UNIVERSIDAD COMPLUTENSE DE MADRID

FACULTAD DE CIENCIAS FÍSICAS

QUARK MASS AND "Nc" DEPENDENCE OF MESON-MESON SCATTERING AND LIGHT RESONANCES WITHIN UNITARIZED CHIRAL PERTURBATION THEORY

MEMORIA PARA OPTAR AL GRADO DE DOCTOR
PRESENTADA POR

Jenifer Nebreda Manjón

Bajo la dirección del doctor
José Ramón Peláez Sagredo

Madrid, 2012

Quark mass and N_c dependence of meson-meson scattering and light resonances within unitarized Chiral Perturbation Theory

by

Jenifer Nebreda Manjón

under the supervision of

Dr. José Ramón Peláez Sagredo

Thesis submitted for the Degree of Doctor in Physics in the
Universidad Complutense de Madrid
-January 2012-

Contents

Preface

Quantum Chromodynamics (QCD) is the theory that explains, in terms of quarks and gluons, the strong interactions. Thanks to its property of asymptotic freedom, which means that the interaction becomes weaker as the energy is increased, it allows for perturbative calculations of processes with a large momentum transfer, domain in which its validity has been largely proved. On the other hand, in the low-energy region its coupling constant grows, preventing us from studying QCD perturbatively. In this regime, quarks and gluons become confined, giving rise to a vast number of particles, called hadrons.

Nevertheless, at very low energies, the existence of a very light octet of pseudoscalar particles, formed by the pions, the kaons and the eta, separated from the resonant region by a gap of several hundreds of MeV, allows us to develop an effective field theory in which resonances are integrated out and the pseudoscalars are the only degrees of freedom. Moreover, the dynamics of these particles are highly constrained by the symmetries of QCD and, in particular, by its spontaneous chiral symmetry breaking. The effective Lagrangian method built on this basis is called Chiral Perturbation Theory (ChPT) and was introduced by Weinberg in 1979 [1]. Later, Gasser and Leutwyler [2, 3, 4, 5] developed the technique and calculated the light-meson scattering amplitudes and other observables, such as masses and form factors, up to one loop in perturbation theory.

The importance of this formalism lies on the fact that the theory is renormalizable and depends only on the masses and decay constants of the light pseudoscalar octet, as well as on a set of phenomenological parameters, known as low energy constants (LECs), which contains the information of the heavier degrees of free-

dom [6, 7] and of the underlying fundamental theory. Once these parameters are determined by means of fits to experimental data, it is possible to make predictions for other processes. ChPT has indeed proved to be very successful in describing the low energy hadron phenomenology. Here we refer the reader to some detailed reviews [8, 9, 10, 11].

However, since ChPT is unfortunately limited to low energies, below roughly 500 MeV, big efforts have been made over the last years in order to improve the high energy behavior of its amplitudes by means of non-perturbative methods. Such methods include the explicit introduction of heavier resonant states in the Lagrangian [6, 12, 7, 13, 14, 15, 16], resummation of diagrams in a Lippmann-Schwinger or Bethe-Salpeter approach [17, 18, 19, 20, 21, 22, 23, 24], the K matrix [25], the Chiral Unitary approach [21, 18], the N/D method [15] and other unitarization techniques like the Inverse Amplitude Method (IAM) [26, 27, 28, 29, 30], which has been largely used for this work.

These unitarization methods not only extend the validity of the amplitudes to higher energies, but also generate light resonances, which are out of reach for standard ChPT. In particular, the IAM can generate the vector resonances $\rho(770)$ and $K^*(892)$ and the scalars $f_0(600)$ or σ, $K_0^*(800)$ or κ, $a_0(980)$ and $f_0(980)$ without a priori assumptions about their existence or nature and without the need of any parameter beyond those of ChPT.

This kind of systematic, model-independent approach is particularly important in the case of the controversial light scalar sector. Although light scalar resonances play a relevant role in various fields, from QCD and Nuclear Physics to Cosmology, their precise properties and even their existence, as in the case of the $K_0^*(800)$, are still subject to intense debate. Both the $f_0(600)$ and the $K_0^*(800)$ are indeed extremely wide, so that they barely propagate and are very hard to see experimentally. This is the reason why many authors have been reluctant to consider them as resonances, with the result that it has taken many years for the $f_0(600)$, or σ, to be included as a "well established" state in the reviews of the Particle Data Group [31], and the $K_0^*(800)$, or κ, still "needs confirmation" and is omitted from the summary table. The $a_0(980)$ lies just below the threshold of the $K\bar{K}$ channel,

to which it strongly couples. This generates a cusp-like behavior in the amplitude that distorts the mass and width parameters. Finally, the $f_0(980)$ overlaps strongly with the $f_0(600)$ and with other resonances and is also close to the $K\bar{K}$ threshold (see "Note on Scalar Mesons" in [31] for an brief account and references).

Whether these resonances belong to the same scalar nonet is still unclear. The issue at stake is their nature, since if they were usual $\bar{q}q$ states [32, 33, 34, 35], one would expect their masses to lie around 1.2 GeV, and not below 1 GeV as they indeed do. Moreover, the mass ordering in a $\bar{q}q$ nonet is opposite to that found for the light scalar resonances. Alternatively, these states have been interpreted as tetraquarks (i.e. two-quark, two-antiquark states) in the MIT Bag Model [36, 37, 38, 39, 40], as hadronic molecules [41, 42, 43, 44], glueballs [45, 46] or hybrids [45]. Most likely, they are a mixture of all these different states. Let us remark that, within the so-called Chiral Unitary approach [21, 18], it has been shown that the $a_0(980)$, $f_0(980)$, κ and σ resonances form an octet and a singlet when the quark masses are degenerated [47].

Regarding the importance of these resonances, let us first focus on the $f_0(600)$. It appears in the scattering of two pions, in the $I = J = 0$ channel. The correlated exchange of two pions in this channel is known to play a key role in the nucleon-nucleon attractive interaction [48], usually modeled as the exchange of a scalar-isoscalar meson, the so-called 'sigma' resonance. Thus, the $f_0(600)$ becomes important for Nuclear Physics. In particular, it is very relevant for the nucleosynthesis processes and, consequently, for anthropic considerations [49, 50, 51] and for the study of the cosmological variation of fundamental constants [52, 53, 54].

On the other hand, the $f_0(600)$ is the lightest meson with the vacuum quantum numbers. Consequently, it is important for the realization of the QCD spontaneous symmetry breaking in models like the linear sigma model or the Nambu-Jona-Lasinio model [55, 56]. Moreover, this breaking, although with relevant differences, is closely related to the Higgs mechanism in the Electroweak Symmetry Breaking Sector in the Standard Model [57, 58, 59]. Also, the quantum numbers of this resonance are the same as those of the glueball, a characteristic feature of the non-

abelian nature of QCD. Since the lightest glueball is expected at energies around 1.5 GeV [60, 61], it can mix up with the $f_0(600)$.

As for ChPT itself, it turns out that, while its low energy constants will, in principle, receive contributions from the meson resonances integrated out of the Lagrangian, it turns out that the one-loop parameters are basically saturated by vector resonance exchange [6, 7]. Thus, it remains to be explained why the light scalar resonances play such a small role, if any at all, in the values of the LECs.

In order to shed some light on these issues, in this work we have followed several different approaches. First, the fact that ChPT depends explicitly on the masses of the quarks has allowed us to study the dependence of the resonances and phase shifts on the quark masses. On the one hand, we have calculated the derivatives of the lightest meson masses with respect to the light and strange quark masses. These values are of interest for the spectroscopic classification of the resonances, and also for studies on the cosmological variability of the fundamental parameters [52, 53, 54]. On the other hand, we have increased the quark masses in order to compare with the results of the studies in lattice QCD.

Let us recall that lattice studies consist on simulating a reticular space-time, where a mathematically well-defined, first-principle formulation of QCD can be carried out numerically, and then extrapolating the results to the physical continuum space-time. Unfortunately, the computational cost of these calculations is very high and it increases fast with decreasing quark masses, so that generally lattice QCD calculations are performed at masses heavier than the physical ones. For this reason, it is interesting for us to increase the mass of the quarks in ChPT so that we can cross-check the results of both methods. Moreover, recent developments in their algorithms are bringing the possibility of phase-shift calculations in different channels and at quark masses closer to the physical ones [62, 63, 64]. Thus, our studies extrapolating ChPT phase shifts to higher quark masses can be useful as a guideline and as a test of compatibility for forthcoming lattice results.

A second approach that I have followed in this work to gain more insight into the scalars puzzle is the study of the amplitudes dependence on another parameter of

the QCD Lagrangian, the number of colors, N_c. QCD amplitudes can be expanded on $1/N_c$ at all energies [65, 66] and the importance of this expansion lies on the fact that different kinds of states depend on N_c very distinctly. For instance, quark-antiquark states are known to become bound as N_c is taken to infinity and their mass and width to scale as $\mathcal{O}(1)$ and $\mathcal{O}(1/N_c)$ respectively. However, since the physical number of colors is only three, a suppression of $\sim 1/3$ of the width over the mass does not seem a very conclusive evidence to assess that a resonance is or is not predominantly made up of a quark-antiquark state. Nevertheless, stronger arguments can be found in various ways. For example, thanks to the fact that the $1/N_c$ expansion can be systematically implemented in ChPT, we have increased the number of colors to make the suppression stronger. We have also built up observables that are suppressed by higher powers of $1/N_c$, so that there is no need to move away from the physical world.

This thesis is presented in the 'article format', which means that the original publications stemming from my post-graduate work are presented after a brief summary and discussion of their main results. Chapter 1 consists on an introduction to the basic concepts and tools used in this thesis. Chapter 2 collects our results: the first section encloses our works on the quark mass dependence of phase shifts and resonances and the second section is dedicated to our studies on the nature of resonances from their $1/N_c$ behavior. Finally, in the third chapter we present the conclusions of this thesis.

List of Publications

The research activity performed in this thesis has produced the following list of peer-reviewed articles:

[1] J. Nebreda and J. R. Peláez,
Strange and nonstrange quark mass dependence of elastic light resonances from SU(3) unitarized chiral perturbation theory to one loop,
Phys. Rev. D 81, 54035 (2010).

[2] J. R. Peláez, J. Nebreda and G. Ríos,
Properties of light resonances from unitarized Chiral perturbation theory: N_c behavior and quark mass dependence,
Prog. Theor. Phys. Suppl. 186, 113 (2010).

[3] J. Nebreda, J. R. Peláez and G. Ríos,
Chiral extrapolation of pion-pion scattering phase shifts within standard and unitarized Chiral Perturbation Theory,
Phys. Rev. D 83, 094011 (2011).

[4] J. Nebreda, J. R. Peláez and G. Ríos,
Enhanced non-quark-antiquark and non-glueball N_c behavior of light scalar mesons,
Phys. Rev. D 84, 074003 (2011).

Also, the work developed in this thesis has been presented in several international congresses giving rise to the following contributions to conference proceedings:

As author

[1] J. Nebreda, J. R. Peláez,
$f_0(600)$, $\kappa(800)$, $\rho(770)$ and K(892) quark mass dependence from unitarized SU(3) Chiral Perturbation Theory*,
in "Hadron 2009: Proceedings of the XIII International Conference on Hadron Spectroscopy", **AIP Conf. Proc. 1257, 500 (2010)**

[2] J. Nebreda, J. R. Peláez,
Dependence on the quark masses of elastic phase shifts and light resonances within standard and unitarized Chiral Perturbation Theory,
to appear in the proceedings of "12th International Conference on Meson-Nucleon Physics and the Structure of the Nucleon (MENU 2010)", **arXiv:1010.3982**

[3] J. Nebreda, J. R. Peláez,
Quark mass dependence of light resonances and phase shifts in elastic $\pi\pi$ and πK scattering,
in "Chiral10 International Workshop on Chiral Symmetry in Hadrons and Nuclei", **AIP Conf. Proc. 1322, 399 (2010)**

[4] J. Nebreda, J. R. Peláez,
Chiral extrapolation of elastic meson-meson scattering: Phase shifts and resonance poles,
in "9th Conference On Quark Confinement And The Hadron Spectrum (Confinement IX)", **AIP Conf. Proc. 1343 277-279, (2011)**

[5] J. Nebreda, J. R. Peláez, G. Ríos,
Mass dependence of pion-pion phase shifts within standard and unitarized ChPT versus Lattice results,
to appear in the proceedings of "XIV International Conference on Hadron Spectroscopy (Hadron 2011)", **arXiv:1108.5980**

As co-author

[6] J. R. Peláez, C. Hanhart, J. Nebreda, G. Ríos,
Unitarized Chiral Perturbation Theory and the meson spectrum,
in "HADRON 2009: Proceedings of the XIII International Conference on Hadron Spectroscopy", AIP Conf. Proc. **1257**, 141 (2010),

Chapter 1

Introduction

The basic concepts and tools used in this thesis are presented in this chapter. In the first section 1.1, we introduce the main ideas of Chiral Perturbation Theory (ChPT). Next, in Section 1.2, we review the unitarization of the ChPT meson-meson scattering amplitudes and present the Inverse Amplitude Method. Section 1.3 provides a compilation of different phenomenological determinations of the effective coupling constants contributing to the meson-meson scattering amplitudes. In Section 1.4, we study how the analytic continuation of the unitarized scattering amplitudes allows us to find poles associated to the lightest resonances. The spectroscopic properties of these lightest mesons are considered in Section 1.5. Finally, Section 1.6 is dedicated to the QCD $1/N_c$ expansion and its implementation in ChPT.

1.1 Chiral Perturbation Theory

The effective Lagrangian method is a very useful tool to implement the symmetry constraints of a theory in its low energy limit. The most general Lagrangian consistent with the symmetries of the theory is written down in the form of an energy expansion, such that only a few terms are relevant in the low energy limit. The effects of the heavy particles are encoded in some set of constants whose values need to be determined from the experimental data.

Chiral Perturbation Theory (ChPT) is the effective Lagrangian method for the strong interactions at low energy. It was first developed by Weinberg in 1979 [1] and is based on the invariance of the QCD Lagrangian under global chiral transformations. In this section, I will first review how the chiral symmetry is implemented in the strong interactions and how it is spontaneously broken, giving rise to the Goldstone bosons that become the degrees of freedom of ChPT. Next, I will introduce the ChPT Lagrangian at leading order and at higher orders in perturbation theory in $SU(3)$. Finally, the $SU(2)$ Lagrangian will be considered.

1.1.1 Chiral symmetry in the strong interactions

Let us consider the fermionic sector of the QCD Lagrangian

$$\mathcal{L} = \bar{\psi}(i\not{D} - M)\psi, \tag{1.1}$$

where ψ is a vector that contains the N_f quark flavors, D_μ is the covariant derivative $D_\mu = \partial_\mu + igA_\mu$, A_μ is the gluonic field and M is the diagonal mass matrix. If we decompose the quark field into chiral fields

$$\psi = \psi_L + \psi_R \tag{1.2}$$

with

$$\psi_L = \frac{1}{2}(1+\gamma_5)\psi \qquad \text{and} \qquad \psi_R = \frac{1}{2}(1-\gamma_5)\psi, \tag{1.3}$$

the Lagrangian can be rewritten as

$$\mathcal{L} = i\bar{\psi}_R\not{D}\psi_R + i\bar{\psi}_L\not{D}\psi_L + \bar{\psi}_R M\psi_L + \bar{\psi}_L M\psi_R. \tag{1.4}$$

We shall consider now the limit $M \to 0$, which is a good approximation in SU(2) and SU(3), since the mass of the quarks is of the order of a few MeV while that of the mesons is of hundreds of MeV. In this limit, the Lagrangian is invariant under

global chiral $SU_R(N_f) \times SU_L(N_f)$ transformations

$$\psi_{L,R}(x) \to \exp(-i\alpha^a_{L,R}\tau^a)\psi_{L,R}(x) \tag{1.5}$$

where τ^a are the generators of $SU(N_f)$. Equivalently, the Lagrangian is invariant under the vector and axial $SU_V(N_f) \times \ SU_A(N_f)$ transformations

$$\psi(x) \to (\exp(-i\alpha^a_V\tau^a) + \exp(-i\alpha^a_A\tau^a\gamma_5))\psi(x). \tag{1.6}$$

If this axial and vector symmetries were realized in nature in the Wigner-Weyl mode, we should find both isospin multiplets and parity doubling. However, while there is an approximate isospin degeneracy (only approximate due to the non-vanishing quark masses), the vector and axial resonances are not even nearly degenerated: in the vector multiplet we find the resonance $\rho(770)$, with a mass of 770 MeV, whereas the axial resonance $a_1(1260)$ is 490 MeV heavier. This difference, which is also found in the rest of the hadrons, is too big to be accounted for by the explicit breaking of the symmetry due to the mass of the quarks.

The chiral symmetry is indeed realized as the Goldstone mode. At least for the lightest quarks ($N_f = 2$ or 3), the symmetry is spontaneously broken following the pattern

$$SU_R(N_f) \times SU_L(N_f) \to SU_V(N_f), \tag{1.7}$$

implying, by the Goldstone theorem [67, 68, 69], that for each generator spontaneously broken there should be a massless boson with the same quantum numbers. This amounts to three massless bosons in $SU(2)$ and eight in $SU(3)$. The pseudoscalar mesons are good candidates for the Nambu-Goldstone bosons, namely, the triplet of pions if we consider only two flavors, plus the kaons and the eta if we consider $N_f = 3$. The reason why they are not massless is because the chiral symmetry is not only spontaneously but also explicitly broken, due to the non-zero quark masses. Nevertheless, since the mass of these pseudo-Nambu-Goldstone

bosons (NGB) is much smaller than that of the rest of the hadrons, we can deal with it perturbatively.

We must also take into account that the quark s is much heavier than the quarks u and d. This implies that the flavor symmetry $SU_V(3)$ is also explicitly broken, explaining the differences in the masses of the NGB, that range from ~ 140 MeV for the pions to ~ 547 MeV for the eta.

Finally, let us make a comment on the η'. In the quark model, the eight NGB have the quantum numbers necessary to form an $SU(3)$ octet. This suggests the existence of a ninth state, the $SU(3)$ singlet. The lightest candidate for such a state is the $\eta'(960)$, which is however very heavy. The responsible for its big mass, which, moreover, does not vanish in the chiral limit, and for the fact that it is not a NGB, is the axial $U(1)$ anomaly. If this anomaly was not present, there would exist an almost conserved current for the $U_A(1)$ symmetry and it could be dynamically broken, so that the η' would also be a NGB.

1.1.2 Chiral Perturbation Theory at leading order

We can now consider that these pseudo-Nambu-Goldstone bosons are the degrees of freedom relevant at low energy and construct an effective theory in which the heavier particles are integrated out. This effective theory is called Chiral Perturbation Theory (ChPT).

As explained in the introduction of this chapter, it must have the same symmetries as QCD, such as invariance under Lorentz transformations, parity and charge conjugation, but also the same pattern of spontaneous and explicit chiral symmetry breaking. At lowest order, this is accomplished by the following effective Lagrangian, which contains all the matrix elements between NGB:

$$\mathcal{L}_{LO} = \frac{F^2}{4}\langle \partial_\mu U \partial^\mu U^\dagger + 2B_0 \mathcal{M}(U + U^\dagger)\rangle, \tag{1.8}$$

where U is the unitary $N_f \times N_f$ matrix $U(\phi) = \exp\left(i\sqrt{2}\phi/F\right)$ that collects the NGB through the $SU(N_f)$ matrix ϕ, F is an energy parameter that we will find later to be the boson decay constant in the chiral limit, $\mathcal{M}$ is the quark mass matrix, B_0 is a constant that relates the quark masses and the NGB masses in the chiral limit and the angular brackets stand for the trace of the matrices. The normalization factor is taken such that the usual kinetic term for the NGB is recovered when U is expanded in terms of the boson fields.

This exponential representation is equally valid for $N_f = 2$ and $N_f = 3$, but in the former case, it is customary to use the four-vector representation that Gasser and Leutwyler adapted from the $O(4)$ nonlinear σ model in their pioneer work on $SU(2) \times SU(2)$ Chiral Perturbation Theory [2]. For this reason, we are going to restrict ourselves to the $SU(3)$ case in this section and in Sect. 1.1.4 we will briefly explain the $SU(2)$ chiral Lagrangian in the $O(4)$ representation.

In $SU(3)$ the matrix ϕ is then given by

$$\phi(x) = \frac{\lambda^a \pi^a(x)}{\sqrt{2}}, \tag{1.9}$$

where the λ^a are the Gell-Mann matrices, which are the generators of $SU(3)$, and π^a is a vector containing the eight NGB. After a rotation in the isospin space, we have

$$\phi(x) = \begin{pmatrix} \frac{1}{\sqrt{2}}\pi^0 + \frac{1}{\sqrt{6}}\eta & \pi^+ & K^+ \\ \pi^- & -\frac{1}{\sqrt{2}}\pi^0 + \frac{1}{\sqrt{6}}\eta & K^0 \\ K^- & \bar{K}^0 & -\frac{2}{\sqrt{6}}\eta \end{pmatrix}. \tag{1.10}$$

Consider now the Lagrangian in (1.8). In order for its kinetic term to be invariant under chiral $SU_R(3) \times SU_L(3)$ transformations, the matrix U must transform as

$$U \to LUR^\dagger \tag{1.11}$$

for L, R in $SU(3)$. The symmetry gives rise to the conserved axial and vector Noether currents

$$V_a^\mu = R_a^\mu + L_a^\mu = -i\frac{F^2}{4}\langle\lambda_a(U^\dagger\partial^\mu U + U\partial^\mu U^\dagger)\rangle,$$
$$A_a^\mu = R_a^\mu - L_a^\mu = i\frac{F^2}{4}\langle\lambda_a(U^\dagger\partial^\mu U - U\partial^\mu U^\dagger)\rangle. \tag{1.12}$$

If we calculate the matrix element of the axial current between a one-boson state and the vacuum, by expanding the axial current in powers of ϕ, we find that

$$\langle 0|A_a^\mu|\pi_b\rangle = ip^\mu F\delta_{ab}, \tag{1.13}$$

which allows the identification of F as the meson decay constant in the chiral limit, as we anticipated before.

On the other hand, the mass term is responsible for the explicit breaking of the symmetry. Since we work in the isospin limit, the matrix $\mathcal{M}$ is given by $\mathcal{M} = \text{diag}(\hat{m}, \hat{m}, m_s)$, with $\hat{m} = (m_u + m_d)/2$, so that the masses of the NGB in the chiral limit are

$$\begin{aligned} M_{0\pi}^2 &= 2\hat{m}B_0, \\ M_{0K}^2 &= (\hat{m} + m_s)B_0, \\ M_{0\eta}^2 &= \frac{2}{3}(\hat{m} + 2m_s)B_0, \end{aligned} \tag{1.14}$$

where we see that they satisfy the Gell-Mann-Okubo relation $4M_{0K}^2 - M_{0\pi}^2 = 3M_{0\eta}^2$ [70, 71]. If the mass term in (1.8) had been written differently, this relation would not have been obtained at tree level [72].

The meson-meson scattering amplitudes can be calculated to leading order using the Lagrangian (1.8) to obtain the tree-level Feynman diagrams. In the following section we introduce the next-to-leading order Lagrangian.

1.1.3 Chiral Perturbation Theory at higher orders

In order to calculate higher energy contributions, we write down all the possible terms invariant under chiral transformations. They can be ordered by the dimensionality of their operators, each factor of $\mathcal{M}$ being equivalent to two derivatives, according to (1.14), and each derivative contributing in a factor p/Λ_χ, where p is the momentum of the NGB and $\Lambda_\chi \simeq 4\pi F \simeq 1$ GeV is the typical scale of symmetry breaking. Moreover, since every term must have an even number of derivatives to fulfill the Lorentz invariance, the general Lagrangian will be of the form:

$$\mathcal{L}_{\text{eff}} = \mathcal{L}_2 + \mathcal{L}_4 + \mathcal{L}_6 + \cdots , \tag{1.15}$$

where each subindex indicates the chiral power of the term. At lowest order, only the leading order $\mathcal{O}(p^2/\Lambda_\chi)$, given by the Lagrangian (1.8), is needed. The most general $SU(3)$ $\mathcal{O}(p^4/\Lambda_\chi)$ term is given by:

$$\begin{aligned}
\mathcal{L}_4 = \quad & L_1\langle\partial_\mu U^\dagger \partial^\mu U\rangle^2 \;+\; L_2\langle\partial_\mu U^\dagger \partial_\nu U\rangle\langle\partial^\mu U^\dagger \partial^\nu U\rangle \\
+ \quad & L_3\langle\partial_\mu U^\dagger \partial^\mu U \partial_\nu U^\dagger \partial^\nu U\rangle \;+\; L_4\langle\partial_\mu U^\dagger \partial^\mu U\rangle\langle U^\dagger M_0 + M_0^\dagger U\rangle \\
+ \quad & L_5\langle\partial_\mu U^\dagger \partial^\mu U (U^+ M_0 + M_0^+ U)\rangle \;+\; L_6\langle U^\dagger M_0 + M_0^+ U\rangle^2 \\
+ \quad & L_7\langle U^\dagger M_0 - M_0^\dagger U\rangle^2 \;+\; L_8\langle M_0^\dagger U M_0^\dagger U + U^\dagger M_0 U^\dagger M_0\rangle,
\end{aligned} \tag{1.16}$$

where the terms that couple to external sources have been omitted since they do not contribute to meson-meson scattering. Thus, at this order we have eight coupling constants L_i which account for the heavier degrees of freedom [6] and whose value must be determined experimentally. These parameters, known as low-energy constants (LECs), will have a finite part $L_i^r(\mu)$, where μ is the renormalization scale, and an infinite part that will cancel the divergencies introduced by loop diagrams with lower order vertices, allowing the theory to be renormalizable order by order.

The $\mathcal{O}(p^4)$ $SU(3)$ meson-meson scattering amplitudes and other observables, such as masses and form factors, can then be obtained from this Lagrangian in

terms of eight low-energy constants [5, 8, 73, 74, 75]. At higher orders the theory loses predictivity because the number of LECs increases very quickly [76].

1.1.4 $SU(2)$ chiral Lagrangian

In the SU(2) case it is more useful to parametrize the U fields as an $O(4)$ vector, as first done by Gasser and Leutwyler [2]. Namely, $U \equiv (U^0, U^j)$ with $j = 1, 2, 3$, and U^0, U^j real fields, with the constraint $U^T U = 1$. The U^j correspond to the fields of the pions $U^j = \pi^j$ and so $U^0 = \sqrt{1 - \vec{\pi}^2}$. After a rotation in the isospin space we have

$$\pi^+ = \frac{\pi^1 + i\pi^2}{\sqrt{2}}, \qquad \pi^- = \frac{\pi^1 - i\pi^2}{\sqrt{2}}, \qquad \pi^0 = \pi^3. \tag{1.17}$$

With this notation, the $SU(2)$ chiral Lagrangian up to $\mathcal{O}(p^4)$ reads

$$\begin{aligned}
\mathcal{L}_{SU(2)} &= \frac{F^2}{2}\nabla_\mu U^T \nabla^\mu U + l_1(\nabla^\mu U^T \nabla_\mu U)^2 \\
&+ l_2(\nabla_\mu U^T \nabla_\nu U)(\nabla^\mu U^T \nabla^\nu U) + l_3(\chi^T U)^2 \\
&+ l_4(\nabla^\mu \chi^T \nabla_\mu U) + l_5(U^T F_{\mu\nu} F^{\mu\nu} U) \\
&+ l_6(\nabla^\mu U^T F_{\mu\nu} \nabla^\nu U) + l_7(\tilde{\chi}^T U)^2 \\
&+ h_1 \chi^T \chi + h_2 F_{\mu\nu} F^{\mu\nu} + h_3 \tilde{\chi}^T \tilde{\chi},
\end{aligned} \tag{1.18}$$

where the covariant derivative is defined as

$$\begin{aligned}
\nabla_\mu U^0 &= \partial_\mu U^0 + a^i_\mu(x) U^i, \\
\nabla_\mu U^i &= \partial_\mu U^i + \epsilon^{ikl} v^k_\mu(x) U^l - a^i_\mu(x) U^0,
\end{aligned} \tag{1.19}$$

with a_μ and v_μ the external axial and vector currents. The tensor $F_{\mu\nu}$ is defined by

$$(\nabla_\mu \nabla_\nu - \nabla_\nu \nabla_\mu) U = F_{\mu\nu} U, \tag{1.20}$$

and the vectors χ, $\tilde{\chi}$ are proportional to the external scalar and pseudoscalar fields, s and p:

$$\begin{aligned} \chi &= 2B_0(s^0, p^i), \\ \hat{\chi} &= 2B_0(p^0, -s^i). \end{aligned} \tag{1.21}$$

Since in this work we will only calculate scattering amplitudes, we can set $v_\mu = a_\mu = 0$, $s^i = p = 0$ and $s^0 = \hat{m}$.

At tree level the amplitudes only depend on F_π and M_π, and thus they are called 'low energy theorems' and correspond to the current algebra results obtained by Weinberg in the sixties [77]. One order higher in perturbation theory, the $\mathcal{O}(p^4)$ pion-pion scattering amplitudes, obtained from the Lagrangian (1.18), depend on four low energy constants, l_1 to l_4.

Furthermore, the $\mathcal{O}(p^6)$ $SU(2)$ Lagrangian can be written in terms of only six independent combinations of low energy constants [78]. Thus, in our works in $SU(2)$ we will go up to two loops using the $\pi\pi$ scattering amplitudes given in [79]. A discussion on the $SU(2)$ and $SU(3)$ low energy constants and a compilation of the different phenomenological determinations used throughout this thesis will be presented in section 1.3.

To end this section dedicated to Chiral Perturbation Theory, let us note that, despite its great success in describing the low-energy region in a complete model-independent and systematic manner, ChPT presents an important limitation: its scattering amplitudes, which are polynomials in masses and momenta, violate the unitarity bounds as the energy is increased and break down in the presence of resonances.

In the next section we study the unitarization of the ChPT amplitudes, which allows to overcome this problem and, furthermore, to generate poles that are associated to resonances.

1.2 Unitarity and the Inverse Amplitude Method

As stated above, the validity of the chiral expansion is naturally limited to low energies and, in particular, in resonant channels it must fail in the resonance region, due to the unitarity condition, as we will see.

In the last years, many unitarization techniques have been developed to overcome this problem, for instance, the explicit introduction of resonances [6, 12, 7, 13, 14, 15, 16], the K matrix [25], the resummation of diagrams in a Lippmann-Schwinger or Bethe-Salpeter approach [17, 18, 19, 20, 21, 22, 23, 24], the Chiral Unitary approach [21, 18], the N/D method [15] and the Inverse Amplitude Method (IAM) [26, 27, 28, 29, 30], which is the unitarization technique used throughout this work.

The main advantage of the IAM with respect to other approaches is that it implements the fully renormalized ChPT expansion at low energies without introducing any spurious parameter in the unitarization procedure. For the elastic scattering, it can indeed be justified within a dispersive approach, which allows us to extend the unitarized amplitudes to the complex plane and find poles associated to the resonances without introducing further model-dependent assumptions. However, there is no dispersive derivation for the coupled-channel case, where the other methods thus become equally useful, but simpler to implement.

Since in our work we want to avoid the appearance of any spurious parameter not present in the ChPT Lagrangian, we will use the IAM for the unitarization of our amplitudes. I am going to devote the rest of this section to explain the rudiments of this method. I will start by introducing the scattering amplitudes and their unitarity constraint. Next, I will show how, by inserting this unitarity condition into a dispersion relation, the IAM can be derived. Finally, I will make some remarks about the validity of this method and present a generalization that allows its use in the region near the Adler zeros.

1.2.1 Partial waves, phase shifts and unitarity

In particle physics the amplitudes are usually projected in partial waves of definite isospin I and angular momentum J. The partial wave t_{ab}^{IJ} for a process $a \to b$, where a and b are two-body states, is then defined as

$$t_{ab}^{IJ}(s) = \frac{1}{32K\pi}\int_{-1}^{1} d(x)P^J(x)T_{ab}^I(s,t,u), \tag{1.22}$$

where $T_{ab}^I(s,t,u)$ is the isospin combination with total isospin I, $P^J(x)$ is the J^{th} Legendre polynomial, $x = \cos\theta$ is the scattering angle in the center of mass frame and s, $t(s,x)$ and $u(s,x)$ are the Mandelstam variables, given by the kinematics of the process. The normalization of the partial waves includes a factor K, whose value is $K = 2$ if the particles are identical and $K = 1$ otherwise. The acceptable combination of total isospin I and angular momentum J also depends on the particular process: if the NGB are identical, as in the case of the pions in the isospin limit, the total amplitude must be symmetric (because they obey Bose statistics) and consequently, the quantity $I + J$ must be even. Note also that the different isospin projections are related by crossing symmetry and that $t_{ab} = t_{ba}$ due to the invariance under temporal inversion.

The relation between the partial wave and the S-matrix, whose elements describe the dispersion from channel a to channel b, is given by

$$S_{ab} = \delta_{ab} + 2i\sqrt{\sigma_a\sigma_b}\, t_{ab}, \tag{1.23}$$

where we have dropped the superindexes IJ and the dependence on s to simplify the notation and σ_a is the phase space of the two-particle channel $|\, a \,\rangle = |\, \alpha\beta \,\rangle$ at the energy $\sqrt{s}$,

$$\sigma_a = \sqrt{\left(1 - \frac{(M_\alpha + M_\beta)^2}{s}\right)\left(1 - \frac{(M_\alpha - M_\beta)^2}{s}\right)}. \tag{1.24}$$

From the unitarity of the S-matrix, $SS^\dagger = \mathbb{1}$, we can obtain a relation for the partial waves. For elastic scattering, we have that the partial wave t must satisfy

$$\operatorname{Im} t = \sigma |t|^2 \quad \Rightarrow \quad \operatorname{Im} t^{-1} = -\sigma, \tag{1.25}$$

meaning that it can be parametrized with a single parameter $\delta(s)$ as

$$t = \frac{1}{\sigma} e^{i\delta} \sin\delta. \tag{1.26}$$

Thus, the modulus of the scattering amplitude is bounded, $|t| < 1/\sigma$, and it reaches its maximum in the resonance region, where the phase shift is $\delta = \pi/2$.

Up to this point we have discussed exact elastic amplitudes, but let us remind that the amplitudes in ChPT are obtained as a truncated expansion in masses and momenta

$$t = t_2 + t_4 + t_6 + ..., \tag{1.27}$$

with $t_k \sim \mathcal{O}(p^k)$. Thus, the amplitudes being a polynomial, they cannot satisfy the unitarity condition (1.25) exactly. Nevertheless, they do satisfy a *perturbative unitarity condition*

$$\begin{aligned} \operatorname{Im} t_2 &= 0, \\ \operatorname{Im} t_4 &= \sigma\ t_2^2, \\ &..., \end{aligned} \tag{1.28}$$

The deviations between the exact unitarity condition (1.25) and the perturbative one (1.28) grow bigger at high energies and at the resonance region and this is one of the motivations for modifying the ChPT amplitudes so that they satisfy the unitarity condition exactly. The other reason is that we want to make poles appear in the complex plane, because they are associated to the resonances, as we shall see later.

1.2.2 Unitarity and dispersion relations

We are going to review now how to implement simultaneously chiral constraints and unitarity on the amplitudes, making use of their analytic structure when the Mandelstam variable s is extended to the complex plane. Further details on this topic can be found in [80].

Partial waves obtained from a relativistic quantum field theory present a characteristic structure in the complex plane. On the one hand, they have a non-vanishing imaginary part from the threshold energy to infinity, due to the existence of intermediate states. On the other hand, they obey the Schwarz reflection principle, by virtue of which

$$t(s^*) = t^*(s). \tag{1.29}$$

As a consequence of these two properties, the amplitudes must posses a cut over the right hand side of the real axis. Moreover, since the amplitudes in the u and t channels are related to the amplitude in the s channel by crossing symmetry, their respective cuts become, for the partial waves, new cuts on the left hand side of the real axis. Finally, causality prevents the analytic extension of the amplitudes to have poles in the first Riemann sheet.

Given this analytic structure, we can use the Cauchy integral formula over the contour C shown in Fig. 1.1 to write

$$t(s) = \frac{1}{2\pi i}\int_C \frac{t(s')}{s'-s}\,ds'. \tag{1.30}$$

If we assume that $t \to 0$ as $|s| \to \infty$, then Eq. (1.30) can be written as

$$t(s) = \frac{1}{\pi}\int_{s_{th}}^{\infty} \frac{\mathrm{Im}\, t(s')}{s'-s}\,ds' + \frac{1}{\pi}\int_{-\infty}^{0} \frac{\mathrm{Im}\, t(s')}{s'-s}\,ds'. \tag{1.31}$$

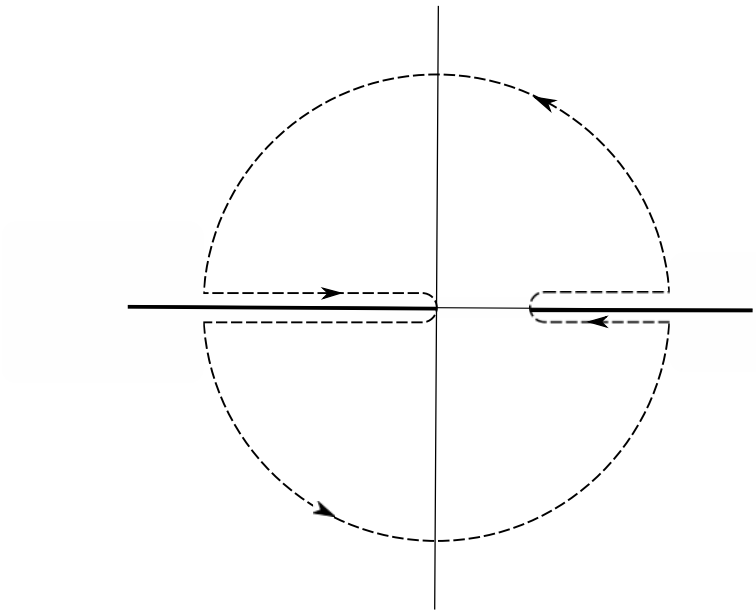

Figure 1.1: Contour of integration in the complex s-plane

where, for real values of s, $\mathrm{Im}\, t(s)$ means the limit of $\mathrm{Im}\, t(s+i\epsilon)$ when $\epsilon \to 0^+$, and so

$$\mathrm{Im}\, t(s) \equiv \mathrm{Im}\, t(s+i\epsilon) = \frac{1}{2i}[t(s+i\epsilon) - t(s-i\epsilon)]. \tag{1.32}$$

Relations of the type of Eq. (1.31) are usually known as *dispersion relations*. Although the assumption that the amplitudes increase sufficiently slow for the integral to converge when $|s| \to \infty$ cannot be made, it is still possible to write down a similar relation by applying Cauchy's theorem to the function

$$G(s) = \frac{t(s)}{(s-s_1)(s-s_2)...(s-s_N)}, \tag{1.33}$$

which, for a sufficiently high N, has the desired $G(s) \to 0$ limit. The price to be paid is that we have to include now the residues of these N poles, so that we need to know the value of the amplitude evaluated at the points s_1, s_2,...,s_N, which are called the *subtraction points*. It is usually preferable to make all the subtractions

at the same point s_1, in which case the Cauchy integral formula reads

$$t(s) = \frac{(s-s_1)^N}{2\pi i}\int_C \frac{t(s')}{(s'-s_1)^N(s'-s)}\,ds' + \sum_{r=1}^{N}\frac{1}{N-r}\,t^{(N-r)}(s_1)(s-s_1)^{N-r}, \tag{1.34}$$

so that we have an *N-times-subtracted dispersion relation* of the form

$$t(s) = \sum_{r=1}^{N} C_r\,(s-s_1)^{N-r} + \frac{(s-s_1)^N}{\pi}\int_{s_{th}}^{\infty}\frac{\mathrm{Im}\,t(s')}{(s'-s_1)^N(s'-s)}\,ds' + I_{LC}(t), \tag{1.35}$$

where the N constants C_i are usually known as *subtraction constants* and $I_{LC}(t)$ is the left cut contribution.

1.2.3 The Inverse Amplitude Method

The dispersion relations studied in the previous section can be used to modify the elastic ChPT amplitudes so that they respect the unitarity condition (1.25). This has been made in many contexts and for different processes, but we are going to focus in one particular method, which is very simple and yields extremely good results: the *Inverse Amplitude Method* [26, 27, 28, 29, 30, 81].

The ChPT partial waves can be used to calculate perturbatively the subtraction constants and the integrand inside Eq. (1.35). Let us consider the elastic scattering amplitudes at order $\mathcal{O}(p^4)$. They are a second order polynomial in s, so that we can write down the perturbative three times subtracted dispersion relations

$$\begin{aligned} t_2 &= a_0 + a_1 s, \\ t_4 &= b_0 + b_1 s + b_2 s^2 + \frac{s^3}{\pi}\int_{s_{th}}^{\infty}\frac{\sigma\, t_2(s')^2}{s'^3(s'-s)}\,ds' + I_{LC}(t_4), \end{aligned} \tag{1.36}$$

where we have used the perturbative unitarity condition (1.28) and the subtraction constants have been expanded in terms of the masses, such that $C_0 = a_0 + b_0$, $C_1 = a_1 + b_1$ and $C_2 = b_2$.

Let us now consider the function

$$G(s) = \frac{t_2(s)}{t(s)}, \tag{1.37}$$

which has the same cut structure as $t(s)$ and the same or even better $s \to \infty$ limit. We can then write its three times subtracted dispersion relation, which reads

$$G(s) = G_0 + G_1 s + G_2 s^2 + \frac{s^3}{\pi} \int_{s_{th}}^{\infty} \frac{\mathrm{Im}\, G(s') ds'}{s'^3 (s' - s)} + I_{LC}(G) + PC, \tag{1.38}$$

where PC stands for the pole contribution in $G(s)$ coming from the zeros of $t(s)$. We can use now the unitarity condition (1.25) to rewrite the imaginary part of $G(s)$ on the physical cut as

$$\mathrm{Im}\, G = t_2^2\, \mathrm{Im}\, \frac{1}{t} = -t_2^2\, \sigma. \tag{1.39}$$

On the other hand we can replace the imaginary part of $G(s)$ on the left cut by its perturbative expansion

$$\mathrm{Im}\, G = t_2^2\, \mathrm{Im}\, \frac{1}{t} \simeq t_2^2\, \mathrm{Im}\, \frac{1}{t_2 + t_4} \simeq -\mathrm{Im}\, t_4. \tag{1.40}$$

and the same with the subtraction constants, $G_0 \simeq a_0 - b_0$, $G_1 \simeq a_1 - b_1$ and $G_2 \simeq -b_2$. The dispersion relation finally reads

$$G(s) = a_0 + a_1 s - b_0 - b_1 s - b_2 s^2 - \frac{s^3}{\pi} \int_{s_{th}}^{\infty} \frac{\sigma(s)\, t_2^2(s) ds'}{s'^3 (s' - s)} - I_{LC}(t_4). \tag{1.41}$$

The pole contribution has been neglected because it is generally small. Nevertheless, we will see later a modified version in which it is considered.

Comparing Eqs. (1.36) and (1.41) we find that

$$G(s) = \frac{t_2^2(s)}{t(s)} \simeq t_2(s) - t_4(s), \tag{1.42}$$

and therefore

$$t(s) \simeq \frac{t_2^2(s)}{t_2(s) - t_4(s)} \equiv t_{\rm IAM}(s). \tag{1.43}$$

The amplitude $t_{\rm IAM}(s)$ calculated with this approximation, known as the *Inverse Amplitude Method* (IAM) [26, 27, 28, 29, 30], satisfies exact unitarity

$$\mathrm{Im}\, t_{\rm IAM}^{-1}(s) = \mathrm{Im}\, \frac{t_2(s) - t_4(s)}{t_2^2(s)} = -\sigma, \tag{1.44}$$

and, if it is re-expanded at low energies, the ChPT expansion is recovered:

$$t_{\rm IAM}(s) = \frac{t_2^2(s)}{t_2(s) - t_4(s)} \simeq t_2(s) + t_4(s) + \mathcal{O}(p^6). \tag{1.45}$$

Let us remark that in this approach we have not made any model dependent assumption, but just approximations to a given order. The generalization to higher orders is straightforward. For instance, the unitarized amplitude at $\mathcal{O}(p^6)$ [82, 83, 30] reads simply

$$t_{\rm IAM}(s) = \frac{t_2^2(s)}{t_2(s) - t_4(s) + \frac{t_4^2(s)}{t_2(s)} - t_6(s)}. \tag{1.46}$$

Validity of the Inverse Amplitude Method

We are going to study now how the approximations made in the previous derivation affect the applicability of the IAM.

First, we have neglected the terms of order $\mathcal{O}(p^6)$ when replacing $\mathrm{Im}\, G(s)$ by $-\mathrm{Im}\, t_4(s)$ on the left cut, as well as the contributions coming from zeros in the

amplitude, which would appear as poles of the inverse function. However, on the one hand, the denominator $s'(s'-s)$ ensures that these integrals are suppressed at high energies, while, on the other hand, Eq. (1.45) shows that the IAM only differs from the ChPT result by $\mathcal{O}(p^6)$ at low energies. Nevertheless, we must be careful with the existence of the so-called *Adler zeros* below threshold in scalar partial waves. We will consider in the next section a slightly modified method that takes into account the poles arising from these Adler zeros [81].

Second, $t_2(s)$ vanishes for all partial waves with $J \geqslant 2$, which means that the expressions (1.43) and (1.46) cannot be used for D-waves and above. Moreover, since $t_2(s) = 0$ implies by Eq. (1.28) that $\operatorname{Im} t_4(s) = 0$, we would need to go up to $\mathcal{O}(p^8)$ to be able to generalize the previous derivation. This is the reason why in section 2.1.3 we calculate the chiral extrapolation of the S, P and D waves in standard ChPT but only for the S and P waves for unitarized ChPT.

Third, the elastic unitarity condition (1.28), which has been used to rewrite the imaginary part of $G(s)$ on the physical cut, only holds below the lowest-lying inelastic threshold. The first inelastic channels are the four-particle intermediate states, the four-pion state in $\pi\pi$ scattering and the $\pi K\pi\pi$ state in πK scattering, but their contribution is strongly suppressed by the four particle phase space and we expect the IAM to give a good approximation. However, there are other intermediate states not suppressed by phase space that open up within the range of energies we are interested in, such as the $K\bar{K}$, opening in the $I = 0, J = 0$ channel at 985 MeV. Above that threshold, the unitarity condition involves two channels and a new, non-negligible integral appears, so that the IAM cannot be trusted anymore. In $\pi\pi$ scattering we find indeed that the resonance $f_0(980)$, whose nature is closely related to the $K\bar{K}$ channel, cannot be reproduced using the elastic IAM.

Nevertheless, the Inverse Amplitude Method can be extended to the coupled-channel case [18, 21, 84, 85, 86], although there is still no dispersive derivation for that method.

Keeping in mind these limitations, let us note again that the dispersion relations in the derivation of the IAM are exact on the right cut, whereas the left cut and

the subtraction constants have been approximated within ChPT in the low energy region, where its use is well justified. Moreover, the unitarized amplitudes are fully renormalized and no spurious parameters have been introduced.

Finally, the fact that the IAM can be directly derived from the analytic structure of the general two-body elastic scattering using dispersion relations allows us to expand the unitarized amplitudes to the complex plane. When doing so, we will find that they provide the correct analytic structure required from relativistic quantum field theory, namely, they present a left and a right cut, which were already present in plain ChPT, and poles on the second Riemann sheet related to the physical resonances.

Modified Inverse Amplitude Method

As we commented above, chiral symmetry requires the existence of Adler zeros below threshold in scalar waves, which turn into poles for the inverse amplitude. Let us denote by s_A the Adler zero of the 'complete' partial wave, such that $t(s_A) = 0$ and let s_2 be the approximation to the Adler zero at LO, such that $t_2(s_2) = 0$. Thus, $G(s)$ has a pole at s_A that has been neglected in the derivation of the unitarized amplitude $t_{\rm IAM}(s)$ and at the same time, $t_{\rm IAM}(s)$ has a zero at s_2 and not at s_A. Moreover, $t_{\rm IAM}(s)$ has a spurious pole at an enery s_0 such that $t_2(s_0) - t_4(s_0) = 0$, which must lie near s_2 since $t_4(s)$ is expected to be small compared to $t_2(s)$. Thus, the unitarized amplitudes do not present the correct behavior in the vicinity of s_A and s_2 and one should be careful not to take the subtraction points in that region.

However, if we repeat the dispersive derivation of the IAM including the pole contributions, we can obtain a *Modified Inverse Amplitude Method* (mIAM)[81] that solves all these problems without yielding any significant deviation over the standard IAM in the physical region. The mIAM amplitude at $\mathcal{O}(p^4)$ reads

$$t_{\rm IAM}(s) = \frac{t_2^2(s)}{t_2(s) - t_4(s) + A(s)}, \tag{1.47}$$

where $A(s)$ is a complicated expression such that $A(s_2) = t_4(s_2)$ and $A(s) = \mathcal{O}(p^6)$ for $s \neq s_2$ and that, in the simplest case of the dispersion of two NGB with equal masses, reads

$$A(s) = t_4(s_2) - \frac{(s_2 - s_A)(s - s_2)}{s - s_A}[t_2'(s_2) - t_4'(s_2)]. \tag{1.48}$$

In the case of the $I = 1/2$, $J = 0$ πK scattering amplitude, the LO partial wave has two zeros instead of one, leading to a more complicated expression for $A(s)$:

$$A^{mIAM}(s) = \frac{t_2(s)^2}{t_2'(s_{2+})^2}\left[\frac{t_4(s_{2+})}{(s - s_{2+})^2} - \frac{(s_{2+} - s_A)}{(s - s_{2+})(s - s_A)} \times \left(t_2'(s_{2+}) - t_4'(s_{2+}) + \frac{t_4(s_{2+})t_2''(s_{2+})}{t_2'(s_{2+})}\right)\right]. \tag{1.49}$$

The modified amplitudes do not appreciably differ from the results using the simple IAM formula in the physical and resonance regions. However, we will need to use the modified version of the IAM in section 2.1.2, where the σ and κ poles move into the subthreshold region when increasing the pion mass.

1.3 The low energy constants

The study of the ChPT amplitudes involves a phenomenological determination of its low energy constants. However, the LECs from the literature are not always quoted with systematic uncertainties and some of them are not even compatible. For this reason, and also because we will use unitarized ChPT, which typically covers higher energy ranges and absorbs part of the higher order corrections, in this thesis new sets of LECs have been obtained for both $SU(2)$ and $SU(3)$ ChPT. In this section, I present a compendium of the existing and new sets used throughout the thesis. Among other issues, a comparison between the different determinations will give an idea of the size of the systematic errors.

$\mathcal{O}(p^4)$ $SU(2)$ low energy constants

We first consider the four LECs l_1 to l_4 contributing to the $\pi\pi$ scattering amplitudes at order $\mathcal{O}(p^4)$. In the first part of table 1.1 we quote some LECs of standard ChPT evaluated at $\mu = 770$ MeV:

- Set I comes from a Roy-Steiner analysis using $\mathcal{O}(p^4)$ $SU(3)$ ChPT (the $SU(2)$ LECs are recast from the $SU(3)$ ones using the relations given in [5]) [87].
- Set II comes from an analysis of the K_{l4} data using $\mathcal{O}(p^4)$ $SU(3)$ ChPT [88].
- Set III comes from the same analysis as set II but from a $\mathcal{O}(p^6)$ calculation [88].
- Set IV comes from a dispersive analysis using $\mathcal{O}(p^6)$ $SU(2)$ ChPT [89].
- Set V comes from a dispersive analysis using $\mathcal{O}(p^6)$ $SU(3)$ ChPT [90].

Note that the values of the LECs vary sizably between the $\mathcal{O}(p^4)$ and $\mathcal{O}(p^6)$ calculations, even if they come from the same analysis. This happens because the two-loop leading log contributions, which at low energies are numerically dominant over other terms of the same order, do not depend on the $O(p^6)$ LECs, but just on the one-loop l_i.

Another important remark is that, if we consider the $SU(2)$ Lagrangian in Eq. (1.18), we observe that l_1 and l_2 multiply terms that only depend on the pion field derivatives, while l_3 and l_4 multiply terms proportional to the quark masses. Thus, the former are best determined when looking at the energy or momentum dependence of the amplitudes. In contrast, the latter specify the dependence of the amplitude on the quark masses and are thus better estimated from lattice calculations. That is the reason why in our work, whenever we use the set IV [89] from standard ChPT, we substitute the value for l_3 by the one estimated in a recent and very detailed review of lattice results [91]. In the second part of table 1.1 we give some examples of lattice determinations:

- MILC 10A uses $SU(2)$ NLO fits [92].

- ETM 10 also uses $SU(2)$ NLO fits (NNLO fits were used to estimate the systematic error from the truncation of ChPT but they concluded that it is unobservable at their current level of precision) [93].

- FLAG is a working group that has reviewed lattice results relevant for pion and kaon physics. Taking into account the precision of each reviewed analysis, they give an estimate for l_3, but not for l_4 since they find that, for the moment, lattice results are not consistent enough [91].

Finally, in order to use the IAM to study the resonances, we need some sets of LECs obtained from fits to experimental data in the resonance region. Of course, these LECs should still be similar to those from standard ChPT. In fact, since the one-loop IAM generates correctly only the s-channel leading logs of the two-loop calculation, which are dominant at low energies, its LECs are expected to lie somewhere in between the one- and two-loop ChPT analysis. For the same reason, we will see that the LECs obtained using the $\mathcal{O}(p^6)$ IAM, which takes into account leading log terms from $\mathcal{O}(p^8)$ and higher orders, differ somewhat from the $\mathcal{O}(p^6)$ ChPT estimates.

In the third part of table 1.1, we collect the $SU(2)$ $\mathcal{O}(p^4)$ LECs that have been used for the IAM amplitudes throughout this work. The set highlighted in boldface is indeed a result of this thesis.

- Set 1 was obtained for the publication 2.1.3 ([94]) included in this thesis. l_1 and l_2 were obtained from fitting the $\mathcal{O}(p^4)$ mIAM to the dispersive data analysis of [95]. l_3 was fixed to the lattice estimate from FLAG (the reason why it is different to the number given in the table is because at the time of the publication of our paper [96] only a preprint of the review was available. In the published version of that review [91], the value of l_3 changed within the errors). l_4 was fixed to the value of set IV.

- Set 2 was obtained in [97] by fitting the $\mathcal{O}(p^4)$ mIAM to data up to the resonance region. l_3 and l_4 were fixed to the values from [2].

Set	$10^3\, l_1^r$	$10^3\, l_2^r$	$10^3\, l_3^r$	$10^3\, l_4^r$
Set I[87]	-4.9 ± 0.6	5.2 ± 0.1	-	17 ± 10
Set II [88]	-4.5	5.9	2.1	5.7
Set III [88]	-3.3 ± 2.5	2.8 ± 1.1	1.2 ± 1.7	3.5 ± 0.6
Set IV[89]	-4.0 ± 0.6	1.9 ± 0.2	0.8 ± 3.8	6.2 ± 1.4
Set V [90]	-4.0 ± 2.1	1.6 ± 1.0	-	-
ETM 10 [93]	-	-	-0.45(0.11)(0.41)	7.94(0.19)(0.63)
MILC 10A [92]	-	-	$0.8(1.3)\binom{+0.6}{-1.5}$	$3.6(2.0)\binom{+3.2}{-1.8}$
FLAG [91]	-	-	0.3 ± 1.3	-
Set 1 [94]	$\mathbf{-3.9 \pm 0.2}$	$\mathbf{4.3 \pm 0.4}$	$\mathbf{0.2 \pm 1.1}$	$\mathbf{6.2 \pm 1.4}$
Set 2 [97]	-3.7 ± 0.2	5.0 ± 0.4	0.8 ± 3.8	6.2 ± 5.7
Set 3 [98]	-5.0	1.7	0.8	6.5
Set 4 [98]	-4.0	1.2	0.8	6.5

Table 1.1: $\mathcal{O}(p^4)$ $SU(2)$ LECs evaluated at $\mu = 770$ MeV. The first group of LECs come from standard ChPT determinations, the second group are estimates from lattice studies and the third group are IAM determinations. Set 1 is highlighted in boldface because it has been obtained for the publication 2.1.3 ([94]), which is part of this thesis.

- Set 3 and Set 4 correspond to the $\mathcal{O}(p^6)$ fits A and D of [98], considered the best among four fits, particularly because their LECs are quite compatible with the values of the standard $\mathcal{O}(p^4)$ LECs and reasonably close to the crude expectations for the $\mathcal{O}(p^6)$ ones.

$\mathcal{O}(p^6)$ $SU(2)$ low energy constants

At $\mathcal{O}(p^6)$ six more LECs, r_{1-6}, contribute to the scattering amplitudes. These constants are very poorly known and rely on a resonance saturation analysis [99], which gives an order of magnitude estimate. The LECs of that analysis are given in

Set	$10^4\, r_1^r$	$10^4\, r_2^r$	$10^4\, r_3^r$	$10^4\, r_4^r$	$10^4\, r_5^r$	$10^4\, r_6^r$
RS [99]	-0.6	1.3	-1.7	-1.0	1.1	0.3
Set IV [89]	-0.6 ± 0.4	1.3 ± 0.7	-1.7 ± 1.0	-1.0 ± 0.6	1.5 ± 0.4	0.40 ± 0.04
Set 3 [98]	-0.6	1.3	-1.7	2.0	2.0	-0.6
Set 4 [98]	-1.0	1.3	-0.3	4.2	2.3	-1.0

Table 1.2: $\mathcal{O}(p^6)$ $SU(2)$ LECs. In the first row we show the resonance saturation estimates (RS) [99]. The value of the scale μ that should be used when applying the RS estimates is not known. The other sets are calculated at $\mu = 770$ MeV. We do not show lattice determinations because there are still few $\mathcal{O}(p^6)$ results.

the first row of table 1.2. In the second row we give the $\mathcal{O}(p^6)$ LECs corresponding to set IV [89], already presented in the previous section. To obtain that set, the resonance saturation values for r^r_{1-4} were taken as an input, considering equally likely all values in the interval from 0 to twice the central value. In the third and fourth rows of the table we give the $\mathcal{O}(p^6)$ LECs corresponding to fits 3 and 4 (A and D in [98]), for which the r_i^r of the previous set were used as constraints.

The NNLO scattering amplitudes can indeed be described in terms of only six parameters b_{1-6} that multiply each of the energy dependent polynomials allowed by Lorentz invariance and chiral symmetry [79]. However, these b_i parameters carry an implicit dependence on M_π, so that the knowledge of all the l_i and r_i constants will be needed when extrapolating to unphysical values of M_π. The expressions that relate the b_i parameters to the l_i and r_i constants can be found in the Appendix B of [79]. In Table 1.3 we present the sets IV, 3 and 4 translated into b_i's.

$SU(3)$ low energy constants

Let us now consider the $SU(3)$ parameters. To one-loop eight of them contribute to the scattering amplitudes. We have not used the $SU(3)$ two-loop amplitudes

Set	$\bar{b}_1^r$	$\bar{b}_2^r$	$\bar{b}_3^r$	$\bar{b}_4^r$	$\bar{b}_5^r$	$\bar{b}_6^r$
Set IV [89]	-8.0 ± 2.1	10.0 ± 1.0	3.6 ± 3.6	3.7 ± 3.1	3.5 ± 2.1	2.4 ± 0.2
Set 3 [98]	-9.3	11.4	3.3	3.7	2.4	-0.4
Set 4 [98]	-8.1	10.1	3.6	3.6	4.3	-1.4

Table 1.3: $\bar{b}_i$ parameters evaluated at $\mu = 770$ MeV. They are normalized in order to be of order unity: $\bar{b}_i = N\, b_i$ for $i = 1, .., 4$ with $N = 16\pi^2$ and $\bar{b}_i = N^2\, b_i$ for $i = 5, 6$. The sets are labeled after the l_i and r_i sets from which they have been calculated.

in our works because they depend on so many parameters that they lack of any predictive power.

In table 1.4 we present the sets of $SU(3)$ LECs used in this thesis. We divide them, as before, in three groups:

- The first group corresponds to standard ChPT determinations. Sets II and III come from an analysis of the K_{l4} data using $SU(3)$ ChPT at $\mathcal{O}(p^4)$ [88] and $\mathcal{O}(p^6)$ [88]. Sets II and III in the preceding sections are nothing but the $SU(2)$ LECs recast from these $SU(3)$ sets and thus we use the same label. Set VI comes from a πK dispersive analysis using the Roy-Steiner formalism [87].

- In the second part of the table we present the results of the lattice study MILC 09A, which uses $SU(3)$ NLO fits [100]. We have chosen this one because of its small errors and because the quality of their analysis is good according to the FLAG review [91].

- In the third part of the table we present the IAM sets 5 and 6. They were obtained for the publication 2.1.2 ([101]), which makes part of this thesis, by fitting to experimental data in the elastic region, as well as lattice results on M_π, M_K, f_π, f_K and scattering lenghts [102, 103, 104, 105] within an elastic IAM approach.

LECs	Set II [88]	Set III [88]	Set VI [87]	MILC 09A [100]	**Set 5 [101]**	**Set 6 [101]**
$10^3\, L_1^r$	0.53 ± 0.25	0.46	1.05 ± 0.12	-	**0.64**	**1.10**
$10^3\, L_2^r$	0.71 ± 0.27	1.49	1.32 ± 0.03	-	**1.03**	**1.11**
$10^3\, L_3$	-2.72±1.12	-3.18	-4.53 ± 0.14	-	**-2.83**	**-4.02**
$10^3\, L_4^r$	0 (fixed)	0 (fixed)	0.53 ± 0.39	0.04(13)(4)	**0.00**	**-0.06**
$10^3\, L_5^r$	0.91 ± 0.15	1.46	3.19 ± 2.40	0.84(12)(36)	**1.26**	**1.35**
$10^3\, L_6^r$	0 (fixed)	0 (fixed)	-	0.07(10)(3)	**-0.01**	**0.15**
$10^3\, L_7$	-0.32± 0.15	-0.49	-	-	**-0.49**	**-0.44**
$10^3\, L_8^r$	0.62± 0.20	1.00	-	0.36(5)(7)	**1.06**	**0.95**

Table 1.4: $O(p^4)$ chiral parameters ($\times 10^3$) evaluated at $\mu = 770$ MeV. The roman-numbered sets are standard ChPT determinations. The reason why we repeat here the labels II and III is because these are the $SU(3)$ sets from which the $SU(2)$ sets II and III in table 1.1 were recast. The MILC 09A set comes from a lattice analysis [100]. The arabic-numbered sets are IAM determinations and they are highlighted in boldface because they have been obtained for the publication 2.1.2 ([101]), which is part of this thesis.

For the sake of completeness, we also provide in table 1.5 the three sets of LECs that we use in section 2.1.4 to estimate the errors on the calculation of the resonance derivatives using an alternative unitarization method:

- Sets a, b and c were obtained by fitting to the meson-meson scattering phase shifts within a coupled-channel Chiral Unitary approach [18, 21, 84]. The hat is used to differentiate them from those obtained within standard ChPT. The Chiral Unitary amplitudes depend on a cut-off and the LECs are not renormalized, but their value is expected to be similar to the standard ones once the renormalization scale is chosen appropriately, at roughly $\mu \sim 1.2 q_{\rm max}$ (see ref. [21]).

LECs	$10^3\,\hat{L}_1$	$10^3\,\hat{L}_2$	$10^3\,\hat{L}_3$	$10^3\,\hat{L}_4$	$10^3\,\hat{L}_5$	$10^3\,\hat{L}_7$	$10^3\,(2\hat{L}_6+\hat{L}_8)$	$q_{\rm max}$ (MeV)
Set a	0.91	1.61	-3.65	-0.25	1.07	-0.4	0.58	666
Set b	0.91	1.61	-3.65	-0.25	1.07	0.05	0.58	751
Set c	0.88	1.54	-3.66	-0.27	1.09	0.10	0.68	673

Table 1.5: $SU(3)$ parameters from fits within the Chiral Unitary approach [84]. As explained in the text, the Chiral Unitary amplitudes depend on a cut-off, $q_{\rm max}$. We write these LECs, which are not renormalized, with a hat to differentiate them from the standard ChPT LECs.

1.4 Poles and resonances

As we commented before, the unitarization of the ChPT amplitudes generates poles in the complex plane that can be related to resonances. In the same way that a stable particle corresponds to a pole in the partial wave amplitude in the real axis below threshold, resonances are associated to poles in the analytic continuation of the amplitudes to the complex plane, always on unphysical sheets.

The physical sheet is the one which is continuous with the scattering amplitude in the physical region of s when we approach the real axis from above. We can then define an unphysical Riemann sheet continuous with the physical one along the cut. Since poles can only appear in unphysical sheets, a resonant shape in our amplitudes will be associated to a pole in the lower half of the unphysical sheet. Moreover, every pole will have a conjugate partner in the upper half of the unphysical sheet, due to the Schwartz reflection principle, which will be introduced in the next section. We can define the mass M and width Γ of the associate resonance, with propagator $\sim \frac{1}{s-(M-i\Gamma/2)^2}$, attending to the position of these poles. A natural definition is $\sqrt{s_{\rm pole}} = M - i\Gamma/2$. For a pedagogical introduction see [80].

Therefore, if we extend the IAM amplitudes to the complex plane, we can look for poles which will help us to determine the properties of the corresponding resonances. This analytic continuation is well justified for the elastic IAM, since it has been derived from a dispersion relation [30].

Analytic continuation of single-channel scattering amplitudes

Let us remember that the analytic continuation of $S(s)$ to the complex plane is the function $S(z)$, $z \in \mathbb{C}$, that matches $S(s)$, $s \in \mathbb{R}$, when we approach the real axis from the upper half plane. Such function presents right cuts from the thresholds to infinity and left cuts from $s = 4(M_\alpha^2 - M_\beta^2)$ to $-\infty$, with M_α and M_β the masses of the two NGB and $M_\alpha > M_\beta$. In addition, poles can be found between the origin and the first threshold, as explained in the preceding section, as well as circular cuts stemming from the kinematics of the process. In the processes that we will study these latter cuts are numerically negligible. The function $S(z)$ is analytic in the rest of the complex plane.

For the cases of interest in this thesis, there are no poles associated to bound states, and we are only concerned with poles associated to resonances, which can only appear in the second Riemann sheet. The analytic continuation of $S(s)$ to the lower half of the complex plane in the second Riemann sheet, $S^{II}(z)$, is defined such that it is continuous with $S(s)$ in the real axis above threshold, $S(s + i\epsilon) = S^{II}(s - i\epsilon)$. Equivalently, for the elastic scattering amplitude we have

$$t(s + i\epsilon) = t^{II}(s - i\epsilon), \tag{1.50}$$

which, together with the Schwartz reflection principle

$$t(z) = t^\dagger(z^*) = t^*(z^*), \tag{1.51}$$

yields

$$t^{II}(s + i\epsilon) = t^*(s + i\epsilon). \tag{1.52}$$

Taking into account the unitarity condition

$$\operatorname{Im} t(s) = \frac{t(s) - t^*(s)}{2i} = \sigma(s)\, t(s) t^*(s), \tag{1.53}$$

we can finally write

$$t^{II}(z) = \frac{1}{1 + 2i\sigma(z)\, t(z)} t(z). \tag{1.54}$$

We will make extensive use of these equations in sections 2.1.2, 2.1.3 and 2.2.3, where we will study the poles associated to the lightest elastic resonances, which are presented in the next section.

1.5 Spectroscopic classification of the lightest mesons

In section 1.1.1 we saw that, if we consider only the two or three lightest quarks, the QCD symmetry $SU(N_f)_R \times SU(N_f)_L$ is spontaneously and explicitly broken to $SU(N_f)_V$. If we consider $N_f = 3$, the $SU(3)_V$ symmetry, or flavor symmetry, $SU(3)_F$, is also broken due to the fact that the strange quark is much heavier than the up and down quarks. This is the reason why the masses of the NGB are so different depending on their quark content.

However, we should still be able to classify the resonances into $SU(3)_F$ multiplets: resonances without strangeness would be almost degenerate and there would be a mass increment of about 150-300 MeV for each additional strange valence quark or antiquark in the meson composition. This is the case for the pseudoscalars and the vector mesons, which are easily classified into the $8 \oplus 1$ multiplets $J^{PC} = 0^{-+}$ and 1^{--}, respectively, if they are assumed to be $\bar{q}q$ states. These nonets are depicted in panels (a) and (b) of figure 1.2 and the properties of the resonances that make them up are listed in table 1.6.

On the other hand, whether the lightest scalar resonances, namely the $a_0(980)$, the $K_0^*(800)$ or κ, the $f_0(600)$ or σ and the $f_0(800)$, form a nonet is still not clear (see "Note on Scalar Mesons" in [31]). If considered as $\bar{q}q$ states [32, 33, 34, 35], they do not satisfy the mass hierarchy, as can be seen in Table 1.6. However, the mass

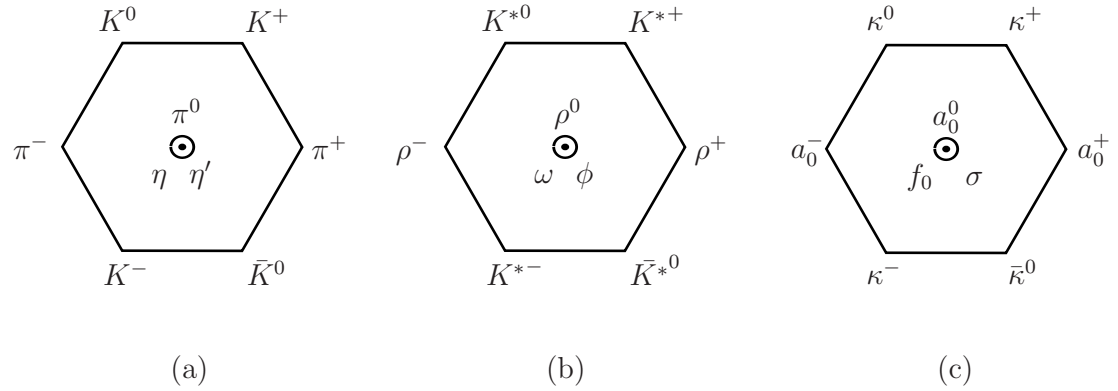

Figure 1.2: Panel (a): pseudoscalar-meson nonet $J^{PC} = 0^{-+}$. Panel (c): vector-meson nonet $J^{PC} = 1^{--}$. Panel (c): scalar-meson nonet $J^{PC} = 0^{++}$.

J^{PC}	I=1	I=1/2	I=0
0^{-+}	$\pi(140)$	$K(496)$	$\eta(548)$, $\eta'(958)$
1^{--}	$\rho(770)$	$K^*(892)$	$\phi(1020)$, $\omega(782)$
0^{++}	$a_0(980)$	$K_0^*(800)$	$f_0(980)$, $f_0(600)$

Table 1.6: Lightest resonances and their approximate masses (see the particle listings in [31] for a detailed account of their properties).

ordering can indeed be explained assuming a tetraquark nature [36, 37, 38, 39, 40]. Other non-ordinary compositions can be attributed to them: they could be meson-meson states [41, 42, 43, 44], hybrids [45] or, in the scalar-isoscalar channel, we could have the lightest glueball [45, 46], whose mass is expected around 1.6 GeV. Most probably, the scalar resonances below $\sim$1 GeV are a mixture of all these possible states. For general reviews on this issue see [106, 45, 107].

Their classification into multiplets is also complicated by the presence of another group of scalar resonances above 1 GeV: the $a_0(1450)$, $K_0^*(1430)$, $f_0(1370)$, $f_0(1500)$ and $f_0(1710)$. In the picture that is emerging over the last years, the scalars below 1 GeV would form a nonet of non-ordinary states, shown in panel (c) of Fig. 1.2, and the others would correspond to an ordinary nonet and a glueball, with an important mixture between the f_0 states above 1 GeV (see "Note on Scalar Mesons" in [31]

and references therein). In particular, it has been shown within the Chiral Unitary approach [21, 18] that the resonances below 1 GeV form an octet and a singlet when the quark masses are degenerated [47].

The main part of this thesis is devoted to the study of the properties of the resonances below 1 GeV, with the aim of throwing some light into the still unclear nature of the light scalars. The simultaneous study of the well-known vector resonances serves as a benchmark for the different methods used.

1.6 The $1/N_c$ expansion

As explained before, QCD does not have any obvious free parameter that could be used as an expansion parameter in the low energy regime. However, as 't Hooft pointed out [65], we can generalize QCD from a $SU(3)$ gauge group to a $SU(N_c)$ gauge group with N_c colors, in the hope that the theory gets simplified in the large N_c limit, so that it can be systematically expanded in $1/N_c$. It is indeed the case: at $N_c = \infty$ mesons are pure $\bar{q}q$ states and, together with glueballs, are free, stable and non-interacting.

In section 2.2 we will make use of these ideas in order to study the nature of the lightest resonances through their leading behavior close to $N_c = 3$. The basic concepts needed to understand the $1/N_c$ expansion of $\bar{q}q$ and glueball states and how it is implemented in ChPT are introduced next. Further details can be found in [66, 108].

1.6.1 N_c counting rules for Feynman diagrams

At large N_c, the sum over the many intermediate states gives rise to large combinatoric factors. The gluon field is a traceless $N_c \times N_c$ matrix $A^i_{\mu j}$ and thus has $N_c^2 - 1$ components, while the quark and antiquark fields, q^i and $\bar{q}_i$, are vectors of N_c components.

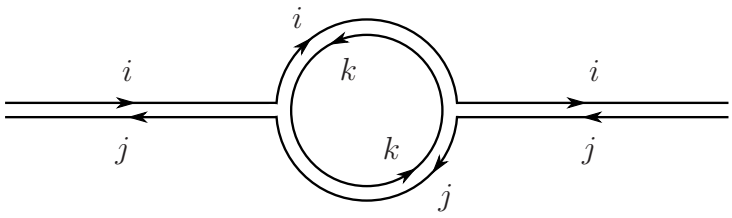

Figure 1.3: Gluon propagator in the double-line notation.

Let us use a very helpful diagrammatic technique introduced by 't Hooft [65]. Since the gluon field, as written above, has one upper index like the quark and one lower index like the antiquark, from the point of view of the symmetry transformations the gluon can be though of as a quark-antiquark combination. In a Feynman diagram we will then represent quarks and antiquarks as a single line with an arrow whose direction distinguishes them, as usual, and the gluons as a double line made up from a quark line and an antiquark one.

In this double-line notation, the one-loop gluon vacuum polarization is drawn as shown in figure 1.3. In the diagram, the color index of the lines at the edge of the loop are contracted with those of the final and initial states, so that their quantum numbers i and j are fixed once the initial and final states are specified. However, the color k of the internal closed line is unspecified, giving a combinatoric factor of N_c when we sum over k. The other dependence of the diagram on the number of colors comes from the two interaction vertices. From the integration of the renormalization group equation for the β function to one loop,

$$\alpha_s(q^2) = \frac{48\pi^2}{(11\,N_c - 2\,N_f)\log(q^2/\Lambda^2_{QCD})}, \tag{1.55}$$

where $\alpha_s = g_s^2/4\pi$, we see that the coupling constant scales as $1/\sqrt{N_c}$. The diagram in figure 1.3 is then of order $(1/\sqrt{N_c})^2 N_c = 1$. Similarly, in order to obtain the leading scaling of any diagram, one must keep track of the contributions from vertices and closed loops.

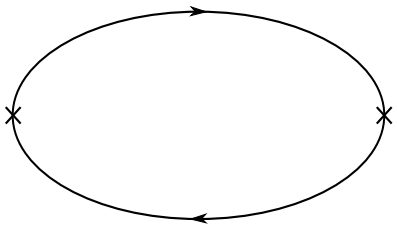

Figure 1.4: Propagator of a $\bar{q}q$ state. The crosses indicate the $\bar{q}q$ states, which are normalized with $1/\sqrt{N_c}$ each. The closed quark line contributes with a combinatoric factor of N_c and, hence, the diagram is $\mathcal{O}(1)$.

Let us introduce now the concept of *planar* diagrams. We say that a diagram is planar when it can be drawn on the plane without line crossings at points where there are no interaction vertices. It turns out that the leading diagrams for large N_c are the planar diagrams with a minimum number of quark loops. Each quark loop suppresses a diagram by a factor of $1/N_c$, whereas adding internal gluon lines does not change the order. If quark loops must be present, the dominant diagram will be the one with the quark lines at the edge [65]. These statements will be illustrated with some examples in the next section, where we will study the leading $1/N_c$ behavior of $\bar{q}q$ and glueball states.

1.6.2 Leading $1/N_c$ behavior of $\bar{q}q$ and glueball states

We will discuss $\bar{q}q$ and glueball states by considering matrix elements of operators that have the appropriate quantum numbers. Let us start with the $\bar{q}q$ states. They are created by quark bilinears $J(x)$, such as the scalar $\bar{q}q$ or the pseudoscalar $\bar{q}\gamma^\mu q$, acting on the vacuum. Assuming that confinement persists at large N_c, it can be shown that $J(x)$ acting on the vacuum creates only one-meson states. Since we must sum over the N_c colors in order to form a color singlet $\bar{q}q$ state, we must introduce a $1/\sqrt{N_c}$ factor in the meson wave function to normalize it properly.

The simplest diagram for the $\bar{q}q$ propagator is depicted in figure 1.4. It has a factor of N_c from the quark loop and a factor of $(1/\sqrt{N_c})^2$ from the normalization of the initial and final meson states. It is then independent of N_c. Having in

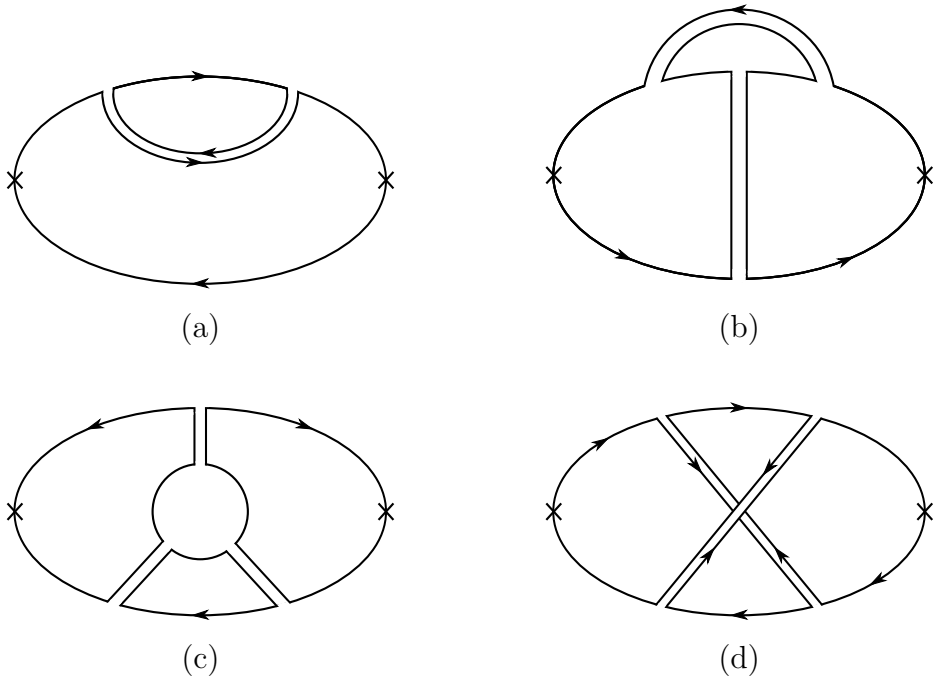

Figure 1.5: Some examples of diagrams contributing to the $\bar{q}q$ propagator: (a) this two-loop correction is of order$(1/\sqrt{N_c})^4 N_c^2 = 1$ (in fact, all the similar diagrams with external quark lines and only internal gluon lines will have the same behavior); (b) this three-loop correction illustrates how a gluon line at the edge of the diagram suppreses it by a factor $1/N_c$; (c) similarly, an internal quark loop also suppreses the diagram by a factor $1/N_c$; (d) this diagram is an example of non-planar diagram and is of order $\mathcal{O}(1/N_c^2)$. These and other diagrams are explained in detail in [66].

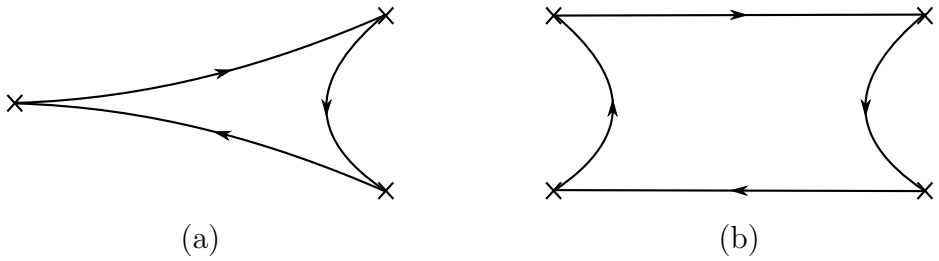

Figure 1.6: Leading diagrams for: (a) the decay of a $\bar{q}q$ state into two $\bar{q}q$ states, of order $\mathcal{O}(1/\sqrt{N_c})$; (b) the scattering of two $\bar{q}q$ states, of order $\mathcal{O}(1/N_c)$.

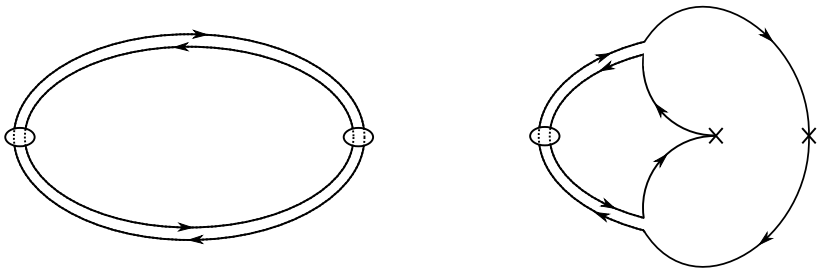

(a) (b)

Figure 1.7: Panel (a): glueball propagator. Panel (b): glueball decay to two $\bar{q}q$ states.

mind the selection rules stated in the previous section, it can be shown that other possible contributions to the $\bar{q}q$ propagator have the same leading behavior or are subdominant in $1/N_c$ [65]. In figure 1.5 we show some examples of possible corrections, which are at most $\mathcal{O}(1)$.

Thus, the propagator of a $\bar{q}q$ state and, hence, its mass, behave as $\mathcal{O}(1)$. Likewise, the leading diagrams of the decay of a $\bar{q}q$ meson into two $\bar{q}q$ mesons and the scattering of two of these states are those shown in Fig. 1.6, whose order is $\mathcal{O}(1/\sqrt{N_c})$ and $\mathcal{O}(1/N_c)$, respectively.

Regarding the glueballs, the simplest color-singlet gluonic state is created by two gluon fields and thus the normalization of its wave function involves a sum over two color indices. Consequently, it carries a normalization factor of $1/N_c$.

The leading diagram for the glueball propagator, depicted in panel (a) of figure 1.7, is therefore $\mathcal{O}(1)$ because it has two of these normalization factors and two color loops. The leading diagram for the decay of a glueball into two mesons is displayed in panel (b) of the same figure. It has two color loops, one normalization factor from the glueball state, two from the $\bar{q}q$ states, and two vertices. Thus it is of order $N_c^2(1/N_c)(1/\sqrt{N_c})^2(1/\sqrt{N_c})^2 = \mathcal{O}(1/N_c)$. Glueballs can also decay to other glueballs when kinematically allowed. Nevertheless, in our work we will only consider the lightest glueball, which can only decay into $\bar{q}q$ states.

1.6.3 The $1/N_c$ expansion in ChPT

In Chiral Perturbation Theory, the dependence on the number of colors is carried by the chiral parameters. The only parameters contributing at tree level are the masses and decay constants of the NGB. Since, for counting issues, the NGB can be considered as $\bar{q}q$ states, their mass must scale as $\mathcal{O}(1)$ [5]. The scaling of their decay constant can be inferred from its relation with the matrix element of the axial current, given in (1.13), namely, $\langle 0|A_a^\mu|\pi_b\rangle = ip^\mu F\delta_{ab}$. The axial current introduces a factor of N_c due to the sum over color indices and the normalization of the meson state introduces a factor of $1/\sqrt{N_c}$, which implies that F scales as $\sqrt{N_c}$.

At higher orders, the N_c dependence of the low energy constants can be derived by observing the structure of the term they multiply [5]. If we consider the NLO $SU(3)$ Lagrangian 1.16, we have terms with one trace and others with two traces. Since traces are taken over flavor indices, each of them amounts to a sum over quark flavors, which takes place in a quark loop. Thus, terms with two flavor traces are suppressed relative to those with one trace by a power of $1/N_c$. On the other hand, taking into account that scattering amplitudes are $\mathcal{O}(1/N_c)$, as stated in the previous section, and that contributions to them from the NLO Lagrangian go as $\sim L_i/F^4$, the terms with only one trace should have $L_i \sim \mathcal{O}(N_c)$, whereas those with two traces will have $L_i \sim \mathcal{O}(1)$.

There is one subtlety that has to be taken into account. The operator

$$\langle \partial_\mu U^\dagger \partial_\nu U \partial^\mu U^\dagger \partial^\nu U\rangle \tag{1.56}$$

does not appear in the $O(p^4)$ Lagrangian because for $N_f = 3$ it is expressible as a linear combination of the terms multiplied by L_1, L_2 and L_3. However, for a larger number of flavors this relation does no longer hold and we have to append this term to the Lagrangian, multiplied by a constant c. Moreover, having a single trace, this term is dominant and so c is $\mathcal{O}(N_c)$. When we go back to three flavors, the low energy constants L_{1-3} receive a contribution from c:

$$L_1' = L_1 + \frac{c}{2}, \quad L_2' = L_2 + c, \quad L_3' = L_3 + c. \tag{1.57}$$

Thus, although L_1 and L_2 where expected to be suppressed, they are also of order $\mathcal{O}(N_c)$, while $2L_1 - L_2$ remains of order unity.

Another subtlety concerns the L_7. In [5] it was considered to be of $\mathcal{O}(N_c^2)$ due to the contribution from the η', which is integrated out of the Lagrangian. However, in the $N_c \to \infty$ limit, the η' becomes a Goldstone boson, and thus it is inconsistent to integrate it out. This inconsistency was solved in [109] by enlarging the chiral $SU(3)$ group to chiral $U(3)$. In the chiral U(3) effective Lagrangian there is an $\mathcal{O}(p^4)$ L_7-like term, which is at most of $\mathcal{O}(N_c)$ at large N_c. Nevertheless, the role of the η' is irrelevant as long as N_c is kept below ~ 20, which is always the case in our works.

Summarizing:

$$\begin{aligned} L_1,\, L_2,\, L_3,\, L_5,\, L_8 \quad & \text{are of order } \mathcal{O}(N_c) \\ 2L_1 - L_2,\, L_4,\, L_6,\, L_7 \quad & \text{are of order } \mathcal{O}(1). \end{aligned} \tag{1.58}$$

Similarly, one can derive the N_c behavior of the low energy constants in the $SU(2)$ Lagrangian: the one-loop constants l_{1-4} are of order $\mathcal{O}(N_c)$ and the two-loop constants r_{1-6} are $\mathcal{O}(N_c^2)$.

Once that we know the N_c behavior of the ChPT scattering amplitudes, we can study the physical scenario $N_c = 3$, as well as vary the number of colors. Moreover, we can implement the N_c scaling in unitarized ChPT in order to study the behavior of the light resonances. Our works on this issue [110, 111] are presented in section 2.2.

Chapter 2

Results

In this chapter I present the main results of this thesis, divided into two sections. Section 2.1 encloses our works on the quark mass dependence of phase shifts and resonances, and section 2.2 is dedicated to our studies on the nature of resonances from their $1/N_c$ behavior.

2.1 Quark mass dependence of the ChPT amplitudes

As we have seen in the introduction, the ChPT amplitudes depend explicitly on the quark masses, which brings us the possibility to study the effect of changing these masses to unphysical values. This kind of study is relevant for lattice calculations, as we will see next, but also for anthropic considerations [49, 50, 51] and the study of the cosmological variability of fundamental constants [52, 53, 54]. In this section, I review our work based on the dependence of the standard and unitarized ChPT amplitudes on the quark masses. It consists of two publications 2.1.2 and 2.1.3, and some recent results 2.1.4 which have not been published yet and are presented here for the first time.

2.1.1 Summary and discussion of results

One of the main objectives of the extrapolation of the ChPT amplitudes to unphysical quark masses, also known as 'chiral extrapolation', is to rise the quark masses in order to compare with lattice results.

Lattice QCD can provide, in principle, a rigorous way to calculate non-perturbative quantities from QCD, such as the spectrum of the lightest meson resonances. However, implementing the light u and d quark masses has a big computational cost, and current calculations are done with unphysical heavy masses. Nevertheless, recent developments in lattice algorithms are allowing a great progress on the treatment of many technical complications, such as the implementation of chiral symmetry or the existence of quarkline disconnected diagrams, that have for long hindered calculations in the mesonic sector, in particular, those involving the isoscalar channels. Very recently, lattice results have become available for the $\rho(770)$ and $f_0(600)$, resonance masses [112, 113, 114, 115, 116], the pion decay constant and even for some pion-pion scattering lengths [103, 117] and phase shifts [62, 63, 64].

On the side of the Inverse Amplitude Method, the quark mass dependence of the subtraction constants and the left cut of the dispersion relation from which it is derived is correctly predicted by ChPT. Thus, we can study the dependence of both the standard and unitarized scattering phase-shifts at higher energies and the resonances generated, which is interesting to serve as a guide to lattice studies. This is the aim of publications 2.1.2 and 2.1.3.

Publication 2.1.2 is a generalization to $SU(3)$ of a recent study [97] performed within $SU(2)$. In [97], the $SU(2)$ elastic ChPT amplitudes unitarized with the IAM were used to calculate the dependence of the $\rho(770)$ and $f_0(600)$, or σ, resonances on the pion mass, or equivalently on the averaged u and d quark mass, $\hat{m}$. In publication 2.1.2, we include the strange quark within an $SU(3)$ ChPT formalism, so that we can generate the $K^*(892)$ and $K_0^*(800)$, or κ, resonances and study the dependence on both the light and the strange quark masses. Let us remark that the $K_0^*(800)$ resonance, despite being a scalar and very similar to the $f_0(600)$, is

more feasible for lattice calculations [118, 119] because of its non-zero isospin and strangeness.

We restrict ourselves to the elastic resonances because the one-channel IAM is exclusively derived from elastic unitarity, analyticity in the form of a dispersion relation, and ChPT, which is only used at low energies, and does not depend on any spurious parameter that could hide an unknown quark mass dependence.

The main results of publication 2.1.2 are the following:

Dependence on the light quark mass

- Previous determinations of the low energy constants come from fitting only to experiment [85, 86], and therefore are mostly sensitive to the LECs that govern the s dependence of partial waves. In order to get better determinations of the LECs that multiply terms with an explicit meson mass dependence, in this work we have performed some new fits including lattice results on M_π, M_K, f_π, f_K and scattering lenghts [102, 103, 104, 105].

- The results on the $\rho(770)$ and σ dependence on M_π are very consistent with those found in $SU(2)$ [97] and the estimations for the two first coefficients of the M_ρ chiral expansion [120].

- Both vector resonances, $\rho(770)$ and $K^*(892)$, behave very similarly: their masses increase smoothly, but much slower than M_π. As a consequence there is a strong phase space suppression which accounts by itself for the width decrease, without a dynamical effect through the couplings $g_{\rho\pi\pi}$ and $g_{K^*\pi K}$, that are remarkably constant, which confirms an assumption made in lattice studies of the $\rho(770)$ width [121].

- For the vectors we find that the Kawarabayashi-Suzuki-Riazuddin-Fayyazuddin (KSRF) relation [122, 123], which approximates their couplings to two mesons by $g \approx M_V/(2\sqrt{2}f_\pi)$, holds to less than 5% when changing the light quark mass from 0 to 9 times its physical value.

- The scalars σ and κ behave very differently to the vectors. The most prominent feature is the splitting of their masses into two branches. This happens when the associated pair of conjugated poles in the second Riemann sheet, which are approaching each other as the quark mass increases, join in a single pole below threshold to split again and remain in the real axis.
- The growth of the σ mass before the 'splitting point' is much faster than that of the κ.
- Their width decrease cannot be attributed to the phase space reduction because their coupling to two mesons is shown to depend strongly on the quark mass.

Dependence on the strange quark mass

- As it could be expected, we find that the properties of the $\rho(770)$ and σ non-strange resonances are almost independent of the strange quark mass within the range of study.
- The $K^*(892)$ and the κ show a strong m_s dependence. As the strange quark is made heavier, their masses grow much faster than they did when increasing the light quark mass, but much slower than the kaon mass.
- In the case of the vector resonance $K^*(892)$, the width decreases almost exactly as it would be expected from phase space suppression only, and its coupling to $K\pi$ is almost constant. In contrast, the width decrease of the scalar κ deviates significantly from that behavior, in agreement with the fact that its coupling to $K\pi$ depends quite strongly on the strange quark mass.
- The KSRF relation is also a fairly good approximation in the whole m_s range, although not as good as in the case of the non-strange quark mass variation.

In publication 2.1.3 we study the chiral extrapolation of the phase-shifts in elastic pion-pion scattering, using both standard and unitarized ChPT to one and two loops. In the standard ChPT approach, which is completely model independent

but is limited to low momenta, we study the S, P and D waves. Unitarization with the elastic IAM extends the analysis to energies of around 1 GeV, being compatible with standard ChPT at low energies for the S and P waves. We have also performed a Montecarlo analysis to provide an estimation of the uncertainties. Finally, we have increased the pion mass up to higher values and we have compared our results to those of lattice QCD. From this work we obtain the following results:

- Using standard ChPT we find that the dependence of the phase shifts on M_π is very soft at one loop and somewhat stronger at two loops, specially for the I=2, J=2 channel.
- Within unitarized ChPT we find that the dependence on the pion mass is again quite soft, specially for the I=2, J=0 channel and stronger at two loops than at one loop.
- In order to compare with lattice results [62, 63, 64] in channels (I,J) = (2,0), (2,2) and (1,1) we go to higher pion masses, up to 444 MeV. The results at such high masses should be considered just qualitatively, since this energy region is above the applicability limit of our method, which was studied in [98]. Standard ChPT shows a good agreement with lattice results below $p \simeq 200$ MeV up to pion masses of 400-450 MeV, while a nice improvement above 200 MeV is found when using unitarized ChPT for the scalar and vector channels.
- We include in this summary a new calculation for the I=1, J=1 phase shift that does not appear in publication 2.1.3. It was presented in the proceedings of a recent conference [96] in order to compare with some lattice results [64] also presented at that conference. In figure 1 we show the $I = J = 1$ phase shift, calculated within standard and unitarized ChPT, to one and two loops, at a pion mass of 266 MeV, compared to the lattice results in [64]. We find a softer dependence of the phase shift on M_π at high momentum than that predicted by the lattice calculations.

In section 2.1.4, which will be part of a future publication [124], we calculate the derivatives of the lightest resonances with respect to the light and strange quark

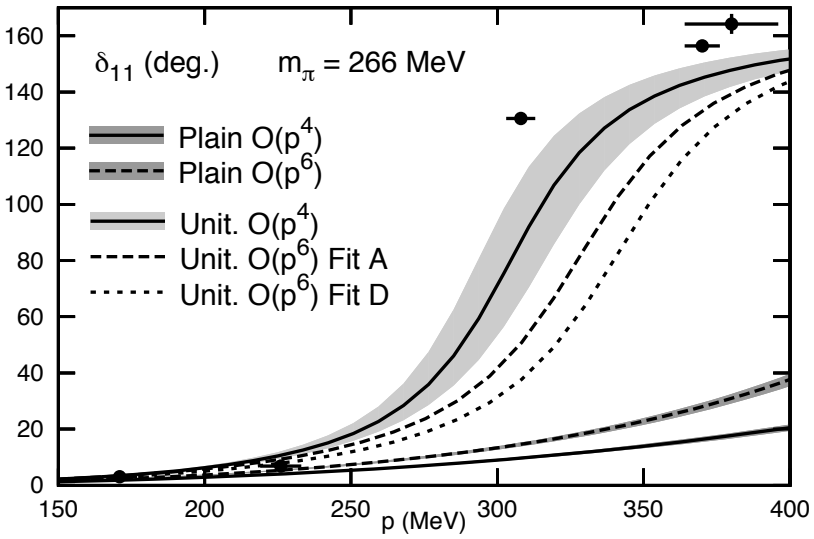

Figure 2.1

masses. Those values are useful for the spectroscopic classification of resonances, but also for the calculation of the variation of nature's fundamental parameters predicted by some models of unification [125, 54].

We find the following results:

- We calculate the adimensional parameters

$$K_R^f = \frac{m_f}{M_R}\frac{\partial M_R}{\partial m_f}$$

  for the pion, kaon, $\rho(770)$, $K^*(892)$, $f_0(600)$ or σ, and $K_0^*(800)$ or κ, resonances.

- For the pion and kaon these parameters are calculated from their ChPT expansions. We find that they are much better determined for the light quarks than for the strange one. The corrections to the leading order calculations are of the same size or smaller than the uncertainty in the higher order results.

- We repeat these calculations with the LECs that will be used for unitarized ChPT and check that the results are compatible with those obtained with the standard ChPT LECs.
- Then, we use the IAM to calculate the K_R^f parameters for the light elastic resonances. In order to estimate the systematic error, we repeat the calculations using the Chiral Unitary Approach [21, 18], which is simpler but does not include the whole mass dependence and has spurious parameters in the form of cutoffs or subtraction constants.
- The results for the scalar resonances are more reliable than those for the vectors because the latter depend strongly on the LECs while the former depend more on chiral loops.
- In particular, we find a small negative value for K_σ^s, in contrast to the estimate used in some studies on the cosmological variation of the fundamental parameters [53], $K_\sigma^s \approx 0.54$. If our result is used instead of theirs, we obtain a somewhat less constraining limit on the magnitude $|\delta(m_s/\Lambda_{\rm QCD})/(m_s/\Lambda_{\rm QCD})|$.

2.1.2 Publication: J. R. Pelaez and J. Nebreda, **Strange and nonstrange quark mass dependence of elastic light resonances from SU(3) unitarized ChPT to one loop,** Phys. Rev. D81, 054035 (2010)

PHYSICAL REVIEW D **81,** 054035 (2010)

Strange and nonstrange quark mass dependence of elastic light resonances from SU(3) unitarized chiral perturbation theory to one loop

J. Nebreda and J. R. Peláez

Departamento de Física Teórica II, Universidad Complutense, 28040 Madrid, Spain

(Received 28 January 2010; published 31 March 2010)

We study the light quark mass dependence of the $f_0(600)$, $\kappa(800)$, $\rho(770)$, and $K^*(892)$ resonance parameters generated from elastic meson-meson scattering using unitarized one-loop chiral perturbation theory. First, we show that it is possible to fit simultaneously all experimental scattering data up to 0.8–1 GeV together with lattice results on decay constants and scattering lengths up to a pion mass of 400 MeV, using chiral parameters compatible with existing determinations. Then, the strange and nonstrange quark masses are varied from the chiral limit up to values of interest for lattice studies. In these amplitudes, the mass and width of the $\rho(770)$ and $K^*(892)$ present a similar and smooth quark mass dependence. In contrast, both scalars present a similar nonanalyticity at high quark masses. Nevertheless, the $f_0(600)$ dependence on the nonstrange quark mass is stronger than for the $\kappa(800)$ and the vectors. We also confirm the lattice assumption of quark mass independence of the vector two-meson coupling that, in contrast, is violated for scalars. As a consequence, vector widths are very well approximated by the Kawarabayashi-Suzuki-Riazuddin-Fayyazuddin relation, and their masses are shown to scale like their corresponding meson decay constants.

DOI: 10.1103/PhysRevD.81.054035 PACS numbers: 14.40.−n, 12.39.Fe, 13.75.Lb

I. INTRODUCTION

Although QCD is well established as the theory of strong interactions, the fact that its coupling becomes large at energies below 1–2 GeV keeps the hadronic realm beyond the reach of perturbative calculations. In that regime, lattice methods are a useful tool to calculate QCD observables, although the discretization involved in this technique introduces complications of its own, in particular, related to chiral symmetry breaking and the implementation of realistic small masses for the light quarks. Despite the remarkable success of lattice studies, results on light meson resonances are few and usually obtained at very large quark masses compared with their physical values [1,2]. This is particularly so for the light scalars, very relevant for nuclear attraction, but whose calculations are hindered by the so-called ''disconnected diagrams.'' Very recently [3], an alternative technique, based on chiral perturbation theory (ChPT) and dispersion relations, has been applied to calculate the dependence of the $f_0(600)$ (or ''sigma'') and $\rho(770)$ resonances on the pion mass—in practice, the average mass of the u and d quarks. Now the starting parameters are physical and resonances appear in amplitudes that describe real data on $\pi\pi$ scattering. The predicted dependence for the $\rho(770)$ compares remarkably well with previous and later lattice predictions. For the scalar sigma it shows a nonanalyticity that should be taken into account when extrapolating future lattice data to physical values. In this work we extend this study to include the strange quark mass within an SU(3) ChPT formalism. Our aim is threefold: first, to confirm previous results within a more general formalism. Second, to analyze the dependence on the average mass of the u and d quarks of the $K^*(892)$ and $\kappa(800)$ strange resonances. The latter, despite being a scalar, and very similar to the $f_0(600)$, is much more feasible for lattice calculations within the next few years [4] due to its nonzero isospin and strangeness. Third, we also study the dependence of all the $f_0(600)$, $\kappa(800)$, $\rho(770)$, and $K^*(892)$ parameters in terms of the strange quark mass. Finally, let us remark that the dependence of hadronic observables, meson masses in particular, is not only of relevance for lattice calculations, but also for anthropic considerations [5] or the study of the cosmological variability of fundamental constants [6].

Thus, in the next two sections we introduce very briefly the basic notation of ChPT, explain the relation between pseudoscalar meson and quark masses, and review the unitarization procedure. In Sec. II, we show the fits to the existing experimental data on elastic scattering as well as to lattice results on pion and kaon masses, their decay constants, and scattering lengths on the highest isospin channels. Section III is devoted to the dependence of light resonance properties on the nonstrange quark masses. In Sec. IV we then study the dependence with the strange quark mass and in Sec. V we present our summary and conclusions.

A. Chiral perturbation theory

As is well known, pions, kaons, and etas can be identified with the Nambu-Goldstone bosons (NGB) of the spontaneous chiral symmetry breaking of QCD. If quarks were massless, so should be the NGB and they would be separated by a mass gap of the order of 1 GeV from other hadrons, thus becoming the only relevant QCD degrees of freedom at low energies. Of course, quarks are not mass-

less, but the u, d, and s flavors have a sufficiently light mass to be considered as a perturbation. It is thus possible to write a low energy effective Lagrangian out of pion, kaon, and eta fields, known as chiral perturbation theory [7]. This Lagrangian is built as the most general derivative and mass expansion that respects the symmetries of QCD, particularly its chiral symmetry breaking pattern. Except for the leading order (LO), fixed by symmetry and the scale of spontaneous symmetry breaking, all terms in the Lagrangian are multiplied by a low energy constant (LEC) that contains the information on the underlying QCD dynamics and also renormalizes the loop diagrams with vertices from lower orders. In this way, pion, kaon, and eta observables are obtained as a *model independent* expansion in powers of momenta and masses over the chiral scale $4\pi f_0 \simeq 1.2$ GeV, where f_0 is the pion decay constant in the chiral limit (as it is customary, for quantities at leading order in the quark mass expansion we will use the 0 subscript).

In particular, partial wave amplitudes for elastic meson-meson scattering are obtained within ChPT as an expansion

$$t(s) = t_2(s) + t_4(s) + \cdots, \qquad t_{2k} = O(p^{2k}), \tag{1}$$

where p denotes either momenta or meson masses. Actually, these partial waves carry definite isospin I and total angular momentum J, but we have momentarily suppressed these labels for clarity. As we have just commented, the leading order $t_2(s)$ corresponds to the current algebra results and only depends on the scale of spontaneous chiral symmetry breaking f_0. The next-to-leading order $t_4(s)$ contains one-loop diagrams made of vertices from the lowest order Lagrangian, plus tree level diagrams of $O(p^4)$. Within the SU(3) formalism, these tree level diagrams are multiplied by LECs, denoted as L_i, which are independent of masses or momenta, and have been determined from different experiments. In Table I we provide several sets for the eight L_i that appear in meson-meson scattering to one loop. Those with an r superscript carry a dependence on the regularization scale μ [7], customarily chosen at $\mu = M_\rho$. Of course, that scale dependence cancels in the calculation of physical observables. The values in the second column come from the ''main fit'' of a K_{l4} analysis to two loops [8], whereas those in the third column come from the same reference, but to one loop. Naively one would expect the LECs obtained in our unitarized one-loop fits to lie somewhere in between these two sets of values, since unitarization reproduces one of the most relevant numerical contributions from the two-loop calculation, namely, the s-channel leading logs. As one of our main interests is πK scattering and the $K^*(892)$ and $\kappa(800)$ resonances, we also provide the values obtained from a very rigorous treatment of $K\pi$ scattering lengths in terms of the Roy-Steiner dispersion relations [9]. The rest of the columns correspond to unitarized ChPT fits that we will explain in Sec. II.

In this work, we are interested in the quark mass dependence of the amplitudes, which appears in ChPT through Lagrangian terms that contain the quark mass matrix $\mathcal{M} = \mathrm{diag}(\hat{m}, \hat{m}, m_s)$, that is treated as a perturbation. Note that we work in the isospin limit $\hat{m} \sim m_u = m_d = (m_u^{\mathrm{phys}} + m_d^{\mathrm{phys}})/2$. Chiral symmetry is explicitly broken by these mass terms and the NGB acquire masses, which, at leading order, read [7]

$$M_{0\pi}^2 = 2\hat{m}B_0, \qquad M_{0K}^2 = (\hat{m} + m_s)B_0, \qquad M_{0\eta}^2 = \frac{2}{3}(\hat{m} + 2m_s)B_0. \tag{2}$$

Let us recall that the constant B_0 is defined from the values *in the chiral limit* of the chiral condensate and the pion decay constant as follows: $B_0 = -\langle 0|\bar{q}q|0\rangle_0/f_0^2$, and thus it carries no quark mass dependence. To one loop, there are some corrections, and the physical meson masses now read

TABLE I. $O(p^4)$ chiral parameters ($\times 10^3$) evaluated at $\mu = M_\rho$. The second and third columns come from the two- and one-loop analysis listed in [8], where L_4 and L_6 were set equal to zero. The fourth column comes from a careful πK dispersive analysis [9] using the Roy-Steiner formalism. The IAM III column is one of the sets obtained from an older fit with the coupled channel IAM [10] (only statistical uncertainties are shown). The columns labeled Fit I and Fit II correspond to the simultaneous fit to experiment and lattice data performed in this work, which are described in Sec. II together with their uncertainties.

LECs	Ref. [8] $O(p^6)$	Ref. [8] $O(p^4)$	Ref. [9]	IAM III	Fit I	Fit II
L_1^r	0.53 ± 0.25	0.46	1.05 ± 0.12	0.6 ± 0.09	1.10	0.74
L_2^r	0.71 ± 0.27	1.49	1.32 ± 0.03	1.22 ± 0.08	1.11	1.04
L_3	-2.72 ± 1.12	-3.18	-4.53 ± 0.14	-3.02 ± 0.06	-4.03	-3.12
L_4^r	0 (fixed)	0 (fixed)	0.53 ± 0.39	0 (fixed)	-0.06	0.00
L_5^r	0.91 ± 0.15	1.46	3.19 ± 2.40	1.9 ± 0.03	1.34	1.26
L_6^r	0 (fixed)	0 (fixed)	$\cdots$	-0.07 ± 0.20	0.15	-0.01
L_7	-0.32 ± 0.15	-0.49	$\cdots$	-0.25 ± 0.18	-0.43	-0.49
L_8^r	0.62 ± 0.20	1.00	$\cdots$	0.84 ± 0.23	0.94	1.06
$L_8^r + L_6^r$	0.62 ± 0.20	1.00	3.66 ± 1.52	0.7 ± 0.46	1.24	1.04
$2L_1^r - L_2^r$	0.35 ± 0.57	-0.57	0.78 ± 0.24	-0.02 ± 0.20	1.09	0.44

$$M_\pi^2 = M_{0\pi}^2\Big[1 + \mu_\pi - \frac{\mu_\eta}{3} + \frac{16M_{0K}^2}{f_0^2}(2L_6^r - L_4^r) + \frac{8M_{0\pi}^2}{f_0^2}(2L_6^r + 2L_8^r - L_4^r - L_5^r)\Big], \tag{3}$$

$$M_K^2 = M_{0K}^2\Big[1 + \frac{2\mu_\eta}{3} + \frac{8M_{0\pi}^2}{f_0^2}(2L_6^r - L_4^r) + \frac{8M_{0K}^2}{f_0^2}(4L_6^r + 2L_8^r - 2L_4^r - L_5^r)\Big], \tag{4}$$

$$M_\eta^2 = M_{0\eta}^2\Big[1 + 2\mu_K - \frac{4}{3}\mu_\eta + \frac{8M_{0\eta}^2}{f_0^2}(2L_8^r - L_5^r) + \frac{8}{f_0^2}(2M_{0K}^2 + M_{0\pi}^2)(2L_6^r - L_4^r)\Big] + M_{0\pi}^2\Big[-\mu_\pi + \frac{2}{3}\mu_K + \frac{1}{3}\mu_\eta\Big] + \frac{128}{9f_0^2}(M_{0K}^2 - M_{0\pi}^2)^2(3L_7 + L_8^r),$$

$$\mu_P = \frac{M_{0P}^2}{32\pi^2 f_0^2}\log\frac{M_{0P}^2}{\mu^2}, \qquad P = \pi, K, \eta. \tag{5}$$

Note, however, that all the quark mass dependence always appears through the leading order masses M_{0P}^2 defined in Eq. (2). As a matter of fact, this also happens in the ChPT amplitudes, which means that studying the quark mass dependence, keeping B_0 fixed, is nothing but studying the meson mass dependence. In practice, and in order to get rid of the B_0 constant, we will recast all our results in terms of masses normalized to their physical values:

$$\frac{\hat{m}}{\hat{m}_{\rm phys}} = \frac{M_{0\pi}^2}{M_{0\pi\,\rm phys}^2}, \tag{6}$$

$$\frac{m_s}{m_{s\,\rm phys}} = \frac{M_{0K}^2 - M_{0\pi}^2/2}{M_{0K\,\rm phys}^2 - M_{0\pi\,\rm phys}^2/2}. \tag{7}$$

Note that, from now on, a quantity with a "phys" subscript refers to the value of that quantity in the physical case. Thus, in this work we will change quark masses, that, using Eqs. (3)–(5), imply a change in meson masses, which are the ones appearing explicitly in the ChPT scattering amplitudes. There are many advantages in using meson masses as the variation parameter, since, contrary to quark masses that have a complicated and scale dependent definition on the QCD renormalization scheme, meson masses are observables, with no scale dependence and a straightforward physical interpretation. Actually, many lattice results are also recast in terms of pion or kaon mass variations. Unfortunately the simple relations in Eqs. (6) and (7) are exact only when written in terms of the leading order masses M_{0P}, not the observable ones. Nevertheless, the one-loop corrections become numerically small when taking ratios so that, to a good degree of approximation, the reader still can think in terms of physical meson masses instead of their leading order values. Actually, in Fig. 1 we show that within the range of quark mass variations that we will consider in this work, the naive, but intuitive, relations

$$\frac{\hat{m}}{\hat{m}_{\rm phys}} \simeq \frac{M_\pi^2}{M_{\pi\,\rm phys}^2}, \quad \text{keeping } m_s = m_{s\,\rm phys}, \tag{8}$$

$$\frac{m_s}{m_{s\,\rm phys}} \simeq \frac{M_K^2}{M_{K\,\rm phys}^2}, \quad \text{keeping } \hat{m} = \hat{m}_{\rm phys} \tag{9}$$

are a very good approximation—within less than 10% error—to the correct ratios in Eqs. (6) and (7) that we actually use. To make our presentation of the results more intuitive we will give, when possible, our results both in terms of quark mass variation and the corresponding meson mass variation. At this point we have to address the question of how much we can vary the quark masses before our approach breaks down. First we want the pion

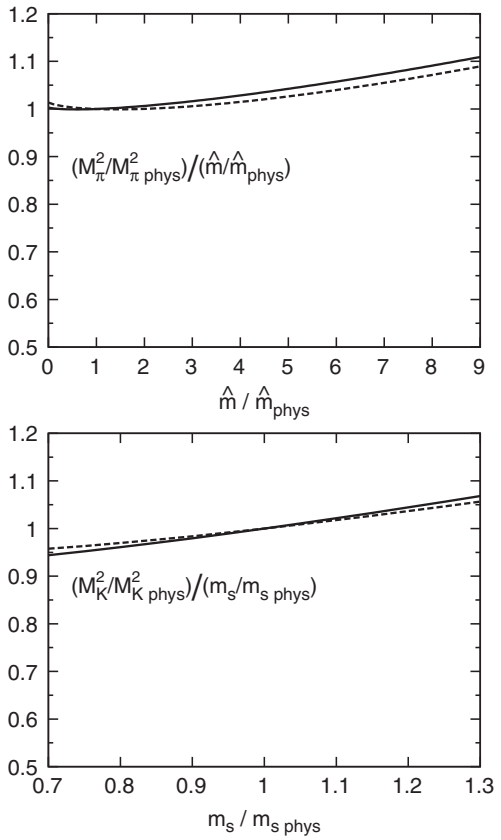

FIG. 1. Top panel: The ratio $(M_\pi^2/M_{\pi\,\rm phys}^2)/(\hat{m}/\hat{m}_{\rm phys})$; bottom panel: $(M_K^2/M_{K\,\rm phys}^2)/(m_s/m_{s\,\rm phys})$. Within the range of variation of this work, a relative variation of a quark mass can be also understood as the same relative variation in the corresponding meson mass squared to within ~10% accuracy. The continuous and dashed lines correspond to fit I and II sets of LECs given in Table I.

always lighter than the kaon and eta since otherwise the elastic approximation would make no sense for $\pi\pi$ or $K\pi$ scattering. Second, ChPT seems to work for masses as high as 500 MeV, since we already know that it provides a fairly good description of low energy $K\pi$ scattering, even though $M_K \sim 500$ MeV. Thus, when changing the nonstrange quark mass, keeping m_s fixed, we will show results up to $M_\pi < 440$ MeV but not beyond, since then $M_K \simeq 600$ MeV. Equivalently, this means $\hat{m}/\hat{m}_{\rm phys} \leq 9$. Concerning the strange quark variation with $\hat{m}$ fixed, we will consider $0.7 < m_s/m_{s\,\rm phys} < 1.3$, since M_π barely changes and 400 MeV $< M_K <$ 585 MeV. This ensures that the $m_K + m_\eta$ is not below the m_{K^*} mass so that we would need a coupled channel formalism. Of course, the closer to the estimated applicability limits the less reliable our formalism will be. The SU(3) $\pi\pi$ and $K\pi$ one-loop amplitudes were first calculated in [11], although for technical reasons explained in [12] needed for the implementation of exact unitarity later on, we use the expressions in the appendix of [12], but written in terms of all physical constants M_π, M_K, M_η, f_π, f_K, f_η as explained in [10]. For completeness we show here the decay constant dependence on meson masses.

$$
\begin{aligned}
f_\pi &= f_0\Big[1 - 2\mu_\pi - \mu_K + \frac{4M_{0\pi}^2}{f_0^2}(L_4^r + L_5^r) + \frac{8M_{0K}^2}{f_0^2}L_4^r\Big],\\
f_K &= f_0\Big[1 - \frac{3\mu_\pi}{4} - \frac{3\mu_K}{2} - \frac{3\mu_\eta}{4} + \frac{4M_{0\pi}^2}{f_0^2}L_4^r\\
&\quad + \frac{4M_{0K}^2}{f_0^2}(2L_4^r + L_5^r)\Big],\\
f_\eta &= f_0\Big[1 - 3\mu_K + \frac{4L_4^r}{f_0^2}(M_{0\pi}^2 + 2M_{0K}^2) + \frac{4M_{0\eta}^2}{f_0^2}L_5^r\Big].
\end{aligned}
\tag{10}
$$

Of course, for $\pi\pi$ and $K\pi$ elastic scattering the most relevant quark mass dependence comes via M_π, M_K and f_π, f_K (since etas only appear in loops). Consequently, the LECs that play the most important role are L_4, L_5, L_6, and L_8, since they appear in Lagrangian terms that contain explicitly powers of the quark mass matrix. In contrast, the Lagrangian terms proportional to the L_1, L_2, and L_3 constants only contain derivatives and thus are somewhat less relevant for the quark mass dependence, but more relevant in terms of s dependence. Finally, let us remark that despite the fact that their effect is encoded in the LECs, the ChPT amplitudes, being an expansion, cannot describe resonances and their associated poles in the second Riemann sheet. Actually, resonances are usually identified with a saturation of the unitarity constraints, which for elastic partial waves of definite isospin I and angular momentum J read

$$
\mathrm{Im}\, t_{IJ}(s) = \sigma(s)|t_{IJ}(s)|^2 \Rightarrow |t_{IJ}(s)| \leq 1/\sigma(s), \tag{11}
$$

where $\sigma(s) = 2k/\sqrt{s}$ and k is the center of mass momentum. The above equations imply that the partial wave can be recast in terms of a single phase or ''phase shift'':

$$
t_{IJ}(s) = \exp i\delta_{IJ}(s) \sin\delta_{IJ}(s)/\sigma(s). \tag{12}
$$

In this work we are only interested in the $(I, J) = (0, 0)$, (1, 1), and (2, 0) channels for $\pi\pi$ scattering and $(I, J) = (1/2, 0)$, $(1/2, 1)$, and $(3/2, 0)$ for πK scattering. For simplicity we will drop the IJ subindex when discussing general properties of elastic partial waves. Note, however, that the ChPT expansion Eq. (1), being basically a polynomial in energy, violates the bound in Eq. (11) as the energy increases and cannot generate poles. Still, ChPT satisfies elastic unitarity perturbatively:

$$
\mathrm{Im}\, t_2(s) = 0, \qquad \mathrm{Im} t_4(s) = \sigma|t_2(s)|^2, \ldots. \tag{13}
$$

But, of course, elastic unitarity can be badly violated if the ChPT series is extrapolated close to a resonance. For these reasons, the resonance region lies beyond the reach of standard ChPT. However, we will see next that ChPT can be used in an alternative way.

B. Dispersion relations, unitarity, and ChPT

Instead of simply extrapolating its series to higher energies, ChPT can be used to calculate the subtraction constants of a dispersion relation for the two-body amplitude. These constants correspond to the values of the amplitude or its derivatives at a low energy point where the use of ChPT is well justified. The remaining information to build the amplitude comes from the strong constraints of analyticity and unitarity.

First of all, it is straightforward to rewrite the strong nonlinear elastic unitarity constraint given in Eq. (11), as follows:

$$
\mathrm{Im}\, 1/t(s) = -\sigma(s). \tag{14}
$$

This means that, from unitarity, we know *exactly* the imaginary part of $1/t$ in the elastic region. We are only left to determine the real part of $1/t$.

Concerning the analyticity constraints, for simplicity let us consider first the case of two identical particles, as in $\pi\pi$ scattering. Then, the analytic structure in the complex s plane is rather simple: it has a ''right'' or ''physical'' cut on the real axis from threshold to $+\infty$, and a ''left'' cut from $-\infty$ to $s = 0$. By means of the Cauchy theorem, a dispersion relation provides the amplitude anywhere inside the cut complex plane in terms of a weighted integral of its imaginary part over the cuts.

In our case, instead of t we are interested in a dispersion relation for $1/t$ since we know exactly its imaginary part in the elastic region thanks to Eq. (14). For convenience, and since t_2 is real, instead of $1/t$ we define $G = t_2^2/t$, that also has a right cut (RC) and a left cut (LC). Since scalar waves are known to have dynamical Adler zeros in the low energy region below threshold, we will also allow for a pole

contribution PC in $G(s)$. All in all, we can write a dispersion relation for $G(s)$ as follows:

$$G(s) = G(0) + G'(0)s + \frac{1}{2}G''(0)s^2 + \frac{s^3}{\pi} \times \int_{RC} ds' \frac{\mathrm{Im}G(s')}{s'^3(s'-s)} + LC(G) + PC. \quad (15)$$

In the elastic region, unitarity in Eq. (11), together with Eq. (13), allows us to evaluate exactly $\mathrm{Im}G = -\sigma t_2^2 = -\mathrm{Im}t_4$ on the RC. Note the three $1/s'$ factors—called subtractions—that we have introduced to suppress the high energy part and, in particular, the inelastic contributions, so that the integrals are dominated by the low energy region. But once the integrals are dominated by the low energy, it is well justified to use ChPT inside the integrals and thus, for instance, the LC integral to one loop ChPT is given by $LC(G) \simeq LC(-t_4) + \cdots$.

The price to pay for the three subtractions is that analyticity only determines the function up to a second order polynomial $G(0) + G'(0)s + \frac{1}{2}G''(0)s^2$. However, note that its coefficients correspond to the values of the amplitude or its derivatives at $s = 0$, where ChPT can be safely applied. In particular, to one loop, $G(0) \simeq t_2(0) - t_4(0)$, $G'(0) \simeq t_2'(0) - t_4'(0)$, and $G''(0) = -t_4''(0)$, since $t_2''(0)$ vanishes. Let us neglect for the moment the pole contribution, which is of higher order and only numerically relevant below threshold. Then one finds that all contributions can be recast in terms of the leading $t_2(s)$ and next-to-leading $t_4(s)$ ChPT amplitudes. Finally, we arrive at the so-called inverse amplitude method (IAM) [13,14]:

$$t(s) \simeq \frac{t_2^2(s)}{t_2(s) - t_4(s)}. \quad (16)$$

Remarkably, this simple equation ensures elastic unitarity, matches ChPT at low energies, and, using LECs compatible with existing determinations, describes fairly well data up to somewhat less than 1 GeV, generating the ρ, K^*, σ, and κ resonances as poles on the second Riemann sheet. It has been shown [15] that the scalars can actually be generated mimicking the LEC, tadpole, and crossed channel diagrams by a cutoff of natural size, and thus it is said that scalars are "dynamically generated" from, essentially, meson-meson dynamics (meson loops). In contrast, to generate the vectors, a precise knowledge of the LECs is needed, namely, of the underlying, non-meson-meson QCD dynamics.

Here we will update this description of experimental data but furthermore we will simultaneously describe the existing lattice results for decay constants and some scattering lengths.

The IAM equation above is just the one-loop result, but it can be easily and systematically extended to higher orders of ChPT or generalized within a coupled channel formalism [10,12,16], generating also the $a_0(980)$, $f_0(980)$ and the octet ϕ. However note that there is no dispersive justification for the coupled channel approach formula[1] and that is the main reason, apart from simplicity, why we have restricted our analysis to the elastic case.

For completeness, and even though it will be negligible except for very high masses near the applicability limits of our approach, let us now include the pole contribution PC ignored so far. Its contribution can be calculated explicitly from its residue [17] and, to one loop, we find a modified IAM (mIAM) formula:

$$t^{\mathrm{mIAM}} = \frac{t_2^2}{t_2 - t_4 + A^{\mathrm{mIAM}}},$$
$$A^{\mathrm{mIAM}} = t_4(s_2) - \frac{(s_2 - s_A)(s - s_2)[t_2'(s_2) - t_4'(s_2)]}{s - s_A}, \quad (17)$$

where s_A is the position of the Adler zero in the s plane, and s_2 its LO approximation. The standard IAM is recovered for $A^{\mathrm{mIAM}} = 0$, which holds exactly for all partial waves except the scalar ones. Above, and in the usual IAM derivation [14] A^{mIAM} was neglected, since it formally yields a next-to-next-to-leading-order (NNLO) contribution and is numerically very small, except near the Adler zero, where it diverges. However, if A^{mIAM} is neglected, the IAM Adler zero occurs at s_2, correct only to LO, it is a double zero instead of a simple one, and a spurious pole of the amplitude appears close to the Adler zero. All of these caveats are removed with the mIAM, Eq. (17). The differences in the physical and resonance region between the IAM and the mIAM are less than 1%. However, as we will see, for large M_π the σ and κ poles "split" into two virtual poles below threshold, one of them moving toward zero and approaching the Adler zero region, where the IAM fails. Thus, we will use for our calculations the mIAM, although it is only relevant for the mentioned second σ and κ poles, and only when they are very close to their corresponding Adler zeros.

Finally, we want to comment on the unequal mass case, since we also want to describe $K\pi$ elastic scattering. The main difference now is that the left cut extends from $-\infty$ to $s = (M_1 - M_2)^2$, and also that there is a circular cut, centered at $s = 0$ with radius $|M_1^2 - M_2^2|$. Again their main contribution comes from a region where ChPT can be applied. This time, however, $t_2(s)$ has *two* zeros instead of one,

$$s_{2\pm} = \tfrac{1}{5}(M_K^2 + M_\pi^2 \pm 2\sqrt{4M_K^4 - 7M_K^2M_\pi^2 + 4M_\pi^4}),$$

and the modification to the IAM reads

[1]If we followed a similar approach the left cuts would mix when calculating the inverse matrix and produce spurious analytic structures.

$$A^{\mathrm{mIAM}}(s) = \frac{t_2(s)^2}{t_2'(s_{2+})^2}\left[\frac{t_4(s_{2+})}{(s-s_{2+})^2} - \frac{(s_{2+}-s_A)}{(s-s_{2+})(s-s_A)} \times \left(t_2'(s_{2+}) - t_4'(s_{2+}) + \frac{t_4(s_{2+})t_2''(s_{2+})}{t_2'(s_{2+})}\right)\right]. \quad (18)$$

Once again we note that this modification will be numerically negligible except in the close vicinity of the Adler zero. The poles of the resonances under study will only come close to that region for very high values of the quark masses, in the limit of applicability of ChPT and our approach.

Before describing our fits, we want to remark that, in the IAM derivation above, ChPT does not play any role outside its applicability limits. By including three subtractions we have suppressed strongly all contributions to the integrals in high energy regions where ChPT results are not reliable. Finally, the three subtraction constants, which correspond to values of the amplitudes or their derivatives at $s = 0$ are well calculated with ChPT. Of course, this is just a one-loop calculation, although the generalization to higher orders is tedious but straightforward. Hence, our approach does not model the left or inelastic cuts, but just uses the corresponding ChPT approximation that, in principle, can be improved order by order, eventually including more subtractions.

II. FITS TO DATA AND LATTICE RESULTS

As commented before, it has been known for a long time [14] that with the one-loop elastic IAM (the mIAM is almost identical) in Eq. (16) it is possible to obtain a remarkable description of $\pi\pi$ and $K\pi$ experimental data up to somewhere below 1 GeV. Simultaneously, the IAM generates the poles associated to the $f_0(600)$, $\rho(770)$, $K^*(892)$, and $\kappa(800)$ resonances and this is achieved using parameters compatible with those of standard ChPT [12]. However, that description was obtained from a fit to experimental data, and therefore it is mostly sensitive to the LECs L_1, L_2, L_3 that predominantly govern the s dependence of partial waves, but much less so to the rest of the LECs that carry an explicit meson mass dependence. Of course, since now we want to extrapolate the IAM fits to nonphysical masses, it is very important that we use a good description of the mass dependence in observables like masses, decay constants, etc. before extracting conclusions about resonance behavior. For that reason, we are presenting here an updated IAM description of experimental data simultaneously fitted to the available lattice results on the mass dependence of M_π/f_π, M_π/f_K, and M_K/f_K as well as scattering lengths for the doubly charged channel in $\pi\pi$, $K\pi$, and KK scattering. Note that for the moment, these lattice data are only available in the highest isospin combination for each particle pair.

In order to change the masses and decay constants according to Eqs. (3)–(5) and (10), we need first to extract the tree level quantities: $M_{0\pi}^2$, M_{0K}^2, and f_0 from the physical values of the pion, kaon, and eta masses as well as the three decay constants f_π, f_K, and f_η. Note that $M_{0\eta}^2$ will be obtained from the Gell-Mann-Okubo relation: $4M_{0K}^2 - M_{0\pi}^2 - 3M_{0\eta}^2 = 0$. Since there are more physical values than tree level constants, for a given set of LECs we actually use the tree level constants that best fit the physical ones. Thus, the physical masses and decay constants that we will obtain when recovering them from the tree level ones will be only approximate. This is, of course, the consequence of using a truncated expansion—ChPT to one loop—to describe observables.

We have made two fits whose resulting LEC sets are given in the two last columns of Table I. Since there are many parameters, there are strong correlations. Thus, sets with quite different parameters can give raise to acceptable descriptions of data, depending on how one weights experiment and lattice results. On fit I we have fitted to experimental data coming from [18] and to lattice results given in [19]. Despite we show in Fig. 1 these data, for the $(I, J) = (0, 0)$ and $(2, 0)$ waves, where many different experiments are actually incompatible, we have fitted to the phase shifts arising from the dispersive analysis of the experimental data in [20], where a complete set of forward dispersion relations and Roy equations was constrained on a phenomenological fit to all waves. For the (1, 1) wave we have used also the phenomenological phase shifts from that solution since, apart from the dispersive constraints, it fits the data of the electromagnetic form factor of the pion, which is much more reliable and precise than the existing experiments on (1, 1) pion-pion scattering. Anyway, since for πK and other waves we are still using scattering, and also because the method has an intrinsic error due to the NLO approximation on the integrals, we have added in quadrature to the experimental data errors a constant error of 2 degrees and a variable error of 5% of the phase shift and to lattice results on masses over decay constants 5% of their values also in quadrature to their errors. We have also introduced a constraint so that the LECs do not differ much from those found in the K_{l4} analysis to two loops of [8], by weighting also in the χ^2 the LECs with the values in [8]. On fit II we have given an additional weight to the large $1/N_c$ constraint $2L_1 - L_2 = 0$ (dividing its error by 10 when calculating the χ^2) whereas we have relaxed the constrains on δ_{11} and $\delta_{1/20}$ (dividing their χ^2 by 1.5).

For comparison, also in Table I we provide three typical sets of LECs available in the literature obtained from data analyses using dispersive techniques plus ChPT. Those on the first and the second columns come from a one- and two-loop analysis of K_{l4} decays [8], where L_4 and L_6 were set equal to zero (following leading order $1/N_c$ arguments). The "Roy-Steiner" column comes from a dispersive analysis of πK scattering [9]. Note that the LECs in these

sets are frequently within more than 2 standard deviations from one another, and we consider that their difference is indicative of the typical size of systematic uncertainties in our knowledge of LECs. As commented above, since the one-loop IAM generates correctly only the s-channel leading logs of the two-loop calculation, which are dominant at low energies, it is not clear whether we should compare with the LECs obtained in the one- or two-loop ChPT analysis. Actually, all of our IAM LECs lie very close, or within the uncertainties, of at least one of the previous determinations given in the table. Taking into account the uncertainties in these nonunitarized determinations, we consider that the agreement between the IAM LECs and previous determinations is fair. Let us remark that the relevant fact about this comparison is to note that we do not need to make any fine-tuning of the LECs, like changing well-established signs, changing order of magnitude, etc., to describe the experimental and lattice data simultaneously.

Finally, we also provide in Table I, the IAM III set of LECs, which corresponds to one of the three fits obtained using the coupled channel IAM in [10]. This set was fitted to experimental data only and the uncertainties quoted are just statistical. Taking into account that we are using the single channel IAM instead of the coupled channel one, and the estimate of systematic uncertainties discussed above, we see that our new fits, including new experimental data and lattice results, are not too different from those already obtained in [10].

In Fig. 2 we show the results of our fits compared with experimental data on $\pi\pi$ and πK elastic scattering phase shifts. The best description is given by fit I (continuous line), whereas fit II gives a somewhat too heavy $\rho(770)$ vector resonance (by roughly 50 MeV, i.e., a 6% error). For comparison, we show as a dotted line the results of the IAM if we used the ChPT LECs obtained from the two-loop analysis of K_{l4} decays listed in Table I. We also show as a dot-dashed line the results that would be obtained if the nonunitarized ChPT one-loop results, using the same set of LECs, are extrapolated to higher energies. Note that the IAM results describe rather well both the resonant and nonresonant shapes up to 1 GeV or slightly above, except for the scalar-isoscalar δ_{00} that is only described up to 800 MeV. This is due to the presence of the sharp rise caused by the $f_0(980)$ resonance that decays mostly to two kaons and can only be described with the coupled channel

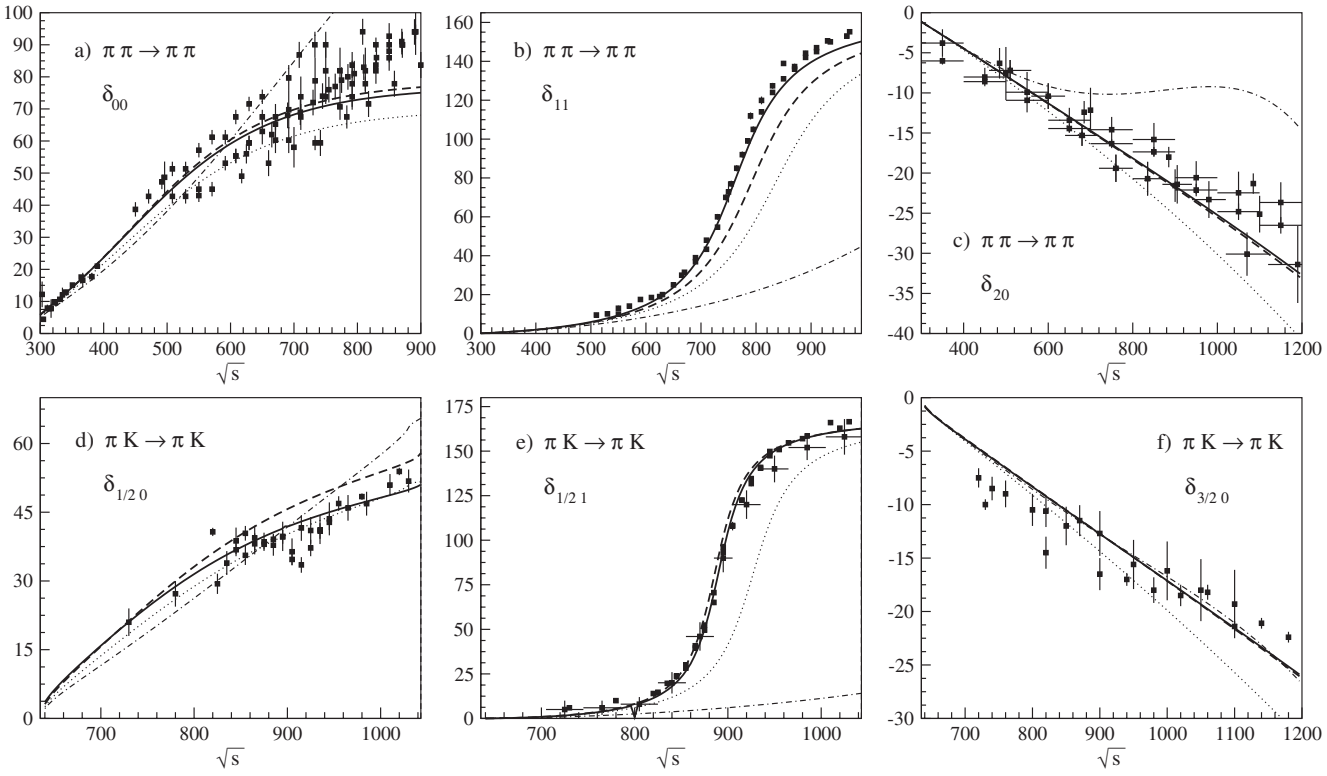

FIG. 2. Results of our IAM fits versus experimental data on $\pi\pi$ and πK scattering. The continuous and dashed lines correspond, respectively, to fits I and II, whose parameters are given in Table I. For comparison we show the results of the IAM if we used the ChPT LECs obtained from the two-loop analysis of K_{l4} decays listed also in Table I (dotted lines) as well as the results of standard nonunitarized ChPT with the same set of LECs (dot-dashed lines). The plotted data correspond to experimental results [18], which are often incompatible. For that reason, in our fits, and for $\pi\pi$ scattering, we have actually used the results of a dispersive analysis of these data [20].

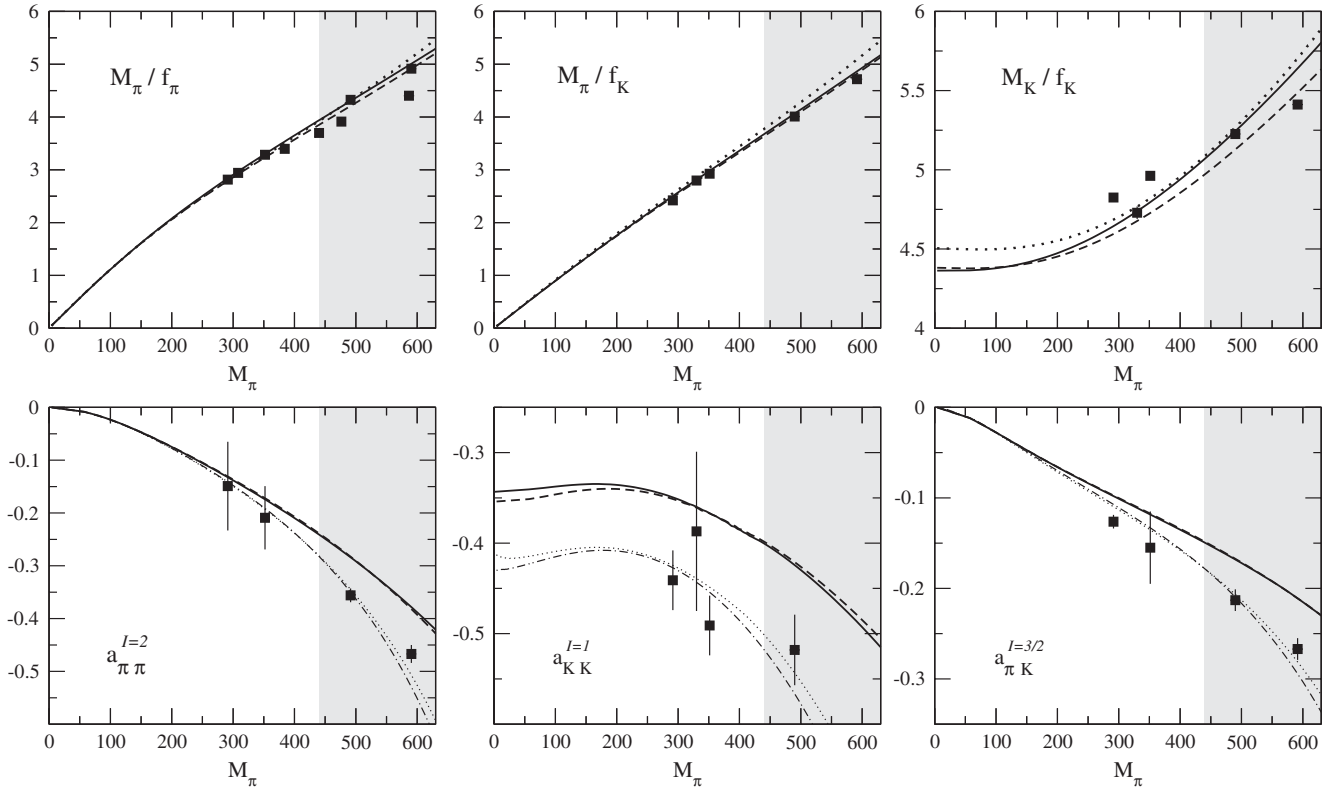

FIG. 3. Result of the unitarized fits to lattice calculations of M_π/f_π, M_π/f_K, M_K/f_K and the $\pi^+\pi^+$, K^+K^+, $K^+\pi^+$ scattering lengths. The continuous and dashed lines correspond, respectively, to fits I and II, whose parameters are given in Table I. For comparison we show the results of the IAM if we used the ChPT LECs obtained from the two-loop analysis of K_{l4} decays listed also in Table I (dotted lines) as well as the results of standard nonunitarized ChPT with the same set of LECs (dot-dashed lines). Lattice results come from [19]. The gray area lies beyond our applicability region; however, it is useful to check that our description does not deteriorate too rapidly.

IAM formalism, [10,12,16], that we do not use here for the reasons explained above.

Those results are, of course, well known, and these fits would just be an update of [10] if we had not also included lattice data on the fit that we show in Fig. 3. Note that we are fitting results on M_π/f_π, M_π/f_K, and M_K/f_K and the $\pi^+\pi^+$, K^+K^+, and $K^+\pi^+$ scattering lengths [19]. Once again we show fits I and II as continuous and dashed lines, respectively, together with IAM results using the LECs from a two-loop analysis of K_{l4} decays listed in Table I (dotted line) and nonunitarized ChPT to one loop with the same set of LECs (dot-dashed line). As explained above, we do not consider that our method should be trusted for pion masses heavier than 440 MeV, being optimistic, and that is why the heavier mass region is shown as a gray area.

III. DEPENDENCE ON *u* AND *d* QUARK MASSES

Now that we have a good description of both the energy dependence of pion-pion amplitudes together with the mass dependence of the few observables available from lattice, we can change the value of the light quark mass, keeping m_s fixed, and predict the behavior of the resonances generated within the IAM.

A. Light vector mesons: The $\rho(770)$ and $K^*(892)$

The $\rho(770)$ and $K^*(892)$ vector resonances are well-established $q\bar{q}$ states belonging to an SU(3) octet. The first is produced in $\pi\pi$ scattering, and its quark mass dependence was already studied within SU(2) ChPT [3]. Here we will just check that we reobtain very similar results within the SU(3) formalism, while describing simultaneously the lattice observables shown in Fig. 3. However, the $K^*(892)$ appears in πK scattering and can only be obtained using SU(3) ChPT as we do here.

1. Mass and width

Thus, in Fig. 4, we show the dependence of the light vector resonances on the nonstrange quark masses, using one-loop SU(3) ChPT unitarized with the IAM. For each resonance, these masses and widths are defined from the position of their associated pole in the second Riemann sheet, through the usual Breit-Wigner identification: $\sqrt{s_{\rm pole}} \equiv M - i\Gamma/2$. We show the results for fits I and II

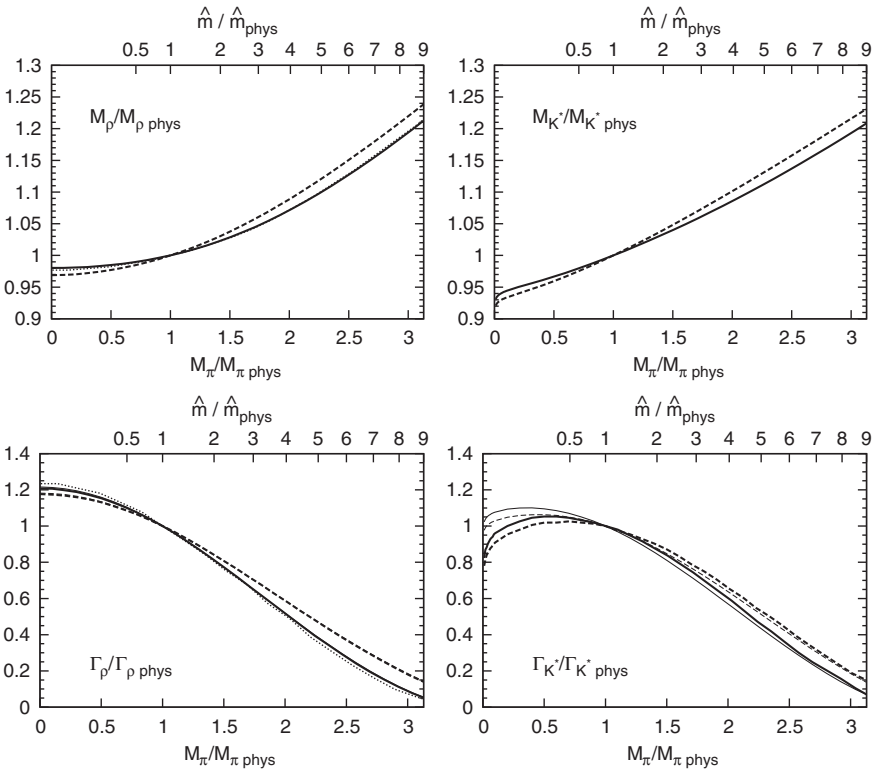

FIG. 4. Dependence of the $\rho(770)$ and $K^*(892)$ mass and width with respect to the nonstrange quark mass $\hat{m}$ (horizontal upper scale), or the pion mass (horizontal lower scale). Note that we give all quantities normalized to their physical values. The thick continuous and dashed lines correspond, respectively, to fits I and II described in the text with unitarized SU(3) ChPT. For the ρ these results are very compatible with those in [3] using SU(2) ChPT (dotted lines). The continuous (dashed) thin line shows the M_π dependence of the widths from the change of phase space only, assuming a constant coupling of the resonances to two mesons, $\rho(770)$ to $\pi\pi$ and $K^*(892)$ to πK, calculated from the dependence of masses and momenta given by fit I (II). For the $\rho(770)$ the thin and dashed lines overlap completely.

as continuous and dashed lines, respectively. The results for both fits are very consistent and their difference can be taken as an estimation for systematic uncertainties in the choice of LECs. To suppress *systematic uncertainties* we give all quantities normalized to their physical values. Note that we provide two scales for the mass variation: In the upper horizontal axis, we show the variation of the quark mass in terms of $\hat{m}/\hat{m}^{\rm phys}$, whereas in the lower horizontal axis we show the variation of the pion mass in terms of $M_\pi/M_\pi^{\rm phys}$. The one-loop ChPT relation between these two scales is given by Eqs. (2) and (3). To be precise, this relation changes for different LECs, but, as we already showed in Fig. 1, the difference is too small to be observed with the naked eye in the axes of Fig. 4.

In the left panels we also show, as a dotted line, the SU(2) ChPT result already obtained in [3], which is fairly consistent with the new SU(3) results. Of course, the difference is somewhat larger when the pion mass is closer to the kaon mass, and the kaons start playing a more prominent role. Of course, since the SU(2) results [3] already described fairly well the available lattice calculations for the $\rho(770)$ mass, so it happens with the SU(3) results here. In addition, this ensures that the M_ρ dependence on M_π agrees nicely with the estimations for the two first coefficients of its chiral expansion [21], which was already checked in the SU(2) case [3].

Since the vertical scale is the same for the $\rho(770)$ and $K^*(892)$ plots, the similarity of their behavior is very evident. Both their masses increase smoothly as the quark mass increases, but much slower than the pion mass. Some differences can be observed for small $\hat{m}$, but this is due to the fact that the SU(3) breaking between the $\rho(770)$ and the $K^*(892)$ is more evident since we keep m_s fixed to its large physical value. What is interesting to observe is that the naive rule of thumb frequently used in the literature [22], that $\partial M_R/\partial\hat{m} = N_R^v$, where N_R^v is the number of valence nonstrange quarks, yields the correct order of magnitude (and this is how it has been used in [22]) but would predict a 2:1 relation for the slope of the $\rho(770)$ with respect to that of the $K^*(892)$, which is not observed for light quarks.

Continuing with our analysis, we note that, as the quark mass increases, the two-pion and pion-kaon threshold grow faster than the masses of the resonances and, as a consequence, there is a strong phase space suppression than can

account exclusively for the decrease of their widths. We show in the lower panels the M_π dependence of Γ_ρ and Γ_{K^*} normalized to their physical values. The decrease of the widths is largely kinematical, following remarkably well the expected reduction from phase space as the masses of the NGB increase [thin continuous and dashed lines corresponding to fits I and II, respectively, although for the $\rho(770)$ they overlap so well that the thin lines are not seen]. This result was already found for the $\rho(770)$ within the SU(2) formalism and is nicely confirmed here. This suggests that there is no dynamical effect through the vector coupling to two mesons, as we will analyze next.

2. Coupling to two mesons

The dynamics of resonance-meson-meson interaction is encoded in the coupling constant that we obtain from the residue of the amplitude at the pole position as follows:

$$g^2 = -16\pi \lim_{s\to s_{\rm pole}} (s - s_{\rm pole}) t(s) \frac{3}{4k^2}, \tag{19}$$

where the normalization factors are chosen to recover the usual expression for the two-meson width of narrow vector resonances:

$$\Gamma_V = |g|^2 \frac{1}{6\pi} \frac{|\mathbf{k}|^3}{M_V^2}, \tag{20}$$

$|\mathbf{k}|$ being the modulus of the meson three-momentum. Actually, by identifying $\sqrt{s_{\rm pole}} = M_V - i\Gamma_V$, we have explicitly checked that we obtain the same numerical value for the coupling with both equations. We find $|g_{\rho\pi\pi}| \simeq 6.1$ and $|g_{K^*\pi K}| \simeq 5.5$.

Then, in Fig. 5 we show the dependence of the $g_{\rho\pi\pi}$ (left panel) and the $g_{K^*\pi K}$ (right panel) couplings with respect to the pion mass (lower horizontal scale) or the nonstrange quark mass $\hat{m}$ (upper horizontal scale). In order to suppress systematic uncertainties, we have normalized the couplings to their physical values. Note that the $g_{\rho\pi\pi}$ is remarkably constant, deviating from its physical value by 2% at most, despite the fact that the quark mass is changed by a factor of 9. It is also relevant because it justifies the constancy assumption made in lattice studies of the $\rho(770)$ width [23]. The $g_{K^*\pi K}$ is also quite independent of the nonstrange quark mass, deviating by 10% at most in the chiral limit and by less than 4% when the quark mass is increased by a factor of 9. The results for fits I and II are almost indistinguishable.

The constancy of the vector-meson-meson couplings, together with the classic KSRF relation [24], provides a striking connection between the quark mass dependence of the rho mass and the pion decay constant. Actually, the KSRF relation, obtained from the partially conserved axial current and vector meson dominance, reads

$$g_{\rho\pi\pi}^2 \simeq M_\rho^2/8f_\pi^2. \tag{21}$$

Note that in our calculation we are obtaining M_ρ from a one-loop ChPT unitarized calculation, whereas f_π comes simply from the next-to-leading-order ChPT calculation, but, of course, without unitarization. It is therefore quite remarkable that the ratio M_ρ/f_π obtained from our amplitudes, shown in Fig. 6, is constant within less than 5% accuracy, when the quark mass varies by a factor of 9, or the pion mass by a factor of 3. Note that, as usual, in Fig. 6 we have normalized the ratio to its physical value. It seems that the simple KSRF relation holds remarkably well up to surprisingly large values of the nonstrange quark mass, and therefore the M_ρ quark mass dependence can be recast with the same factor as that for f_π.

A similar result is found for the $K^*(892)$ whose ratio M_{K^*}/f_π is also shown in Fig. 6 to deviate by less than 2% from its physical value. Note that, according to the second reference in [24], the f_K dependence does not show up in the relation. Actually, had we used $M_{K^*}/\sqrt{f_\pi f_K}$ instead, the deviation would have been a factor of 3 larger.

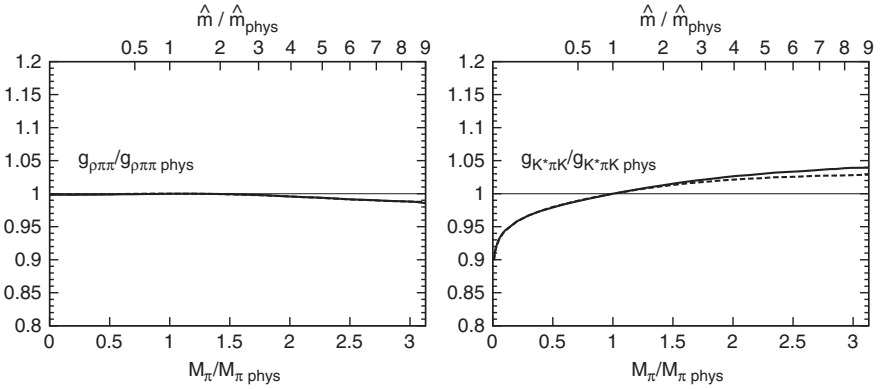

FIG. 5. Two-meson-vector coupling dependence with respect to the nonstrange quark mass $\hat{m}$ (horizontal upper scale), or the pion mass (horizontal lower scale). Note we normalize the couplings to their physical values. We show on the left the $\rho(770)$ coupling to two pions and on the right that of the $K^*(892)$ to πK (continuous and dashed lines correspond to fits I and II, respectively).

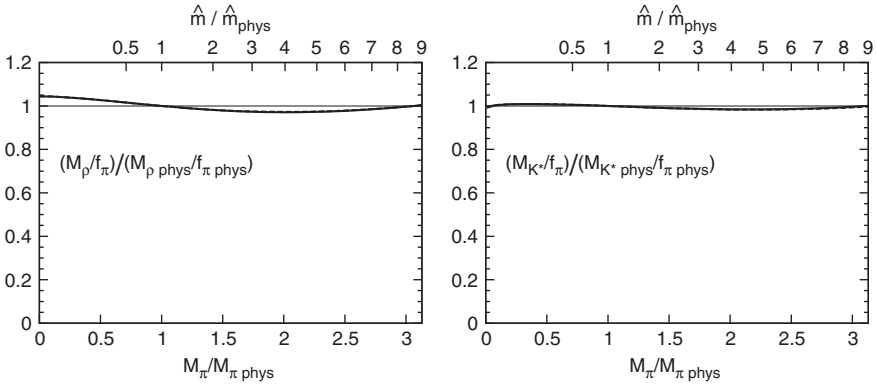

FIG. 6. Ratio of vector resonance masses to the pion decay constant dependence on the nonstrange quark mass (horizontal upper scale), or the pion mass (horizontal lower scale). Once again, we normalize all quantities to their physical values. We show the M_ρ/f_π on the left and M_{K^*}/f_π on the right (continuous and dashed lines correspond to fits I and II, respectively). Both masses seem to follow the f_π quark mass dependence up to less than 5% and 2%, respectively.

B. Light scalar mesons: The $f_0(600)$ and $\kappa(800)$

The $f_0(600)$, or sigma, and the $\kappa(800)$ scalar mesons are still somewhat controversial. The main problem is their huge width that makes their experimental identification complicated. Despite the fact that their pole mass and width has been determined by several groups with the help of model independent dispersive techniques (with and without ChPT input) and a fairly reasonable agreement (see [9,14,25] for recent determinations), they are still cited with extremely cautious and conservative estimates in the PDG [26]. Their nature is even more controversial, and as commented above, there are no present lattice calculations with realistic quark masses that could shed some light on the problem. It is therefore even more interesting to obtain predictions on their quark mass dependence. Compared with the vector case, there is an additional complication because now we do not necessarily expect a similar behavior between the $\kappa(800)$ and the $f_0(600)$, since although the former should belong to an SU(3) octet, the latter could be in the singlet, the octet, or have a significant mixture of both. As a matter of fact, there are indications that its singlet component is actually dominant [27,28].

1. Mass and width

As the data show in Fig. 2, the sigma and kappa resonances do not present a peak nor a Breit-Wigner shape in the meson-meson scattering $(I, J) = (0, 0)$ and $(1/2, 0)$ waves, respectively. Once again, these masses and widths are defined from the position of their associated pole in the second Riemann sheet, as follows: $\sqrt{s_{\rm pole}} \equiv M - i\Gamma/2$, but one should keep in mind that these scalar states do not present the typical Breit-Wigner shape, so there is no immediate equivalence of the mass in terms of a peak in the cross section or a time delay in the propagation.

In Fig. 7 we show the pole mass and width dependence of light scalar resonances on the nonstrange quark mass. As in Fig. 4, we show quantities normalized to their physical values and we provide two scales for the horizontal axis: $\hat{m}/\hat{m}_{\rm phys}$ (upper horizontal axis) and $M_\pi/M_{\pi\,\rm phys}$ (lower horizontal axis). Once again, the continuous line represents the results for fit I, the dashed line those of fit II, and the dotted line stands for the results of unitarized SU(2) ChPT for the $f_0(600)$. As before we find that the fits I and II are very consistent with each other, and, for the $f_0(600)$ also with the existing SU(2) calculation of [3].

The most prominent feature of the scalars behavior is the appearance of two branches for the mass as defined above, already observed for the σ in [3]. The reason is that for physical values of the quark mass, the poles associated with resonances appear as conjugated poles in the second Riemann sheet, i.e., there are poles at $\sqrt{s_{\rm pole}} \equiv M \pm i\Gamma/2$. Of course, only the one in the lowest half plane is continuous with the physical amplitude in the real axis, and this is the one responsible for the physical resonance. However, as the quark mass increases these poles move closer to the real axis until they join in a single pole below threshold, but still in the second Riemann sheet. If the quark mass is increased further, the poles split again but without leaving the real axis. The position of each one of these poles corresponds to each one of the branches that we show in the upper panels of Fig. 7.

Although this qualitative behavior is a well-known possibility for potentials in scalar channels, one-loop unitarized ChPT is predicting the quark mass value for which it occurs, which is a genuine prediction for QCD. For scalar-isoscalar $\pi\pi$ scattering it was already observed in the SU(2) case [3]. Here we are confirming this position when using SU(3) instead of SU(2) ChPT, but we see it also happening for the $\kappa(800)$, although the point at which it happens depends more on the set of LECs. For this reason, we think that the existence of this nonanalyticity of the $\kappa(800)$ pole is robust, but not so much the precise quark mass value where it occurs.

This "apparent splitting" cannot occur for higher partial waves since they all carry a k^{2J} factor that forces the

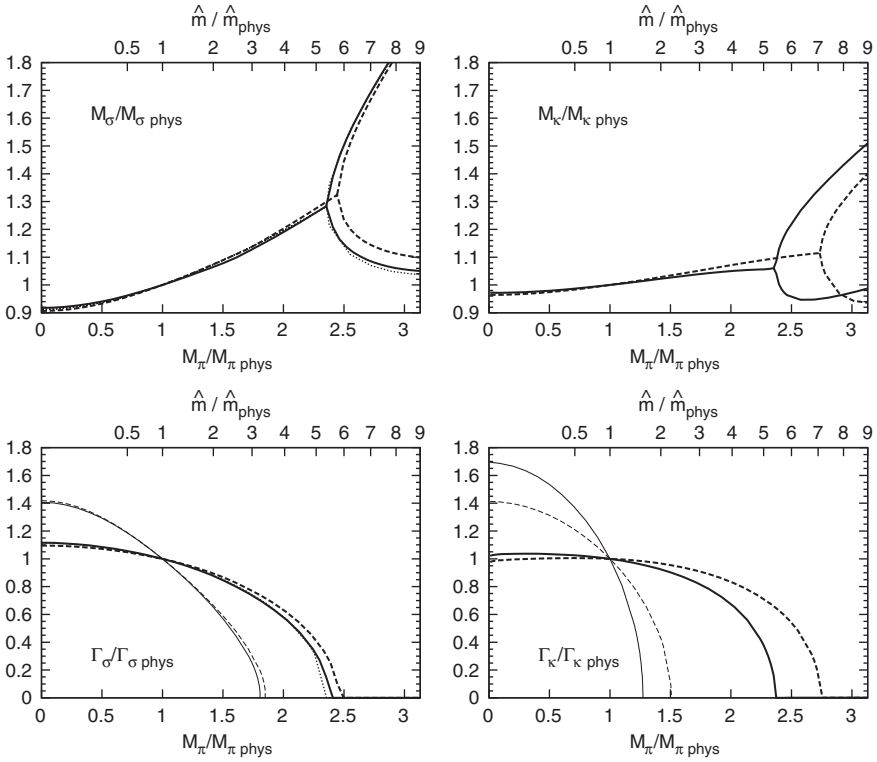

FIG. 7. Dependence of the $f_0(600)$ and $\kappa(800)$ mass and width with respect to the nonstrange quark mass $\hat{m}$ (horizontal upper scale), or the pion mass (horizontal lower scale). Note that we give all quantities normalized to their physical values. The thick continuous and dashed lines correspond, respectively, to fits I and II described in the text with unitarized SU(3) ChPT. For the $f_0(600)$ these results are very compatible with those in [3] using SU(2) ChPT (dotted lines). Let us remark that both resonances, being scalar, develop two poles on the real axis for sufficiently high masses. The thin lines show the decrease of the widths if it were only due to phase space reduction (the thin continuous lines correspond to fit I and the dashed ones to fit II).

conjugated poles to join the real axis exactly at threshold, and then one of them jumps to the first Riemann sheet.

Apart from the evident qualitative similarities between the behavior of the $f_0(600)$ and the kappa, it is also clear that quantitatively they behave somewhat differently. In particular, the growth of the $\kappa(800)$ mass before the ''splitting point'' is much softer than for the $f_0(600)$, and even softer than the $\rho(770)$ and $K^*(892)$ growth shown in Fig. 4 (please note the difference in scales between both figures).

In the lower panels of Fig. 7 we show the quark mass dependence of the sigma and kappa widths. On the left we show that the decrease of the sigma width we find with the SU(3) one-loop IAM is very consistent between fits I and II, and confirm the previous results within SU(2) [3]. On the right we show the results for the $\kappa(800)$ width. We also show that the width decrease for both of them cannot be attributed to the phase space reduction, due to the increase of pion and kaon masses, naively expected from the narrow width approximation

$$\Gamma_S = |g|^2 \frac{1}{8\pi} \frac{|p|}{M_S^2}, \tag{22}$$

which we show as a thin continuous (dashed) line corresponding to fit I (II). Despite the fact that the shape of the decrease is slightly different for the σ and κ, both scalars behave very differently than vector mesons. Actually, we will see next that this implies that the scalar couplings to two mesons have a much stronger quark mass dependence than the vector ones.

2. Coupling to two mesons

As we have just seen, the narrow width approximation in Eq. (22) above is of little use for scalars. But, of course, we can still extract the coupling constant from the residue as we did for vectors, although now the equation reads

$$g^2 = -16\pi \lim_{s \to s_{\rm pole}} (s - s_{\rm pole}) t(s). \tag{23}$$

We find $|g_{\sigma\pi\pi}| \simeq 2.86$ GeV and $|g_{\kappa\pi K}| \simeq 3.6$ GeV, to be compared to $|g_{\sigma\pi\pi}| \simeq 2.97 \pm 0.04$ GeV and $|g_{\kappa\pi K}| \simeq 4.94 \pm 0.07$ GeV, obtained in [28] or the $|g_{\sigma\pi\pi}| \simeq 2.2$ average obtained in [29]. The agreement is fairly reasonable, taking into account that the data that have been used, the σ and κ poles, and the models in those references differ substantially for each reference.

Thus, in Fig. 8 we show the quark mass dependence (upper horizontal scale) or pion mass dependence (lower

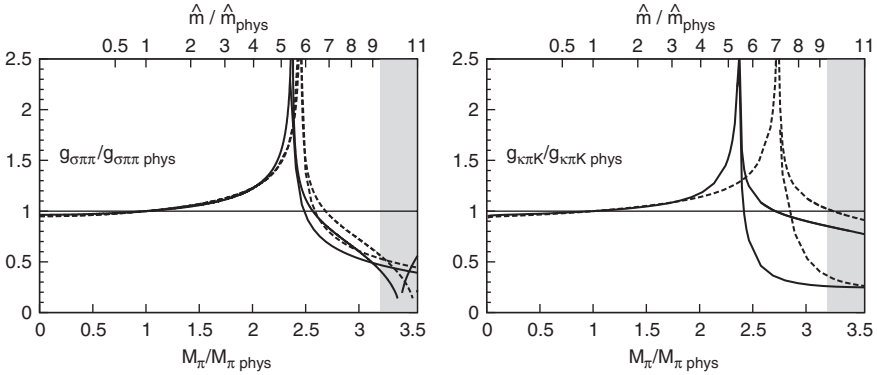

FIG. 8. Two-meson-scalar coupling dependence with respect to the nonstrange quark mass $\hat{m}$ (horizontal upper scale), or the pion mass (horizontal lower scale). Note we normalize the couplings to their physical values. We show on the left the $f_0(600)$ or sigma coupling to two pions and on the right that of the $\kappa(800)$ to πK. Let us remark that the two poles in the real axis show different couplings, which explains the doubling of the lines above the double branch point.

horizontal scale) of $g_{\sigma\pi\pi}$ and $g_{\kappa\pi K}$. As usual, all quantities are normalized to their physical values. Compared with Fig. 5 (note the different scales), we see that these couplings show a much stronger quark mass dependence. Moreover, they increase dramatically near the point of the apparent splitting. Beyond that point there are two nonconjugate poles lying on the real axis below threshold in the second Riemann sheet. For this reason, after the splitting point we plot two curves for each fit. The lowest curve corresponds to the pole closest to the threshold that eventually jumps into the first Riemann sheet. This threshold crossing from one sheet to the other corresponds to the point where the coupling tends to zero in the figures, in good agreement with the well-known result in [30]. Actually this can be checked numerically, because, as shown in [31] the coupling is inversely proportional to the energy derivative of the one-loop function [$G(s)$ in [31] and $J(s)$ in ChPT [12]], which is divergent at threshold. Despite this consistency check, within our approach this occurs at pion masses close to the naive applicability limit, and therefore the exact M_π value when this happens is not very reliable.

IV. DEPENDENCE ON THE STRANGE QUARK MASS

Up to here we have only been changing the values of the nonstrange quark mass keeping m_s fixed. However, since we are dealing with the full SU(3) ChPT formalism, we are now able to change the strange quark, keeping $\hat{m}$ fixed. The dependence of hadronic observables on the strange quark mass is also of interest for lattice studies and for cosmological considerations [6]. As we explained in Sec. I A we will only vary the strange quark mass in the limited range $0.7 < m_s/m_{s\,\mathrm{phys}} < 1.3$ to ensure that the kaon does not become too heavy to spoil the ChPT convergence nor too light to require a coupled channel formalism to deal with the $K^*(892)$ or $\kappa(800)$ resonances, thus introducing additional model dependences in our approach.

A. Light vector mesons: The $\rho(770)$ and $K^*(892)$

1. Mass and width

As in previous sections we define the mass and width of the vector resonances from the position of their associated poles. Thus, in the upper panels of Fig. 9 we show the quark mass dependence (or kaon mass dependence in the lower horizontal scale) of the ρ and $K^*(892)$ masses. In the lower panels we show the dependence of their widths. As usual, all quantities are normalized to their physical values to suppress systematic uncertainties.

As could be expected, both the mass and width of the $\rho(770)$, being nonstrange, are almost independent of the strange quark mass within the range of study. Note that the ρ mass actually decreases very slightly, by roughly 1%. Since the pion mass almost remains constant—see Eq. (3) and the L_6, L_4 values in Table I—this implies that phase space decreases slightly for smaller strange quark mass and the $\rho(770)$ width decreases accordingly. Actually, we can check in Fig. 9 that the width reduction follows remarkably well the phase space reduction expected from Eq. (20) (thin continuous and dashed lines).

Looking now at the right panels of Fig. 9, we notice that, as expected, the $K^*(892)$ shows a much stronger dependence than the $\rho(770)$ on the strange quark or the kaon masses. On the one hand, when the kaon mass is made lighter, the $K^*(892)$ mass decreases, as it happened when changing the light quark mass, although much faster, i.e., up to 5% when the kaon mass decreases by 20%. Nevertheless, and contrary to what happened when reducing $\hat{m}$, the $K^*(892)$ width increases significantly, up to 40%. This is due to the fact that the $K^*(892)$ decays to πK, but the kaon mass decrease is faster than that of the $K^*(892)$. On the other hand, when the kaon mass is made heavier, the $K^*(892)$ mass grows, but much slower than the kaon mass, so that phase space shrinks and the resonance width decreases once more. We are also showing as thin lines the expected variation of the widths if their only quark mass dependence came from the change in the particles

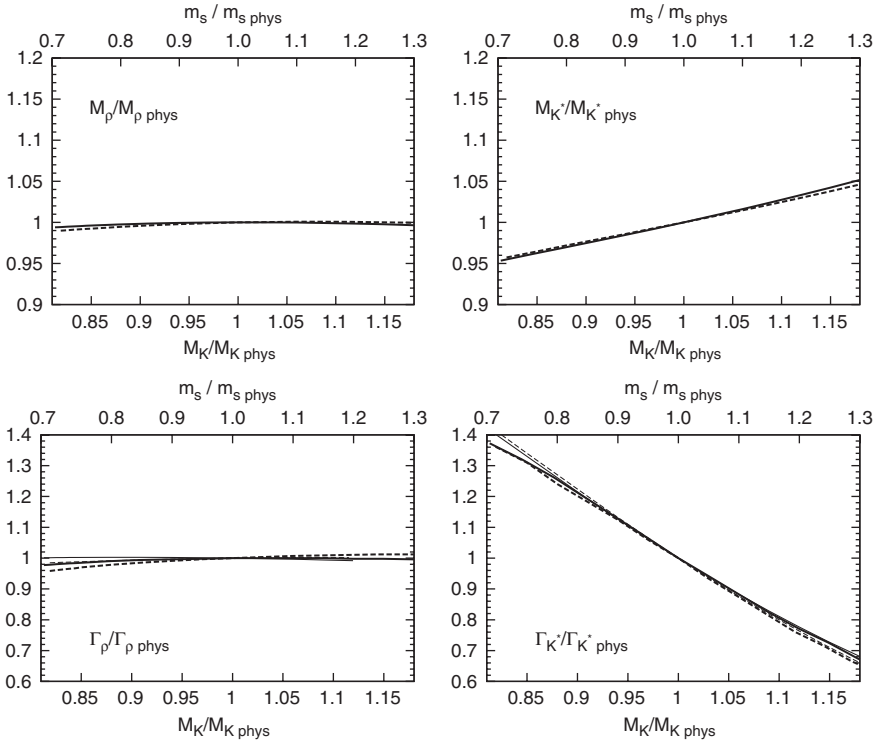

FIG. 9. Dependence of the $\rho(770)$ and $K^*(892)$ mass and width with respect to the strange quark mass m_s (horizontal upper scale), or the kaon mass (horizontal lower scale). Note that we give all quantities normalized to their physical values. The thick continuous and dashed lines correspond, respectively, to fits I and II described in the text with unitarized SU(3) ChPT. The thin lines show the decrease of the widths as if it were only due to phase space reduction (the thin continuous lines correspond to fit I and the dashed ones to fit II).

masses and the naive phase space suppression in Eq. (20) (thin continuous lines for fit I and thin dashed lines for fit II). We see that they are in very good agreement with our results from the IAM, which suggest that their coupling to two mesons is almost independent of the quark masses, which we will see next.

2. Coupling to two mesons

Thus, in Fig. 10 we show the dependence both on m_s and kaon masses of the vector to meson-meson couplings. As usual everything is normalized to their physical values. It can be noted that within the range of variation under study, which is 30% for the strange quark mass in either direction, both the $g_{\rho\pi\pi}$ and $g_{K^*\pi K}$ couplings change by 1% at most.

In Fig. 11 we show the results for the KSRF relation variation in terms of the strange quark mass. Since the ρ coupling has virtually no dependence on m_s, the relation remains trivially constant. For the $K^*(892)$ the relation is well satisfied (to within less than 5% from the physical value) in the whole m_s range of our study.

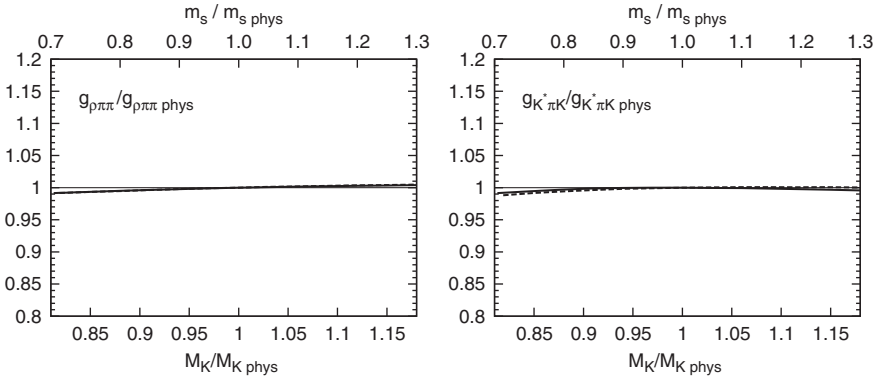

FIG. 10. Two-meson-vector coupling dependence with respect to the strange quark mass m_s (horizontal upper scale), or the kaon mass (horizontal lower scale). Note we normalize the couplings to their physical values. We show on the left the $\rho(770)$ coupling to two pions and on the right that of the $K^*(892)$ to πK.

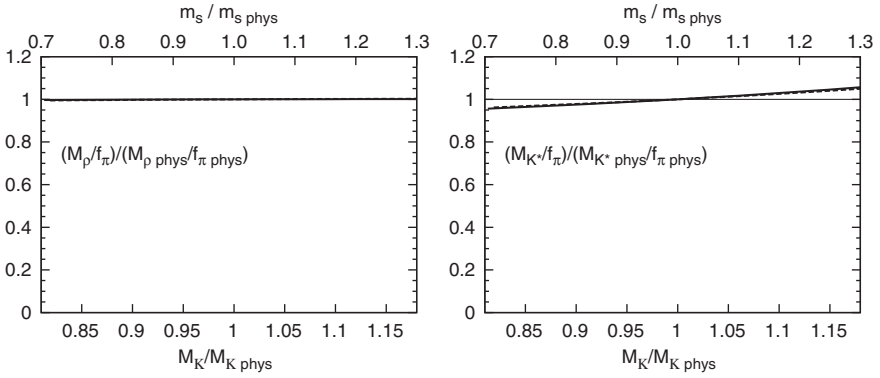

FIG. 11. Ratio of vector resonance masses to the pion decay constant dependence on the strange quark mass (horizontal upper scale), or the kaon mass (horizontal lower scale). Once again, we normalize all quantities to their physical values. We show the M_ρ/f_π on the left and M_{K^*}/f_π on the right (continuous and dashed lines correspond to fits I and II, respectively). For the ρ the result is trivial since we have already shown that its coupling does not depend on m_s. However the $K^*(892)$ mass deviates from the f_π quark mass dependence by less than 5% with respect to the physical value.

B. Light scalar mesons: The $f_0(600)$ and $\kappa(800)$

We simply repeat the procedure we used to study the light quark variation in Sec. III B, but this time changing the strange quark mass instead, and keeping $\hat{m}$ fixed.

1. Mass and width

Thus, in Fig. 12, we show the variation of the sigma and $\kappa(800)$ masses and widths with respect to the kaon mass variation (lower horizontal scale) or the strange quark mass (upper horizontal scale). Once again all masses are normalized to their physical values. As could be expected, we see in the left panels that the change on the sigma is smaller than 1% on both mass and width (beware we have changed the scale with respect to the previous Fig. 7 to make the changes more visible).

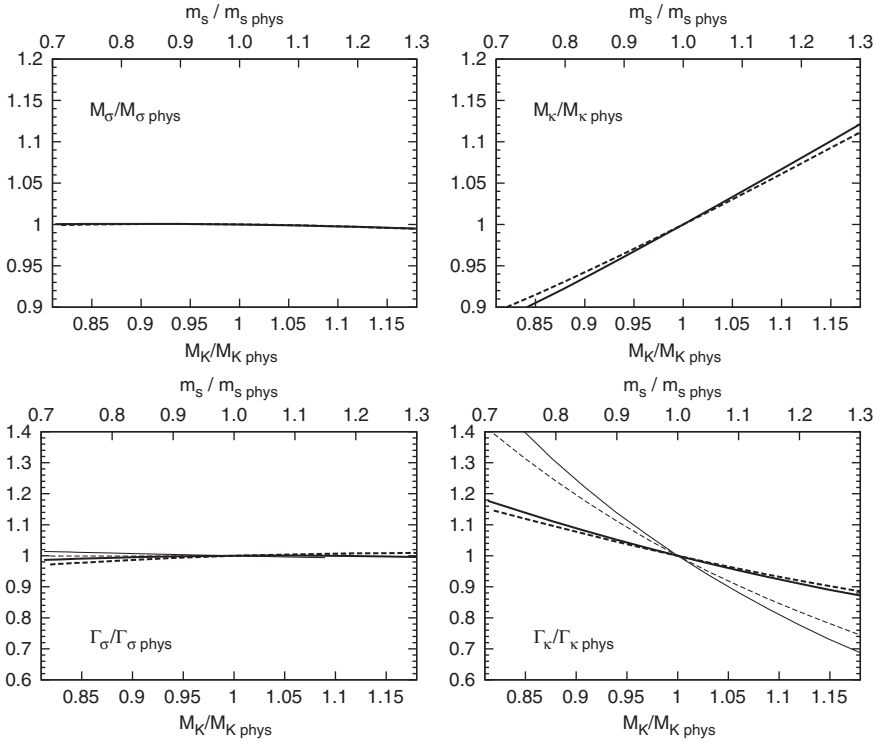

FIG. 12. Dependence of the $f_0(600)$ and $\kappa(800)$ mass and width with respect to the strange quark mass m_s (horizontal upper scale), or the kaon mass (horizontal lower scale). Note that we give all quantities normalized to their physical values. The thick continuous and dashed lines correspond, respectively, to fits I and II described in the text with unitarized SU(3) ChPT. The thin lines show the decrease of the widths as if it were only due to phase space reduction (the thin continuous lines correspond to fit I and the dashed ones to fit II).

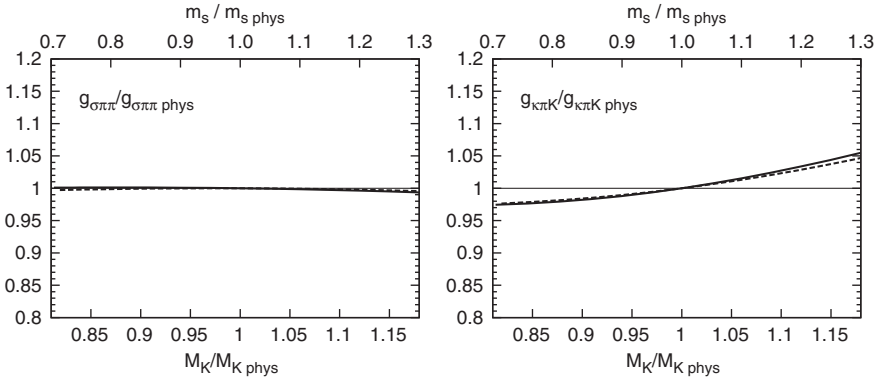

FIG. 13. Two-meson-scalar coupling dependence with respect to the strange quark mass m_s (horizontal upper scale), or the kaon mass (horizontal lower scale). Note we normalize the couplings to their physical values. We show on the left the $f_0(600)$ or sigma coupling to two pions and on the right that of the $\kappa(800)$ to πK.

A much bigger effect is seen for the $\kappa(800)$ in the right panels, whose mass changes by as much as 12% from its physical value within the range of study, whereas the width changes by as much as 20%. However, its mass dependence, despite being somewhat stronger than for its vector counterpart $K^*(892)$, is still softer than for the kaon itself. This is the reason why, as the $\kappa(800)$ becomes lighter its width increases, and vice versa.

In the lower panels we have also plotted the expected naive phase space reduction. This time, however, as the sigma properties barely depend on the strange quark mass, we only see a significant deviation from that naive behavior in the case of the $\kappa(800)$.

2. Coupling to two mesons

For all means and purposes, with respect to strange quark mass variations, the sigma coupling to two mesons turns out to be a constant within our approximation, as can be seen in the left panel of Fig. 13.

In contrast, the $g_{\kappa\pi K}$ coupling shows some dependence on the strange quark mass. Actually, it grows by 6% when the kaon mass is increased by 18% from its physical value.

V. SUMMARY AND CONCLUSIONS

In this work we have studied the quark mass dependence of the light vector and scalar resonances generated as poles of meson-meson scattering elastic amplitudes within unitarized one-loop chiral perturbation theory. This dependence is of interest to relate lattice results to hadronic observables, but also for anthropic and cosmological considerations. The use of an SU(3) formalism extends previous studies within SU(2), allowing us to study the behavior of strange resonances like the $\kappa(800)$ and $K^*(892)$, but also to study variations not only of the light u and d quark masses, but also of the strange quark mass.

After a brief introduction on how ChPT provides a model independent expansion of pion, kaon, and eta masses and decay constants, as well as their two-body interaction amplitudes, we have reviewed how this series can be used inside a dispersion theory formalism to construct the so-called inverse amplitude method amplitudes that satisfy elastic unitarity while respecting the ChPT expansion. It has been known for a long time that the elastic IAM reproduces well the meson-meson elastic scattering data up to 800–1000 MeV, including the resonance region. Note that we have refrained for the moment to use the very successful coupled channel IAM precisely because at present it lacks a dispersive derivation, and we want to avoid as much model dependence as possible. Of course the experimental data may fix rather well the energy dependence but not so well the mass dependence. For that reason we have presented here a new IAM analysis including simultaneously the existing lattice results on meson masses, decay constants, and scattering lengths. We obtain a fairly good description of experiment and lattice data using chiral parameters rather similar to existing one- and two-loop determinations. No fine-tuning of parameters is required. Once this is done, we have varied the quark masses within certain ranges that ensure the applicability of the elastic IAM for the resonances under study: $\hat{m}/\hat{m}_{\rm phys} \leq 9$ and $0.7 < m_s/m_{s\,\rm phys} < 1.3$ ($\hat{m}$ is the average mass of the u and d quarks). In practice, in ChPT we have changed the squared pion and kaon masses, which, at leading order, are proportional to quark masses. Although we have shown in Fig. 1 that this simple approximation works within roughly 10% accuracy, we have carefully included the full one-loop corrections, and shown the quark and meson mass variation independently in all plots.

In the second Riemann sheet of these amplitudes, the IAM generates the—conjugated pairs of—poles associated to the vector $\rho(770)$, $K^*(892)$ and scalar $f_0(600)$ and $\kappa(800)$ resonances. Light vector resonances are well established and there is little relevance on whether we refer to their ''pole'' or Breit-Wigner mass and widths. In contrast, the scalar $f_0(600)$, or sigma and the $\kappa(800)$ are rather controversial due to their large apparent width and the lack of a Breit-Wigner shape in the meson-meson scattering phase shifts. To avoid complications, we have always

presented our results in terms of pole definitions of masses, widths, and couplings.

For the $f_0(600)$ and $\rho(770)$ resonances, which appear in $\pi\pi$ scattering, we have nicely confirmed the similar unitarized one-loop SU(2) ChPT analysis performed in [3]. When increasing $\hat{m}$ both the sigma and ρ masses grow faster than the pion mass, whereas their widths decrease. However, the $\rho(770)$ mass behaves smoothly in the whole quark mass range, whereas, roughly at $M_\pi \sim 340$ MeV, the $f_0(600)$ pole and its conjugated pair meet in the second Riemann sheet below threshold, producing a nonanalyticity—or apparent splitting in two branches—of the sigma mass in terms of M_π. In addition, we confirm that the $\rho(770)$ width decrease, as $\hat{m}$ grows, follows remarkably well the simple expectations of phase space reduction already found within the SU(2) formalism. Once again, such a simple behavior is not observed for the sigma.

Of course, the SU(3) formalism allows us now to study also the $K^*(892)$ and $\kappa(800)$ resonances in πK scattering. We find that both the mass and width of the $K^*(892)$ behave qualitatively and quantitatively in a very similar way to those of the $\rho(770)$, which could be expected given the fact that they belong to the same octet. In addition, we have explicitly calculated here their couplings to two mesons, from the residue of the partial wave at their associated pole, finding that they are both remarkably independent of the nonstrange quark mass, as suggested from the width behavior. The $K^*(892)$ coupling is quite well approximated by a constant, although not so well as in the ρ case. This could be of relevance when computing its width on the lattice as it has already been done for the ρ [23].

It therefore seems that light quark masses play no significant role in the *dynamics* of the dominant decay modes of vector mesons, namely $\rho \to \pi\pi$ and $K^* \to \pi K$, since their couplings seem to be independent of light quark masses and all their width variation can be attributed to the phase space modification due to changes in the masses of all particles.

Furthermore, this provides a hint, checked here by explicit calculation, that the KSRF relation, that approximates these couplings by $g \simeq M_V/2\sqrt{2}f_\pi$, holds to less than 5% when changing $\hat{m}$ from 0 to 9 times its physical value. It is remarkable that this relation is so well satisfied, first, because ours is a one-loop calculation, which, in principle includes higher order pion mass corrections to KSRF, and the pion mass becomes rather large, but, second, because our resonance masses come from unitarized amplitudes whereas f_π stems from the nonunitarized ChPT truncated series.

Concerning the $\kappa(800)$, its behavior is qualitatively similar to that of the sigma, including the apparent mass splitting in two branches, which is a feature that can only occur for scalars. However, the $\kappa(800)$ nonstrange quark mass dependence is softer than for the sigma. Still the pion mass where the $\kappa(800)$ apparent mass splitting occurs is similar to that of the sigma, although with bigger uncertainties $M_\pi \sim 340$–400 MeV. Of course, contrary to the vector case, one could now expect some differences between the two scalars since they do not necessarily belong to the same octet and actually, the sigma is believed to be predominantly the singlet state [27,28], and it could even allow for a glueball component. As we did with the vectors, in this work we have also calculated explicitly the behavior of the scalar couplings to two mesons under quark mass variations. We find a qualitatively similar behavior for both $g_{\sigma\pi\pi}$ and $g_{\kappa\pi K}$: contrary to vectors, they cannot be considered constant within the variation range, particularly when M_π comes close to the apparent mass splitting value, where it suffers a dramatic enhancement.

Finally, since we use the SU(3) formalism, we have been able to study the dependence of light resonance properties on the strange quark mass. Because of the fact that the physical mass of the kaons is already quite high but also because we want the $M_K + M_\eta$ threshold to be significantly above the $K^*(892)$ mass, we have limited our study to the range $0.7 < m_s/m_{s\,\mathrm{phys}} < 1.3$. As could be naively expected, and in contrast to strange resonances, the masses and widths of both the nonstrange ρ and σ are remarkably independent of the strange quark mass. This time, the $\kappa(800)$ mass has a much stronger dependence than that of the $K^*(892)$—actually, it grows a factor of 3 faster. Once again, the $K^*(892)$ width follows remarkably well the behavior dictated by phase space only, and we have checked that its πK coupling is almost independent of m_s. The KSRF relation is also a fairly good approximation in the whole energy range, although not as good as in the case of the nonstrange quark. Concerning the $\kappa(800)$, once again its coupling is strongly dependent on the quark mass, so that its width does not follow the naive phase space behavior.

In summary, we have presented an exhaustive study on the strange and nonstrange quark mass dependence of light scalar and vector resonances appearing in elastic Goldstone bosons scattering. For the future, this work could be extended to other light scalar mesons like the $f_0(980)$ and $a_0(980)$ using a coupled channel formalism, that is somewhat less rigorous as it has no dispersive derivation, and also is much more complicated due to the presence of the $K\bar{K}$ threshold.

To conclude, and apart from the interest for studies of constraints on hadronic properties from cosmological or anthropic considerations, we think that the quark mass dependence studied here will be within the reach of lattice studies in the not too distant future—it is already so for the ρ meson—and we expect our results to be useful in the chiral extrapolation of lattice results to physical values.

ACKNOWLEDGMENTS

We thank C. Hanhart, E. Oset, and G. Ríos for useful discussions, J. A. Oller for suggesting us to include the

KSRF relation in our study, and W. Dunwoodie for providing us with lists of experimental $K\pi$ data. This work was partially supported by the Spanish Ministerio de Educación y Ciencia research Contracts No. FPA2007-29115-E, No. FPA2008-00592, and No. FIS2006-03438, U. Complutense/Banco Santander Grants No. PR34/07-15875-BSCH and No. UCM-BSCH GR58/08 910309. We acknowledge the support of the European Community-Research Infrastructure Integrating Activity Study of Strongly Interacting Matter (acronym HadronPhysics2, Grant Agreement No. 227431) under the Seventh Framework Programme of EU.

[1] S. Aoki *et al.*, Phys. Rev. D **60**, 114508 (1999).
[2] K. F. Liu, Prog. Theor. Phys. Suppl. **168**, 160 (2007); C. McNeile and C. Michael, Phys. Rev. D **74**, 014508 (2006); M. G. Alford and R. L. Jaffe, Nucl. Phys. **B578**, 367 (2000); T. Kunihiro *et al.*, Phys. Rev. D **70**, 034504 (2004).
[3] C. Hanhart, J. R. Pelaez, and G. Rios, Phys. Rev. Lett. **100**, 152001 (2008).
[4] J. Nagata, S. Muroya, and A. Nakamura, Phys. Rev. C **80**, 045203 (2009); S. Prelovsek and D. Mohler, Phys. Rev. D **79**, 014503 (2009).
[5] C. J. Hogan, Rev. Mod. Phys. **72**, 1149 (2000); H. Oberhummer *et al.*, Science **289**, 88 (2000); T. Damour and J. F. Donoghue, Phys. Rev. D **78**, 014014 (2008); T. E. Jeltema and M. Sher, Phys. Rev. D **61**, 017301 (1999).
[6] J. K. Webb *et al.*, Phys. Rev. Lett. **82**, 884 (1999); V. V. Flambaum and E. V. Shuryak, Phys. Rev. D **67**, 083507 (2003); **65**, 103503 (2002).
[7] J. Gasser and H. Leutwyler, Nucl. Phys. **B250**, 465 (1985).
[8] G. Amoros, J. Bijnens, and P. Talavera, Nucl. Phys. **B602**, 87 (2001).
[9] P. Buettiker, S. Descotes-Genon, and B. Moussallam, Eur. Phys. J. C **33**, 409 (2004); S. Descotes-Genon and B. Moussallam, Eur. Phys. J. C **48**, 553 (2006).
[10] J. R. Pelaez, Mod. Phys. Lett. A **19**, 2879 (2004).
[11] V. Bernard, N. Kaiser, and U. G. Meissner, Phys. Rev. D **43**, R2757 (1991); Nucl. Phys. **B357**, 129 (1991); Phys. Rev. D **44**, 3698 (1991).
[12] A. Gomez Nicola and J. R. Pelaez, Phys. Rev. D **65**, 054009 (2002).
[13] T. N. Truong, Phys. Rev. Lett. **61**, 2526 (1988); **67**, 2260 (1991); A. Dobado *et al.*, Phys. Lett. B **235**, 134 (1990).
[14] A. Dobado and J. R. Peláez, Phys. Rev. D **47**, 4883 (1993); **56**, 3057 (1997).
[15] J. A. Oller and E. Oset, Nucl. Phys. **A620**, 438 (1997); **652**, 407(E) (1999).
[16] J. A. Oller, E. Oset, and J. R. Pelaez, Phys. Rev. Lett. **80**, 3452 (1998); Phys. Rev. D **59**, 074001 (1999); **62**, 114017 (2000); F. Guerrero and J. A. Oller, Nucl. Phys. **B537**, 459 (1999); **B602**, 641(E) (2001).
[17] A. Gomez Nicola, J. R. Pelaez, and G. Rios, Phys. Rev. D **77**, 056006 (2008).
[18] S. D. Protopopescu *et al.*, Phys. Rev. D **7**, 1279 (1973); P. Estabrooks and A. D. Martin, Nucl. Phys. **B79**, 301 (1974); G. Grayer *et al.*, Nucl. Phys. **B75**, 189 (1974); C. D. Froggatt and J. L. Petersen, Nucl. Phys. **B129**, 89 (1977); W. Hoogland *et al.*, Nucl. Phys. **B126**, 109 (1977); M. J. Losty *et al.*, Nucl. Phys. **B69**, 185 (1974); N. B. Durusoy *et al.*, Phys. Lett. **45B**, 517 (1973); P. Estabrooks, R. K. Carnegie, A. D. Martin, W. M. Dunwoodie, T. A. Lasinski, and D. W. G. Leith, Nucl. Phys. **B133**, 490 (1978); D. Aston *et al.*, Nucl. Phys. **B296**, 493 (1988); D. Linglin *et al.*, Nucl. Phys. **B57**, 64 (1973); L. Rosselet *et al.*, Phys. Rev. D **15**, 574 (1977); S. Pislak *et al.* (BNL-E865 Collaboration), Phys. Rev. Lett. **87**, 221801 (2001); P. Truoel, arXiv:hep-ex/0012012.
[19] S. R. Beane *et al.* (NPLQCD Collaboration), Phys. Rev. D **77**, 094507 (2008); **77**, 014505 (2008); **74**, 114503 (2006); Ph. Boucaud *et al.* (ETM Collaboration), Comput. Phys. Commun. **179**, 695 (2008).
[20] R. Kaminski, J. R. Pelaez, and F. J. Yndurain, Phys. Rev. D **77**, 054015 (2008).
[21] P. C. Bruns and U.-G. Meißner, Eur. Phys. J. C **40**, 97 (2005).
[22] P. Gerber and H. Leutwyler, Nucl. Phys. **B321**, 387 (1989); A. Nyffeler, Z. Phys. C **60**, 159 (1993); A. Dobado and J. R. Pelaez, Phys. Rev. D **59**, 034004 (1998).
[23] S. Aoki *et al.* (CP-PACS Collaboration), Phys. Rev. D **76**, 094506 (2007).
[24] K. Kawarabayashi and M. Suzuki, Phys. Rev. Lett. **16**, 255 (1966); Riazuddin and Fayyazuddin, Phys. Rev. **147**, 1071 (1966).
[25] I. Caprini, G. Colangelo, and H. Leutwyler, Phys. Rev. Lett. **96**, 132001 (2006); F. J. Yndurain, R. Garcia-Martin, and J. R. Pelaez, Phys. Rev. D **76**, 074034 (2007); R. Kaminski, R. Garcia-Martin, P. Grynkiewicz, and J. R. Pelaez, Nucl. Phys. B, Proc. Suppl. **186**, 318 (2009).
[26] C. Amsler *et al.* (Particle Data Group), Phys. Lett. B **667**, 1 (2008).
[27] D. Black, A. H. Fariborz, F. Sannino, and J. Schechter, Phys. Rev. D **59**, 074026 (1999).
[28] J. A. Oller, Nucl. Phys. **A727**, 353 (2003).
[29] R. Kaminski, G. Mennessier, and S. Narison, Phys. Lett. B **680**, 148 (2009).
[30] S. Weinberg, Phys. Rev. **130**, 776 (1963); V. Baru, J. Haidenbauer, C. Hanhart, Yu. Kalashnikova, and A. E. Kudryavtsev, Phys. Lett. B **586**, 53 (2004).
[31] D. Gamermann, J. Nieves, E. Oset, and E. R. Arriola, Phys. Rev. D **81**, 014029 (2010).

2.1.3 Publication: J. Nebreda, J. R. Pelaez, G. Rios, **Chiral extrapolation of pion-pion scattering phase shifts within standard and unitarized ChPT,** Phys. Rev. D83, 094011 (2011)

PHYSICAL REVIEW D **83,** 094011 (2011)

Chiral extrapolation of pion-pion scattering phase shifts within standard and unitarized Chiral Perturbation Theory

J. Nebreda, J. R. Peláez, and G. Ríos

Departamento de Física Teórica II. Universidad Complutense, 28040, Madrid. Spain
(Received 27 December 2010; revised manuscript received 29 March 2011; published 11 May 2011)

We calculate the pion-pion elastic scattering phase shifts for pion masses from the chiral limit to values of interest for lattice studies. At low energies, we use the standard Chiral Perturbation Theory expressions to one and two loops. In addition, we study the phase shifts' mass dependence in the resonance region by means of dispersion theory in the form of unitarized Chiral Perturbation Theory and the inverse amplitude method. We pay particular attention to the case when resonances are close to threshold, illustrating the different behavior between scalar and vector resonances. We also provide the estimation of uncertainties, which are dominated by those of the $O(p^6)$ chiral parameters.

DOI: 10.1103/PhysRevD.83.094011 PACS numbers: 14.40.Be, 12.39.Fe, 13.75.Lb

I. INTRODUCTION

Elastic pion-pion scattering has been an object of study for many decades due to several reasons. In particular, pions are very relevant in the description of final states in other hadronic processes. Also, the two-pion correlated exchange in the scalar-isoscalar channel is the main contribution to nucleon-nucleon attraction, and has been interpreted for long as a scalar ''sigma'' resonance [1] whose existence, mass, and width have been the subject of an intense debate. Actually, this resonance, nowadays called $f_0(600)$, appears as a pole deep in the second Riemann sheet of the scattering amplitude (see the ''Note on scalar mesons'' in [2] for a detailed account). Finally, the pion-pion interaction at low energies is also relevant for the determination of light quark mass ratios and the size of the chiral condensate [3].

On the theory side, unfortunately, neither the elastic resonance region nor the low-energy region are accessible to perturbative QCD calculations. In order to describe these processes in terms of quarks and gluons, one should rely on lattice techniques. For a long time, these techniques have found little applications in this low-energy realm due to complications on the implementation of chiral symmetry, the small physical values of the light quarks and other technicalities as the existence of quarkline disconnected diagrams in some channels. However, very recently, lattice results have become available for the $\rho(770)$ and $f_0(600)$ resonance masses [4–8], the pion decay constant, or even the isospin 2 scattering length [9,10], obtained with pion masses which are not too far from the physical values. Recent developments [11] in algorithms may make disconnected diagrams for multihadron calculations tractable in the not too distant future. This means that pion-pion scattering phase-shifts might be calculable soon within lattice-QCD. Actually, some first results for the isospin 2 waves have been obtained for still somewhat large pion masses [12,13]. Of course, lattice calculations still have systematic uncertainties which are hard to estimate and they always rely on modified actions, finite volumes, and other complications so that their physical results are actually extrapolations to the physical limit. It is, therefore, necessary to understand how these chiral or physical extrapolations should be carried out.

Fortunately, even though we cannot rely on perturbative QCD at low energies, we can still use its effective low-energy theory, known as Chiral Perturbation Theory (ChPT) [14], which provides a rigorous, systematic and model independent expansion of hadronic observables in terms of the external meson momenta and the relatively small pion mass. We will very briefly review ChPT in Sec. II, mostly to introduce the required notation.

Within ChPT, the quark mass dependence appears in a model independent way through the pion mass squared, which is also described as an expansion. Remarkably, the isospin $I = 2$ scattering length m_π dependence found on the lattice is rather well described by just leading order ChPT up to surprisingly large pion masses [9,10], and the one-loop corrections seem to be rather small. In this work we will first study the evolution of the lowest five pion-pion scattering phase-shifts, with definite isospin and angular momentum $(I, J) = (0, 0))$, (1,1), (2,0), (0, 2), and (2, 2), using the one and two-loop standard ChPT expressions, estimating the uncertainties due to the relatively poor knowledge of the low-energy constants—particularly those at two loops. Of course, this approach is limited to low masses and momenta and cannot be used to describe resonances, although, in principle it should be able to describe their low-energy tails, through, for instance, the low-energy scattering phase-shifts. This is the reason why one of the aims of this work is to study the evolution of all $\pi\pi$ scattering phase-shifts at low-energy within standard ChPT.

Beyond the low-energy regime, it is still possible to obtain the quark mass dependence of hadronic observables, by combining ChPT with dispersion relations. Thus, in Sec. V, we briefly review the inverse amplitude method (IAM) [15–17], obtained by using the elastic

approximation together with ChPT, to calculate the subtraction constants and the left cut contribution of a dispersion relation for the inverse of the partial waves. This technique provides a description of meson-meson scattering which is simultaneously compatible with the ChPT low-energy description but also generates the lightest elastic resonance on each channel. By applying this technique to the $\pi\pi$ scattering amplitude to one-loop in SU(2) ChPT, some of us have calculated the pion mass dependence of the $\rho(770)$ and $f_0(600)$ masses and widths [18]. Interestingly, this method had already been applied to study only the $f_0(600)$ quark mass dependence and its influence, through the nucleon-nucleon interaction, on the production of carbon and oxygen and its anthropic implications [19]. Recently [20], some of us have also calculated the $\kappa(800)$ and $K^*(892)$ mass and width dependence with respect to the non strange-quark mass, as well as the dependence of all these four resonances with respect to the strange-quark mass. And even more recently [21], we have extended to two loops the analysis of the $\rho(770)$ and $f_0(600)$ resonances within unitarized elastic $\pi\pi$ scattering.

The IAM results for the m_π dependence of the $\rho(770)$ agree nicely with the estimations for the two first coefficients of its chiral expansion [22], and also with the existing lattice results [4–8]. The comparison with lattice is relatively straightforward in this case since the $\rho(770)$ is not extremely wide and it is actually calculated as a state of the spectrum.

Unfortunately, the comparison of the IAM with lattice results will not be so straightforward for the scalar channels. First, we find of particular interest the repulsive $I = 2$ channels. Note that these channels have no resonances, so that neither the spectroscopic studies on the lattice nor our pole studies with the IAM [18,20,21] address this case. However, this is the simplest channel for scattering lattice studies and, as commented above, there are already some lattice results for the scattering length down to relatively low pion masses [9,10] and for phase-shifts but only for $m_\pi \simeq 400$ MeV or higher [12,13].

Second, we are also interested in the much debated isoscalar channel. Of course, given the status of the σ or $f_0(600)$, reliable lattice results would be most welcome. Unfortunately, lattice calculations in this channel are hard due to disconnected diagrams, but also their interpretation would be complicated because this resonance is extremely wide (see [2] and references therein). In addition, it was shown in [18,20] that, for sufficiently high masses, the $f_0(600)$, being a scalar, becomes a virtual state—a pole in the second Riemann sheet below threshold—which is not a physical state of the spectrum. Therefore, since spectroscopic (or ''pole'') lattice studies of the σ may be rather complicated, a study of the scalar phase shift, as the one presented here, deserves more interest.

These are the motivations to study the chiral extrapolation of phase shifts either from standard or unitarized ChPT. This will be done first for standard ChPT to next to leading order (NLO) in Sec. III A, and then to next to next to leading order (NNLO) in Sec. III B. Surprisingly, in both cases, the predicted behavior for the phase shift in the $\rho(770)$ may look counterintuitive when compared with present lattice calculations of the $\rho(770)$ mass m_π dependence. This discussion deserves a separate section, in which we also evaluate the pion mass dependence of the ''size'' of the $\rho(770)$. Next, we will present the IAM results for NLO ChPT in Sec. VI A and for NNLO in Sec. VI B. We will discuss and summarize all our findings in Sec. VIII.

II. CHIRAL PERTURBATION THEORY

Pions are the Goldstone bosons associated to the spontaneous chiral symmetry breaking of QCD. If quarks were strictly massless, pions would be massless too and separated by a gap of the order of 1 GeV from the rest of hadrons, becoming the relevant QCD low-energy degrees of freedom. Chiral Perturbation Theory (ChPT) [14] is nothing but the most general Lagrangian built out as an expansion in pion momenta (i.e., derivatives) respecting the QCD symmetries. In real life, though, the u and d quarks have a very small mass, that we will take in the isospin limit as $\hat{m} = (m_u + m_d)/2$, which can be treated as a perturbation within ChPT. As a consequence, pions have a physical mass of $m_\pi = 139.57$ MeV, whose model independent perturbative expansion in terms of $\hat{m}$ is given by ChPT. In summary, the QCD low-energy theory we will use is SU(2) ChPT [14], which corresponds to considering the u and d quarks only and integrating out the other four quarks, whose effect will be included in the low-energy constants (LECs) that multiply each term of the ChPT Lagrangian. In this way, only pions will circulate in the loops. Hence, by varying the pion mass while keeping the ChPT low-energy constants fixed, we are sensitive to the light quark mass dependence for constant s, c, b and t masses.

Perturbative $\pi\pi$ scattering within ChPT

Pion-pion elastic scattering is customarily described in terms of partial wave amplitudes $t_J^{(I)}(s)$ of definite isospin I and angular momentum J, where s is the Mandelstam variable, although for simplicity we will drop these indices when there is no possible confusion. From ChPT, these partial waves are obtained as a series expansion $t = t_2 + t_4 + t_6 \cdots$, with $t_k = O(p/4\pi f_\pi)^k$, where p stands generically for center of mass momenta or pion masses. The leading order (LO) t_2 is $O(p^2)$ and is universal [23] in the sense that it only depends on the scale $f_\pi \simeq 92.4$ MeV and m_π. The NLO calculation yields t_4 [14] and is obtained from one-loop diagrams with LO vertices and tree diagrams from the NLO Lagrangian terms, which are multiplied by some low-energy constants (LECs), called $l_i^r(\mu)$. These LECs absorb the dependence

TABLE I. ChPT low-energy constants from [24] that contribute to $\pi\pi$ scattering to $O(p^4)$ and $O(p^6)$ that we use in our standard ChPT calculations. The value for $l_3^r(\mu)$ comes from a recent analysis of the lattice results [25]. The renormalization scale is set to $\mu = 770$ MeV. Errors are only statistical or "only account for the noise seen in the calculations" of [24]. The first four r_i and their uncertainties are obtained from resonance saturation. The $r_f^r(\mu)$ value is from [26].

$O(p^4)$	LECs ($\times 10^{-3}$)	$O(p^6)$	LECs ($\times 10^{-4}$)
$l_1^r(\mu)$	-3.98 ± 0.62	$r_1^r(\mu)$	-0.60 ± 0.35
$l_2^r(\mu)$	1.89 ± 0.23	$r_2^r(\mu)$	1.28 ± 0.74
$l_3^r(\mu)$	0.18 ± 1.11	$r_3^r(\mu)$	-1.68 ± 0.97
$l_4^r(\mu)$	6.17 ± 1.39	$r_4^r(\mu)$	-1.00 ± 0.58
		$r_5^r(\mu)$	1.52 ± 0.42
		$r_6^r(\mu)$	0.40 ± 0.04
		$r_f^r(\mu)$	0.00 ± 1.20

on the loop regularization scale μ, and are determined by the underlying QCD dynamics. Their measured values can be found in Table I. Something similar happens with the NNLO result t_6 [27], which has two-loop contributions with LO vertices, one-loop contributions with one LO vertex and one NLO vertex containing some l_i, plus tree level diagrams with NNLO vertices, whose LECs appear only in six combinations now called $r_i^r(\mu)$, whose estimated values are listed also in Table I. All these LECs carry a scale dependence that cancels that from loop integrals, so that observables are scale independent and finite order by order.

Let us remark that we write the $\pi\pi$ scattering amplitude in terms of the physical constants m_π and f_π, which are obtained as expansions in powers of the LO pion mass. Actually, l_3 and l_4 appear at NLO in $\pi\pi$ scattering through these m_π and f_π expansions, but in contributions that depend stronger on the pion mass and softer on the energy than those containing the other LECs. Thus, l_3 and l_4 are harder to determine experimentally and have the largest uncertainty. This is particularly severe for l_3, and that is why we have used its lattice determination [25] quoted in Table I.

At NNLO, the expansion of f_π on the physical pion mass [28] requires an additional parameter r_f, also listed in Table I. Note that there is an additional $O(p^6)$ constant, r_M, which appears in the NNLO chiral expansion of the physical pion mass m_π in powers of the quark mass $\hat{m}$, but such a constant would only be needed in order to study the quark mass dependence of observables. However, quark masses carry some renormalization scale and scheme dependence and most lattice results provide their results in terms of the physical pion mass. That is why here we will study the dependence of scattering phases on the physical pion mass and not on the quark mass. Therefore, we do not need r_M.

We show in Table I the estimated statistical uncertainties of the LECs (for r_5, r_6 they are described as the noise in the dispersive calculation of [24]). Systematic uncertainties are large and harder to estimate; for illustration, we also provide in Table II other values found in the literature at $O(p^4)$ and $O(p^6)$. We consider the spread on these values as a crude indication of the size of systematic uncertainties. From the sets in [30] we note that, even for the same analysis, the values of the $O(p^4)$ LECs can be somewhat different whether they are obtained from a pure $O(p^4)$ calculation or including the $O(p^6)$ corrections. Hence, it should not come as a surprise later that the $O(p^6)$ values obtained from a unitarized fit, which includes part of the higher order corrections, may also come out somewhat different from the values obtained in a pure ChPT $O(p^6)$ analysis.

As a final comment concerning ChPT parameters, it is possible and usual to write the NNLO $\pi\pi$ scattering amplitude in terms of just six parameters $b_1, \ldots, b_6$, multiplying each one of the energy dependent polynomials allowed by Lorentz invariance and chiral symmetry. Thus, the knowledge of 6 constants is enough to describe $\pi\pi$ scattering to that order. However, these b_i parameters do carry a dependence on m_π and the full knowledge of all the l_i and r_i constants is needed to extrapolate to unphysical values of m_π, which is the object of this work, and the reason why we need to determine 11 parameters instead of just six.

TABLE II. Samples of other sets of LECs: First row: SU(3) analysis of πK scattering using Roy-Steiner equations. Second and third rows: K_{l4} analysis to $O(p^4)$ and $O(p^6)$, respectively. Naively, we have combined quadratically the SU(3) LECs errors there. Fourth row: Roy equations analysis. Uncertainties from imaginary parts and unknown $O(p^6)$ LECs combined quadratically. Last row, values used in [18] with the one-loop IAM. All LECs are evaluated at the scale $\mu = 770$ MeV.

Analysis	$10^3 l_1^r$	$10^3 l_2^r$	$10^3 l_3^r$	$10^3 l_4^r$
ChPT $O(p^4)$ [29]	-4.9 ± 0.6	5.2 ± 0.1		17 ± 10
ChPT $O(p^4)$ [30]	-4.5	5.9	2.1	5.7
ChPT $O(p^6)$ [30]	-3.3 ± 2.5	2.8 ± 1.1	1.2 ± 1.7	3.5 ± 0.6
ChPT $O(p^6)$ [31]	-4.0 ± 2.1	1.6 ± 1.0		
IAM $O(p^4)$ [18]	-3.7 ± 0.2	5.0 ± 0.4	0.8 ± 3.8	6.2 ± 5.7

Now, elastic unitarity implies for partial waves, at physical values of s, that:

$$\mathrm{Im}\, t(s) = \sigma(s)|t(s)|^2 \Rightarrow \mathrm{Im}1/t(s) = -\sigma(s), \quad (1)$$

where $\sigma(s) = 2p/\sqrt{s}$, p being the center of mass momentum. As a consequence, the modulus of $t(s)$ is related to its phase:

$$t(s) = |t(s)|e^{i\delta(s)} = e^{i\delta(s)} \sin\delta(s)/\sigma(s). \quad (2)$$

This ''phase-shift'' $\delta(s)$, which determines completely the amplitude, is the usual way to parametrize partial waves that we will use next to predict the amplitude variation when the pion mass is changed. Of course, before extrapolating to other pion masses, we will compare the ChPT amplitudes, with and without unitarization, with the existing experimental data.

ChPT amplitudes, being an expansion, satisfy unitarity only perturbatively:

$$\mathrm{Im}\, t_2 = 0, \quad \mathrm{Im}t_4 = \sigma|t_2|^2, \quad \mathrm{Im}t_6 = 2t_2\,\mathrm{Re}t_4 \ldots. \quad (3)$$

In particular, ChPT partial waves are expected to violate unitarity as s increases, since they are basically polynomials in s. In Sec. V, we will use ChPT inside dispersion relations to obtain amplitudes that, while respecting the ChPT expansion at low energies, satisfy unitarity and allow and provide a good description of experiment up to higher energies.

After this brief introduction to ChPT and its notation, we are now ready to present our first calculations.

III. RESULTS WITHIN STANDARD CHPT

Using the equations above, the phase shift within standard ChPT is obtained as a series expansion (see [32] for a prescription on how to perform this expansion):

$$\begin{aligned} \delta &= \sigma(t_2 + \mathrm{Re}t_4) + O(p^6), \\ \delta &= \sigma(t_2 + \mathrm{Re}t_4 + \mathrm{Re}t_6) + \frac{2}{3}(\sigma t_2)^3 + O(p^8), \end{aligned} \quad (4)$$

which are the expressions used in our one-loop and two-loop calculations, respectively, that we detail next.

Now, let us recall that the pion—and quark—mass dependence of the partial waves $t(s)$ within ChPT comes from two different sources: from kinematics, through pion propagators, or from the dynamics encoded in the vertices. In particular, the threshold shift is purely of a kinematic nature and rather trivial to understand. Therefore, although $\pi\pi$ phase shifts are customarily presented in terms of $\sqrt{s}$, we are showing them here as a function of the center of mass momentum p, which is also more convenient to compare to lattice studies. With this kinematic threshold effect ''subtracted'', the remaining m_π dependence is rather mild for most partial waves. As we will see, this soft dependence of the $\delta_{IJ}(p)$ on m_π has been also found for $I = 2$ waves in very recent lattice calculations [12].

A. One-loop ChPT

In Fig. 1 we show the phase shifts from the one-loop ChPT, i.e. $O(p^4)$, for the $(I, J) = (0, 0)$, (2, 0), (1, 1) $\pi\pi$ scattering waves. Note that for the (1, 1) channel, the description fails much before $p \simeq 300$ MeV. This momentum is typically below the $\rho(770)$ resonance region, which is a natural applicability bound for the ChPT series. This resonance has a relatively narrow shape, corresponding to a pole close to the real axis in the second Riemann sheet, which, of course, is completely missed by one-loop ChPT except in its very low-energy tail. In contrast, one-loop ChPT is giving a fairly good description of the (0, 0) channel even up to, say $p = 350$ or 400 MeV. In this case, there is also a resonance—the scalar σ (or $f_0(600)$)— but it is very wide and its pole is deep in the complex plane, so that it is not seen in the real axis as the typical sharp rise in the phase. For this reason, and despite being an expansion which has no such a pole in the complex plane, ChPT results are not very different qualitatively from the data in this channel. Finally, we see that the one-loop description of the (2, 0) channel is also reasonably good up to such high momentum, mostly due to the fact that this channel has no resonances and also that the data are not particularly precise.

The gray areas in the figure cover the uncertainties due to the statistical error in the LECs detailed in the previous section. In order to calculate these areas we have used a Monte Carlo sampling. For each phase-shift calculation we have generated 5000 different samples of LECs using a Gaussian distribution with variances equal to the errors quoted in Table I. To avoid a confusing overlapping between uncertainty bands, we only show the one corresponding to the physical pion mass. In the appendix we provide a detailed study of the evolution of these uncertainties with m_π. As a general feature for both scalar and vector waves, the relative uncertainty of the phase at a given momentum grows slowly with m_π.

Once we have checked where one-loop ChPT calculations provide an acceptable description of data, we can now compare, also in Fig. 1, with the results obtained if we change the pion mass from its physical value to $m_\pi = 230$, 300 and 350 MeV. The first observation is that the sign of the phase derivative does not change when increasing the pion mass, at least up to 350 MeV, which means that the attractive or repulsive nature of each wave is conserved.

In that figure, we have represented with an arrow the direction of the phase movement as m_π increases. Thus, the next observation is that both scalar phase shifts increase in absolute value as m_π grows, whereas the phase of the vector channel decreases.

The behavior of the phase at low momentum in the vector channel may seem surprising at first, because

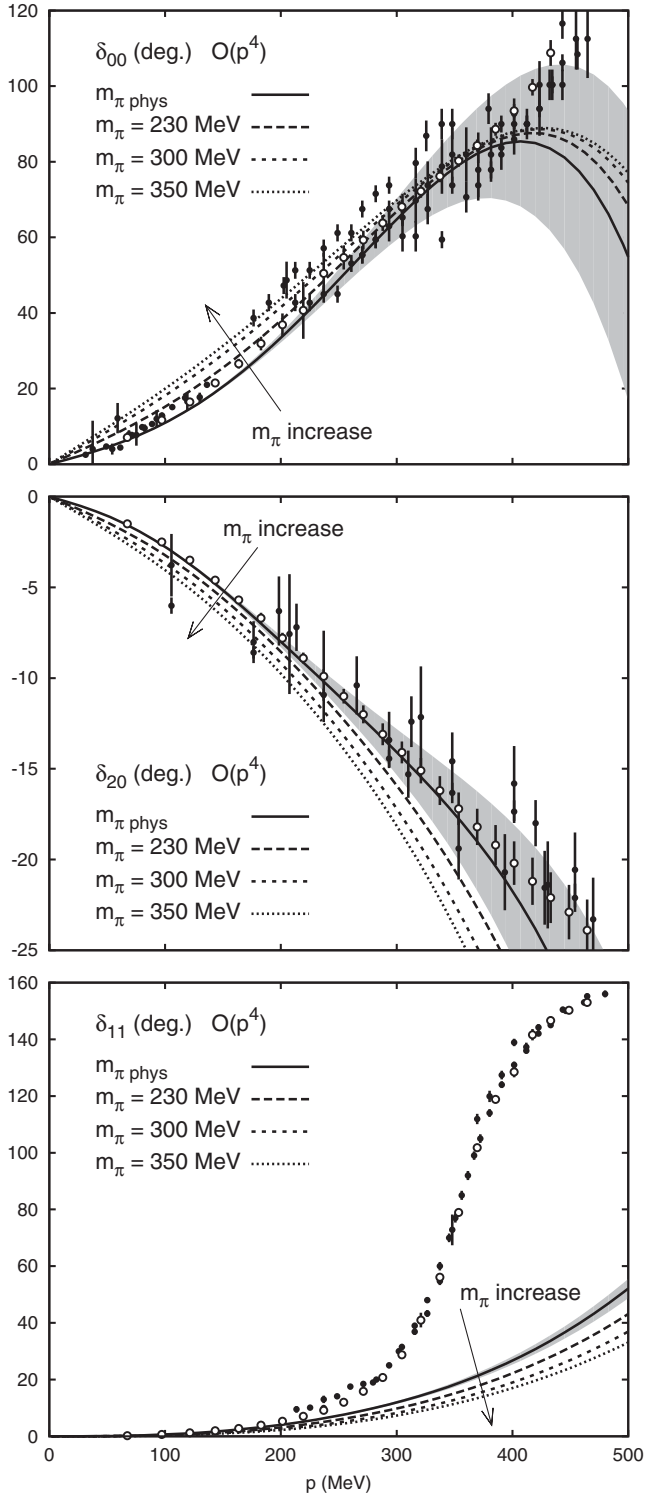

FIG. 1. S and P wave $\pi\pi$ phase shifts from standard ChPT up to one loop. Different lines stand for different pion masses $m_\pi = 139.57$, 230, 300 and 350 MeV, respectively. Since the lines are too close to each other, we only show error bands for the physical mass. Experimental data come from [33] (black circles) and the precise model independent dispersive data analysis from [34] (white circles). The arrows show the direction of increasing m_π.

several lattice works [4–8], the chiral effective treatment [22], as well as the IAM [18], predict that the $\rho(770)$ mass increases much slower than the 2π threshold as m_π grows. But then, when the $\rho(770)$ peak reaches a given momentum, the phase there should be $\pi/2$ to a very good approximation. Therefore, one would expect naively the phase at low momentum to rise as m_π grows. However, the model independent ChPT analysis tells us otherwise. We will see in detail in Sec. IV why this intuitive picture fails and the phase shift actually has to decrease at first and increase later on.

Finally, in Fig. 2, we show the one-loop ChPT results for the D waves: $(I, J) = (0, 2)$ and $(2, 2)$. We show these separately because both of them vanish at $O(p^2)$, so that the one-loop $O(p^4)$ calculation is just their LO contribution. Actually, they are both very small at low energies.

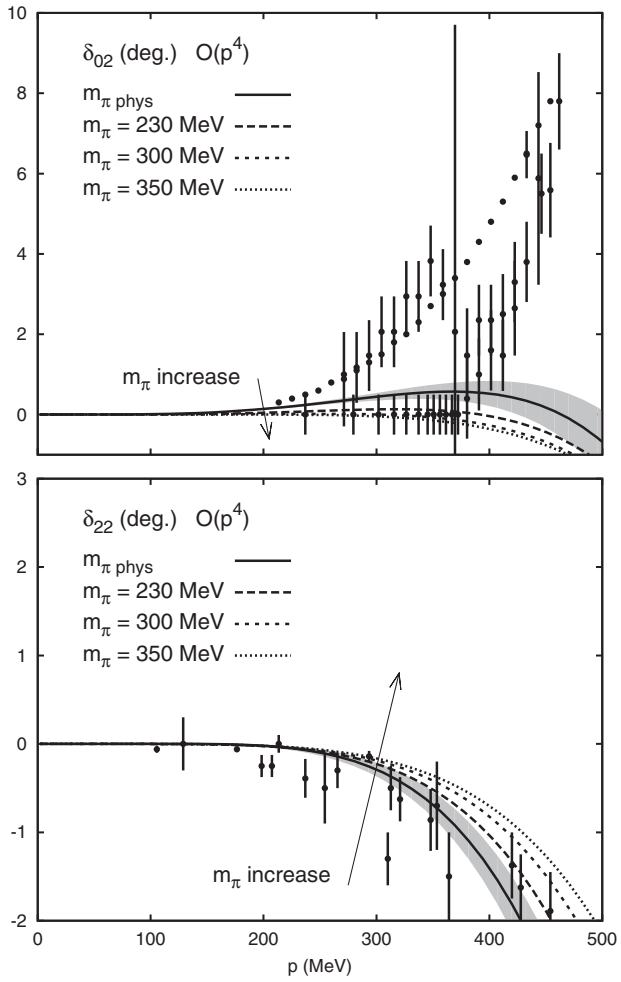

FIG. 2. D wave $\pi\pi$ phase shifts from standard ChPT up to one loop. Different lines stand for different pion masses $m_\pi = 139.57$, 230, 300 and 350 MeV, respectively. Since the lines are too close to each other, we only show error bands for the physical mass. Experimental data come from [33]. The arrows show the direction of increasing m_π.

We can see in the figures that the one-loop ChPT calculation provides an acceptable solution for the (2, 2) wave up to relatively high momentum, but obviously it cannot reproduce the resonance shape of the $f_2(1270)$ resonance in the (0, 2) channel. As before, we only show the uncertainty band due to the statistical errors on the LECs for the physical pion mass, obtained again from a Monte Carlo Gaussian sample. Relative uncertainties for different pion masses are detailed in the appendix.

Note that, in contrast to the scalar waves, both tensor phase shifts decrease in absolute value as the pion mass increases not too far from its physical value. In this sense, they are more similar to the vector channel behavior. Remarkably, for larger pion masses and momentum the (0, 2) phase shift even changes sign and the derivative becomes negative. However, this behavior is not found at two loops, as we will see in the next subsection.

B. Two-loop ChPT

We use the two-loop $\pi\pi$ scattering calculation in [27]. Note, however, that instead of the usual $b_1 \ldots b_6$ parameters, in order to implement the m_π dependence we need to use the one-loop $l_1 \ldots l_4$ and r_i parameters in Table I. In Fig. 3 we show the resulting phase shifts for the $(I, J) = (0, 0)$, (1, 1), and (2, 0) waves for the physical m_π but also for $m_\pi = 230$, 300, and 350 MeV.

The uncertainty bands, which we show only for the physical pion mass—see the appendix for other masses—are once again calculated with a Monte Carlo Gaussian sampling of 5000 sets of LECs, using as standard deviations the uncertainties quoted in Table I. The only exception are the $r_{1\ldots4}$ parameters, which are estimated from resonance saturation and, as in [24], we have assumed that all values in the interval from 0 to twice the estimation are equally likely. Of course, we want to emphasize that this is just an estimate of the values of the $O(p^6)$ parameters, which are rather difficult to determine. Possible improvements in their determinations could come from future lattice-QCD calculations, as it has already been done with the $O(p^4)$ LECs (see [25] for a review) or from the use of recent dispesive data analysis like that in [34] inside threshold parameter sum rules [35].

Also, since the renormalization scale μ where the estimates for $r_{1\ldots4}$ and r_f apply is not known, another source of uncertainty appears. Our calculations are made at $\mu = 770$ MeV so, in order to account for the uncertainty due to that choice, we have followed [24] again and we have calculated the shift occurring in the phase shift if $r_{1\ldots4}$ are fixed and the scale is changed to $\mu = 500$ MeV and $\mu = 1$ GeV. That shift is added in quadrature to the errors given by the Monte Carlo sampling.

The general features of the one-loop description still apply to the two-loop case. Namely, all waves keep their attractive or repulsive nature, and both scalar phases increase in absolute value as m_π grows, whereas the vector

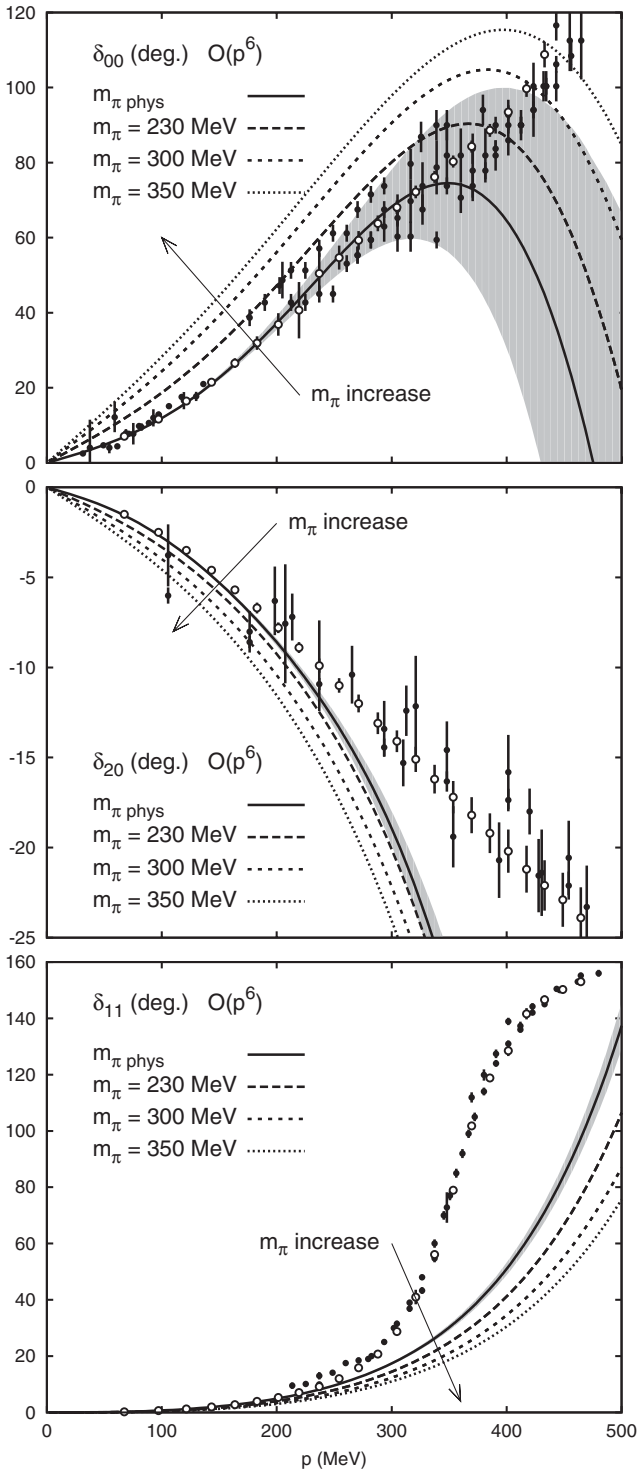

FIG. 3. S and P wave $\pi\pi$ phase shifts from standard ChPT up to two loops. Different lines stand for different pion masses: continuous, long dashed, short dashed and dotted for $M_\pi = 139.57$, 230, 300 and 350 MeV, respectively. Since the lines are too close to each other, we only show error bands for the physical mass. Experimental data (black circles) come from [33] and the precise model independent dispersive data analysis from [34] (white circles). The arrows show the direction of increasing m_π.

channel phase decreases. The counterintuitive behavior of the $\rho(770)$ is therefore a robust prediction of ChPT. In the next section, we will explain with a simple model why chiral symmetry requires this behavior. Still, the description of the (0,0) wave is fair only up to $p = 300$ or 350 MeV, although it has improved remarkably in the low-energy region, where the data are most recent and reliable, as they come from $K_{\ell 4}$ decays. The (1, 1) phase is now much closer to the experimental data, and thus it seems to provide a fairly good representation up to, say $p = 200$ MeV. However, the description of the (2, 0) has deteriorated for higher momenta, and seems to be good only up to, roughly, 200 or 250 MeV.

However, despite the qualitative m_π dependence being similar to the one-loop case, quantitatively the effect is stronger. In absolute value all S-wave phase shifts grow faster with m_π to two loops than they did to one loop.

In Fig. 4, we show the two-loop result for the D waves. As commented before, these waves have no $O(p^2)$ term, so, this $O(p^6)$ calculation is just a next to leading order calculation. We can see that the differences with the one-loop case are dramatic. The $(I, J) = (0, 2)$ phase suffers a remarkable improvement, being able to describe the tail of the $f_2(1275)$ resonance up to momentum of the order of 450 MeV. Contrary to the one-loop case, within the m_π range of this study, the (0, 2) phase does not become negative. Finally, the (2, 2) phase shift fails to describe even the sign of the data, and is only relatively close to the data points below 150 MeV. Furthermore, the one-loop m_π phase-shift dependence was opposite to the two-loop case: from more negative to less negative for the former versus from positive to negative for the second. The predictions for this channel are therefore not very robust, which is also corroborated by the large uncertainties for higher m_π that can be found in the appendix.

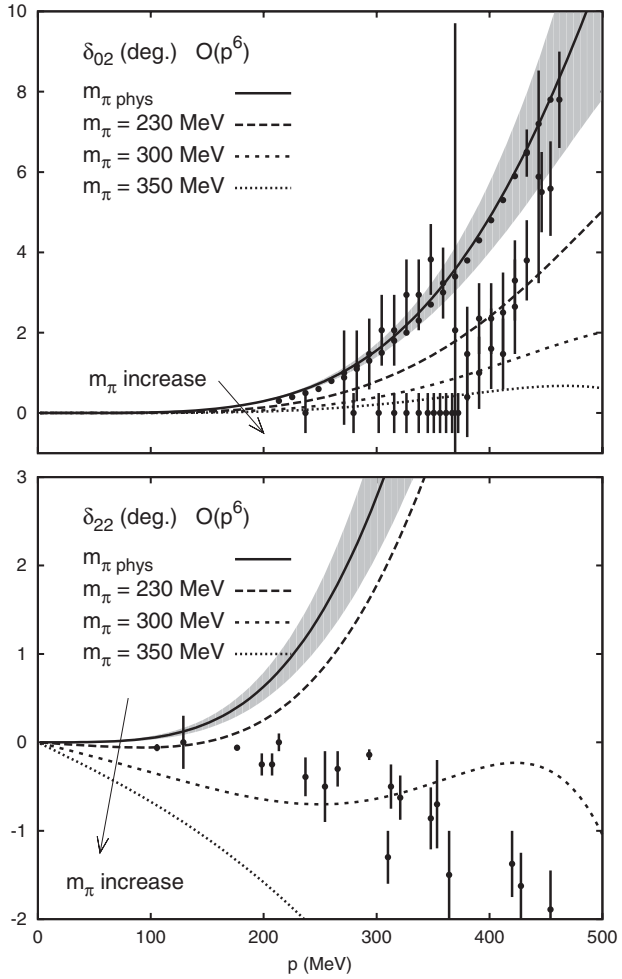

FIG. 4. D wave $\pi\pi$ phase shifts from standard ChPT up to two loops. Different lines stand for different pion masses: continuous, long dashed, short dashed and dotted for $m_\pi = 139.57$, 230, 300 and 350 MeV, respectively. Since the lines are too close to each other, we only show error bands for the physical mass. Experimental data (black circles) come from [33]. The arrows show the direction of increasing m_π.

C. Comparison with lattice results for $I = 2$ and $m_\pi > 350$ MeV

As we have already commented, there are very recent lattice results on phase shifts for the $I = 2$, $J = 0$ [12,13] and $J = 2$ channels [12]. In Figs. 5 and 6 we compare the one and two-loop calculations within standard ChPT, first for the physical mass versus experimental data, and then for $m_\pi = 396$, 420, 444, and 524 MeV, versus lattice results.

When we examine Fig. 5, corresponding to the $I = 2$, $J = 0$ phase shifts, the first observation is that all lattice points with $p < 200$ MeV are well described within the uncertainties of one-loop ChPT, even up to $m_\pi = 444$ MeV. From the figure, we observe that a pion mass of 524 MeV seems out of reach and will not be considered any longer. Beyond that momentum, the ChPT calculation bends downwards and misses all other lattice results with higher momenta. Remarkably, the two-loop ChPT results do not improve this agreement. Actually, the two-loop calculation describes somewhat worse the lattice data and seems to move consistently to more negative values than those observed on the lattice, as m_π grows higher. Let us remark that the curvature downwards is larger in the two-loop result than just to one loop. In view of the figures it seems that the standard ChPT applicability limit is, at best, somewhere around $p \simeq 150$–200 MeV, up to m_π of the order of 400–440 MeV.

Unfortunately, for the $I = 2$, $J = 2$ channel, shown in Fig. 6, there are no lattice results available at low momentum. Surprisingly, the one-loop calculation agrees quite nicely with the lattice values up to around $p \simeq 500$ MeV, even for the highest pion mass. However, the two-loop results show a very strong m_π dependence that is in complete disagreement with the behavior predicted by the

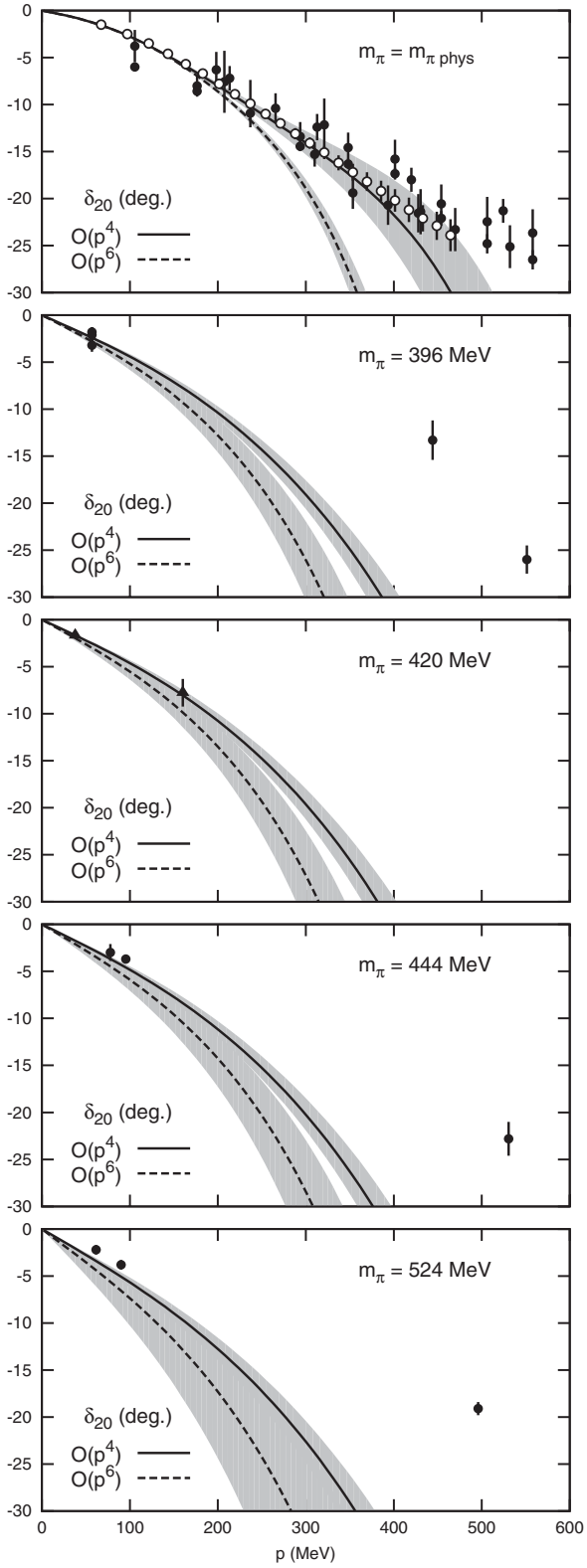

FIG. 5. One and two-loop standard ChPT phase shifts for the $I = 2$, $J = 0$ channel. Top panel: results compared to data from [33] (black circles) and [34] (white circles). Rest of panels: results compared to lattice results coming from [12] (circles) and [13] (triangles).

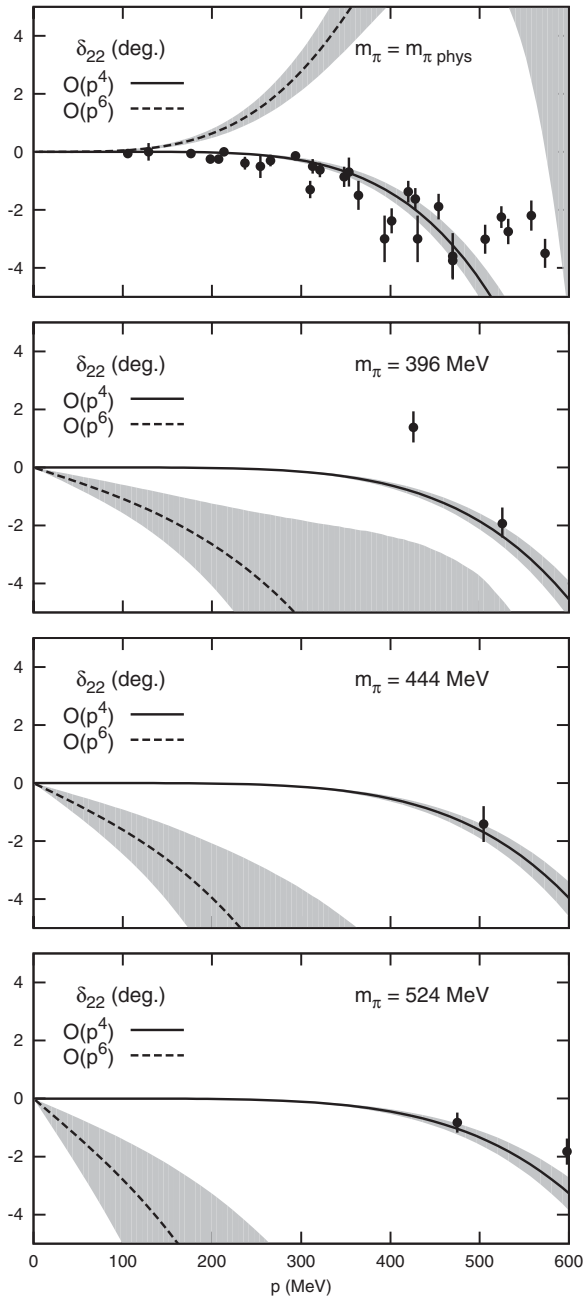

FIG. 6. One and two-loop standard ChPT phase shifts for the $I = 2$, $J = 2$ channel. Top panel: results compared to data from [33] (black circles). Rest of panels: results compared to lattice results coming from [12] (circles). Note the large difference between one and two-loop results.

lattice simulations. Even the tendency is wrong, since the absolute value of the phase seems to grow with m_π, whereas lattice results may suggest a decrease. Let us, nevertheless, recall that for D-waves the tree level amplitude vanishes, so that one and two-loop calculations correspond only to leading and next to leading order results. Higher order calculations may be needed to improve and stabilize the D wave description.

IV. RECONCILING THE PHASE SHIFT AND RESONANCE BEHAVIOR IN THE VECTOR CHANNEL

We have seen that, within ChPT, the low momentum phase shift of the vector channel is found to decrease as m_π grows. This is a model independent result and looks rather robust since it is obtained both at one and two loops. However, lattice results [4–8], the chiral effective treatment [22], as well as the IAM [18] predict that, in terms of momentum, the $\rho(770)$ peak gets closer and closer to threshold. Thus, for any low momentum choice, and as m_π increases, the $\rho(770)$ peak reaches that given momentum so that the phase there should be $\pi/2$. Therefore, one would naively expect the phase shift for any fixed low momentum to grow with m_π.

Actually, this is what one would find if, to describe the $\rho(770)$ resonance pole, one uses the very simple and intuitive (but, as we will see below, incomplete) Breit-Wigner model

$$t(s) = \frac{-\sqrt{s}M\Gamma(p)/2p}{s - M^2 + iM\Gamma(p)} \tag{5}$$

where, $p^2 = s/4 - m_\pi^2$ and the width is:

$$\Gamma(p) = \Gamma_R\left(\frac{p}{p_R}\right)^3, \tag{6}$$

where M is the resonance mass and p_R is the pion momentum at the resonance energy $p_R^2 = M^2/4 - m_\pi^2$ so that $t(s)$ behaves correctly at threshold, $t(s) \sim p^{2l}$. Note that $\Gamma_R = g^2 p_R^3/6\pi M^2$ is the $\rho(770)$ decay width.

For the sake of simplicity, let us now assume that the resonance mass M and coupling remain constant when changing the pion mass m_π. This implies that M and $\Gamma(p)$ are m_π independent. For our illustration purposes here, this is a fairly good approximation to what has been found on the lattice or with the IAM, and it could be considered as the leading order term in the m_π expansion (see [36] for the $\rho(770)$ mass).

In such case, however, the phase-shift m_π dependence near threshold does not follow what is obtained from ChPT (or the IAM, as we will see below). In particular, since

$$\tan\delta(p) = -\frac{M\Gamma(p)}{4p^2 - 4p_R^2}, \tag{7}$$

the only m_π dependence in δ (for a given p) is through p_R (and $d(p_R^2)/d(m_\pi^2) = -1$) so that

$$\frac{\partial\delta}{\partial(m_\pi^2)} = -\frac{\partial\delta}{\partial(p_R^2)} = \frac{4M\Gamma(p)}{(4p^2 - 4p_R^2)^2 + M^2\Gamma(p)^2} > 0. \tag{8}$$

However, in ChPT, for low p we have shown in Figs. 1 and 3 that $\partial\delta/\partial(m_\pi^2) < 0$.

Of course, it is very well known that a simple Breit-Wigner vector formalism is not consistent with the chiral expansion unless there are some additional low-energy contributions—or contact terms in the Lagrangian formalism [37]. Just to keep things very simple we can use a modification of the Breit-Wigner parametrization, which is widely used in analysis of $\pi\pi$ scattering and other phenomenology involving decays into light mesons [38], and reads

$$\Gamma(p) = \Gamma_R\left(\frac{p}{p_R}\right)^{2l+1}\frac{D_l(p_R r)}{D_l(pr)} \equiv \tilde{\Gamma}(p)\frac{D_l(p_R r)}{D_l(pr)}. \tag{9}$$

Here $\tilde{\Gamma}(p)$ is m_π independent and $D_l(pr)$ are the Blatt-Weisskopf centrifugal barrier functions [39], that for $l = 1$ read $D_1(pr) = 1 + (pr)^2$. All the m_π dependence is carried by p_R and the new parameter r, which is usually interpreted as a crude estimate of the size of the meson, although it should not be identified with its mean square charge radius. At low momentum we now find

$$\frac{\partial\delta(p)}{\partial(m_\pi^2)} \simeq \frac{1 + p_R^4(r^2)'}{4p_R^4}M\tilde{\Gamma}(p), \tag{10}$$

where $(r^2)'$ stands for $dr^2/d(m_\pi^2)$. In order to have a decreasing phase shift at low p when increasing m_π, we just need $1 + p_R^4(r^2)' < 0$. We will see below that this is actually required by chiral symmetry at leading order in the pion mass expansion. This would explain the phase decrease seen in ChPT for not too large m_π, even though the $\rho(770)$ is approaching threshold as m_π grows. Of course, when m_π grows too large, and particularly in the limit when the $\rho(770)$ tends to threshold, so that $p_R \to 0$, the derivative is positive, and the phase shift increases, as one would have expected naively.

Let us then check that chiral symmetry actually requires $1 + p_R^4(r^2)' < 0$, at least for low pion masses. We can estimate the leading m_π dependence of r by comparing the low momentum and mass expansion of the amplitude in Eqs. (5) using (9), with that of ChPT. In particular, since in this simple model we have only one parameter, r, we will only compare the scattering lengths. Our aim is just to reproduce the leading order m_π dependence, since we have already made additional approximations and simplifications (like the constancy of the $\rho(770)$ mass and coupling). We define the scattering length, a, as $\mathrm{Re}t \simeq p^2(a + bp^2 + \cdots)$. The low p expansion of the amplitude in Eq. (5) using (9) leads to

$$\begin{aligned} a_{BW} &= \frac{m_\pi M\Gamma_R(1 + (p_R r)^2)}{4p_R^5} \\ &= \frac{m_\pi\Gamma_R}{Mp_R^3}\left(1 + \frac{1}{4}M^2r^2 + O(m_\pi^2)\right). \end{aligned} \tag{11}$$

This result has to be compared with that of ChPT: $a_{\mathrm{ChPT}} = 1/24\pi f_\pi^2 + O(m_\pi^2)$. Matching with ChPT we obtain for r^2

$$r^2 = \frac{p_R^3}{6\pi f_\pi^2 M\Gamma_R}\frac{1}{m_\pi} + O(m_\pi^0) \tag{12}$$

$$\equiv \frac{1}{g^2 f_\pi^2}\frac{M}{m_\pi} + O(m_\pi^0) \simeq (4.3\ \mathrm{GeV}^{-1})^2. \qquad (13)$$

The value obtained with this ChPT estimation is compatible with what is found in the literature ($r \sim 4$–$5\ \mathrm{GeV}^{-1}$) [38].

Note that the size r explodes as $m_\pi \to 0$. However, this is a very well known feature of hadrons, at least for the charge radius. Actually, the squared charged radius of the pion and the nucleon show a $\log m_\pi^2$ singularity [14,40,41] and the Pauli radius of the nucleon an additional $1/m_\pi$ singularity [40]. Nevertheless, as we have commented, our r^2 parameter should not be directly identified with the $\rho(770)$ charged radius, although our results suggest that they may have a similar singularity.

With this m_π dependence for r we find that

$$1 + p_R^4 (r^2)' = 1 - \frac{M p_R^4}{2 g^2 f_\pi^2 m_\pi^3}, \qquad (14)$$

which is negative for the physical values of the parameters. This guarantees that $\partial\delta(p)/\partial(m_\pi^2) < 0$ for m_π not far from m_π^{phys}, and sufficiently low p, as is obtained in ChPT.

The decrease is a robust feature of ChPT, although the pure chiral expansion cannot reproduce the $\rho(770)$ resonance. Of course, the model we have presented here is very simple and naive, but provides a qualitative and intuitive explanation of why chiral symmetry implies that the vector phase-shift at low momenta first decreases, although it may increase later as m_π grows. This model cannot be pushed too far. In particular, we cannot reproduce the chiral behavior of the scattering length beyond leading order or even the slope parameter.

It is, however, possible to incorporate simultaneously the $\rho(770)$ pole and the full low-energy ChPT expansion to one and two loops. In the next section, we will explain the technique in detail and later on we will show how it describes the existing lattice data up to much higher momentum than standard ChPT. Actually, we will check how the vector phase-shift decreases first and then increases as m_π grows.

V. UNITARIZED CHPT: THE INVERSE AMPLITUDE METHOD

As we have already commented in Sect. II, the partial waves obtained from the ChPT expansion are basically a truncated series in momenta or energies and cannot satisfy elastic unitarity, Eq. (1), exactly, but only perturbatively, as in Eq. (3).

There is, however, a well known technique, known as unitarization, to obtain expressions for partial waves that satisfy elastic unitarity, have the correct analytic structure in terms of cuts in the complex plane, and simultaneously respect the ChPT expansion up to a given order. Here we will make use of the elastic inverse amplitude method (IAM)—or a slightly modified version—that implements the fully renormalized one or two-loop ChPT expansion at low energies but does not introduce any spurious parameter in the unitarization procedure. Had we used other, possibly simpler but very successful, unitarization techniques with spurious parameters, like cutoff or any other regulator, we should have had to worry about the unknown m_π dependence of that scale.

The IAM [17] uses elastic unitarity and the ChPT expansion to evaluate a once subtracted dispersion relation for the inverse amplitude. The analytic structure of $1/t$ consists on a right cut from threshold to ∞, a left cut from $-\infty$ to 0, and possible poles coming from zeros of t. We can write then a once subtracted dispersion relation for $1/t$, the subtraction point being s_A,

$$\frac{1}{t(s)} = \frac{s - s_A}{\pi}\int_{RC} ds' \frac{\mathrm{Im}1/t(s')}{(s' - s_A)(s' - s)} + LC(1/t) + PC(1/t), \qquad (15)$$

where $LC(1/t)$ stands for a similar integral over the left cut and $PC(1/t)$ is the contribution of the pole at s_A. The choice of s_A is, in principle, arbitrary, but since we want to use the information encoded in the ChPT series, we are then limited to the low-energy region, preferably, below threshold. Now, scalar waves vanish at the so called Adler zero that lies in the real axis below threshold and in practice this is a very convenient choice for s_A, which has actually motivated our notation. For other waves, there is no such an Adler zero, and the subtraction point can be taken, for instance, at $s = 0$. It is important to remark that the choice of subtraction point, as long as it lies between the left and right cut, has only a very small numerical effect [17] on the physical region. Up to here everything is exact. The most relevant observation is that, following Eq. (1), on the elastic cut we know exactly $\mathrm{Im}1/t = -\sigma$.

Now we are going to derive the IAM within one-loop ChPT. First, the Adler zero position can be approximated as, $s_A = s_2 + s_4 + \cdots$, where t_2 vanishes at s_2, $t_2 + t_4$ vanishes at $s_2 + s_4$, and so on. On the right cut we can evaluate exactly $\mathrm{Im}1/t = -\sigma = -\mathrm{Im}t_4/t_2^2$, as can be read from Eqs. (1) and (3). Since the left cut is weighted at low energies we can use one-loop ChPT to approximate $LC(1/t) \simeq LC(-t_4/t_2^2)$. The pole contribution $PC(1/t)$ can be safely calculated with ChPT since it involves derivatives of t evaluated at s_A, which is a low-energy point where ChPT is perfectly justified. Altogether, we arrive to a modified one-loop IAM (mIAM) formula [17]:

$$t^{\mathrm{mIAM}} = \frac{t_2^2}{t_2 - t_4 + A^{\mathrm{mIAM}}}, \qquad (16)$$
$$A^{\mathrm{mIAM}} = t_4(s_2) - \frac{(s_2 - s_A)(s - s_2)[t_2'(s_2) - t_4'(s_2)]}{s - s_A},$$

where the prime denotes the first derivative with respect to s and where we use for s_A in the numerical calculations its NLO approximation $s_2 + s_4$. The standard IAM formula is

recovered for $A^{\mathrm{mIAM}} = 0$, which is indeed the case for all partial waves except the scalar ones. In the original IAM derivation [15,16] A^{mIAM} was neglected since it formally yields a higher order contribution and is numerically very small except near the Adler zero. However, if A^{mIAM} is neglected, the IAM Adler zero occurs at s_2, correctly only to LO, is a double zero instead of a simple one, and a spurious pole appears close to the Adler zero. All of these caveats disappear with the mIAM, and the differences between the IAM and the mIAM in the physical and resonance region are of the order of 1%.

It is important to remark that ChPT has *not* been used *at all* for calculations of $t(s)$ for positive energies above threshold. Note that the use of ChPT is well justified to calculate s_A, and $PC(1/t)$, since these are low-energy calculations. ChPT has also been used to calculate the left cut integral, which, despite extending to infinity, is heavily weighted at low energies, which once again justifies the use of ChPT. The left cut and the elastic approximation are the only approximations used to obtain the IAM, but no other model dependent assumptions have been made. In particular there are no spurious parameters included in the IAM derivation, but just the ChPT LECs, m_π and f_π.

Remarkably, these simple equations (either the IAM or the mIAM) ensure elastic unitarity, match ChPT at low energies and, using LECs compatible with existing determinations, describe fairly well data up to somewhat less than 1 GeV, generating the ρ, K^*, σ, and κ resonances as poles on the second Riemann sheet [16].

The extension to two loops is very similar and straightforward for the IAM [16,42] or the mIAM [21]:

$$t^{\mathrm{mIAM}} = \frac{t_2^2}{t_2 - t_4 + t_4^2/t_2 - t_6 + A^{\mathrm{mIAM}}},$$

$$\begin{aligned} A^{\mathrm{mIAM}} = {} & t_4(s_2) - \frac{2t_4(s_2)t_4'(s_2)}{t_2'(s_2)} - \frac{t_4^2(s_2)}{t_2'(s_2)(s - s_2)} + t_6(s_2) \\ & + \frac{(s - s_2)(s_A - s_2)}{s - s_A}\left(t_2'(s_2) - t_4'(s_2) - t_6'(s_2)\right. \\ & \left. + \frac{t_4'(s_2)^2 + t_4''(s_2)t_4(s_2)}{t_2'(s_2)}\right). \end{aligned} \tag{17}$$

Let us now remark that both in the one and two-loop derivations above, we have assumed that t_2 is not identically zero. However, this is only the case for scalar and vector partial waves. Unfortunately, as seen in Eq. (3), when $t_2(s) \equiv 0$ the first imaginary part appears at $O(p^8)$, namely, at three loops. Therefore, we cannot recast the dispersion relation in terms of the full ChPT expansion unless we make use of $t_8(s)$, a calculation that does not exist. In [43], and using only the t_8 term of the form cs^4, it was shown that the $f_2(1275)$ shape could be fairly well fitted with the IAM and a c value of the correct order of magnitude expected from dimensional grounds. This was justified because the f_2 resonance appears at high $s \gg m_\pi^2$ and the other $O(p^8)$ terms, containing pion mass powers, could be neglected. However, in this work we want to make m_π much larger than its physical value and we need the m_π dependence. It is, therefore, not so well justified to neglect all the t_8 terms except cs^4. For that reason, we are limited to use the IAM for scalar and vector partial waves.

Hence, using the IAM or the mIAM, we can study how the generated ρ and σ poles evolve by changing m_π in the one-loop IAM amplitudes [18] or two-loop amplitudes [21], and describe the dependence of their masses, widths, and couplings on m_π. In [18] the mIAM was used for the ρ and σ chiral extrapolation, because, for the scalar and at high m_π, one resonance pole gets near the IAM spurious pole, a problem that is nicely solved with the mIAM. Nevertheless, in the physical region and near the other generated poles, the differences between IAM and mIAM approaches are almost negligible, even for high pion masses.

Of course, the poles are not the only object of study on the lattice. Actually, lattice results are already available for phase shifts in $I = 2$ channels, where no pole exists. Moreover, these channels were not studied in [18,21]. It is also very likely that lattice results on phase shifts for other channels will be available soon. For these reasons, we will now let m_π vary within our unitarized ChPT expressions, with the aim of extending the phase-shift predictions based on ChPT, up to higher masses and momenta.

VI. RESULTS WITH THE IAM AND CHPT

Let us first recall, as already explained in some of the very first works on the IAM [16], and repeated in many other instances [21,44,45], that when the central values of the standard LECs are used, the IAM only improves ChPT up to a couple of hundred MeV higher and resonances are only reproduced qualitatively. For a semiquantitative description of resonances, which is what we will do next, one has to fit the data and the resulting LECs are slightly modified from those obtained from pure ChPT. Since the IAM contains contributions that count as higher order in ChPT (in particular, the numerically relevant s-channel logarithms), one would very naively expect the LECs from the one-loop IAM to lie somewhere in between the one and two-loop values from ChPT. This is actually observed, since the $O(p^4)$ IAM LECs in Table III lie somewhere between the one and two-loop analysis of pure ChPT listed in Table II, although closer to the ChPT $O(p^4)$ analysis in the two first rows of that table. In contrast, the $O(p^4)$ values of the LECs for the two-loop IAM in Table IV are closer to the two-loop analyses like that in Table I or those in the third and fourth row of Table II. Let us emphasize that the variation between the $O(p^4)$ LECs values between the one and two-loop analyses already occurs in pure ChPT—particularly for l_2^r. The IAM simply follows a similar pattern.

TABLE III. LECs used in this work for the one-loop IAM, obtained from a fit to the dispersive data analysis of [34]. Both l_3 and l_4 are fixed to the standard values given in Table I. The scale is set to $\mu = 770$ MeV.

$O(p^4)$	LECs ($\times 10^{-3}$)
$l_1^r\ (\mu)$	-3.9 ± 0.2
$l_2^r\ (\mu)$	4.3 ± 0.4
$l_3^r\ (\mu)$	0.18 ± 1.11
$l_4^r\ (\mu)$	6.17 ± 1.39

Before changing the pion mass, let us note that for the IAM, we are assuming the elastic approximation and therefore, when increasing m_π, we should allow for some $\pi\pi$ elastic regime, which is guaranteed if $m_\pi < 500$ MeV, although it has been found that relatively stable unitarized results can be obtained for all waves only up to $m_\pi \simeq$ 300–350 MeV [21]. Of course, some waves are more stable than others. In particular, the elastic IAM approximation is quite good up to larger energies for the $(I, J) = (2, 0)$ (roughly up to $\sqrt{s} \simeq 1200$–1300, see [44]), since it has no resonances and does not couple to $\bar{K}K$. We will actually check that for this channel we can stretch the applicability range and still get fairly good agreement with recent lattice results for relatively large pion masses.

A. One-loop IAM

In Fig. 7 we show the IAM results to one-loop in ChPT, using the LECs in Table III, obtained by an updated fit to

TABLE IV. Low-energy constants obtained from fits [21] to experimental data on elastic $\pi\pi$ scattering and lattice results on f_π, M_ρ and the isospin 2 scattering length as well as a $1/N_c$ leading behavior of a pure $\bar{q}q$ state for the $\rho(770)$. Many of these sets are not quite compatible with each other and suffer large systematic uncertainties. These two fits correspond to different ways of weighting the existing experimental and lattice data sets, which are detailed in [21]. The values correspond to the scale $\mu = 770$ MeV.

	Set A	Set D
$O(p^4)(\text{x}10^{-3})$		
$l_1^r\ (\mu)$	-5.0	-4.0
$l_2^r\ (\mu)$	1.7	1.2
$l_3^r\ (\mu)$	0.8	0.8
$l_4^r\ (\mu)$	6.5	6.5
$O(p^6)(\text{x}10^{-4})$		
$r_1^r\ (\mu)$	-0.6	-0.6
$r_2^r\ (\mu)$	1.3	1.5
$r_3^r\ (\mu)$	-1.7	-3.3
$r_4^r\ (\mu)$	2.0	0.9
$r_5^r\ (\mu)$	2.0	1.7
$r_6^r\ (\mu)$	-0.6	-0.7
$r_f^r\ (\mu)$	-1.4	-1.8

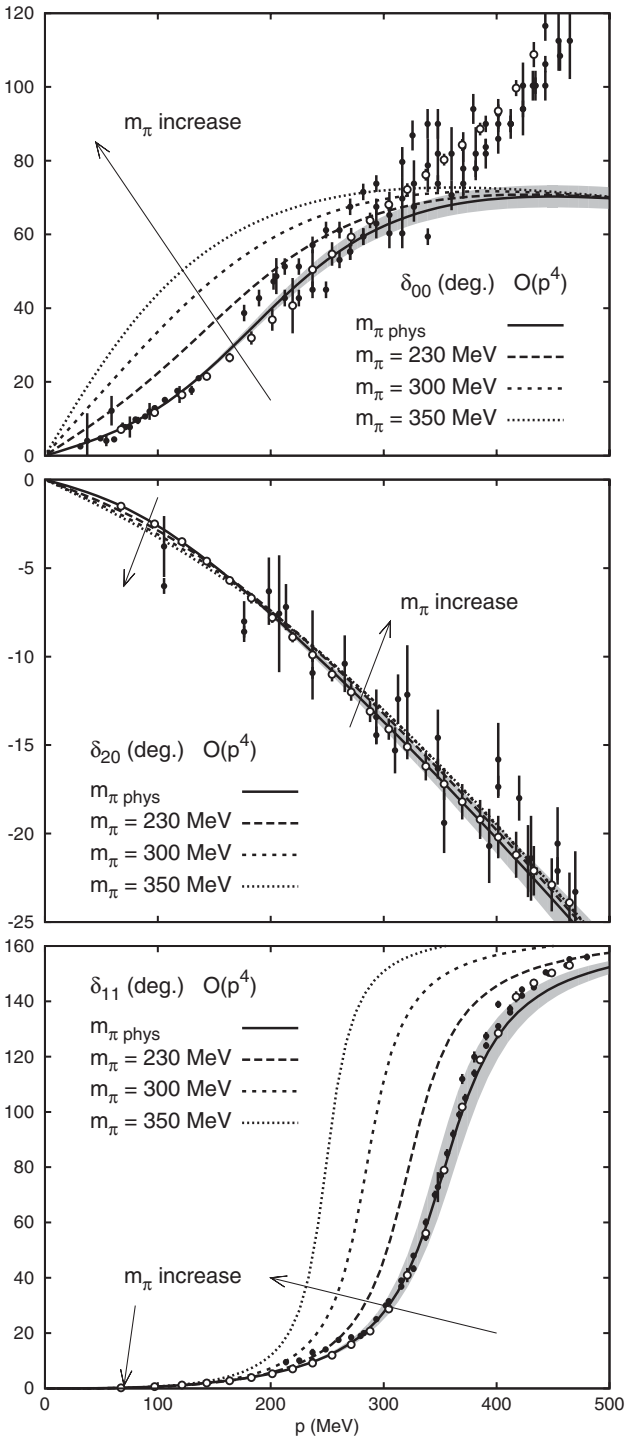

FIG. 7. S and P wave $\pi\pi$ phase shifts from unitarized ChPT up to one loop. Different lines stand for different pion masses: continuous, long dashed, short dashed and dotted for $M_\pi = 139.57$, 230, 300 and 350 MeV, respectively. Since the lines are too close to each other, we only show error bands for the physical mass. Experimental data come from [33] (black circles) and the precise model independent dispersive data analysis from [34] (white circles). The arrows show the direction of increasing m_π. See Fig. 8 for a blow up of the low momentum region of the $I = 1$, $J = 1$ phase shift.

the output from the recent and precise dispersive data analysis in [34], and fixing l_3 and l_4 to the updated values in Table I. The uncertainties are mostly systematic, arising from different choices of the maximum energy up to where we make the fit of the (0, 0) channel, which we have chosen between 500 and 800 MeV; the other channels are fitted up to 1 GeV. Note that the resulting LECs are consistent within 1 standard deviation with the results we used in [18], that we list in the last row of Table II. We first note that the experimental data is fairly well described up to the region where inelastic effects (or resonances like the $f_0(980)$) become relevant. This includes the $\rho(770)$ resonance shape, but also the wide shape of the $f_0(600)$. The gray bands in the figures cover the uncertainties in our results obtained from a Monte Carlo Gaussian sampling of the l_i statistical error bars also listed in the table. As usual, and to avoid confusion due to many overlapping gray bands, we only show the uncertainty for the physical pion mass. Details on uncertainties for higher masses can be found in the appendix.

The general features for the scalar-isoscalar channel are very similar to the one-loop nonunitarized results. Namely, the phase shift conserve its positive sign and increases in absolute value as m_π grows.

However, the $I = 2$ channel behavior is rather different. First, the m_π dependence is even milder than for the nonunitarized case. In the very low momentum region, roughly below $p = 200$ MeV, the phase increases in absolute value as it happened with standard one-loop ChPT. However, for larger momentum, the m_π dependence is the opposite, and the phase starts decreasing its absolute value. As we will see later on, this is the behavior found on recent lattice results, which cannot be reproduced by a crude extrapolation of one-loop ChPT to larger momentum.

Something similar occurs in the vector channel, although enhanced by the presence of the $\rho(770)$ resonance that ChPT failed to reproduce. Now we see that the phase increases as the two-pion threshold grows and gets closer to the resonance. This is the intuitive behavior one would expect when getting close to the resonance. However, one should observe that it is *not* incompatible with the phase decrease observed in standard ChPT at low energies. To see this, in Fig. 8, we show a blow up of the very low-energy region of the vector channel, where we can see that the IAM behaves similarly to ChPT, namely, the phase decreases as m_π grows. As explained before, this only happens in the very low momentum regime, since, as seen in the figure, for higher momentum the phase shift increases again since the IAM is able to reconstruct the $\rho(770)$ resonance, which is closer and closer to threshold as m_π grows.

In the next subsection we will see that these general features and improvements with respect to nonunitarized ChPT are even more dramatic when considering the two-loop calculation.

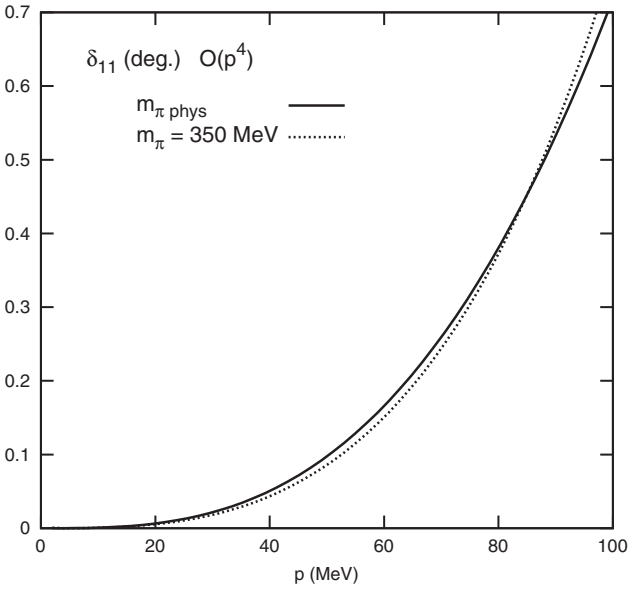

FIG. 8. $\pi\pi$ $I = 1$, $J = 1$ phase shift from unitarized ChPT up to one loop. The continuous line stands for $M_\pi = 139.57$ MeV and the dotted line for $M_\pi = 350$ MeV. Similarly to the ChPT case, in the low momentum region the phase shift decreases as m_π grows. However at higher momentum it increases with the pion mass, due to the presence of the $\rho(770)$ resonance.

B. Two-loop IAM

In Figs. 9 and 10 we show the results of the two-loop IAM for the two best fits in [21], "A" and "D", whose corresponding sets of LECs we provide in Table IV. These fits have been obtained from an IAM fit to experimental data but also to lattice results on f_π, M_ρ and the isospin 2 scattering length. Note that by fitting only the experimental data one determines better the LECs that govern the s dependence, but not so well those governing the m_π dependence. That is the reason why some existing lattice results on f_π, M_ρ and the $I = 2$ scalar scattering length were also included in the fits of [21]. Unfortunately, the experimental data in the resonance region are frequently in conflict with one another, and to a lesser extent, something similar happens for the lattice results mentioned above. Fits A and D correspond to different ways of weighting the conflicting experimental and lattice results, including some educated estimates for systematic uncertainties. The details can be found in [21]. These fits give rather stable results for all observables in the elastic region, up to $m_\pi =$ 300–350 MeV, and somewhat beyond for some particular waves, like $(I, J) = (2, 0)$.

Note that the qualitative behavior of all waves is similar in Figs. 9 and 10. The difference between fit A and D is purely quantitative: in fit A the m_π dependence is just stronger than in fit D.

Remarkably, almost all the features described for the one-loop unitarized case remain in the two-loop unitarized fits. Quantitatively, there are small differences, since the

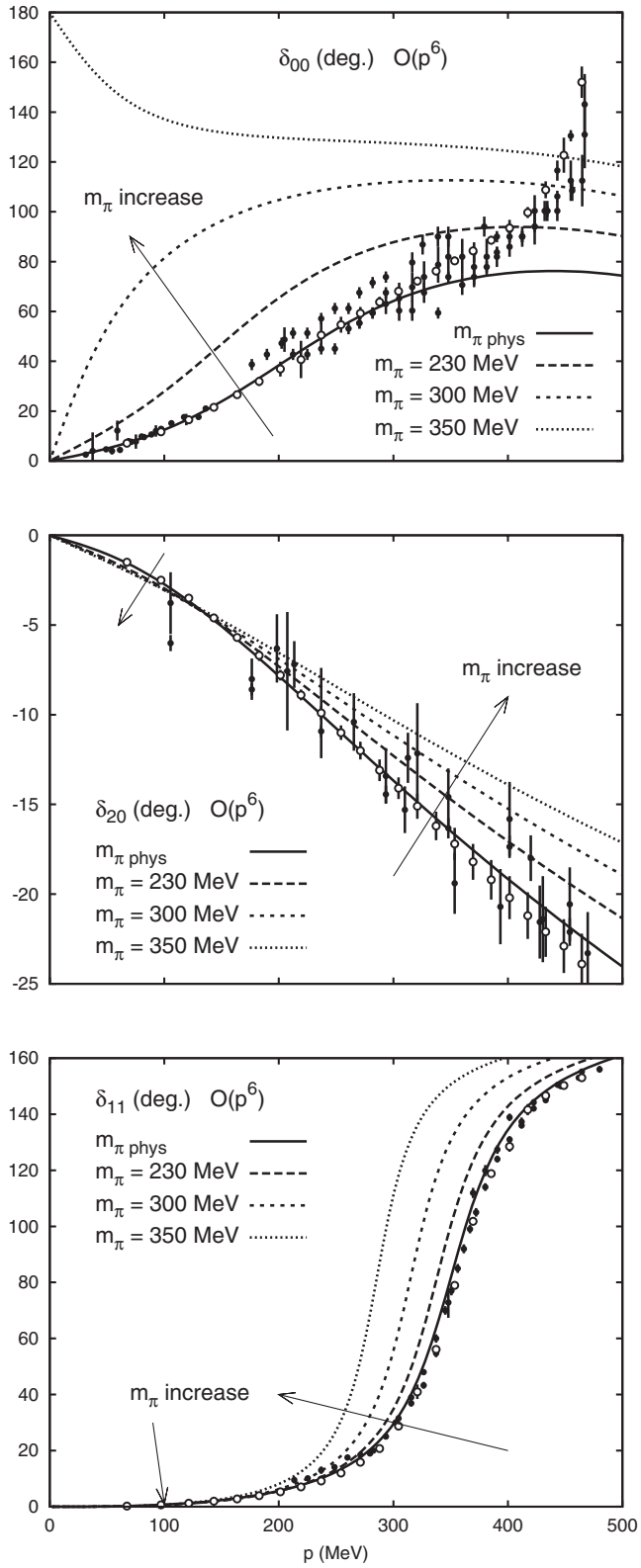

FIG. 9. S and P wave $\pi\pi$ phase shifts from the two-loop IAM "fit A" in [21]. The conventions are as in Fig. 7. The arrows show the direction of increasing m_π. The difference between these curves and those in Fig. 10 are an indication of the order of magnitude of our uncertainties.

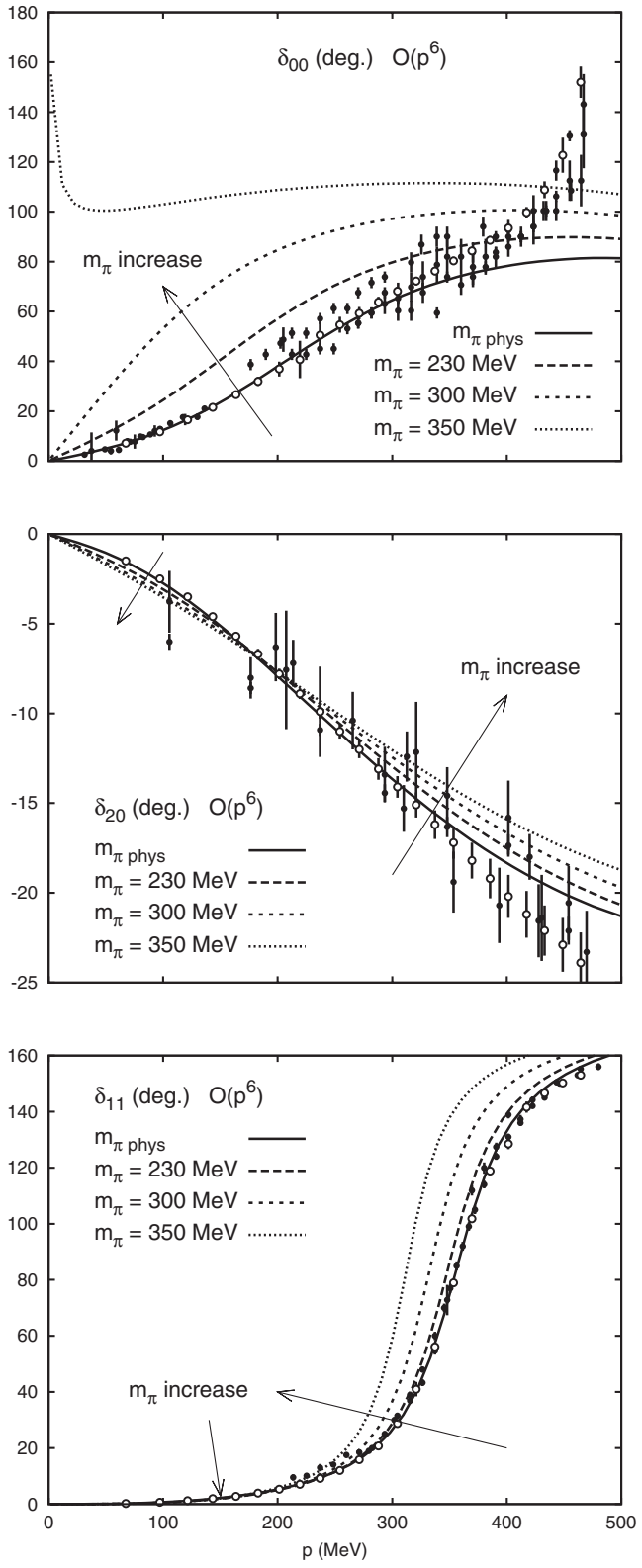

FIG. 10. S and P wave $\pi\pi$ phase shifts from the two-loop IAM "fit D" in [21]. The conventions are as in Fig. 7. The arrows show the direction of increasing m_π. The difference between these curves and those in Fig. 9 are an indication of the order of magnitude of our uncertainties.

m_π dependence at two loops seems somewhat stronger in the scalar waves, and somewhat weaker in the vector channel. This somewhat stronger m_π dependence produces the only significant, and relevant, difference with the one-loop IAM. Both the one and two-loop IAM generate the $f_0(600)$ or σ resonance as a pole deep in the complex plane, which mass grows much slower than the two-pion threshold, so that the '"bump"' that this wide resonance produces in the (0, 0) phase is bigger and gets closer to threshold. Actually, as shown in [18] the two conjugated poles of the $f_0(600)$ move in the second, unphysical, Riemann sheet, until they reach the real axis below threshold, where the two poles are no longer conjugated. As m_π keeps growing one of them jumps into the first Riemann sheet below threshold becoming a bound state. By Levinson's theorem [46], this implies that the phase at threshold increases by π. For the IAM to one-loop this jump occurs for m_π larger than 350 MeV, but since the m_π dependence is stronger for the IAM at two-loops, this jump can already be seen in Figs. 9 and 10 for the $m_\pi = 350$ MeV curve, which behavior thus reflects the existence of a bound state. Let us emphasize that the same behavior would be observed to one loop—although for higher m_π—but it will never be seen in standard ChPT, which cannot generate a pole.

However, when comparing with the nonunitarized two-loop results in Fig. 3, we see that unitarization not only improves the vector channel by describing the $\rho(770)$ resonance, but also the $I = 2$ channel is nicely described up to much higher momentum, even though this channel is nonresonant. We will profit from this lack of complicated resonant structures in the $I = 2$ scalar wave, and also from the fact that this channel does not couple to $\bar{K}K$, to extrapolate to higher pion masses where we will see that the unitarized results are in much better agreement than standard ChPT with some recent lattice results.

VII. COMPARISON WITH LATTICE RESULTS FOR $I = 2$ AND $m_\pi > 350$ MeV

In Fig. 11 we show the results from the one and two-loop IAM with very recent results on the lattice [12,13] for the $I = 2$ scalar channel. Note that the data below $p = 200$ MeV is still fairly well described by the IAM, as it happened with ChPT, but that the IAM is not bending down and getting away from higher momentum data as it happened with standard ChPT results. Actually, the IAM results follow qualitatively the shape of the lattice data. Moreover, the m_π dependence is much milder than for plain ChPT, in better agreement with the findings on the lattice. Let us remark that we do not aim at precision here because pion masses of 400 MeV are probably close to the IAM applicability bound. Our approach should become more reliable below 300–350 MeV, where we expect lattice results to appear soon. Still, the remarkable improvement with respect to the standard ChPT results is pretty clear.

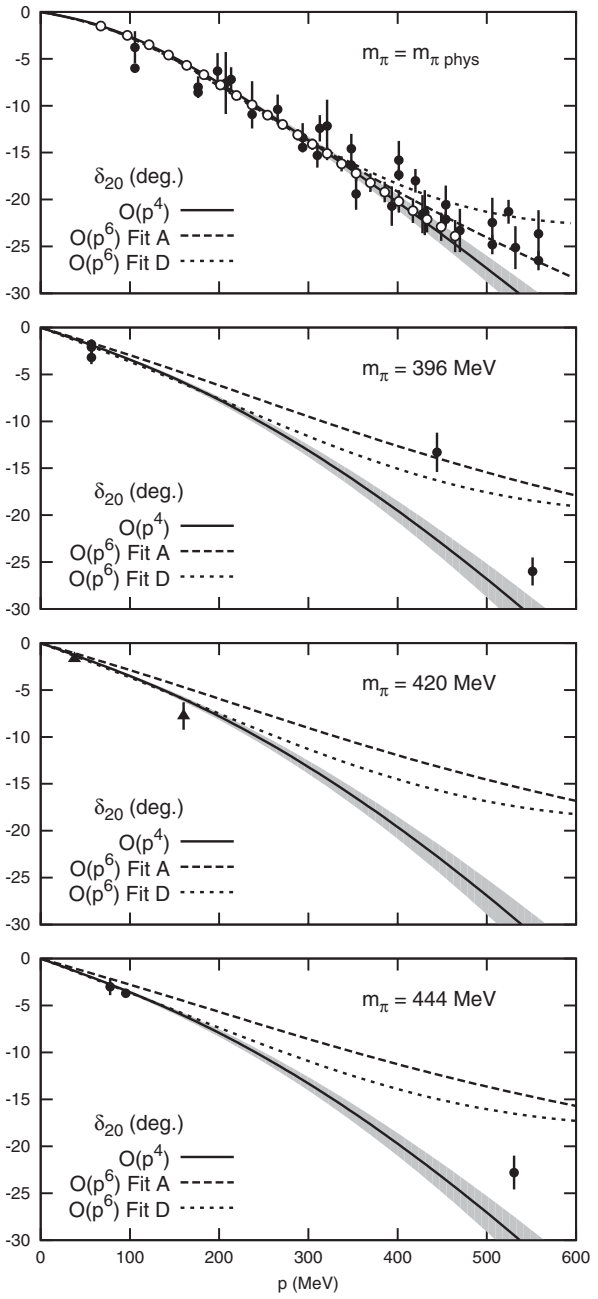

FIG. 11. One and two-loop IAM phase shifts for the $I = 2$, $J = 0$ channel. Top panel: results compared to data from [33] (black circles) and [34] (white circles). Rest of panels: results compared to lattice results coming from [12] (circles) and [13] (triangles). Note that for the two-loop case we provide results for the two best fits, A and D, obtained in [21].

As previously commented, the IAM cannot be directly applied to the D waves, since their tree level contribution vanishes. Further modifications of the IAM would be needed, which are beyond the scope of this work.

VIII. SUMMARY AND DISCUSSION

In this work, we have studied the pion mass dependence of $\pi\pi$ elastic scattering phase shifts.

On the one hand, we have presented results for one and two-loop standard Chiral Perturbation Theory using a set of LECs obtained from a dispersive analysis in the literature. We have seen that this first approach is, of course, limited to low momentum, say below 300 MeV, depending on the channel, and pion masses up to 400–450 MeV. For the scalar and vector waves, we have found a rather stable behavior between the one and two-loop calculations within that momentum range. We have seen that at this very low momentum, the absolute value of scalar phase shifts increases as the pion mass grows, so that these channels enhance their attractive or repulsive nature. We have found that up to momenta less than 200 MeV, the ChPT results are in fair agreement with lattice data for the scalar $I = 2$ channel.

We have found that, surprisingly, the vector phase shift at very low momentum decreases as m_π grows within the applicability region. This may seem counterintuitive, since from lattice and other effective theory techniques, as m_π grows one expects the two-pion threshold to approach fast the $\rho(770)$ mass. We have, nevertheless, shown with a very simple and intuitive model why very basic requirements about chiral symmetry impose such a decrease on the phase for low momentum and not too large m_π.

We have also shown results within standard ChPT for the angular momentum 2 phase shifts. These are much less stable when comparing one and two-loop results. Particularly for the $(I, J) = (2, 2)$ channel, the one and two-loop results show an opposite behavior, and the two-loop calculation is also at odds with the m_π dependence found on the lattice. Of course, one has to keep in mind that for D waves, the one and two-loop calculations correspond to leading and next to leading order calculations, contrary to scalar and vector channels, where they correspond to next to leading and next to next to leading calculations. It is very likely that higher order calculations, or better determinations of LECs, which are highly correlated, may improve this situation for D waves.

Finally, we have used ChPT inside a dispersion relation to extend the analysis of scalar and vector waves to higher momentum by means of the so called inverse amplitude method. This unitarization technique describes remarkably well the data up to energies of the order of 1 or 1.2 GeV, depending on the channel and has been shown to describe well the m_π dependence of several observables like M_ρ, f_π or the $I = 2$ scalar scattering length.

The description provided by this method is, of course, compatible with that of standard ChPT at very low momentum. However, at higher momentum it reconstructs the behavior of the $\rho(770)$ resonance, which, for a given choice of low momentum, translates into a decreasing phase for smaller m_π but a growing phase for larger m_π until the $\rho(770)$ mass coincides with that particular momentum choice. In addition, we have shown that the unitarized $I = 2$ scalar phase shift has the correct qualitative behavior for momentum beyond 200 MeV. Despite being close to the applicability bounds of the approach, we have actually shown that the IAM beyond $p = 150$–200 MeV improves dramatically the description of lattice results with respect to ChPT and explains their very mild m_π dependence.

Intuitively, the phase-shift evolution of the $S0$ and P channels is dominated by the presence of the $f_0(600)$ and $\rho(770)$ resonances and their pion mass dependence, studied in [18,20–22]. Since the masses of both resonances seem to grow slower than the pion mass, they come closer and closer to threshold so that, naively, one would expect the interaction to grow stronger and the phase to raise once the resonance is sufficiently close to the momentum where the phase is measured. Actually, this is what is found for the $S0$ channel, whose phase raises noticeably as m_π grows. At the limit of the range of applicability of the two-loop IAM, the $f_0(600)$ even becomes a bound state and by Levinson's theorem we see the phase to increase by π at threshold. However, the naive expectations may not be met if the resonance is still not close enough to threshold. In such case, the phase may seem to decrease at first due to the finite size of the resonance, the effect of which has been illustrated in a simple model of the $\rho(770)$. Only when the $\rho(770)$ is sufficiently close to threshold, the naively expected behavior is observed. Concerning the $S2$ wave, we have found a very mild m_π dependence for the phase shift, when expressed in terms of the momentum, in good agreement with recent lattice calculations. This can be understood from the absence of resonant structures in this channel. Of course, ChPT can only reproduce the low-energy tails of the resonances, which we have generated by means of ChPT unitarized with the IAM. For the D waves, the IAM cannot be applied to this order, and we have to rely on ChPT only. However, the behavior observed can also be understood from the presence of the $f_2(1270)$ resonance in the $D0$ channel, and a similar behavior to the $\rho(770)$ in its own channel. For the $D2$ channel, the ChPT results are not sufficiently precise to make any conclusive statement.

Apart from understanding the dependence of these observables on QCD parameters on the pion mass, we consider that this work is of interest as a guideline for future studies of lattice QCD.

ACKNOWLEDGMENTS

We thank J. Dudek for lattice results and detailed explanations. Our work was partially supported by the Spanish Ministerio de Educación y Ciencia research Contract Nos.: FPA2007-29115-E, FPA2008-00592 and FIS2006-03438, and U. Complutense/Banco Santander

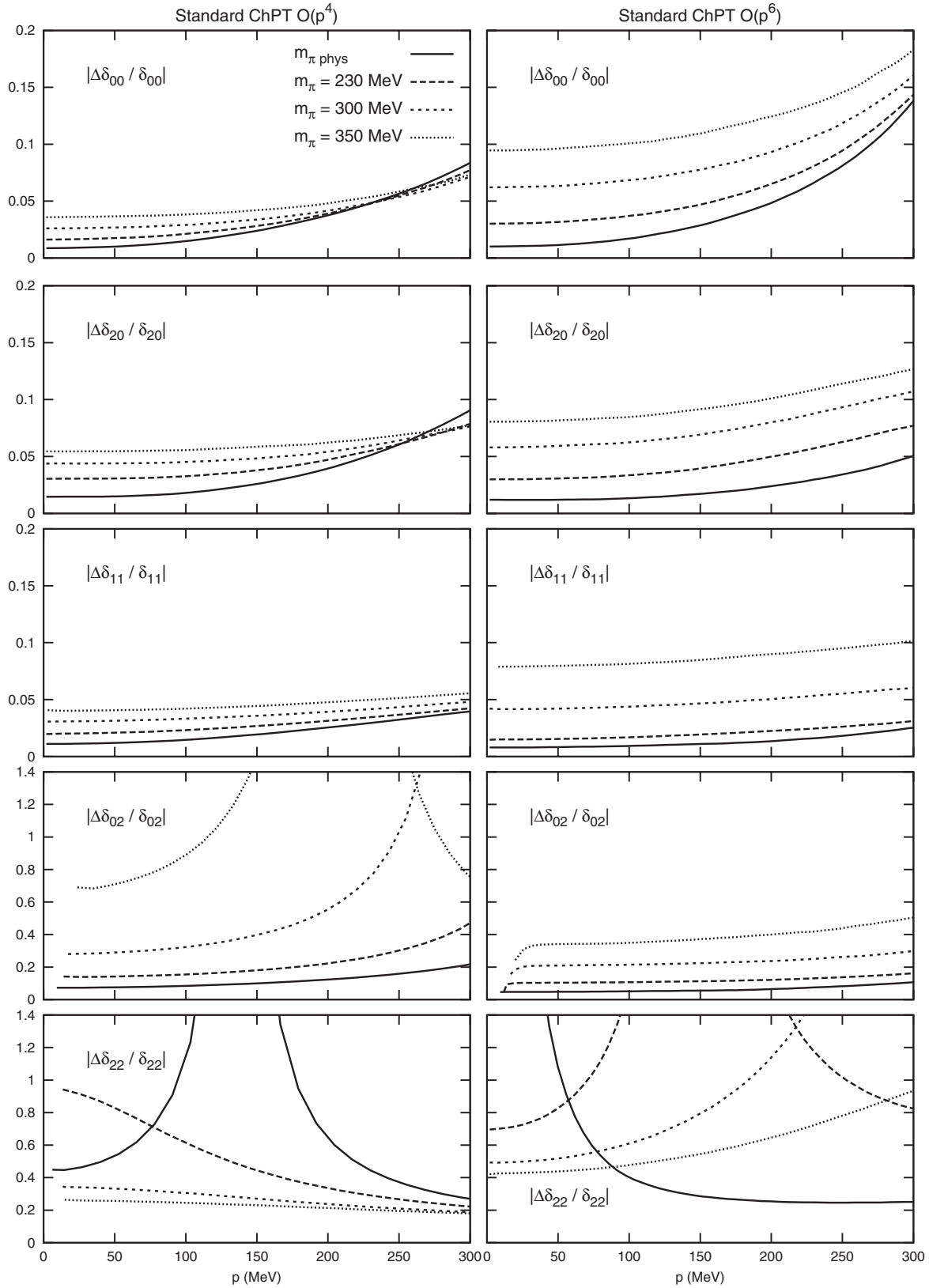

FIG. 12. $\pi\pi$ phase shift errors normalized to the value of the phase shifts in standard ChPT to one loop (left column) and to two loops (right column). Different lines stand for different pion masses: continuous, long dashed, short dashed and dotted for $m_\pi = 139.57$, 230, 300 and 350 MeV, respectively.

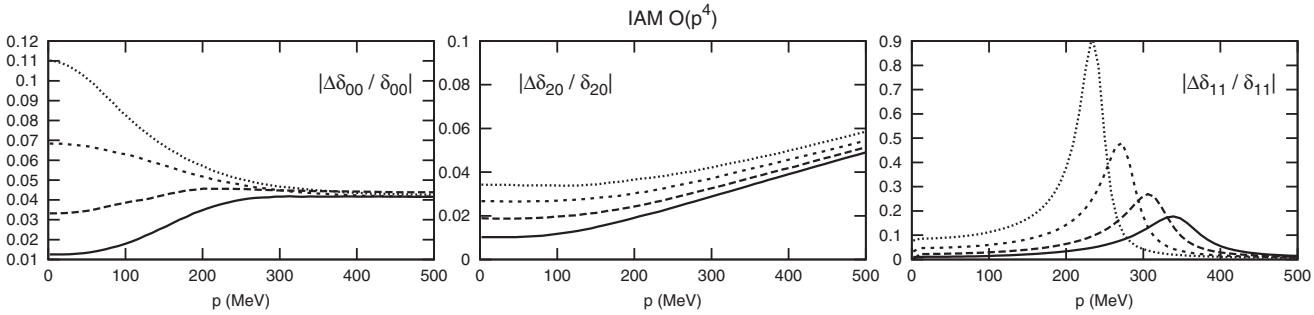

FIG. 13. $\pi\pi$ phase shift errors normalized to the value of the phase shifts in unitarized ChPT to one loop. Different lines stand for different pion masses: continuous, long dashed, short dashed and dotted for $m_\pi = 139.57$, 230, 300 and 350 MeV, respectively.

Grant Nos. PR34/07-15875-BSCH and UCM-BSCH GR58/08 910309. We acknowledge the support of the European Community-Research Infrastructure Integrating Activity Study of Strongly Interacting Matter (acronym HadronPhysics2, Grant Agreement No. 227431) under the Seventh Framework Programme of the European Union.

APPENDIX: PHASE-SHIFT UNCERTAINTIES FOR DIFFERENT m_π

In Fig. 12, we plot the relative uncertainties of the standard ChPT phase-shift calculation. As we have already seen, standard ChPT is limited to low momentum and thus we only show momentum up to $p = 300$ MeV. For the scalar and vector waves we see that in the low momentum region the errors grow with the pion mass. This is in agreement with the fact that the LECs that govern the mass dependence of the partial waves carry the biggest uncertainties. For D-waves, the relative uncertainty is much bigger than for lower angular momentum waves. (Note the difference in scales between the D waves and the rest of the plots). This is due to the fact that for D-waves the tree level calculation vanishes and therefore the one and two-loop results are just leading and next to leading order. In the case of δ_{02} to one loop, the error seems to explode for the highest masses due to the phase shift changing from a positive to a negative value in the region of interest. The same occurs for δ_{22} to one loop for the physical value of the pion mass. Finally, the value of δ_{22} to two loops changes from negative to positive for the lightest masses of the pion.

In Fig. 13, we show the relative uncertainties for the IAM phase shifts. We find again that for scalar waves they grow bigger as the pion mass is increased. The same happens for the vector phase shift below the $\rho(770)$ peak. The highest uncertainty on δ_{11} occurs when the slope of the phase shift reaches its maximum value.

[1] M. H. Johnson and E. Teller, Phys. Rev. **98**, 783 (1955).
[2] K. Nakamura *et al.* (Particle Data Group), J. Phys. G **37**, 075021 (2010).
[3] G. Colangelo, J. Gasser, and H. Leutwyler, Phys. Rev. Lett. **86**, 5008 (2001).
[4] C. W. Bernard *et al.*, Phys. Rev. D **64**, 054506 (2001).
[5] Ph. Boucaud *et al.* (ETM Collaboration), Phys. Lett. B **650**, 304 (2007).
[6] C. Allton *et al.* (RBC and UKQCD Collaborations), Phys. Rev. D **76**, 014504 (2007).
[7] C. R. Allton *et al.*, Phys. Lett. B **628**, 125 (2005).
[8] M. Gockeler *et al.* (QCDSF Collaboration), Proc. Sci., LAT2008 (2008) 136;J. Noaki *et al.*, Proc. Sci., LAT2008 (2008) 107 [arXiv:0810.1360].
[9] S. R. Beane *et al.*, Phys. Rev. D **77**, 014505 (2008).
[10] X. Feng, K. Jansen, and D. B. Renner, Phys. Lett. B **684**, 268 (2010).
[11] J. Bulava, K. J. Juge, C. J. Morningstar, M. J. Peardon, and C. H. Wong, Proc. Sci., LAT2009 (2009) 097 [arXiv:0911.2044]; C. Morningstar *et al.*, *in HADRON 2009: Proceedings of the XIII International Conference on Hadron Spectroscopy*, edited by Volker Crede, Paul Eugenio, and A. Ostrovidov, AIP Conf. Proc. No. 1257 (AIP, New York, 2010).
[12] J. J. Dudek, R. G. Edwards, M. J. Peardon, D. G. Richards, and C. E. Thomas, arXiv:1011.6352.
[13] K. Sasaki and N. Ishizuka, Phys. Rev. D **78**, 014511 (2008).
[14] J. Gasser and H. Leutwyler, Ann. Phys. (N.Y.) **158**, 142 (1984).
[15] T. N. Truong, Phys. Rev. Lett. **61**, 2526 (1988); **67**, 2260 (1991); A. Dobado *et al.*, Phys. Lett. B **235**, 134 (1990).
[16] A. Dobado and J. R. Peláez, Phys. Rev. D **47**, 4883 (1993); **56**, 3057 (1997).
[17] A. Gomez Nicola, J. R. Peláez, and G. Ríos, Phys. Rev. D **77**, 056006 (2008).
[18] C. Hanhart, J. R. Peláez, and G. Ríos, Phys. Rev. Lett. **100**, 152001 (2008).

[19] J. F. Donoghue, Phys. Rev. C **74**, 024002 (2006); T. Damour and J. F. Donoghue, Phys. Rev. D **78**, 014014 (2008).

[20] J. Nebreda and J. R. Peláez, Phys. Rev. D **81**, 054035 (2010).

[21] J. R. Peláez and G. Ríos, Phys. Rev. D **82**, 114002 (2010).

[22] P. C. Bruns and U.-G. Meißner, Eur. Phys. J. C **40**, 97 (2005).

[23] S. Weinberg, Physica A (Amsterdam) **96**, 327 (1979).

[24] G. Colangelo, J. Gasser, and H. Leutwyler, Nucl. Phys. **B603**, 125 (2001).

[25] G. Colangelo *et al.*, arXiv:1011.4408.

[26] G. Colangelo and S. Durr, Eur. Phys. J. C **33**, 543 (2004).

[27] J. Bijnens, G. Colangelo, G. Ecker, J. Gasser, and M. E. Sainio, Nucl. Phys.**B508**, 263 (1997); **B517**, 639(E) (1998).

[28] J. Bijnens, Prog. Part. Nucl. Phys. **58**, 521 (2007).

[29] P. Buettiker, S. Descotes-Genon, and B. Moussallam, Eur. Phys. J. C **33**, 409 (2004); S. Descotes-Genon and B. Moussallam, Eur. Phys. J. C **48**, 553 (2006).

[30] G. Amoros, J. Bijnens, and P. Talavera, Nucl. Phys. **B602**, 87 (2001).

[31] L. Girlanda, M. Knecht, B. Moussallam, and J. Stern, Phys. Lett. B **409**, 461 (1997).

[32] J. Gasser and U. G. Meissner, Phys. Lett. B **258**, 219 (1991).

[33] G. Grayer *et al.*, Nucl. Phys. **B75**, 189 (1974); L. Rosselet *et al.*, Phys. Rev. D **15**, 574 (1977); S. Pislak *et al.* (BNL-E865 Collaboration), Phys. Rev. Lett. **87**, 221801 (2001); J. R. Batley *et al.* (NA48/2 Collaboration), Eur. Phys. J. C **54**, 411 (2008); W. Hoogland *et al.*, Nucl. Phys. **B126**, 109 (1977); M. J. Losty *et al.*, Nucl. Phys. **B69**, 185 (1974); N. B. Durusoy *et al.*, Phys. Lett. B **45**, 517 (1973); S. D. Protopopescu *et al.*, Phys. Rev. D **7**, 1279 (1973); P. Estabrooks and A. D. Martin, Nucl. Phys. **B79**, 301 (1974); B. Hyams *et al.*, Nucl. Phys. **B64**, 134 (1973); D. H. Cohen *et al.*, Phys. Rev. D **7**, 661 (1973).

[34] R. Garcia-Martín, R. Kamiński, J. R. Peláez, J. R. de Elvira, and F. J. Ynduráin, Phys. Rev. D **83**, 074004 (2011).

[35] J. Nebreda, G. Ríos, J. R. Peláez, and F. J. Ynduráin (work in progress).

[36] P. C. Bruns and U. G. Meissner, Eur. Phys. J. C **40**, 97 (2005).

[37] G. Ecker, J. Gasser, H. Leutwyler, A. Pich, and E. de Rafael, Phys. Lett. B **223**, 425 (1989).

[38] F. Von Hippel and C. Quigg, Phys. Rev. D **5**, 624 (1972); H. Becker *et al.* (CERN-Munich Collaboration), Nucl. Phys. **B150**, 301 (1979); V. Chabaud *et al.* (CERN-Cracow-Munich Collaboration), Nucl. Phys. **B223**, 1 (1983); R. Kaminski, L. Lesniak, and K. Rybicki, Z. Phys. C **74**, 79 (1997); S. Kopp *et al.* (CLEO Collaboration), Phys. Rev. D **63**, 092001 (2001).

[39] J. Blatt and V. F. Weisskopf, *Theoretical Nuclear Physics* (Wiley, New York, 1952), p. 361.

[40] M. A. B. Beg and A. Zepeda, Phys. Rev. D **6**, 2912 (1972).

[41] M. K. Volkov and V. N. Pervushin, Nuovo Cimento Soc. Ital. Fis. A **27**, 277 (1975).

[42] J. Nieves, M. Pavon Valderrama, and E. Ruiz Arriola, Phys. Rev. D **65**, 036002 (2002).

[43] A. Dobado and J. R. Pelaez, Phys. Rev. D **65**, 077502 (2002).

[44] A. Gomez Nicola and J. R. Peláez, Phys. Rev. D **65**, 054009 (2002); J. R. Peláez, Mod. Phys. Lett. A **19**, 2879 (2004).

[45] J. R. Peláez, AIP Conf. Proc. **892**, 72 (2007); H. Leutwyler, AIP Conf. Proc. **1030**, 46 (2008).

[46] N. Levinson, K. Dan. Vidensk. Selsk. Mat. Fys. Medd. **25**, 9 (1949); R. G. Newton, *Scattering Theory of Waves and Particles* (McGraw-Hilll, New York, 1966).

2.1.4 Derivatives with respect to the quark masses at the physical values

Throughout this section we have been studying the behavior of the elastic resonances and phase-shifts when changing the quark masses to *unphysical values*. In this last section, we are going to calculate the derivatives of the resonances' masses with respect to the quark masses at their *physical values*. These calculations are useful for the determination of their spectroscopic nature, but also for the study of the cosmological variation of the fundamental constants [125, 54] predicted by some models of unification and suggested by some experimental data [126]. The change on light-meson and nucleon masses is particularly important for the variation of the constants of nature because it can modify the binding energy in deuterium, affecting the Big Bang Nucleosynthesis (BBN) [125]. It would also modify the position of compound resonances in heavy nuclei, which can be measured in the nuclear reactions in the stars and in the Oklo natural reactor [54].

First, we will calculate the derivatives of the Goldstone bosons, whose dependence on the quark masses is given by standard ChPT, which is model independent. The, we will calculate the derivatives of the lightest elastic resonances, $\rho(770)$, $K^*(892)$, $f_0(600)$ and $K_0^*(800)$, using Chiral Perturbation Theory unitarized with the elastic IAM.

Derivatives of the NGB

As stated above, the derivatives of the Goldstone bosons with respect to the quark masses can be directly calculated from their ChPT expansion. Thus, we will calculate them using some sets of LECs that we find in the literature for standard ChPT, as well as with the sets that we will use in the next sections for unitarized ChPT, in order to check that they yield compatible results.

On the one hand, for the pion nonstrange quark mass dependence, we use the SU(2) ChPT expansion up to two-loops [127, 99, 76],

$$\begin{aligned}\frac{M_\pi^2}{M_{0\pi}^2} &= 1+\frac{M_{0\pi}^2}{f_0^2}\left(2l_3^r+\frac{1}{2}L\right)+\frac{M_{0\pi}^4}{f_0^4}\left[\frac{1}{N}\left(l_1^r+2l_2^r-\frac{13}{3}L\right)\right.\\ &+ \frac{163}{96}\frac{1}{N^2}-\frac{7}{2}k_1-2k_2-4\left(l_3^r\right)^2+4l_3^r l_4^r-\frac{9}{4}k_3+\frac{1}{4}k_4+r_M^r\\ &+ \left.\left(2l_3^r+\frac{5}{2}L-2l_4^r+\frac{1}{2N}\right)\left(2l_3+\frac{1}{2}L\right)\right], \qquad (2.1)\end{aligned}$$

where $N=16\pi^2$, $L=\frac{1}{N}\log\frac{M_{0\pi}^2}{\mu^2}$ and $k_i=(4l_i^r-\gamma_i L)L$.

On the other hand, the SU(3) ChPT expansions [5, 3, 4],

$$\begin{aligned}M_\pi^2 &= M_{0\pi}^2\left[1+\mu_\pi-\frac{\mu_\eta}{3}+\frac{16M_{0K}^2}{f_0^2}\left(2L_6^r-L_4^r\right)+\frac{8M_{0\pi}^2}{f_0^2}\left(2L_6^r+2L_8^r-L_4^r-L_5^r\right)\right],\\ M_K^2 &= M_{0K}^2\left[1+\frac{2\mu_\eta}{3}+\frac{8M_{0\pi}^2}{f_0^2}\left(2L_6^r-L_4^r\right)+\frac{8M_{0K}^2}{f_0^2}\left(4L_6^r+2L_8^r-2L_4^r-L_5^r\right)\right],\\ M_\eta^2 &= M_{0\eta}^2\left[1+2\mu_K-\frac{4}{3}\mu_\eta+\frac{8M_{0\eta}^2}{f_0^2}(2L_8^r-L_5^r)+\frac{8}{f_0^2}(2M_{0K}^2+M_{0\pi}^2)(2L_6^r-L_4^r)\right]\\ &+ M_{0\pi}^2\left[-\mu_\pi+\frac{2}{3}\mu_K+\frac{1}{3}\mu_\eta\right]+\frac{128}{9f_0^2}(M_{0K}^2-M_{0\pi}^2)^2(3L_7+L_8^r), \qquad (2.2)\end{aligned}$$

allow us to include kaons and etas and calculate the strange quark mass dependence, although it will be more uncertain than that on the non-strange quark mass.

We then calculate analytically the derivatives of the r.h.s of eqs. (2.1) and (2.2) on the quark masses $\hat{m}$ and m_s. We are going to give the results in terms of the dimensionless and scale-independent parameters K_R, defined as:

$$K_R^f=\frac{m_f}{M_R}\frac{\partial M_R}{\partial m_f}, \qquad (2.3)$$

where m_f denotes the mass of a quark of flavor f and M_R denotes the resonance mass. In terms of the LO masses, $M_{0\pi}$, M_{0K} and $M_{0\eta}$, we can rewrite them as:

$$\begin{aligned} K_R^q &= \frac{M_{0\pi}^2}{M_R}\left(\frac{\partial M_R}{\partial M_{0\pi}^2}+\frac{1}{2}\frac{\partial M_R}{\partial M_{0K}^2}+\frac{1}{3}\frac{\partial M_R}{\partial M_{0\eta}^2}\right) \\ K_R^s &= \frac{M_{0K}^2-M_{0\pi}^2/2}{M_R}\left(\frac{\partial M_R}{\partial M_{0K}^2}+\frac{4}{3}\frac{\partial M_R}{\partial M_{0\eta}^2}\right). \end{aligned} \tag{2.4}$$

We have used two methods to evaluate the derivatives numerically. The difference between them is of a higher order in the ChPT expansion and has been considered as one of the sources of systematic uncertainty.

- Method A: In this method, we get the values of the tree-level quantities $M_{0\pi}$, M_{0K} and f_0 from the equations (2.1) and (2.2) and from the expansions of the decay constants, namely, in SU(2),

$$\begin{aligned} \frac{f_\pi}{f_0} &= 1+\frac{M_{0\pi}^2}{f_0^2}\left(l_4^r-L\right)+\frac{M_{0\pi}^4}{f_0^4}\left[\frac{1}{N}\left(-\frac{1}{2}l_1^r-l_2^r+\frac{29}{12}L\right)\right. \\ &- \frac{13}{192}\frac{1}{N^2}+\frac{7}{4}k_1+k_2-2l_3^rl_4^r+2\left(l_4^r\right)^2-\frac{5}{4}k_4+r_F^r \\ &+ \left.\left(2l_3^r+\frac{5}{2}L-2l_4^r\right)\left(l_4^r-L\right)-\frac{1}{N}\left(2l_3^r+\frac{1}{2}L\right)\right], \end{aligned} \tag{2.5}$$

  and, in $SU(3)$,

$$\begin{aligned} f_\pi &= f_0\left[1-2\mu_\pi-\mu_K+\frac{4M_{0\pi}^2}{f_0^2}\left(L_4^r+L_5^r\right)+\frac{8M_{0K}^2}{f_0^2}L_4^r\right], \\ f_K &= f_0\left[1-\frac{3\mu_\pi}{4}-\frac{3\mu_K}{2}-\frac{3\mu_\eta}{4}+\frac{4M_{0\pi}^2}{f_0^2}L_4^r+\frac{4M_{0K}^2}{f_0^2}\left(2L_4^r+L_5^r\right)\right], \\ f_\eta &= f_0\left[1-3\mu_K+\frac{4L_4^r}{f_0^2}\left(M_{0\pi}^2+2M_{0K}^2\right)+\frac{4M_{0\eta}^2}{f_0^2}L_5^r\right]. \end{aligned} \tag{2.6}$$

In the case of $SU(2)$, we impose the experimental value of M_π and f_π on the left side of the system of equations formed by (2.1) and (2.5) and solve it. In $SU(3)$, there are six physical quantities (three masses and three decay constants), but only three independent tree-level constants, since $M_{0\eta}$ is obtained from the Gell-Mann-Okubo relation $4M_{0k}^2 - M_{0\pi}^2 - 3M_{0\eta}^0 = 0$. Thus, we simply find the tree-level constants that best fit the experimental values.

- Method B: this time, instead of getting a value for the tree-level quantities, we rewrite the derivatives of the NGB masses in terms of the physical constants. The difference between calculating the derivatives in terms of the tree-level constants or in terms of the physical ones is a consequence of using a truncated expansion to describe observables. This difference will be of a higher order in the expansion and will give us an idea of the systematic error in our results.

We have calculated the parameters K_R^f for the pion and the kaon using both methods and different sets from SU(2) and SU(3) standard ChPT. The results are shown in the first eight rows of table 2.1, grouped under the 'ChPT LECs' label. The sets correspond to those introduced in section 1.3, except for the fact that some LECs have been replaced by lattice determinations, best suited for the study of the quark mass dependence: set IIIb corresponds to set III [88], with L_4 and the combinations $2L_6 - L_4$ and $2L_8 - L_5$ taken from the lattice set MILC 09A [100]; set IVb corresponds to set IV [89] in section 1.3 with l_3 replaced by the estimate given in the review of lattice results [91].

We see that the results are very compatible within the errors, which are bigger in the case of the m_s dependence. In table 2.2 we present our estimates: the central value is the average of all the results and the errors are taken to cover all the ChPT values. If we compare these numbers with the leading order calculations, which yield $K_\pi^q = 0.50$, $K_\pi^s = 0$, $K_K^q = 0.02$ and $K_K^s = 0.48$ for $m_s/\hat{m} = 22$ to 30 [31], we find that the higher order corrections are of the same order or smaller that the uncertainty of the results.

	N_f	meth.	set	$10^2\,K_\pi^q$	$10^2\,K_\pi^s$	$10^2\,K_K^q$	$10^2\,K_K^s$
ChPT LECs	$SU(2)$	A	III'	49.6 ± 0.7			
			IV'	49.4 ± 0.4			
		B	III'	49.5 ± 0.6			
			IV'	49.4 ± 0.3			
	$SU(3)$	A	II	49.4	-0.8	2.5	56.8
			III'	$48.9^{+0.5}_{-0.8}$	$2.0^{+3.6}_{-5.5}$	$2.0^{+0.4}_{-0.5}$	$52.2^{+4.3}_{-6.0}$
		B	II	49.6	-0.6	2.4	54.3
			III'	$49.1^{+0.2}_{-0.4}$	$1.6^{+2.9}_{-3.3}$	$2.0^{+0.3}_{-0.4}$	$50.3^{+4.0}_{-5.2}$
IAM LECs	$SU(2)$ $\mathcal{O}(p^4)$	A	1	49.0			
			2	49.2			
		B	1	49.1			
			2	50.3			
	$SU(2)$ $\mathcal{O}(p^6)$	A	3	49.5			
			4	49.4			
		B	3	49.5			
			4	49.4			
	$SU(3)$	A	5	50.2	6.9	2.9	60.6
			6	49.8	-1.1	2.7	58.4
		B	5	48.5	5.5	2.8	56.3
			6	49.9	-0.9	2.6	55.6
Chiral Unitary LECs	$SU(3)$	A	a	49.6	4.7	2.4	55.7
			b	49.6	4.7	2.4	55.7
			c	49.8	4.9	2.5	57.0
		B	a	49.0	4.5	2.4	54.8
			b	49.0	4.5	2.4	54.8
			c	49.0	4.6	2.5	55.8

Table 2.1: Different results for the quantity $10^2\,K_R^f$ as defined in (2.3), where $f = q$ for the non-strange quark mass dependence and $f = s$ for the strange one.

K_π^q	$0.494\,^{+0.009}_{-0.013}$	K_π^s	$0.005\,^{+0.051}_{-0.040}$
K_K^q	$0.022\,^{+0.003}_{-0.007}$	K_K^s	$0.534\,^{+0.043}_{-0.060}$

Table 2.2: Estimates for K_R^f coefficients for the pion and the kaon using low energy constants from ChPT.

K_π^q	$0.495\,^{+0.008}_{-0.010}$	K_π^s	$0.026\,^{+0.043}_{-0.037}$
K_K^q	$0.027\,^{+0.002}_{-0.003}$	K_K^s	0.577 ± 0.029

Table 2.3: Estimates for K_R^f coefficients for the pion and kaon using LECs from unitarized ChPT.

In the next section, where we will calculate the K_R^f parameters for the elastic resonances using unitarized ChPT, we will use sets of LECs that have been obtained by fitting the experimental data up to the resonance region and, in some cases, to lattice results. Before proceeding to these calculations, we are going to check that, if we use those LECs to calculate K_π^f and K_K^f, we get results compatible to those using LECs from standard ChPT. These results are shown in the second and third parts of table 2.2, labeled 'IAM LECs' and 'Chiral Unitary LECs', respectively, according to the unitarization method used for the analysis from which the corresponding LECs come from. The different sets were already presented in section 1.3.

These results are indeed very compatible with those found using standard ChPT low energy constants. In table 2.3 we present the average of the results with the errors taken to include all the values. Nevertheless, we have to take into account that these errors are probably underestimated since no error analysis has been performed for any of the sets.

Derivatives of the lightest elastic resonances

The elastic resonances are obtained from some form of unitarized ChPT, and they depend on quark masses through the ChPT expansion in terms of pion and kaon masses, which appear both kinematically and in interaction vertices. We are going

	N_f	meth.	set	$\hat{K}^q_\rho$	$\hat{K}^q_\sigma$	$\hat{K}^q_{K^*}$	$\hat{K}^q_\kappa$	$\hat{K}^s_\rho$	$\hat{K}^s_\sigma$	$\hat{K}^s_{K^*}$	$\hat{K}^s_\kappa$
IAM LECs	$SU(2)$ $\mathcal{O}(p^4)$	A	1	2.4	**7.9**						
			2	2.4	**7.8**						
		B	1	2.0	**7.7**						
			2	1.9	**7.9**						
	$SU(2)$ $\mathcal{O}(p^6)$	A	3	**6.0**	**7.4**						
			4	**5.6**	**8.7**						
		B	3	**6.0**	**7.4**						
			4	**5.6**	**8.7**						
	$SU(3)$	A	5	2.2	**7.2**	3.7	**2.5**	0.3	**-0.9**	15.9	**40.1**
			6	3.0	**8.1**	4.5	**3.1**	1.5	**-0.8**	13.9	**35.1**
		B	5	1.1	**6.2**	2.9	**2.2**	-1.2	**-2.1**	12.5	**36.5**
			6	2.0	**7.3**	3.7	**2.8**	0.2	**-1.6**	11.2	**32.7**
ChU LECs	$SU(3)$	A	a	3.7	5.9	1.4	1.9	-5.2	-5.9	4.8	30.2
			b	3.9	5.4	1.6	2.3	-4.9	-6.2	6.8	44.1
			c	3.6	5.7	1.5	2.5	-5.0	-5.8	6.4	59.1
		B	a	3.3	5.6	1.4	1.8	-5.3	-8.8	4.7	29.5
			b	3.5	5.1	1.4	1.8	-5.0	-8.2	6.4	35.5
			c	3.2	5.4	1.3	2.1	-5.4	-8.9	5.5	44.1

Table 2.4: Results for the parameter $\hat{K}^f_R = 10^2\, K^f_R$ for the resonances $\rho(770)$, $f_0(600)$ or σ, $K^*(892)$ and $K^*_0(800)$ or κ.

to use two unitarization techniques, the Inverse Amplitude Method [26, 27, 28, 29, 30], which has been explained in the introduction, since it is largely used in this thesis, and the Chiral Unitary approach (ChU) [21, 18], incorporated here only to estimate the systematic error.

The latter approach, which is much simpler despite being a coupled channel approach, contains spurious parameters and does not carry the full mass meson dependence on the scattering, since tadpoles and left cuts are ignored. The IAM, on the other hand, incorporates the fully renormalized ChPT amplitudes into a dispersion relation and does not contain any spurious parameter. Thus, it includes the whole quark mass dependence up to a given order in the ChPT expansion.

In order to calculate the parameters K_R^f, we change the NGB masses and decay constants with the quark masses according to their ChPT expansions (using the two approaches explained in the previous section) and calculate the corresponding change on the resonance masses. The results are shown in table 2.4. It is very important to remark that the dependence of the vector resonances on the quark masses is not so well determined because they depend strongly on the values of the LECs. However, scalars depend more on the chiral loops, which are model independent, and much less on the LECs. For this reason, the predictions for scalars are more reliable than for vectors, as already explained in [98]. In the table we highlight in boldface the most reliable results.

Finally, in table 2.5 we present our estimates for the σ, κ, $\rho(770)$ and $K^*(892)$ resonances. We have used for the central value that of the most reliable results, highlighted in boldface in table 2.4. If there are no 'most-reliable' results, we have simply taken the average of the IAM results. As we commented before, the ChU approach has only been used to enlarge the errors.

It is interesting to compare the value obtained for K_σ^s with the one used in [53] for the study of the cosmological variation of the fundamental parameters. In that work, the possible variation of the ratio of the weak/strong scales ($W = m_s/\Lambda_{\rm QCD}$) is studied. The strange quark mass is identified as the most important quantity,

K^q_ρ	$0.058\,^{+0.002}_{-0.047}$	K^s_ρ	$0.00\,^{+0.01}_{-0.06}$
K^q_σ	$0.08\,^{+0.01}_{-0.03}$	K^s_σ	$-0.01\,^{+0.01}_{-0.08}$
$K^q_{K^*}$	$0.04\,^{+0.01}_{-0.02}$	$K^s_{K^*}$	$0.13\,^{+0.03}_{-0.09}$
K^q_κ	0.03 ± 0.01	K^s_κ	$0.36\,^{+0.23}_{-0.07}$

Table 2.5: Estimates for K^f_R parameters as defined in (2.3) for the resonances $\rho(770)$, $f_0(600)$ or σ, $K^*(892)$ and $K^*_0(800)$ or κ.

and the σ meson mass as the ingredient of the nuclear forces most sensitive to it, compared to the ω and nucleon mass contributions. Using a simple constituent quark picture, assuming additivity of the strange sea, they estimate $K^s_\sigma \approx 0.54$, $K^s_\omega \approx 0.15$ and $K^s_N \approx 0.19$. Adding the dependence of the deuteron binding Q_d on the sigma, omega and nucleon masses

$$\frac{\delta Q_d}{Q_d} \approx -48\frac{\delta m_\sigma}{m_\sigma}, \qquad \frac{\delta Q_d}{Q_d} \approx 50\frac{\delta m_\omega}{m_\omega}, \qquad \frac{\delta Q_d}{Q_d} \approx 6\frac{\delta m_N}{m_N}, \tag{2.7}$$

they obtain

$$\frac{\delta Q_d}{Q_d} = -17\frac{\delta m_s}{m_s}, \tag{2.8}$$

and using the limit $|\delta Q_d/Q_d| < 0.1$ from [54], they get a final constraint on the m_s variation of

$$\left|\frac{\delta(m_s/\Lambda_{\rm QCD})}{(m_s/\Lambda_{\rm QCD})}\right| < 0.006. \tag{2.9}$$

However, we see in table 2.5 that our estimate for K^s_σ is much smaller and negative, $K^s_\sigma \approx -0.01$. Using this number together with their estimates for the ω and nucleon mass dependence, we would get $\delta Q_d/Q_d = 9\,\delta m_s/m_s$, and thus

$$\left|\frac{\delta(m_s/\Lambda_{\rm QCD})}{(m_s/\Lambda_{\rm QCD})}\right| < 0.01. \tag{2.10}$$

In their calculation, a strong cancelation between the σ and ω contributions occurred, whereas, if we use our result for K^s_σ, the σ contribution is much smaller. As a consequence, the sign of the dependence of Q_d on m_s changes. However, since the final result only depends on the absolute value of the variation of Q_d with m_s, the difference is not so big as it could be expected from the very disparate values of K^s_σ.

In [53] they also use a second method to constraint the ratio W based on the fact that the existence of certain isotopes depends on a neutron resonance whose energy varies strongly with the sigma and omega masses. Here there is a similar suppression of the sigma and omega contributions, so that the final result is not so strongly affected by the change of the estimate for K^s_σ. Their result $|\delta(m_s/\Lambda_{\rm QCD})/(m_s/\Lambda_{\rm QCD})| < 1.2 \times 10^{-10}$ changes to

$$\left|\frac{\delta(m_s/\Lambda_{\rm QCD})}{(m_s/\Lambda_{\rm QCD})}\right| < 3.7 \times 10^{-10} \tag{2.11}$$

when using our estimate. In both methods, the use of our K^s_σ leads to a result that is less constraining than theirs. Anyway, a full study of the cosmological variation of the fundamental constants using our values for the K^q_R parameters is now in preparation [124].

2.2 Properties of the light elastic resonances from their N_c behavior

In section 1.6 we introduced the QCD $1/N_c$ expansion. On the one hand, we saw that the $\bar{q}q$ and glueball states have a well determined $1/N_c$ behavior and, on the other hand, that the expansion is easily implemented in Chiral Perturbation Theory. Since the IAM incorporates the fully renormalized ChPT amplitudes into a dispersion relation without introducing cutoffs or subtraction constants, where spurious N_c dependences could hide, it can be used to study the N_c behavior of the

light elastic resonances. Comparing this behavior to the one expected for $\bar{q}q$ and glueball states is a useful tool to study the spectroscopic nature of these resonances.

This section is dedicated to our works on the N_c behavior of the elastic resonances. In publication 2.2.2 we review some recent results [128, 83] on the N_c behavior of the resonances $\rho(770)$ and $f_0(600)$, or σ, as well as our works on the quark mass dependence of resonance parameters. Since the chiral extrapolation has been largely treated in the previous section, we prefer to include publication 2.2.2 here. Next, in publication 2.2.3, we study the nature of the lightest elastic resonances using some highly N_c-suppressed observables.

2.2.1 Summary and discussion of results

Using the N_c dependence of the chiral amplitudes, it was shown in [128] that light vectors follow nicely a diquark behavior, whereas the nature of the light scalars cannot be predominantly $\bar{q}q$. This result was later confirmed at two loops [83] for the $\rho(770)$ and $f_0(600)$ mesons, getting for the latter a hint of a subdominant $\bar{q}q$ component with a mass around 1 GeV arising as N_c grows. This behavior would be most likely due to the mixing between light non-$\bar{q}q$ and heavier $\bar{q}q$ states. Morover, semi-local duality requires that the ρ and σ contributions to the $\pi^+\pi^+$ elastic cross section cancel and, thus, is spoilt at large N_c if these resonances behave very differently [129]. The subdominant $\bar{q}q$ component found in [83] would then be needed to restore the semi-local duality at large N_c. A recent work using unitary resonance chiral dynamics [130] confirms that the $\rho(770)$ is a stable meson in the limit $N_c \to \infty$ and that the σ is not predominantly a $\bar{q}q$ state at $N_c = 3$, but cannot conclude whether the σ resonance completely disappears at large N_c or has a subdominant component in its structure.

Publication 2.2.2 is a review of the results in [128] and [83]. It also includes a discussion on the applicability of the $1/N_c$ expansion within the IAM, which is a motivation for the next publication 2.2.3, as we will see. The main points in the discussion are the following:

- The IAM is not reliable in the $N_c \to \infty$ limit, because the theory becomes weakly interacting and unitarity constraints may not be so determining as other approximations made in the derivation of the method.
- Also, the mass of the η' scales as $1/\sqrt{N_c}$ in the chiral limit, and thus it could become a relevant degree of freedom at sufficiently high N_c. The $N_c \to \infty$ limit including the η' meson within $U(3) \times U(3)$ ChPT is studied in [131].
- Information on the dominant component of the light scalars can only be extracted in the vicinity of $N_c = 3$: since two-meson and some tetraquark states dissolve in the continuum in the $N_c \to \infty$ limit, a subdominant $\bar{q}q$ component could become dominant at large N_c. Moreover, the original mixing could change with N_c.

Thus, in order to obtain information about the physical resonances, we should consider N_c near its physical value. However, $1/N_c$ at $N_c = 3$ may not seem like a very small parameter to perform an expansion. Nevertheless, we can find observables whose next-to-leading order corrections are suppressed by higher orders of $1/N_c$, so that stronger conclusions can be drawn at the physical number of colors. In [132] it was found that, for a $\bar{q}q$ state, the real part of the inverse amplitude, evaluated at the resonance pole mass, scales as $\mathcal{O}(N_c^{-1})$ instead of $\mathcal{O}(N_c)$, and that the correction is of order $\mathcal{O}(N_c^{-3})$ at most. Likewise, it was shown that the correction to the $\mathcal{O}(N_c^{-1})$ leading behavior of $m_R\Gamma_R$ is also suppressed by two powers of N_c.

Making use of these ideas, in publication 2.2.3 we define two adimensional observables whose non-leading corrections are suppressed by two and three powers of N_c for a $\bar{q}q$ state. For a glueball these corrections are even more suppressed because of the fact that its width scales as $1/N_c^2$ instead of just $1/N_c$, as we saw in section 1.6. We calculate the size of these corrections for the lightest elastic resonances *at the physical number of colors* $N_c = 3$. This allows us to make a completely model-independent study, using the recent and very precise output of the data dispersive analyses in [95] and [133], without the need of the IAM. We find the following results:

- We observe that, for the $\rho(770)$ and $K^*(892)$ vector resonances, the suppression of our observables is of the order expected for $\bar{q}q$ states.
- In contrast, for the $f_0(600)$ and $K_0^*(800)$ scalar resonances, we find that the corrections are two orders of magnitude larger than expected for $\bar{q}q$ states, which makes the $\bar{q}q$ interpretation of both scalars very unnatural. For the $f_0(600)$ a dominant glueball component is also discarded.
- Unitarized ChPT is used to show that, for the scalars, the evolution of the corrections with N_c is far from what expected for $\bar{q}q$ states (and glueballs), which explains the need for unnaturally large corrections at $N_c = 3$.

2.2.2 Publication: J. R. Pelaez, J. Nebreda, G. Rios, **Properties of light resonances from unitarized Chiral perturbation theory: N_c behavior and quark mass dependence,** Prog. Theor. Phys. Suppl. 186, 113-123 (2010)

Properties of Light Resonances from Unitarized Chiral Perturbation Theory: N_c Behavior and Quark Mass Dependence

J. R. Peláez,*) J. Nebreda and G. Ríos

Dept. de Física Teórica II, Universidad Complutense, 28040 Madrid, Spain

We review the unitarization of Chiral Perturbation Theory with dispersion relations and how it describes meson-meson scattering data, generating light resonances whose mass, width and nature can be related to QCD parameters like quark masses and the number of colors.

§1. Introduction

Light hadron spectroscopy lies beyond the applicability of perturbative QCD. However, there is an effective field theory, known as Chiral Perturbation Theory[1] (ChPT), which provides a description of the dynamics of the lightest mesons. Despite it is limited to low energies and masses, here we review how, when combined with dispersion relations, it leads to a successful description of meson dynamics, generating resonant states without a priori assumptions on their existence or nature. This "unitarized ChPT" is a useful tool to identify the spectroscopic nature of resonances through their dependence on the QCD number of colors N_c, but also to relate lattice results to physical resonances by studying their quark mass, m_q, dependence.

ChPT is built out of the Goldstone Bosons of the QCD spontaneous chiral symmetry breaking, namely, pions, kaons and etas, as a low energy expansion of a Lagrangian respecting all QCD symmetries. It is organized in powers of p^2/Λ^2, where p stands either for derivatives, momenta or meson masses, and $\Lambda \equiv 4\pi f_\pi$, where f_π denotes the pion decay constant. ChPT is renormalized order by order by absorbing loop divergences in the renormalization of parameters of higher order counterterms, known as low energy constants (LECs) that *carry no energy or mass dependence* and depend on a regularization scale μ. As always after renormalization, the full amplitude is independent of this scale. Their values depend on the QCD dynamics, and are determined from experiment. Up to the desired order, the ChPT expansion provides a *systematic and model independent* description of how meson observables depend on QCD parameters like the light quark masses $\hat{m} = (m_u + m_d)/2$ and m_s, or the leading $1/N_c$ behavior.[2]

§2. Dispersion relations and unitarization

Elastic resonances appear as poles on the second Riemann sheet of the meson-meson scattering partial waves t_{IJ} of definite isospin I and angular momentum J. At physical values of s, elastic unitarity implies

*) Speaker. J.R.P. thanks the NFQCD2010 organizers for the invitation and for their work to create such an exciting workshop.

$$\mathrm{Im}\, t_{IJ}(s) = \sigma(s)|t_{IJ}(s)|^2 \;\; \Rightarrow \;\; t_{IJ} = \frac{1}{\mathrm{Re}\, t_{IJ}^{-1} - i\sigma}, \quad \text{with} \quad \sigma(s) = 2p/\sqrt{s}, \quad (2{\cdot}1)$$

where s is the Mandelstam variable and p is the center of mass momentum. However, ChPT amplitudes, being an expansion $t_{IJ} \simeq t_{IJ}^{(2)} + t_{IJ}^{(4)} + \cdots$, with $t^{(2k)} = O(p^{2k})$, can only satisfy Eq. (2·1) perturbatively

$$\mathrm{Im}\, t_{IJ}^{(2)}(s) = 0,\ \mathrm{Im}\, t_{IJ}^{(4)}(s) = \sigma(s)|t_{IJ}(s)^{(2)}|^2,\ \cdots \Rightarrow\ \mathrm{Im}\, t_{IJ}^{(4)}(s)/{t_{IJ}^{(2)}}^2(s) = \sigma(s), \quad (2{\cdot}2)$$

and cannot generate poles. However, the resonance region can be reached combining ChPT with dispersion theory either for the amplitude[3] or for the inverse amplitude through the Inverse Amplitude Method (IAM).[4–6] We will concentrate on the *one-channel* IAM,[4,5] since it uses ChPT only up to a given order inside a dispersion relation, without additional input or further model dependent assumptions. Other unitarization techniques will be commented below.

2.1. *The one-loop ChPT Inverse Amplitude Method*

For a partial wave $t_{IJ}(s)$, we can write a dispersion relation (that we subtract three times, since we will also use it below for $t_{IJ}^{(4)}$, that grows with s^2)

$$t_{IJ}(s) = C_0 + C_1 s + C_2 s^2 + \frac{s^3}{\pi}\int_{s_{th}}^{\infty} \frac{\mathrm{Im}\, t_{IJ}(s')ds'}{s'^3(s'-s-i\epsilon)} + LC(t_{IJ}). \quad (2{\cdot}3)$$

Note we have explicitly written the integral over the physical cut, extending from threshold, s_{th}, to infinity, but we have abbreviated by LC the equivalent expression for the left cut (from 0 to $-\infty$). We could do similarly with other cuts, if present, as for $\pi K \to \pi K$. Note that from Eq. (2·1) the imaginary part of the *inverse amplitude* is *exactly* known in the elastic regime. We can then write a dispersion relation like that in (2·3) but now for the auxiliary function $G = (t_{IJ}^{(2)})^2/t_{IJ}$, i.e.,

$$G(s) = G_0 + G_1 s + G_2 s^2 + \frac{s^3}{\pi}\int_{s_{th}}^{\infty} \frac{\mathrm{Im}\, G(s')ds'}{s'^3(s'-s-i\epsilon)} + LC(G) + PC,$$

where now PC stands for possible pole contributions in G coming from zeros in t_{IJ}. It is now straightforward to expand the subtraction constants and use that $\mathrm{Im}\, t_{IJ}^{(2)} = 0$ and $\mathrm{Im}\, t_{IJ}^{(4)} = \sigma|t_{IJ}^{(2)}|^2$, so that $\mathrm{Im}\, G = -\mathrm{Im}\, t_{IJ}^{(4)}$. In addition, up to the given order, $LC(G) \simeq -LC(t_{IJ}^{(4)})$, whereas PC is of higher order and can be neglected. Then

$$\frac{t_{IJ}^{(2)2}}{t_{IJ}} \simeq a_0 + a_1 s - b_0 - b_1 s - b_2 s^2 - \frac{s^3}{\pi}\int_{s_{th}}^{\infty} \frac{\mathrm{Im}\, t_{IJ}^{(4)}(s')ds'}{s'^3(s'-s-i\epsilon)} - LC(t_{IJ}^{(4)}) \simeq t_{IJ}^{(2)} - t_{IJ}^{(4)},$$

since the a_i, b_i terms, coming from the G_i expansion, are the subtraction terms of a dispersion relation for $t_{IJ}^{(2)} - t_{IJ}^{(4)}$. Thus we arrive at the so-called IAM:

$$t_{IJ} \simeq t_{IJ}^{(2)2}/(t_{IJ}^{(2)} - t_{IJ}^{(4)}), \quad (2{\cdot}4)$$

that provides an elastic amplitude satisfying unitarity and has the correct ChPT expansion up to the order we have used. The PC contribution has been calculated

explicitly[6] and is not just formally suppressed, but numerically negligible except near the Adler zeros, away from the physical region. It is straightforward to extend the IAM to other elastic channels or higher orders.[5] Naively, the IAM looks like replacing $\mathrm{Re}\, t_{IJ}^{-1}$ by its $O(p^4)$ ChPT expansion in (2·1), but (2·1) is only valid in the real axis, whereas our derivation allows us to consider the amplitude in the complex plane and look for poles associated to resonances. Let us remark that, since ChPT is used *only at low energies* in the dispersion relation, the IAM formula is justified only up to energies where inelasticities become important, even though ChPT does not converge at those energies. Only when the energy is close to the Adler zero one should use a slightly modified version of the IAM.[6] Re-expanding the IAM, ChPT is recovered up to the order it was used as input, as well as partial contributions to higher order, but not the complete series — see Ref. 7) for a discussion of this issue.

In Fig. 1 we present some results[8] of an updated fit of the IAM $\pi\pi$ and πK scattering amplitudes to data, simultaneously fitting the available lattice results on ratios of meson masses and decay constants and some scattering lengths. It is important to remark that the resulting LECs are in fairly good agreement with standard determinations: no fine tuning is required. The $f_0(600)$, $\rho(770)$, $\kappa(800)$ and $K^*(892)$ are *not introduced by hand* but *generated* as poles in the second Riemann sheet of their corresponding partial waves. The fact that we do not need to model the integrands and *the only input parameters are those of ChPT* is relevant since we then know how to relate our amplitudes to QCD parameters like N_c or m_q.

2.2. *Other unitarization techniques within the coupled channel formalism*

Naively one can arrive at (2·4) in a matrix form, ensuring coupled channel unitarity, just by expanding the real part of the inverse T matrix. Unfortunately, *there is still no dispersive derivation* including a left cut *for the coupled channel case.* Being much more complicated, different approximations to $\mathrm{Re}\, T^{-1}$ have been used:

• The fully renormalized one-loop ChPT calculation of $\mathrm{Re}\, T^{-1}$ provides the correct ChPT expansion, with left cuts approximated to $O(p^4)$.[10),12)] Indeed, using LECs consistent with standard ChPT determinations, one can describe[10] below 1.2 GeV all two-body scattering channels made of pions, kaons or etas. Simultaneously, this approach[10] generates poles associated to the $\rho(770)$ and $K^*(892)$ vector mesons, together with the $f_0(980)$, $a_0(980)$, $f_0(600)$ and κ (or $K_0(800)$) scalar resonances.

• Originally,[13] the coupled channel IAM was used neglecting crossed loops and tadpoles. This is considerably simpler, and despite the left cut is absent, since its numerical influence is relatively small, meson-meson data are described with reasonable LECs while generating all poles enumerated above. Note that this approximation keeps the s-channel loops but also the tree level up to $O(p^4)$, which encodes the effect of heavier resonances, like the ρ. Thus, contrary to some common belief, the IAM incorporates the low energy effects of t-channel ρ exchange.

• Finally, if only scalar meson-meson scattering is of interest, it is possible to use just one cutoff (or another regulator) that numerically mimics the combination of LECs appearing in scalar channels. This "chiral unitary approach" is very popular, even beyond the meson-meson framework, due to its great simplicity but remarkable success[14] and also for its straightforward relation to the Bethe-Salpeter formalism[15]

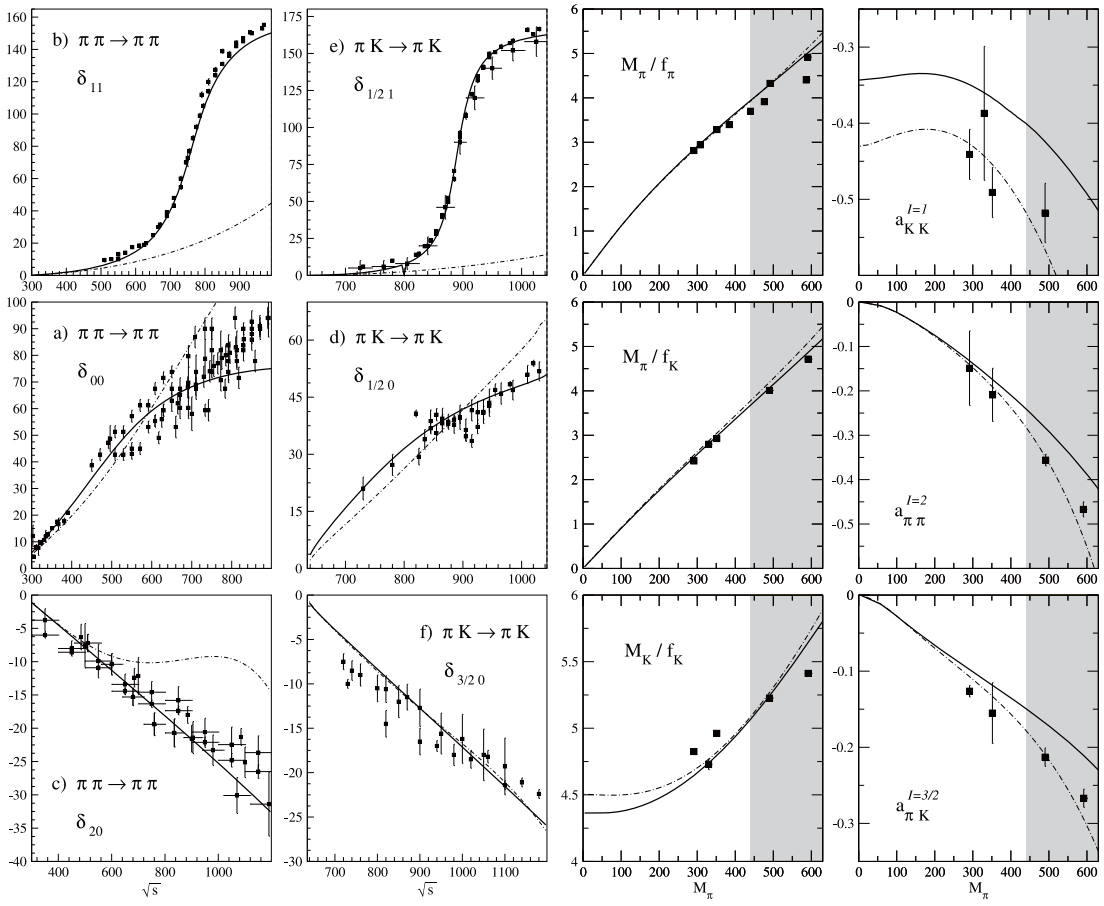

Fig. 1. Updated IAM fit[8] (continuous line). We also show non-unitarized ChPT results with the LECs from the K_{l4} two-loop analysis[9] (dot-dashed line). **Left**: IAM versus data on $\pi\pi$ and πK scattering. **Right**: fit results compared to lattice calculations[11] on ratios of meson masses and decay constants and some scattering lengths. We fit up to $m_\pi = 440$ MeV, but even beyond (grey areas) lattice results are not described badly. Experimental references are detailed in 10).

that provides physical insight on unitarization. With this method it was shown[16] that, assuming no m_q dependence of the cutoff, all light scalar resonances degenerate into an octet and a singlet in the $SU(3)$ limit. Axial-vector mesons have also been generated by using a chiral Lagrangian for the pseudoscalar-vector interaction.[17]

§3. The nature of resonances from their leading $1/N_c$ behavior

The QCD $1/N_c$ expansion,[2] valid in the whole energy region, provides a rigorous definition of $\bar{q}q$ bound states: their masses and widths behave as $O(1)$ and $O(1/N_c)$, respectively. The QCD leading $1/N_c$ behavior of f_π and the LECs is well known, and ChPT amplitudes have no cutoffs or subtraction constants where spurious N_c dependences could hide. Hence, by scaling with N_c the ChPT parameters in the IAM, the N_c dependence of the mass and width of the resonances has been determined to

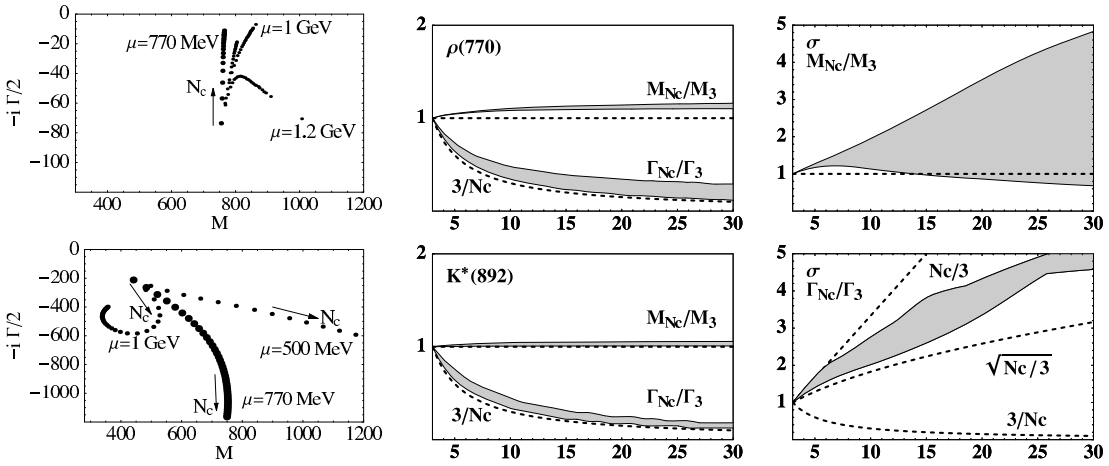

Fig. 2. **Left:** ρ (top) and σ (bottom) pole trajectories for different values of μ, note that for $\mu = 1.2$ GeV the ρ pole goes away the real axis. **Center:** N_c behavior of the ρ (top) and K^* (bottom) mass and width. **Right:** N_c behavior of the σ mass and width.

one and two loops.[18),19)] These are defined from the pole position as $\sqrt{s_{pole}} = M - i\Gamma$. However, *a priori*, one should be careful *not to take N_c too large, because the $N_c \to \infty$ limit is a weakly interacting limit.* As shown above, the IAM relies on the fact that the exact elastic *RC* contribution dominates the dispersion relation. Since the IAM describes data and the resonances within, say, 10 to 20% errors, this means that at $N_c = 3$ the other contributions are not approximated badly. But meson loops, responsible for the *RC*, scale as $3/N_c$ whereas the inaccuracies due to the approximations scale partly as $O(1)$. Thus, we can estimate that those 10 to 20% errors at $N_c = 3$ become 100% errors at, say $N_c \sim 30$ or $N_c \sim 15$, respectively. Hence we never show results[18),19)] beyond $N_c = 30$. Even beyond $N_c \sim 15$ they should be interpreted with care.

Thus, Fig. 2 shows the behavior of the ρ, K^* and σ masses and widths found in 18). The ρ and K^* neatly follow the expected behavior for a $\bar{q}q$ state: $M \sim 1$, $\Gamma \sim 1/N_c$. The bands cover the uncertainty $\mu \sim 0.5 - 1$ GeV where to apply the $1/Nc$ scaling. Note also that *outside this μ range* the ρ meson starts deviating from a $\bar{q}q$ behavior. Something similar occurs to the $K^*(892)$. Hence, we cannot apply the N_c scaling at an arbitrary μ value, if the well established ρ and K^* $\bar{q}q$ nature is to be reproduced.

In contrast, the σ shows a different behavior from that of a pure $\bar{q}q$: *near* $N_c = 3$ both its mass and width grow with N_c, i.e. its pole moves away from the real axis. Of course, far from $N_c = 3$, and for some choices of LECs and μ, the σ pole might turn back to the real axis,[19)–21)] as seen in Fig. 2 (top-right). But, as commented above, the IAM is less reliable for large N_c, and at most this behavior only suggests that there *might be* a subdominant $\bar{q}q$ component.[19)] In addition, we have to ensure that the LECs fit data and reproduce the vector $\bar{q}q$ behavior.

Since loops are important in determining the scalar pole position, but are $1/N_c$ suppressed compared to tree level terms with LECs, we checked the $O(p^4)$ results with an $O(p^6)$ IAM calculation in $SU(2)$.[19)] We defined a χ^2-like function to measure

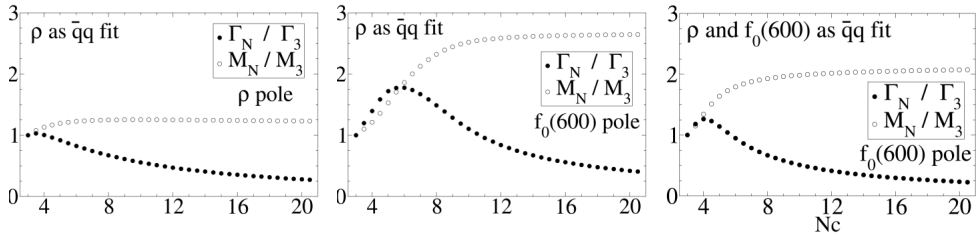

Fig. 3. **Left and center**: N_c behavior of the ρ and σ pole at $O(p^6)$ with the "ρ as $\bar{q}q$ fit". **Right:** Sigma behavior with N_c at $O(p^6)$ with the "ρ and σ as $\bar{q}q$ fit".

how close a resonance is from a $\bar{q}q$ N_c behavior. First, we used it at $O(p^4)$ to show that it is not possible for the σ to behave predominantly as a $\bar{q}q$ while describing simultaneously the data and the ρ $\bar{q}q$ behavior, thus *confirming the robustness of the conclusions for N_c close to 3*. Next, we obtained an $O(p^6)$ data fit where the ρ $\bar{q}q$ behavior was imposed (see Fig. 3, left and center). Note that both M_σ and Γ_σ grow with N_c near $N_c = 3$, confirming the $O(p^4)$ result of a non $\bar{q}q$ dominant component. However, for N_c between 8 and 15, where we still trust the IAM, M_σ becomes constant and Γ_σ starts decreasing. This may hint to a *subdominant $\bar{q}q$ component*, arising as loops become suppressed when N_c grows. Finally, by forcing the σ to behave as a $\bar{q}q$, we found that in the best case (Fig. 3, right) this subdominant $\bar{q}q$ component could become dominant around $N_c > 6 - 8$, at best, but always with an $N_c \to \infty$ mass above ~ 1 GeV instead of its physical ~ 450 MeV value.

Let us emphasize again[22] what can and *what cannot* be concluded from our results and clarify some frequent questions and doubts:

• Most likely, scalars are a mixture of different states, but *the dominant component of the σ and κ in meson-meson scattering does not behave as a $\bar{q}q$*. If the $\bar{q}q$ was *dominant*, they would behave as the ρ or the K^* in Fig. 2. *However, a smaller fraction of $\bar{q}q$ cannot be excluded* and is somewhat favored in our $O(p^6)$ analysis.[19]

• *Two meson and some tetraquark states[23] have a consistent "qualitative" behavior*, i.e., both disappear in the meson-meson scattering continuum as N_c increases. Our results are not able yet to establish the nature of that dominant component. To do so other tools[28),29)] might be necessary. The most we can state is that the behavior of two-meson states or some tetraquarks might be qualitatively consistent.

The $N_c \to \infty$ limit has been studied in 20) and 21). Apart from its mathematical interest, it could have some physical relevance if the data and the large N_c uncertainty on the choice of scale were more accurate. Nevertheless:

• *A priori the IAM is not reliable in the $N_c \to \infty$ limit*, since that is a weakly interacting theory, where exact unitarity becomes less relevant in confront of other approximations made in the IAM derivation. It has been shown[20] that it might work well in that limit in the vector channel of QCD but not in the scalar channel.

• Another reason to keep N_c not too far from 3 is that we have not included the $\eta'(980)$, whose mass is related to the $U_A(1)$ anomaly and scales as $\sqrt{3/N_c}$. Nevertheless, if in our calculations we keep $N_c < 30$, its mass would be $> 310\,\text{MeV}$ and thus pions are still the only relevant degrees of freedom in the σ region.

• *Contrary to the leading $1/N_c$ behavior in the vicinity of $N_c = 3$, the $N_c \to \infty$*

limit does not give information on the "dominant component" of light scalars. The reason was commented above: in contrast to $\bar{q}q$ states, that become bound, two-meson and some tetraquark states dissolve in the continuum as $N_c \to \infty$. Thus, even if we started with an infinitesimal $\bar{q}q$ component in a resonance, for a sufficiently large N_c it may become dominant, and beyond that N_c the associated pole would behave as a $\bar{q}q$ state. Also, since the mixings of different components could change with N_c, a too large N_c could alter significantly the original mixings.

Actually, this is what happens for the one-loop IAM σ resonance for $N_c \to \infty$, but it does *not* necessarily mean that the "correct interpretation [...] is that the σ pole is a conventional $\bar{q}q$ meson environed by heavy pion clouds".[21] That the σ is not conventional is simply seen by comparing it with the "conventional" ρ and K^* in Fig. 2. A large two-meson component is consistent, but so is a tetraquark. Actually, the $N_c \to \infty$ of the one-loop unitarized ChPT pole in the scalar channel limit is not unique[20),21)] given the uncertainty in the chiral parameters. Moreover, despite the one-loop IAM could make sense in the $N_c \to \infty$ limit for the vector channel,[20)] in the scalar channel it can lead to phenomenological inconsistencies[20)] for some LECs, since poles can even move to negative squared mass values (weird), to infinity or to a positive mass square. Hence, robust conclusions on the dominant light scalar component can be obtained not too far from real life, say $N_c < 15$ or 30, for a μ choice between roughly 0.5 and 1 GeV, that simultaneously ensures the $\bar{q}q$ dependence for the ρ and K^* mesons. Note, however, that under these same conditions the two-loop IAM still finds, not only a dominant non-$\bar{q}q$ component, but also a hint of a $\bar{q}q$ subdominant component,[19)] which is not conventional in the sense that it appears at a much higher mass than the physical σ. This subdominant component at that higher mass seems to be needed to ensure fulfillment of local duality[24)] for $Nc > 3$. This may support the existence of a second scalar octet, a $\bar{q}q$ now, above 1 GeV.[25)]

Finally, using not the IAM, but the chiral unitary approach with a natural range for the cutoff N_c dependence, it has also been suggested[26)] that a large, in some cases dominant, non $\bar{q}q$ behavior could exist in axial vector mesons.

§4. Quark mass dependence of resonances

ChPT provides a rigorous expansion of meson masses in terms of m_q (at leading order $M^2_{meson} \sim m_q$). Thus, by changing the meson masses in the amplitudes, we see how the poles generated with the IAM depend on m_q. We report here the $SU(2)$ analysis[27)] of ρ and σ as well the $SU(3)$ analysis[8)] of non-strange, ρ and σ, and strange, $\kappa(800)$ and $K^*(892)$, resonances.

The values of m_π considered should fall within the ChPT range of applicability and allow for some elastic $\pi\pi$ and πK regime below $K\bar{K}$ or $K\eta$ thresholds, respectively. Both criteria are satisfied if $m_\pi \leq 440$ MeV, since $SU(3)$ ChPT still works with such kaon masses, and because for $m_\pi \simeq 440$ MeV, the kaon mass becomes $\simeq 600$ MeV. Of course, we expect higher order corrections, which are not considered here, to become more relevant as m_π is increased. Thus, our results become less reliable as m_π increases due to the $O(p^6)$ corrections which we have neglected.

Figure 4 (left) shows the evolution of the σ and ρ pole positions as m_π is in-

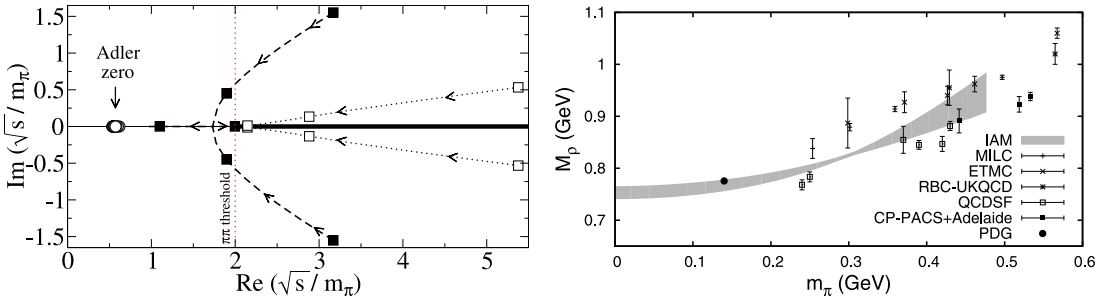

Fig. 4. **Left:** Movement of the σ (dashed lines) and ρ (dotted lines) poles for increasing m_π (direction indicated by the arrows) on the second sheet. The filled (open) boxes denote the pole positions for the σ (ρ) at pion masses $m_\pi = 1,\ 2$, and $3 \times m_\pi^{\rm phys}$, respectively. For $m_\pi = 3m_\pi^{\rm phys}$ three poles accumulate very near the threshold. All poles are always far enough from the Adler zero (circles). **Right:** Comparison of our results for the M_ρ dependence on m_π with some recent lattice results.[32] The grey band covers the error coming from the LECs uncertainties.

creased. In order to see the pole movements relative to the two pion threshold, which is also increasing, we use units of m_π, so the threshold is fixed at $\sqrt{s} = 2$. Both poles move closer to threshold and they approach the real axis. The ρ poles reach the real axis at the same time that they cross threshold. One of them jumps into the first sheet and stays below threshold in the real axis as a bound state, while its conjugate partner remains on the second sheet practically at the very same position as that in the first. In contrast, the σ poles go below threshold with a finite imaginary part before they meet in the real axis, still on the second sheet, becoming virtual states. As m_π increases, one pole moves toward threshold and jumps through the branch point to the first sheet staying in the real axis below threshold, very close to it as m_π keeps growing. The other σ pole moves down in energies away from threshold and remains on the second sheet. These very asymmetric poles could signal a prominent molecular component,[28),29)] at least for large pion masses. Similar movements were found within quark models[30)] and a finite density analysis.[31)]

Figure 4 (right) shows our results for the ρ mass dependence on m_π compared with some recent lattice results,[32)] and the PDG value for the ρ mass. Now the mass is defined as the point where the phase shift crosses $\pi/2$, except for those m_π values where the ρ becomes a bound state, where it is defined again from the pole position. Taking into account the incompatibilities between different lattice collaborations, we find a qualitative good agreement with lattice results. Note also that the m_π dependence in our approach is correct only up to NLO in ChPT, and we expect higher order corrections to be important for large pion masses. The M_ρ dependence on m_π agrees also with estimations for the two first coefficients of its chiral expansion.[33)]

In Fig. 5 (left) we compare the m_π dependence of M_ρ and M_σ (defined from the pole position $\sqrt{s_{pole}} = M - i\Gamma/2$), normalized to their physical values. The bands cover the LECs uncertainties. Both masses grow with m_π, but M_σ grows faster than M_ρ. Below $m_\pi \simeq 2.4\, m_\pi^{\rm phys}$ we only show one line because the two conjugate σ poles have the same mass. Above $2.4\, m_\pi^{\rm phys}$, these two poles lie on the real axis

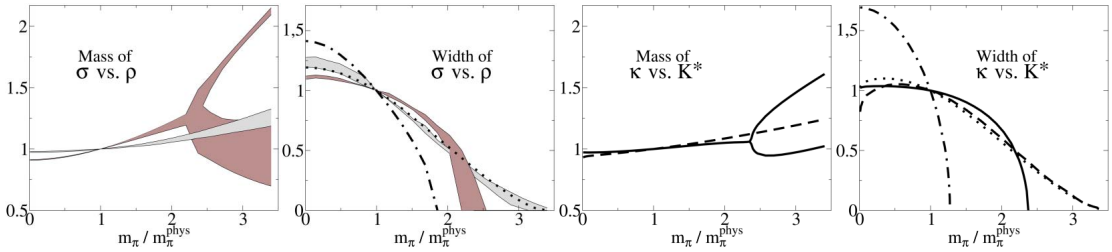

Fig. 5. m_π dependence of resonance masses and widths in units of the physical values. In the two left panels the dark (light) band shows the results for the σ (ρ). The band width reflects the uncertainties in the $SU(2)$ LECs. Similarly, the two right panels, calculated within $SU(3)$,[8] show the behavior for the $K^*(892)$ (continuous) and $\kappa(800)$ (dashed). The (dotted) dot-dashed line shows the m_π dependence of the corresponding vector (scalar) width from the change of phase space only, assuming a constant coupling of the resonance to two mesons.

with two different masses. The heavier pole goes towards threshold and around $m_\pi \simeq 3.3\, m_\pi^{\rm phys}$ moves into the first sheet, but that is beyond our applicability limit.

In the next panel of Fig. 5 we compare the m_π dependence of Γ_ρ and Γ_σ normalized to their physical values: note that both widths become smaller. We compare this decrease with the expected phase space reduction as resonances approach the $\pi\pi$ threshold. We find that Γ_ρ follows very well this expected behavior, which implies that the $\rho\pi\pi$ coupling is almost m_π independent. In contrast, Γ_σ deviates from the phase space reduction expectation. This suggests a strong m_π dependence of the σ coupling to two pions, necessarily present for molecular states.[29),34)]

Finally, in the last two panels of Fig. 5 we compare the mass and width dependence on $\hat{m}$ of the $\kappa(800)$ versus the $K^*(892)$, keeping m_s fixed.[8)] Note that the same pattern of the $\sigma - \rho$ system is repeated. Belonging to the same octet, $K^*(892)$ and ρ behave very similarly, and both their widths follow just phase space reduction. The σ and κ behaviors are only qualitatively similar, the latter being somewhat softer. This might be partly due to a possible significant admixture of singlet state in the σ. The dependence of these resonances on m_s has been also studied in Ref. 8).

§5. Summary

We have reviewed how the Inverse Amplitude Method (IAM)[6)] is derived from the first principles of analyticity, unitarity, and Chiral Perturbation Theory (ChPT) at low energies. It is able to generate, as poles in the amplitudes, the light resonances appearing in meson-meson elastic scattering, without any a priori assumptions. Up to a given order in ChPT, it yields the correct dependences on $\hat{m}, m_s$ and N_c.

The leading $1/N_c$ behavior suggests that the dominant component of light scalars does not behave as a $\bar{q}q$ state as N_c increases not far from $N_c = 3$. When using the two loop IAM result in $SU(2)$, below $N_c \sim 15$ or 30, there is a hint of a subdominant $\bar{q}q$ component, but arising at roughly twice the mass of the physical σ.

We have studied the pion (quark) mass dependence of the $f_0(600), \rho(770), \kappa(800)$ and $K^*(892)$ poles[8),27)] and how they become bound states: softly for vectors and

with a non-analyticity for scalars. We found that the vector-meson-meson coupling constant is almost m_π independent and a qualitative agreement with some lattice results for the ρ mass evolution with m_π. These results may be relevant for studies of the meson spectrum[36] and form factors[35] on the lattice.

Acknowledgements

Work partially supported by Spanish MICINN: FPA2007-29115-E, FPA2008-00592 and FIS2006-03438, U.Complutense/ Banco Santander grant PR34/07-15875-BSCH and UCM-BSCH GR58/08 910309 and the EU-Research Infrastructure Integrating Activity "Study of Strongly Interacting Matter" (HadronPhysics2, Grant n. 227431) under the EU Seventh Framework Programme.

References

1) S. Weinberg, Physica A **96** (1979), 327.
J. Gasser and H. Leutwyler, Ann. of Phys. **158** (1984), 142; Nucl. Phys. B **250** (1985), 465.
2) G. 't Hooft, Nucl. Phys. B **72** (1974), 461.
E. Witten, Ann. of Phys. **128** (1980), 363.
3) I. Caprini, G. Colangelo and H. Leutwyler, Phys. Rev. Lett. **96** (2006), 132001.
S. Descotes-Genon and B. Moussallam, Eur. Phys. J. C **48** (2006), 553.
4) T. N. Truong, Phys. Rev. Lett. **61** (1988), 2526; Phys. Rev. Lett. **67** (1991), 2260.
A. Dobado, M. J. Herrero and T. N. Truong, Phys. Lett. B **235** (1990), 134.
5) A. Dobado and J. R. Peláez, Phys. Rev. D **47** (1993), 4883; Phys. Rev. D **56** (1997), 3057.
6) A. Gomez Nicola, J. R. Pelaez and G. Rios, Phys. Rev. D **77** (2008), 056006.
7) J. Gasser and U.-G. Meißner, Nucl. Phys. B **357** (1991), 90.
8) J. Nebreda and J. R. Pelaez, Phys. Rev. D **81** (2010), 054035.
9) G. Amoros, J. Bijnens and P. Talavera, Nucl. Phys. B **602** (2001), 87.
10) A. Gomez Nicola and J. R. Pelaez, Phys. Rev. D **65** (2002), 054009; AIP Conf. Proc. **660** (2003), 102, hep-ph/0301049.
J. R. Pelaez, Mod. Phys. Lett. A **19** (2004), 2879.
11) S. R. Beane et al. (NPLQCD Collaboration), Phys. Rev. D **77** (2008), 094507; Phys. Rev. D **77** (2008), 014505.
S. R. Beane et al. (NPLQCD Collaboration), Phys. Rev. D **74** (2006), 114503.
Ph. Boucaud et al. (ETM collaboration), Comput. Phys. Commun. **179** (2008), 695.
12) F. Guerrero and J. A. Oller, Nucl. Phys. B **537** (1999), 459 [Errata; **602** (2001), 641].
13) J. A. Oller, E. Oset and J. R. Pelaez, Phys. Rev. Lett. **80** (1998), 3452;Phys. Rev. D **59** (1999), 074001.
14) J. A. Oller and E. Oset, Nucl. Phys. A **620** (1997), 438 [Errata; **652** (1999), 407]; Phys. Rev. D **62** (2000), 114017.
15) J. Nieves and E. Ruiz Arriola, Phys. Lett. B **455** (1999), 30.
16) J. A. Oller, Nucl. Phys. A **727** (2003), 353.
17) M. F. M. Lutz and E. E. Kolomeitsev, Nucl. Phys. A **730** (2004), 392.
L. Roca, E. Oset and J. Singh, Phys. Rev. D **72** (2005), 014002.
L. S. Geng, E. Oset, L. Roca and J. A. Oller, Phys. Rev. D **75** (2007), 014017.
18) J. R. Pelaez, Phys. Rev. Lett. **92** (2004), 102001.
19) J. R. Pelaez and G. Rios, Phys. Rev. Lett. **97** (2006), 242002.
20) J. Nieves and E. R. Arriola, Phys. Rev. D **80** (2009), 045023.
21) Z. X. Sun et al., hep-ph/0411375.
Z. X. Sun et al., hep-ph/0503195.
22) J. R. Pelaez, hep-ph/0509284; *Proceedings of the 11th International Conference on Elastic and Diffractive Scattering, Blois, France, 15-20 May 2005.*
J. R. Pelaez and G. Rios, arXiv:0905.4689; *Proceedings of Excited QCD, Zakopane, Poland, 8-14 Feb 2009.*

23) R. L. Jaffe, *Proc. of the Intl. Symposium on Lepton and Photon Interactions at High Energies, Physikalisches Institut, Univ. of Bonn (1981)*, ISBN: 3-9800625-0-3.
24) J. R. de Elvira, J. R. Pelaez, M. R. Pennington and D. J. Wilson, arXiv:1001.2746.
25) E. van Beveren et al., Z. Phys. C **30** (1986), 615; hep-ph/0606022.
E. van Beveren and G. Rupp, Eur. Phys. J. C **22** (2001), 493.
J. A. Oller and E. Oset, Phys. Rev. D **60** (1999), 074023.
F. E. Close and N. A. Tornqvist, J. of Phys. G **28** (2002), R249.
26) L. S. Geng, E. Oset, J. R. Pelaez and L. Roca, Eur. Phys. J. A **39** (2009), 81.
27) C. Hanhart, J. R. Pelaez and G. Rios, Phys. Rev. Lett. **100** (2008), 152001.
28) D. Morgan, Nucl. Phys. A **543** (1992), 632.
D. Morgan and M. R. Pennington, Phys. Rev. D **48** (1993), 1185.
29) V. Baru et al., Phys. Lett. B **586** (2004), 53.
30) E. van Beveren et al., AIP Conf. Proc. **660** (2003), 353; Phys. Rev. D **74** (2006), 037501.
31) D. Fernandez-Fraile, A. Gomez Nicola and E. T. Herruzo, Phys. Rev. D **76** (2007), 085020.
32) Ph. Boucaud et al. (ETM Collaboration), Phys. Lett. B **650** (2007), 304.
C. Allton et al. (RBC and UKQCD Collaborations), Phys. Rev. D **76** (2007), 014504.
C. W. Bernard et al., Phys. Rev. D **64** (2001), 054506.
C. R. Allton et al., Phys. Lett. B **628** (2005), 125.
M. Gockeler et al. (QCDSF Collaboration), arXiv:0810.5337.
33) P. C. Bruns and U.-G. Meißner, Eur. Phys. J. C **40** (2005), 97.
34) S. Weinberg, Phys. Rev. **130** (1963), 776.
Y. Kalashnikova et al., Eur. Phys. J. A **24** (2005), 437.
35) F. K. Guo, C. Hanhart, F. J. Llanes-Estrada and U. G. Meissner, Phys. Lett. B **678** (2009), 90.
36) S. Prelovsek et al., arXiv:1005.0948.
S. Prelovsek and D. Mohler, Phys. Rev. D **79** (2009), 014503.

2.2.3 Publication: J. Nebreda, J. R. Pelaez, G. Rios, **Enhanced non quark-antiquark and non-glueball N_c behavior of light scalar mesons,** Phys. Rev. D84, 074003 (2011)

PHYSICAL REVIEW D **84,** 074003 (2011)

Enhanced non-quark-antiquark and non-glueball N_c behavior of light scalar mesons

J. Nebreda, J. R. Peláez, and G. Ríos

Departamento de Física Teórica II, Universidad Complutense de Madrid, 28040 Madrid, Spain

(Received 8 July 2011; published 4 October 2011)

We show that the latest and very precise dispersive data analyses require a large and very unnatural fine-tuning of the $1/N_c$ expansion at $N_c = 3$ if the $f_0(600)$ and $K(800)$ light scalar mesons are to be considered predominantly $\bar{q}q$ states, which is not needed for light vector mesons. For this, we use scattering observables whose $1/N_c$ corrections are suppressed further than one power of $1/N_c$ for $\bar{q}q$ or glueball states, thus enhancing contributions of other nature. This is achieved without using unitarized ChPT, but if it is used we can also show that it is not just that the coefficients of the $1/N_c$ expansion are unnatural, but that the expansion itself does not even follow the expected $1/N_c$ scaling of a glueball or a $\bar{q}q$ meson.

DOI: 10.1103/PhysRevD.84.074003 PACS numbers: 12.39.Mk, 11.15.Pg, 12.39.Fe, 13.75.Lb

Light scalar resonances play a relevant role for several fields of Physics: For the nucleon-nucleon interaction, because they are largely responsible for the attractive part [1] (with cosmological and anthropic implications). For the QCD nonabelian nature, because some of these resonances have the quantum numbers of the lightest glueball, also common to the vacuum and hence of relevance for the spontaneous chiral symmetry breaking. Moreover, they are also of interest for the saturation [2] of the low energy constants of Chiral Perturbation Theory (ChPT) [3]. However, the precise properties of these mesons, their nature, spectroscopic classification, and even their existence—as for the $K(800)$ or κ—are still the object of an intense debate. In particular, different models [4] suggest that they may not be ordinary quark-antiquark mesons, but tetraquarks, meson molecules, glueballs, or a complicated mixture of all these. The problem, of course, is that we do not know how to solve QCD at low energies.

However, since the QCD $1/N_c$ expansion is applicable at all energies, and the mass and width N_c dependence of $\bar{q}q$ mesons and glueballs is well known [5], the N_c scaling of resonances becomes a powerful tool to classify them and understand their nature. In [6,7], some of us studied the mass and width behavior of light resonances using ChPT—which is the QCD low-energy effective Lagrangian—and unitarization with a dispersion relation. It was found that the poles of the $\rho(770)$ and $K^*(982)$ vectors behave predominantly as expected for $\bar{q}q$ states, whereas those of the $f_0(600)$, also called σ, and $K(800)$ scalars, do not [6]. Still, a possible subdominant $\bar{q}q$ component for the $f_0(600)$ may arise naturally at two loops [7] within ChPT (less so at one loop), but with a mass around 1 GeV or more.

Of course, all these conclusions rely on unitarized ChPT and the assumption that corrections, suppressed just by $1/N_c$, are of natural size. Since $N_c = 3$ in real life, this may not seem as a large suppression, even more when the meaning of "natural size" may not be clear for dimensional parameters. For that reason, unitarized ChPT was useful to change N_c, and reveal the $1/N_c$ scaling, no matter how unnatural the coefficients may appear.

Here, we will provide adimensional observables with corrections suppressed further than $1/N_c$, that can also be applied directly to real data at $N_c = 3$, without the need to extrapolate to larger N_c using unitarized ChPT.

In particular, resonances appearing in elastic two-body scattering are commonly identified by three criteria. The N_c behavior of one of these criteria—the associated pole in the unphysical sheet—was already studied in [6,7]. A second possibility is to define the mass as the energy where the phase shift reaches $\pi/2$, which both for $\pi\pi$ or πK scattering occurs relatively far from the $f_0(600)$ and $K(800)$ pole positions. This criterion was studied in [8] for the $f_0(600)$ with a relatively inconclusive result about its assumed $\bar{q}q$ behavior. A more reliable parametrization and better data were called for and we will provide them here together with more conclusive results. Third, the phase increases very fast in the resonance region and the mass can be identified with the maximum of the phase derivative. All three criteria roughly coincide for narrow resonances, but the most physical definition is the latest, since it identifies the resonance as a metastable state whose lifetime is the inverse of the width. Note that this is the less evident feature both for the $f_0(600)$ and $K(800)$ and thus the phase derivative will become our preferred observable to test their N_c dependence.

Let us then recall that partial waves generically scale as $1/N_c$, except at the resonance mass m_R. Actually, it has been found [8] that if a resonance pole at $s_R = m_R^2 - i m_R \Gamma_R$ behaves as a $\bar{q}q$ [5], i.e. $m_R \sim O(1)$ and $\Gamma_R \sim O(1/N_c)$, then the phase shift satisfies [9]:

$$\delta(m_R^2) = \frac{\pi}{2} - \underbrace{\left.\frac{\mathrm{Re}t^{-1}}{\sigma}\right|_{m_R^2}}_{O(N_c^{-1})} + O(N_c^{-3}), \tag{1}$$

$$\delta'(m_R^2) = -\underbrace{\left.\frac{(\mathrm{Re}t^{-1})'}{\sigma}\right|_{m_R^2}}_{O(N_c)} + O(N_c^{-1}), \tag{2}$$

where $t(s)$ is the partial wave, $\sigma = 2k/\sqrt{s}$, and k is the meson center of mass momentum. Derivatives are taken with respect to s. The $1/N_c$ counting of the different terms in the equations above comes from the following expansions at $s = m_R^2$ [10]:

$$\mathrm{Re}\, t^{-1} = m_R\Gamma_R\left[\frac{m_R\Gamma_R}{2}(\mathrm{Re}t^{-1})'' - \sigma'\right] + O(N_c^{-3}), \quad (3)$$

$$m_R\Gamma_R = \frac{\sigma}{(\mathrm{Re}t^{-1})'} + O(N_c^{-3}). \quad (4)$$

In brief, the corrections in Eqs. (1)–(4) are suppressed by a further $1/N_c^2$ power due to an expansion on the imaginary part of the pole, which scales like $\Gamma \sim 1/N_c$. As nicely shown in [8], by expanding separately the real and imaginary parts of t^{-1}, only the $1/N_c^{2n+1}$ powers are kept on each expansion, leading to Eqs. (3) and (4).

Since we are interested in adimensional observables whose corrections are suppressed further than just $1/N_c$, we can recast Eqs. (1) and (2) as follows:

$$\left.\frac{\frac{\pi}{2} - \mathrm{Re}t^{-1}/\sigma}{\delta}\right|_{m_R^2} \equiv \Delta_1 = 1 + \frac{a}{N_c^3}, \quad (5)$$

$$\left.-\frac{[\mathrm{Re}t^{-1}]'}{\delta'\sigma}\right|_{m_R^2} \equiv \Delta_2 = 1 + \frac{b}{N_c^2}. \quad (6)$$

Note that we have normalized each equation and extracted the leading $1/N_c$ dependence so that the coefficients a and b should naturally be $O(1)$ or less. It is relatively simple to make a and b much smaller than 1 with cancellations with natural higher order $1/N_c$ contributions, but very unnatural to make them much larger.

Now, in Table I, we show the resulting a and b for the lightest resonances found in $\pi\pi$ and πK elastic scattering. Before describing in detail the calculations, let us observe that *for the* $\rho(770)$ *and* $K^*(892)$ *vector resonances all parameters are of order one or less, as expected for* $\bar{q}q$ *states*. In contrast, *for the* $f_0(600)$ *and* $K(800)$ *scalar resonances we find that all parameters are larger, by two orders of magnitude, than expected for* $\bar{q}q$ *states*. This is one of the main results of this work, and makes the $\bar{q}q$ interpretation of both scalars extremely unnatural.

Let us now describe in detail our calculations and their different degree of precision and reliability. As commented above, the $f_0(600)$ "Breit-Wigner" mass was already studied [8] using Eq. (1), but no conclusion was reached on whether the deviations were consistent with the $1/N_c$ suppression or not. This was partly attributed to the limited reliability of the conformal parametrization or unitarized ChPT, whose phase never reaches $\pi/2$, used in [8]. To overcome this caveat, we are now using the recent, very precise and reliable *output* of the data analysis in [11], constrained to satisfy once-subtracted coupled dispersion relations—or GKPY equations—as well as Roy equations, which is therefore model-independent and specially suited to obtain the $f_0(600)$ pole [12]. Note that this analysis incorporates the very recent and reliable data on K_{l4} decays from NA48/2 [13], which is a key factor in attaining high levels of precision. The analysis in [11,12] is also in good agreement with previous dispersive results based on standard Roy equations [24]. We have followed the same rigorous approach for the $\rho(770)$, although, being so narrow, the conformal unconstrained data analysis and the Inverse Amplitude Method (IAM) yield very similar results. The uncertainties we quote for both the $f_0(600)$ and $\rho(770)$ cover the uncertainties in the output of the dispersive representation.

In this work, we also deal with strange resonances in πK scattering. For the scalar $K(800)$, we have also used a rigorous dispersive calculation, namely, that in [14], which uses Roy-Steiner equations to determine the isospin $1/2$ scalar channel of πK scattering, although this time, we can only provide a central value. Note, however, that the value of m_R^2 obtained in that analysis is located below threshold, so that the phase shift is ill defined at m_R^2. Nevertheless, we have been using the m_R mass definition to allow for an easier comparison with [8], but the definition $\sqrt{s_R} = m - i\Gamma/2$ is equally valid and is actually the standard choice used in the context of scalar mesons. Moreover, the N_c scaling of Eqs. (1) and (2) does not change if we evaluate the quantities at $s = m^2$, instead of m_R^2, since m^2 differs from m_R^2 in $\Gamma^2/4$, which is $O(N_c^{-2})$. Thus, the values for the $K(800)$ in Table I correspond to this choice. For the vector $K^*(892)$, there are no very precise purely dispersive descriptions of the existing data and we therefore rely on a single partial wave dispersion relation and $SU(3)$ ChPT to one-loop to determine its subtraction constants (this is known as ChPT unitarized with the single-channel IAM [15]), which we will briefly explain in the next section. We have applied the same method to the $\rho(770)$ and the results lie within 50% of their central value when using the GKPY dispersive representation. Since the $K^*(892)$ is narrower than the $\rho(770)$, the IAM is likely to provide a better approximation than in the $\rho(770)$ case, but even with that 50% uncertainty, it is enough to check that the a and b parameters are smaller than 1.

There is, of course, another way of interpreting our results, which is that due to the large $1/N_c$ coefficients of the $f_0(600)$ the series simply does not converge. In particular, Eq. (1), which was thoroughly considered in [8], is obtained as an expansion of $\arctan(x) = x - x^3/3\ldots$. In

TABLE I. Normalized coefficients of the $1/N_c$ expansion for different resonances. For $\bar{q}q$ resonances, all them are expected to be of order one or less.

	$\rho(770)$	$K^*(892)$	$f_0(600)$	$K(800)$
a	-0.06 ± 0.01	0.02	-252^{+119}_{-156}	-2527
b	$0.37^{+0.04}_{-0.05}$	0.16	77^{+28}_{-24}	162

this way, we could explain why the $a = -0.06 \pm 0.01$ coefficient is so small for the $\rho(770)$: it is simply the effect of calculating $a = \tilde{a}^3/3$ with $\tilde{a} = 0.56^{+0.03}_{-0.04}$, which is now naturally of $O(1)$. We could try the same procedure for the $f_0(600)$, assuming its series expansion is that of a $\bar{q}q$, to find $\tilde{a} = 9.1$, still rather unnatural, but of course, this value makes no sense since the whole series would not be converging and terms higher than $1/N_c^3$ would become dominant.

This is one of the reasons why despite being only suppressed by $1/N_c^2$ instead of $1/N_c^3$, we also provide the expansion in Eq. (6) obtained from the derivative of the amplitude. In this case, the b/N_c^2 term is not the square of a natural $1/N_c$ quantity, i.e.,

$$\frac{b}{N_c^2} = \frac{\mathrm{Re}t^{-1}}{\sigma}\left[\frac{\sigma'}{(\mathrm{Re}t^{-1})'} - \frac{\mathrm{Re}t^{-1}}{\sigma}\right] + O(N_c^{-4}). \quad (7)$$

Despite containing a cancellation between two $1/N_c$ terms, its value for the $\rho(770)$ is rather natural. However, once again, the value for the scalars is almost two orders of magnitude larger than expected.

In the previous analysis, it is very relevant that the width of the resonance is suppressed with additional $1/N_c$ powers with respect to the mass. Actually, it is rather straightforward to extend the formalism to study the assumption that the $f_0(600)$ could be predominantly a glueball, since then $m_R \sim O(1)$ and $\Gamma_R \sim O(1/N_c^2)$ [5,16]. As a consequence, for the glueball case, the scaling of Eqs. (3) and (4) changes and so does that of $\delta(m_R^2)$ and $\delta'(m_R^2)$:

$$\delta(m_R^2) = \frac{\pi}{2} - \underbrace{\frac{\mathrm{Re}t^{-1}}{\sigma}\bigg|_{m_R^2}}_{O(N_c^{-2})} + O(N_c^{-6}), \quad (8)$$

$$\delta'(m_R^2) = \underbrace{\frac{(\mathrm{Re}t^{-1})'}{\sigma}\bigg|_{m_R^2}}_{O(N_c^{2})} + O(N_c^{-2}). \quad (9)$$

Much as it was done in Eqs. (5) and (6), in order to make explicit this further N_c suppression, we can define some new parameters a' and b' that should be of $O(1)$ if the resonance was a glueball:

$$\Delta_1 = 1 + \frac{a'}{N_c^6}, \qquad \Delta_2 = 1 + \frac{b'}{N_c^4}. \quad (10)$$

Following the same procedure as before, we obtain for the $f_0(600)$, $a' = -6800^{+3200}_{-4200}$ and $b' = 2080^{+760}_{-650}$. In other words, a very dominant or pure glueball nature for the $f_0(600)$ is very disfavored by the $1/N_c$ expansion, even more than the $\bar{q}q$ interpretation. This is because it would require even more unnatural coefficients, this time too large by three to four orders of magnitude.

Of course, as we did for the $\bar{q}q$ case, we could worry about the fact that, due to the $\arctan(x) = x - x^3/3 + \ldots$ expansion, the a' should have been interpreted as $a' = \tilde{a}'^3/3$. But even with that interpretation, we would still find $\tilde{a}' = 27^{+5}_{-7}$, again rather unnatural. Once more, and as happened in the $\bar{q}q$ case, the b' parameter does not correspond to the fourth power of any natural quantity, so that its value is genuinely unnatural, disfavoring the glueball interpretation.

Let us remark that in the case of tetraquarks or molecules, the width is not expected to be suppressed with additional $1/N_c$ powers with respect to the mass of the resonance [16,17]. Thus, our previous formalism does not apply. Furthermore, it is most likely that scalars are a mixture of different components. Therefore, our results, while showing that neither the $\bar{q}q$ or a glueball are favored as dominant components of light scalars, do not exclude that these structures could be mixed with other components that would dominate the $1/N_c$ expansion with a different N_c behavior [18].

In summary, we have shown that if, for the light scalar mesons, we study $\bar{q}q$ or glueball $1/N_c$ expansions as those in Eqs. (5), (6), and (10), their coefficients come out very unnatural, suggesting that these resonances cannot be described as *predominantly* made of a quark and an antiquark or a glueball. Note that, contrary to our previous works [6,7], this conclusion has been reached *from dispersive analyses of data*, without extrapolating to $N_c \neq 3$ using unitarized ChPT.

However, unitarized ChPT will be used next to calculate the $\Delta_i - 1$ observables, in order to show that, for scalars, what really happens is that they do not even follow the $1/N_c$ expansion of $\bar{q}q$ or glueball states given in Eqs. (5), (6), and (10), thus explaining the need for unnatural coefficients if a $\bar{q}q$ or glueball-like expansion is assumed.

A. **The Inverse Amplitude Method:** The elastic IAM [15] uses ChPT to evaluate the subtraction constants and the left cut of a dispersion relation for the inverse of the partial wave. The elastic right cut is exact, since the elastic unitarity condition, $\mathrm{Im}t = \sigma|t|^2$, fixes $\mathrm{Im}t^{-1} = -\sigma$. Note that the IAM is derived only from elastic unitarity, analyticity in the form of a dispersion relation, and ChPT, which is only used at low energies. It satisfies exact elastic unitarity and reproduces meson-meson scattering data up to energies $\sim$1 GeV. It can be analytically continued into the second Riemann sheet where poles associated to resonances are found. In particular, we find the $\rho(770)$ and $f_0(600)$, as well as the $K^*(892)$ and the $K(800)$ resonances as poles in $\pi\pi$ and πK scattering amplitudes, respectively.

The dependence on the QCD number of colors, N_c, is implemented [6,7] through the leading N_c scaling of the ChPT low energy constants (LECs), which is model-independent [3,7,19]. Fortunately, for Eqs. (5) and (6) to hold, only the leading $1/N_c$ behavior is needed. Note also that the IAM does not have any other parameters where uncontrolled N_c-dependence could hide—as it happens in

other unitarization methods—so that the IAM allows us to check the scaling of the $\Delta_i - 1$ in Eqs. (5) and (6).

The $SU(2)$ IAM: Only the nonstrange $f_0(600)$ and $\rho(770)$ resonances can be checked, but we can do it by unitarizing with the IAM the corresponding partial waves either to one or two loops. We simply scale $f_{N_c} \to f\sqrt{N_c/3}$, the one-loop constants, as $l^r_{i,N_c} \to l^r_i N_c/3$ and the two-loop ones as $r_{i,N_c} \to r_i (N_c/3)^2$.

Thus, in the two first columns of Fig. 1, we show, for the $\rho(770)$ and $f_0(600)$ resonances, the scaling of the $\Delta_i - 1$ both to one loop (upper panels) and two loops (lower panels). Note that we have normalized them to their $N_c = 3$ value, in order to cancel the leading part of the a and b coefficients and thus extract the leading $1/N_c^k$ behavior of Eqs. (5) and (6). For the one-loop calculations, we use the set of LECs in [20], whereas for the two-loop calculation, we use the fit D from [20,21]. We have checked that similar results are obtained when using other sets of LECs in these references or the estimates from resonance saturation [2].

We can observe that the scaling for the $\rho(770)$ observables overlaps with the expectation for the leading behavior of $\bar{q}q$ states. However, in the case of the $f_0(600)$, the scaling is completely different. To one loop, the $f_0(600)$ observables grow instead of decreasing. Let us note, however, that for N_c larger than $\sim$10, the $f_0(600)$ pole lies on the third quadrant of the complex plane. Before that happens, the value of m_R^2 becomes less than $4m_\pi^2$ and the phase shift has no physical meaning so that Eqs. (5) and (6) do not hold. This behavior does not occur to two loops. Actually, we find again the $f_0(600)$ behavior already observed in [7], where, for N_c close to 3, the width grows as in the one-loop case (and so do the observables here), but for larger N_c, the $f_0(600)$ starts behaving more as a $\bar{q}q$. Note that this $\bar{q}q$ behavior appears at a mass somewhat bigger than 1 GeV. This was a hint of the $f_0(600)$ being a mixture of a predominantly non-$\bar{q}q$ component and, at least, a subdominant $\bar{q}q$ component with a mass much heavier that the physical one, which is the one that survives at large N_c. In terms of the $\Delta_i - 1$ observables defined here, this translates into a growth close to $N_c = 3$ and a decrease at larger N_c. Therefore, it is not only that the a and b coefficients of the $f_0(600)$ are too large as shown in the previous section, but that the scaling itself does not correspond to a $\bar{q}q$ state (and even less so to a glueball). To two-loops, the $\rho(770)$ does not follow exactly the leading behavior of $\bar{q}q$ states but decreases slightly faster, which can be naturally explained due to subleading effects or to a possible small pion cloud contribution.

The $SU(3)$ IAM: Now we can study the scaling of $\Delta_i - 1$ not only for the $\rho(770)$ and $f_0(600)$, but also for the $K^*(892)$ and $K(800)$ resonances, although in this case, the elastic unitarized amplitudes are available only to one loop [22,23]. We have now eight LECs, called $L_i(\mu)$, that scale [3,19] as $L_{i,N_c} \to L_i(N_c/3)$ for $i = 2, 3, 5, 8$, while $2L_1 - L_2$, L_4, L_6 and L_7 do not change with N_c.

In the third and fourth columns of Fig. 1, we show the results found using the set of LECs called Fit II in [22]. Similar results are obtained with Fit I or the estimates from resonance saturation in [2]. In the upper panels, we simply

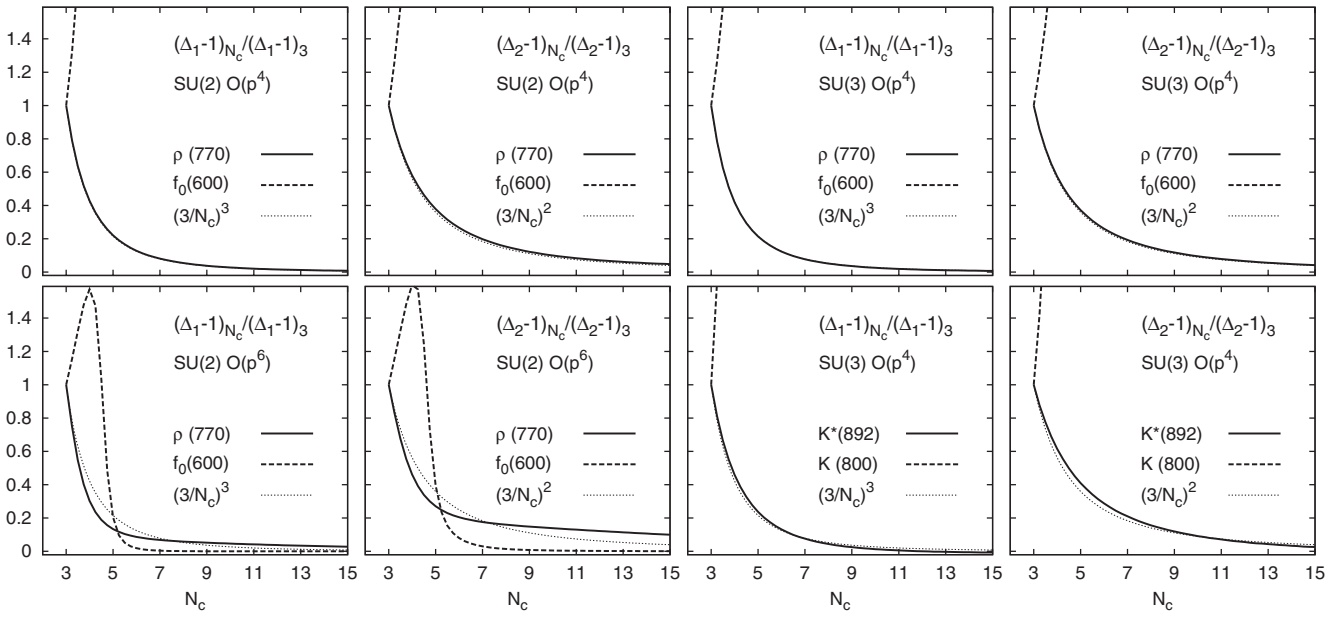

FIG. 1. $1/N_c$ scaling of the $\Delta_i - 1$ observables normalized to their $N_c = 3$ value for light scalar and vector mesons, using unitarized ChPT within $SU(2)$ or $SU(3)$ and to one or two loops, $O(p^4)$ and $O(p^6)$, respectively.

reobtain within the $SU(3)$ formalism the same results we obtained for the $\rho(770)$ and $f_0(600)$ within the $SU(2)$ formalism to one loop. In the lower panels, we show the results for the light vector $K^*(892)$, following nicely the $\bar{q}q$ expectations, as well as the results for the scalar $K(800)$, which has a very similar behavior to the $f_0(600)$, at odds with a dominant $\bar{q}q$ or glueball nature.

Summary: In this work, we have studied the $1/N_c$ expansion of the meson-meson scattering phase-shifts around the pole mass of a $\bar{q}q$ or glueball resonance. In particular, we have defined observables whose corrections are suppressed further than just one power of N_c, paying particular attention to the derivative of the phase, which provides a physical and intuitive definition of a resonance. By using recent and very precise dispersive data analyses, we have shown that if we assume a $\bar{q}q$ or glueball behavior for the $f_0(600)$ and $K(800)$, the coefficients of the expansion of such observables turn out unnaturally large. This is shown without using ChPT or extrapolating beyond $N_c = 3$. Moreover, when using unitarized ChPT, we have shown that it is the very $1/N_c$ scaling of the observables which does not follow the pattern of the $1/N_c$ expansion expected for $\bar{q}q$ or glueball states.

We thank J. Nieves and E. Ruiz-Arriola for useful discussions, checks and suggestions and B. Mussallam for the results of his Roy-Steiner dispersive analysis of the $K(800)$ channel.

[1] M. H. Johnson and E. Teller, Phys. Rev. **98**, 783 (1955).
[2] G. Ecker, J. Gasser, A. Pich, and E. de Rafael, Nucl. Phys. **B321**, 311 (1989); J. F. Donoghue, C. Ramirez, and G. Valencia, Phys. Rev. D **39**, 1947 (1989).
[3] S. Weinberg, Physica A (Amsterdam) **96**, 327 (1979); J. Gasser and H. Leutwyler, Ann. Phys. (Leipzig) **158**, 142 (1984); Nucl. Phys. **B250**, 465 (1985).
[4] R. L. Jaffe, Phys. Rev. D **15**, 267 (1977); AIP Conf. Proc. **964**, 1 (2007); Prog. Theor. Phys. Suppl. **168**, 127 (2007); R. L. Jaffe and F. E. Low, Phys. Rev. D **19**, 2105 (1979); J. D. Weinstein and N. Isgur, Phys. Rev. Lett. **48**, 659 (1982); Phys. Rev. D **27**, 588 (1983); **41**, 2236 (1990); G. Janssen, B. C. Pearce, K. Holinde, and J. Speth, Phys. Rev. D **52**, 2690 (1995); N. N. Achasov and V. V. Gubin, Phys. Rev. D **56**, 4084 (1997); Yad. Fiz. **65**, 1566 (2002) [Phys. At. Nucl. **65**, 1528 (2002)]; P. Minkowski and W. Ochs, Eur. Phys. J. C **9**, 283 (1999); J. A. Oller and E. Oset, Nucl. Phys. A **620**, 438 (1997); **652**, 407(E) (1999); E. van Beveren and G. Rupp, Eur. Phys. J. C **22**, 493 (2001); J. Vijande, A. Valcarce, F. Fernandez, and B. Silvestre-Brac, Phys. Rev. D **72**, 034025 (2005); T. Hyodo, D. Jido, and T. Kunihiro, Nucl. Phys. **A848**, 341 (2010); R. Kaminski, G. Mennessier, and S. Narison, Phys. Lett. B **680**, 148 (2009).H. Forkel, Phys. Lett. B **694**, 252 (2010).
[5] G. 't Hooft, Nucl. Phys. **B75**, 461 (1974); E. Witten, Ann. Phys. (Leipzig) **128**, 363 (1980).
[6] J. R. Pelaez, Phys. Rev. Lett. **92**, 102001 (2004).
[7] J. R. Pelaez and G. Rios, Phys. Rev. Lett. **97**, 242002 (2006).
[8] J. Nieves and E. Ruiz Arriola, Phys. Lett. B **679**, 449 (2009).
[9] Note our $t(s)$ has an opposite sign compared to that in [8].
[10] Note the corrected sign in front of σ' which nevertheless does not affect the results in [8].
[11] R. Garcia-Martin, *et al.*, Phys. Rev. D **83**, 074004 (2011).
[12] R. Garcia-Martin, R. Kaminski, J. R. Pelaez, and J. Ruiz de Elvira, Phys. Rev. Lett. **107**, 072001 (2011).
[13] J. R. Batley *et al.* (NA48-2 Collaboration), Eur. Phys. J. C **70**, 635 (2010).
[14] S. Descotes-Genon and B. Moussallam, Eur. Phys. J. C **48**, 553 (2006).
[15] T. N. Truong, Phys. Rev. Lett. **61**, 2526 (1988); **67**, 2260 (1991); A. Dobado *et al.*, Phys. Lett. B **235**, 134 (1990); A. Dobado and J. R. Peláez, Phys. Rev. D **47**, 4883 (1993); **56**, 3057 (1997).
[16] F. J. Llanes-Estrada, J. R. Pelaez, and J. Ruiz de Elvira, Nucl. Phys. B, Proc. Suppl. **207–208**, 169 (2010).
[17] R. L. Jaffe, *Proceedings of the International Symposium on Lepton and Photon Interactions at High Energies*, Physikalisches Institut (University of Bonn, Bonn, 1981), ISBN 3-9800625-0-3.
[18] For some preliminary attempts at disentangling the composition of light scalars using their leading $1/N_c$ behavior we refer the reader to [16].
[19] A. A. Andrianov, Phys. Lett. B **157**, 425 (1985); A. A. Andrianov and L. Bonora, Nucl. Phys. **B233**, 232 (1984); D. Espriu, E. de Rafael, and J. Taron, Nucl. Phys. **B345**, 22 (1990); S. Peris and E. de Rafael, Phys. Lett. B **348**, 539 (1995).
[20] J. Nebreda, J. R. Pelaez, and G. Rios, Phys. Rev. D **83**, 094011 (2011).
[21] J. R. Pelaez and G. Rios, Phys. Rev. D **82**, 114002 (2010).
[22] J. Nebreda and J. R. Pelaez, Phys. Rev. D **81**, 054035 (2010).
[23] A. Gomez Nicola and J. R. Pelaez, Phys. Rev. D **65**, 054009 (2002).
[24] G. Colangelo, J. Gasser, and H. Leutwyler, Nucl. Phys. **B603**, 125 (2001); B. Ananthanarayan, G. Colangelo, J. Gasser, and H. Leutwyler, Phys. Rep. **353**, 207 (2001).

Chapter 3

Conclusions

Throughout this thesis we have studied the properties of the elastic $\pi\pi$ and πK scattering and of the lightest resonances appearing in it: the well-established vector resonances, $\rho(770)$ and $K^*(892)$, and the controversial scalars $f_0(600)$ and $K_0^*(800)$, also called σ and κ, respectively.

We have made use of the low-energy effective theory known as Chiral Perturbation Theory (ChPT) [1, 2, 3, 4, 5]. For the study of resonances, we have unitarized the ChPT amplitudes using the Inverse Amplitude Method [26, 27, 28, 29, 30], which is obtained from a subtracted dispersion relation of the inverse amplitude, whose imaginary part in the elastic region is known exactly from unitarity. It does not contain any spurious parameter and all dependences on QCD parameters appear through the ChPT expansion, which is used to calculate the low energy subtraction points and the left cut. Moreover, the unitarization generates poles on the second Riemann sheet associated to the light resonances, without a priori assumptions on their existence or nature. This has allowed us to make a systematic study of the dependence of the amplitudes and resonances on two QCD parameters: the quark masses and the number of colors, N_c.

We have studied the chiral extrapolation of the phase-shifts in elastic pion-pion scattering, using both standard and unitarized $SU(2)$ ChPT to one and two loops. In the standard ChPT approach, limited to low momenta, we have studied the S, P and D waves. Then, using unitarized ChPT, we have extended the analysis up to

energies of around 1 GeV for the S and P waves, being compatible with standard ChPT at low energies. We have compared with lattice results [62, 63, 64] and found a good agreement of standard ChPT below $p \sim 200$ MeV for the I=2, J=0 and I=J=1 channels and up to $p \sim 500$ MeV for the I=J=2 channel. We have shown that unitarized ChPT improves the agreement in the scalar and vector channels at higher energies. We have also performed a Montecarlo analysis to provide an estimation of the uncertainties.

The strange and non-strange quark mass dependence of the $f_0(600)$, $K_0^*(800)$, $\rho(770)$ and $K^*(892)$ resonances has been studied using unitarized one-loop $SU(3)$ ChPT. We have fitted simultaneously all experimental scattering data up to 0.8-1 GeV together with lattice results on the pion and kaon parameters and some scattering lengths [102, 103, 104, 105] up to a pion mass of 440 MeV. Then, we have varied the strange and non-strange quark masses from the chiral limit up to values of interest for lattice studies. We have found that the mass and width of the $\rho(770)$ and $K^*(892)$ present a smooth quark mass dependence, whereas both scalars show a similar non-analyticity at high quark masses. We have also confirmed the lattice assumption of quark mass independence of the vector-two-meson coupling, while, for the scalars, we have seen that the coupling depends strongly on the quark masses.

The derivatives of the masses of these resonances with respect to the quark ones have also been calculated using the IAM. We have given results for the adimensional parameters $K_R^f = \frac{m_f}{M_R}\frac{\partial M_R}{\partial m_f}$, where m_f is the mass of the light or the strange quark. We have estimated the systematic errors by using two different methods that only differ by higher orders in the ChPT expansion, and also by repeating the calculations using the Chiral Unitary approach [21, 18], which is simpler than the IAM but does not include the whole mass dependence. Calculating these parameters for the pion and kaon, for which unitarization is not needed, we have checked that the LECs that we use for the IAM calculations yield results that are compatible with those found using standard ChPT LECs. Among the estimates that we provide, we point out that for the σ with the strange quark mass, which is very different from

the value used in some studies on the cosmological variation of the fundamental constants [53].

As far as the the number of colors is concerned, we have reviewed some works [128, 83] on the behavior in the $1/N_c$ expansion of the resonances generated with the IAM. By means of a comparison with the behavior expected for a $\bar{q}q$ state, they showed that the $1/N_c$ behavior of the σ is at odds with being predominantly an ordinary $\bar{q}q$ state. In this review we have also discussed why we cannot take the $N_c \to \infty$ limit within the IAM approach.

Finally, we have presented two new adimensional observables such that their value is known for $\bar{q}q$ and glueball states up to highly suppressed corrections in the $1/N_c$ expansion. These observables have allowed us to extract information on the possible $\bar{q}q$ or glueball nature of the σ and κ mesons at $N_c = 3$, using very reliable dispersive calculations of the $\pi\pi$ and πK scattering phase shifts [95, 133], without the need of unitarization methods. We have shown that, if we assume a $\bar{q}q$ nature for the σ and κ, the $1/N_c$ corrections are two orders of magnitude too big, which strongly disfavors the $\bar{q}q$ interpretation of both scalars, as well as the glueball interpretation for the σ.

Resumen en español

Introducción

La Cromodinámica Cuántica, QCD por sus siglas en inglés, es la teoría que explica, en términos de quarks y gluones, la interacción fuerte. Gracias a su propiedad de libertad asintótica, que consiste en que la interacción se hace más débil a medida que aumenta la energía, los procesos que involucran una transferencia grande de momento pueden ser calculados perturbativamente. De hecho, su validez ha sido sobradamente comprobada en este dominio de energías. Por otro lado, en la región de bajas energías su constante de acoplamiento crece. En este régimen, los quarks y gluones se mantienen confinados, dando lugar a un vasto número de partículas, llamadas hadrones. De este modo, el confinamiento nos impide usar los quarks y gluones como grados de libertad.

Sin embargo, a muy bajas energías, la existencia de un octete de partículas pseudoescalares muy ligeras, formado por los piones, los kaones y la eta y separado por varios centenares de MeV de la zona resonante, nos permite desarrollar una teoría de campos efectiva en la que dichas partículas pseudoescalares son los únicos grados de libertad. La dinámica de estas partículas está además muy constreñida por las simetrías de QCD y, en particular, por la ruptura espontánea de la simetría quiral.

Sobre esta base, Weinberg introdujo en 1979 [1] el método de Lagrangiano efectivo conocido como Teoría de Perturbaciones Quiral (ChPT). Después, Gasser y Leutwyler [2, 3, 4, 5] desarrollaron la técnica y calcularon las amplitudes de dis-

persión de dos mesones ligeros y otros observables, tales como masas y factores de forma, a un loop en teoría de perturbaciones.

La importancia de este formalismo reside en el hecho de que la teoría es renormalizable y depende sólo de las masas y constantes de desintegración del octete pseudoescalar y de un conjunto de parámetros fenomenológicos, conocido como constantes de baja energía (LECs), que contienen información de los grados de libertad más pesados [6, 7] y sobre la teoría subyacente. Una vez que estos parámetros han sido determinados por medio de ajustes a datos experimentales, es posible hacer predicciones para otros procesos y, de hecho, ChPT ha demostrado ser muy eficaz a la hora de describir la fenomenología hadrónica de bajas energías. En este punto, remitimos al lector a algunas memorias que dan cuenta detallada de sus logros: [8, 9, 10, 11].

Sin embargo, puesto que ChPT está limitada a energías por debajo de 500 MeV aproximadamente, durante los últimos años se han dedicado muchos esfuerzos a mejorar el comportamiento de las amplitudes a energías más altas, por medio de métodos de unitarización. Dichos métodos incluyen la introducción explícita de resonancias más pesadas en el Lagrangiano [6, 12, 7, 13, 14, 15, 16], la "resumación" de diagramas usando el método de Lippmann-Schwinger o Bethe-Salpeter [17, 18, 19, 20, 21, 22, 23, 24], el uso de la matriz K [25], el esquema Quiral Unitario [21, 18], el método N/D [15] y el Método de la Amplitud Inversa (IAM) [26, 27, 28, 29, 30]. Ésta última es la técnica principalmente empleada en los trabajos que componen esta tesis.

La unitarización de las amplitudes no sólo extiende su validez a energías más altas, sino que también permite generar resonancias ligeras, lo cual está fuera del alcance de ChPT estándar. El Método de la Amplitud Inversa, en particular, genera las resonancias vectoriales $\rho(770)$ y $K^*(892)$ y las escalares $f_0(600)$, $K(800)$, $a_0(980)$ y $f_0(980)$ sin necesidad de hacer suposiciones a priori sobre su existencia o naturaleza. Esto es de particular importancia en el caso del controvertido sector de las resonancias escalares ligeras.

Las propiedades de dichas resonancias, e incluso su existencia, en el caso de la $K_0^*(800)$, son aún controvertidas, a pesar de que éstas juegan un papel muy relevante en varios campos, desde la Cromodinámica Cuántica y la Física Nuclear hasta la Cosmología. Tanto la resonancia $f_0(600)$ como la $K_0^*(800)$ son extremadamente anchas, de modo que se propagan muy poco y son muy difíciles de observar experimentalmente. Esta es la razón por la que muchos autores se han mostrado reacios a considerarlas como resonancias, de modo que sólo muy recientemente se ha incluido el $f_0(600)$ o σ como un estado "bien establecido" en los compendios del "Particle Data Group" [31] y el $K_0^*(800)$ o κ todavía "necesita confirmación" y se omite de las tablas resumidas. Por su parte, la resonancia $a_0(980)$ se encuentra justo por debajo del umbral del canal de dos kaones, al que se acopla fuertemente, generando en las amplitudes una forma de pico que distorsiona los parámetros de masa y anchura. Por último, la $f_0(980)$ se superpone notablemente con la $f_0(600)$ y otras resonancias y además también está cerca del umbral (en "Note on Scalars Mesons" [31] se puede encontrar un breve informe sobre los mesones escalares y numerosas referencias).

Asimismo, la pertenencia de estas resonancias a un mismo nonete escalar tampoco está clara todavía, puesto que su naturaleza es aún incierta. Si se tratara de estados de dos quarks, $\bar{q}q$ [32, 33, 34, 35], se esperaría que tuvieran una masa de alrededor de 1.2 GeV, y no por debajo de 1 GeV como es el caso. Además, la jerarquía de las masas en un nonete $\bar{q}q$ es justamente la contraria a la de las resonancias escalares. Como alternativa, estos estados se pueden interpretar como tetraquarks, es decir, estados de dos quarks y dos antiquarks [36, 37, 38, 39, 40], como moléculas hadrónicas [41, 42, 43, 44], o incluso como glueballs, es decir, estados puramente gluónicos [45, 46], en el caso de la isoescalar $f_0(600)$. Lo más probable es que su naturaleza sea una mezcla de todos estos estados.

En cuanto a la importancia de estas resonancias, nos centraremos primero en la $f_0(600)$. Aparece en la dispersión de dos piones, en el canal de isospín $I = 0$ y momento angular $J = 0$. El intercambio correlacionado de dos piones en este canal juega un papel clave en la interacción atractiva entre nucleones, modelada generalmente como el intercambio de un mesón escalar-isoescalar, la llamada resonancia

"sigma". Por esta razón, la resonancia $f_0(600)$ resulta ser importante para la Física Nuclear y, en particular, para los procesos de nucleosíntesis, importantes para las consideraciones antrópicas [49, 50, 51] y el estudio de la variación cosmológica de las constantes fundamentales [52, 53, 54].

Por otra parte, la resonancia $f_0(600)$ es el meson más ligero con los números cuánticos del vacío, por lo que es relevante para el proceso de ruptura espontánea en QCD en modelos como el sigma lineal o el de Nambu-Jona-Lasinio [55, 56]. Es más, esta ruptura, aunque con diferencias sustanciales, está intimamente relacionada con el mecanismo de Higgs en el sector de ruptura espontánea de la simetría electrodébil en el Modelo Estándar [57, 58, 59]. Por otro lado, sus números cuánticos son los mismos que los del glueball, un estado característico de la naturaleza no abeliana de QCD. Se estima que la masa del glueball más ligero se encuentra a energías de alrededor de 1.5 GeV, pero su identificación es complicada [60, 61] porque puede mezclarse tanto con mesones $\bar{q}q$ como con posibles estados exóticos, como tetraquarks y moléculas, con los mismos números cuánticos.

En lo que concierne a la propia Teoría de Perturbaciones Quiral, sucede que, aunque sus constantes de baja energía en principio reciben contribuciones de las resonancias mesónicas integradas fuera del Lagrangiano, en la práctica el intercambio de resonancias vectoriales básicamente satura los parámetros de un loop [6, 7]. Por lo tanto, aún tenemos que entender por qué las resonancias escalares ligeras apenas contribuyen a los valores de las LECs.

Con el objetivo de ayudar a esclarecer estos asuntos, en este trabajo he seguido varios enfoques distintos. En primer lugar, el hecho de que ChPT dependa explícitamente de las masas de los quarks nos ha permitido calcular las derivadas de las masas de los mesones más ligeros respecto a la masa tanto de los quarks ligeros como del extraño. Estos valores son interesantes para la clasificación espectroscópica de las resonancias, así como para consideraciones antrópicas [49, 50, 51] y para los estudios sobre la variación cosmológica de los parámetros fundamentales [52, 53, 54]. También hemos aumentado la masa de los quarks para estudiar el comportamiento de los desfases en la dispersión de dos piones y el de las resonancias generadas tanto en la dispersión de dos piones como en la de pion-kaon. Hemos aumentado

las masas de los quarks hasta valores que nos permiten comparar los resultados con los estudios de QCD en el retículo.

Dichos estudios consisten en simular un espacio-tiempo discreto, donde se puede llevar a cabo una formulación matemática de QCD bien definida y a partir de primeros principios, extrapolando después los resultados al límite contínuo. Lamentablemente, el coste computacional de estos cálculos es muy grande y aumenta rápidamente al disminuir la masa de los quarks, de modo que, generalmente, los cálculos de QCD en el retículo se realizan con masas mayores que las físicas. Por lo tanto, nuestros estudios extrapolando las amplitudes de ChPT a masas más altas pueden ser útiles como guía y test de compatibilidad para futuros resultados.

El segundo enfoque usado en esta tesis para estudiar el problema de las resonancias escalares es el estudio de su dependencia con otro parámetro del Lagrangiano de QCD: el número de colores, N_c. Las amplitudes de QCD pueden ser expandidas en $1/N_c$ a cualquier energía [65, 66] y la importancia de esta expansión reside en el hecho de que diferentes tipos de estados dependen del número de colores de manera muy distinta. Por ejemplo, se sabe que los estados quark-antiquark se convierten en estados ligados y su masa y anchura escalan como $\mathcal{O}(1)$ y $\mathcal{O}(1/N_c)$ respectivamente. Puesto que el número de colores es sólo tres, puede parecer que una supresión de $\sim 1/3$ de la anchura respecto a la masa no es lo suficientemente fuerte como para confirmar si una resonancia tiene o no una naturaleza predominantemente $\bar{q}q$. Sin embargo, existen varias formas de encontrar argumentos más contundentes. Por ejemplo, gracias al hecho de que la expansión en $1/N_c$ se puede implementar en ChPT, hemos aumentado el número de colores para hacer la supresión más fuerte. También hemos creado observables que están suprimidos por potencias más altas de $1/N_c$, de modo que para su estudio no hay necesidad de abandonar el mundo físico con tres colores. El hecho de trabajar en $N_c = 3$ nos permite prescindir de los métodos de unitarización y usar análisis dispersivos [95, 133] más rigurosos y precisos.

Resultados

Esta tesis se presenta en el formato 'por artículos', lo que significa que en ella figuran las publicaciones originales fruto de mi trabajo como estudiante predoctoral. A continuación sigue un pequeño resumen y un análisis de los principales resultados obtenidos. En el primer apartado recogemos los resultados del estudio de la dependencia de las resonancias y los desfases con la masa de los quarks y, en el segundo, repasamos nuestros estudios sobre la naturaleza de las resonancias por medio de la expansión en $1/N_c$. Por último se presentan las conclusiones de esta tesis.

Dependencia de las amplitudes de ChPT con la masa de los quarks

Uno de los principales objetivos del cálculo de las amplitudes de dispersión para valores de la masa de los quarks mayores que los físicos es comparar con los resultados de QCD en el retículo. Los cálculos en el retículo proporcionan, en principio, un forma rigurosa de calcular no perturbativamente cantidades de QCD, tales como el espectro de las resonancias mesónicas más ligeras. Sin embargo, como decíamos antes, implementar las ligeras masas de los quarks u y d requiere mucho tiempo computacional, por lo que los cálculos usualmente se llevan a cabo asignando a los quarks masas mucho mayores que las físicas. Recientemente se están realizando grandes progresos en el tratamiento de muchas complicaciones técnicas, como la implementación de la simetría quiral o la existencia de diagramas inconexos, que durante mucho tiempo han complicado los cálculos en el sector mesónico, y, en particular, aquellos que involucran a los canales isoescalares. En los últimos años se han obtenido resultados para las masas de las resonancias $\rho(770)$ y $f_0(600)$ [112, 113, 114, 115, 116], para la constante de decaimiento del pión e incluso para algunas longitudes de dispersión de dos piones [103, 117] y desfases [62, 63, 64]. Puesto que ChPT puede predecir correctamente cómo dependen de la masa de los quarks las constantes de substracción y el corte izquierdo de las relaciones de dispersión de las que se deriva el Método de la Amplitud Inversa, podemos estudiar tanto la dependencia de los desfases como también de las resonancias generadas, lo cual es interesante como guía para los estudios en el retículo.

La publicación 2.1.2 es una generalización a $SU(3)$ de un reciente estudio [97] en $SU(2)$. En [97], las amplitudes de $SU(2)$ ChPT unitarizadas con el IAM fueron utilizadas para calcular la dependencia de las resonancias $\rho(770)$ y $f_0(600)$ con la masa del pión, o, equivalentemente, con la masa promediada de los quarks u y d, $\hat{m}$. En la publicacion 2.1.2, incluímos el quark extraño usando el formalismo de $SU(3)$ ChPT, de modo que también podemos generar las resonancias $K^*(892)$ y $K_0^*(800)$ y estudiar la dependencia tanto con la masa de los quarks ligeros como con la del extraño. La resonancia $K_0^*(800)$, a pesar de ser escalar y muy similar a la $f_0(600)$, es más asequible para los cálculos en el retículo [118, 119], debido a que tiene isospín y extrañeza no nulos. A continuación exponemos esquemáticamente los principales resultados obtenidos en este trabajo.

Dependencia con la masa de los quarks ligeros

- Las anteriores determinaciones de las constantes de baja energía proceden de ajustes sólo a datos experimentales [85, 86], y por lo tanto son más sensitivas a las LECs que gobiernan la dependencia de las ondas parciales con la energía. Para obtener una mejor estimación de las LECs que multiplican términos con una dependencia explícita con las masas, en este trabajo hemos llevado a cabo nuevos ajustes incluyendo resultados del retículo para M_π, M_K, f_π, f_K y las longitudes de dispersión [102, 103, 104, 105].

- Los resultados obtenidos para las resonancias $\rho(770)$ y $f_0(600)$ son muy consistentes con los de $SU(2)$ [97] y con las estimaciones de los dos primeros coeficientes de la expansión quiral de M_ρ [120].

- Ambas resonancias vectoriales, $\rho(770)$ y $K^*(892)$, se comportan de forma muy similar: sus masas aumentan lentamente, mucho más despacio que la del pión. Como consecuencia, hay una gran supresión del espacio de fases, que da cuenta por si misma de la reducción de la anchura, que se produce sin un efecto dinámico a traves de los acoplos $g_{\rho\pi\pi}$ y $g_{K^*\pi K}$. Éstos se mantienen notablemente constantes, lo que confirma una suposición hecha en estudios de la anchura de la $\rho(770)$ en el retículo [121].

- Para los mesones vectoriales encontramos que la relación de Kawarabayashi-Suzuki-Riazuddin-Fayyazuddin (KSRF) [122, 123], que aproxima sus acoplos a dos mesones por $g \approx M_V/(2\sqrt{2}f_\pi)$, se mantiene con una precisión de alrededor de un 5% al cambiar la masa de los quarks ligeros de 0 a 9 veces su valor físico.

- Por su parte, el comportamiento de los escalares $f_0(600)$ y $K_0^*(800)$ es muy distinto al de las resonancias vectoriales. La característica más notable es la bifurcación de la masa en dos ramas. Esto sucede cuando los dos polos conjugados asociados a las resonancias en la segunda hoja de Riemann, los cuales se aproximan el uno al otro a medida que aumenta la masa de los quarks, se juntan en un solo polo por debajo del umbral y después se separan y se mantienen en el eje real.

- El aumento de la masa de la $f_0(600)$ antes de la bifurcación es mucho más rápido que el de la $K_0^*(800)$. La reducción de sus anchuras no se puede atribuir en este caso sólo a la disminución del espacio de fases, porque comprobamos que su acoplo a dos mesones depende muy fuertemente de la masa de los quarks.

Dependencia con la masa del quark extraño

- Como es de esperar, encontramos que las propiedades de las resonancias no extrañas $\rho(770)$ y $f_0(600)$ son prácticamente independientes de la masa del quark extraño en el rango estudiado.

- Las resonancias $K^*(892)$ y $K_0^*(800)$ muestran una dependencia con m_s mucho más fuerte. A medida que el quark extraño se hace más pesado, sus masas crecen mucho más rápido de lo que lo hacían al aumentar la masa de los quarks ligeros, pero más lentamente que la del kaón.

- En el caso de la resonancia vectorial $K^*(892)$, la anchura se reduce tal y como se espera como efecto de la supresión del espacio de fases solamente, pues su acoplo a $K\pi$ es prácticamente constante. Contrariamente, la disminución de la anchura de la resonancia $K_0^*(800)$ se desvía de forma significativa de ese

comportamiento, de acuerdo con el hecho de que su acoplo a $K\pi$ depende muy fuertemente de la masa del quark extraño.

- La relación de KSFR también es una buena aproximación en todo el rango de m_s estudiado, aunque no tan buena como en el caso de la dependencia con $\hat{m}$.

En la publicación 2.1.3 estudiamos la extrapolación quiral de los desfases en la dispersión de dos piones, usando ChPT estándar y unitarizada, a uno y dos loops. Con ChPT estándard, que está limitada a momentos bajos, estudiamos las ondas S, P y D. La unitarización con el IAM extiende el análisis a energías de alrededor de 1 GeV, siendo compatible con ChPT estándar a bajas energías para las ondas S y P. A continuación, hemos llevado a cabo una comparación con los resultados de los cálculos en el retículo. Además hemos realizado un análisis de Montecarlo para ofrecer una estimación de las incertidumbres. Los resultados de este trabajo se exponen a continuación.

- Usando ChPT estándar encontramos que la dependencia de los desfases con la masa del pión es muy suave a un loop y algo más fuerte a dos loops, especialmente para el canal I=J=2.

- Con ChPT unitarizada encontramos una dependencia en la masa del pión también bastante suave, particularmente para el canal I=2, J=0, y ligeramente más fuerte a dos loops que a un loop.

- Con el objetivo de comparar con los resultados de los cálculos en el retículo [62, 63, 64] en los canales (I,J) = (2,0), (2,2) and (1,1), incrementamos la masa del pión hasta 444 MeV. Los resultados para masas tan altas deben ser considerados sólo cualitativamente, puesto que esta región de energía está por encima de los límites de aplicabilidad de nuestro método. ChPT estándar muestra un buen acuerdo con los resultados del retículo por debajo de $p \simeq 200$ MeV hasta masas del pión de unos 400 a 450 MeV, mientras que se obtiene una buena mejora por encima de 200 MeV al usar ChPT unitarizada para los canales escalar y vectorial.

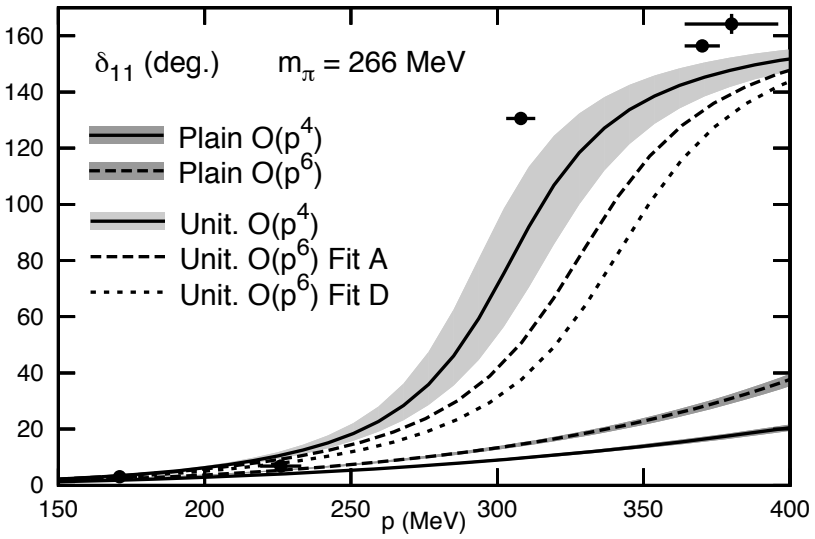

Figure 1

- En este resumen incluimos un nuevo cálculo posterior la publicación del artículo 2.1.3. Dicho resultado se presentó en las actas de una conferencia reciente [96], con el fin de compararlo con nuevos resultados en el retículo [64] presentados en la misma conferencia. Se trata del desfase en el canal I=J=1 a una masa $M_\pi = 266$ MeV, mostrado en la figura 1. En ella se observa que, para momentos por encima de 300 MeV, nuestros desfases dependen de la masa del pión más suavemente de lo que predicen los cálculos en el retículo.

En la sección 2.1.4 calculamos las derivadas de las resonancias más ligeras respecto a $\hat{m}$ y m_s. Estos valores no sólo son de utilidad para el estudio de la naturaleza espectroscópica de las resonancias, sino que también son necesarios para el cálculo de la variación de las constantes fundamentales predicha por algunos modelos de unificación [125, 54].

Los resultados que encontramos son los siguientes:

- Calculamos los parámetros adimensionales

$$K_R^f = \frac{m_f}{M_R}\frac{\partial M_R}{\partial m_f}$$

para el pión, el kaón y las resonancias $\rho(770)$, $K^*(892)$, $f_0(600)$ and $K_0^*(800)$.

- Para el pión y el kaón estos parámetros se calculan a partir de sus expansiones en ChPT. Encontramos que nuestra precisión es mayor para los quarks ligeros que para el extraño. Las correcciones a los cálculos de primer orden son del mismo tamaño o más pequeñas que la incertidumbre en los resultados a órdenes superiores.

- Repetimos los cálculos con las LECs que usaremos para ChPT unitarizada y comprobamos que son compatibles con los resultados encontrados con las LECs de ChPT estándar.

- A continuación usamos el IAM para calcular el parámetro K_R^f para las resonancias elásticas. Para estimar el error sistemático, repetimos los cálculos usando aproximación chiral unitaria (Chiral Unitary approach) [21, 18], que es más sencilla pero no incluye toda la dependencia en la masa y contiene parámetros espurios.

- Los parámetros K_R^f para las resonancias escalares son más fiables que para las vectoriales porque estas últimas dependen fuertemente de las LECs mientras que las escalares dependen más de los loops quirales.

- En particular, encontramos para K_σ^s un valor negativo y pequeño, al contrario que el estimado para algunos estudios sobre la variación cosmológica de las constantes fundamentales [53], $K_\sigma^s \approx 0.54$. Si usamos nuestro resultado en lugar del suyo, obtenemos un límite algo menos restrictivo para la cantidad $|\delta(m_s/\Lambda_{\rm QCD})/(m_s/\Lambda_{\rm QCD})|$.

Propiedades de las resonancias elásticas ligeras a partir de su comportamiento con $1/N_c$

Como comentábamos anteriormente, las amplitudes de QCD admiten una expansión en $1/N_c$ a cualquier energía [65, 66]. En esta sección nos servimos del hecho de que los estados $\bar{q}q$ y los glueballs tienen un comportamiento bien determinado con $1/N_c$

y, por otra parte, de que la expansión se puede implementar en ChPT con facilidad. Puesto que el IAM no introduce cutoffs o constantes de substracción que podrían ocultar una dependencia en N_c desconocida, podemos usarlo para estudiar el comportamiento de las resonancias elásticas ligeras. La comparación de este comportamiento con el esperado para estados de $\bar{q}q$ y glueballs sirve como herramienta para el estudio de la naturaleza espectroscópica de estas resonancias.

Usando esta técnica, en [128] se demostró que las resonancias vectoriales ligeras siguen claramente un comportamiento $\bar{q}q$, mientras que la dependencia de las escalares está reñida con una naturaleza predominantemente $\bar{q}q$. Este resultado fue después confirmado a dos loops [83] para los mesones $\rho(770)$ y $f_0(600)$, encontrándose para este último indicios de la aparición, al aumentar N_c, de una componente $\bar{q}q$ subdominante con una masa alrededor de 1 GeV. Este comportamiento estaría principalmente debido a la mezcla entre estados ligeros no $\bar{q}q$ y estados $\bar{q}q$ más pesados. Además, la dualidad semi-local requiere que las contribuciones de las resonancias ρ y σ a la sección eficaz de colisión elástica de $\pi^+\pi^+$ se cancelen y, por lo tanto, se dejaría de satisfacer al aumentar N_c si ambas resonancias no se comportaran de un modo similar [129]. La componente $\bar{q}q$ subdominante encontrada en [83] sería entonces necesaria para restaurar la localidad semi-dual a N_c alto. Un trabajo reciente [130], basado en el esquema SRA (single-resonance approximation), confirma que la resonancia $\rho(770)$ es un meson estable en el límite $N_c \to \infty$ y que el estado predominante en la σ no es $\bar{q}q$ en $N_c = 3$. Sin embargo, no puede concluir si la resonancia σ desaparece completamente en el límite $N_c \to \infty$ o si contiene una componente subdominante en su estructura.

En la publicación 2.2.2, tras repasar los principales resultados de [128] y [83], así como nuestros trabajos sobre la dependencia de los parámetros de las resonancias con la masa de los quarks, presentamos una discusión sobre la aplicabilidad de la expansión en $1/N_c$ dentro del IAM. No se espera que esta expansión proporcione resultados fiables en el límite $N_c \to \infty$ y debe ser considerada sólo en las proximidades de $N_c = 3$, lo cual, como veremos, es una motivación para nuestra siguiente

publicación 2.2.3. Los principales puntos de este análisis sobre la aplicabilidad de la expansión son los siguientes:

- El IAM no es fiable en el límite $N_c \to \infty$ porque las interacciones de la teoría se hacen débiles y la condición de unitariedad puede no ser tan determinante como otras aproximaciones hechas en la derivación del método.
- Además, la masa de la η' escala como $1/\sqrt{N_c}$ en el límite quiral y, por lo tanto, podría convertirse en un grado de libertad relevante a un N_c lo suficientemente alto. El límite $N_c \to \infty$ incluyendo el mesón η' en $U(3) \times U(3)$ ChPT se estudia en [131].
- Sólo se puede extraer información acerca de la componente dominante en los escalares ligeros en las cercanás de $N_c = 3$: puesto que las moléculas de dos mesones y algunos estados de tetraquark se disuelven en el contínuo en el límite $N_c \to \infty$, una componente $\bar{q}q$ subdominante podría volverse dominante a un cierto N_c lo suficientemente alto. Además, la mezcla original podría cambiar con N_c.

Por otra parte, $1/N_c$ a $N_c = 3$ puede parecer un parámetro no lo suficientemente pequeño para realizar una expansión. Sin embargo, podemos encontrar observables cuyas correcciónes estén suprimidas por órdenes más altos de $1/N_c$, de modo que se pueden extraer conclusiones más fuertes a partir de los datos experimentales manteniendo el número físico de colores. En [132] se encontró que, para un estado $\bar{q}q$, la parte real de la amplitud inversa, evaluada en la masa del polo de la resonancia, escala como $\mathcal{O}(N_c^{-1})$, en lugar de $\mathcal{O}(N_c)$, y que la corrección es de orden $\mathcal{O}(N_c^{-3})$. Del mismo modo, se demostró que la corrección al comportamiento dominante $\mathcal{O}(N_c^{-1})$ del observable $m_R\Gamma_R$ es también de orden $\mathcal{O}(N_c^{-3})$.

Haciendo uso de estas ideas, en la publicación 2.2.3 definimos dos observables adimensionales cuyas correcciones están suprimidas por dos y tres potencias de N_c para un estado $\bar{q}q$. Para un glueball, estas correcciones están aún más suprimidas, gracias a que su anchura es $\mathcal{O}(1/N_c^2)$ en lugar de $\mathcal{O}(1/N_c)$. Calculamos entonces el tamaño de estas correcciones *en el número físico de colores* $N_c = 3$ para las

resonancias elásticas ligeras usando los recientes y muy precisos análisis dispersivos de datos experimentales [95] y [133], encontrando los siguientes resultados:

- Observamos que, para las resonancias vectoriales $\rho(770)$ y $K^*(892)$, la supresión de nuestros observables es del orden esperado para estados $\bar{q}q$.
- Por el contrario, para los escalares $f_0(600)$ y $K_0^*(800)$, encontramos que las correcciones son dos órdenes de magnitud más grandes, lo que hace muy poco natural una interpretación de estas resonancias como estados $\bar{q}q$. Asimismo, para la $f_0(600)$ una componente glueball dominante queda también descartada.
- Usamos además ChPT unitarizada para mostrar que, para los escalares, las evolución de las correcciones con N_c se aleja mucho de la esperada para un estado $\bar{q}q$ (y glueball), lo que explica la necesidad de correcciones demasiado grandes en $N_c = 3$ para obtener los valores esperados a primer orden en $1/N_c$.

Conclusiones

A lo largo de esta tesis hemos estudiado las propiedades de la dispersión elástica de $\pi\pi$ y πK y de las resonancias más ligeras que aparecen en ella: las vectoriales $\rho(770)$ y $K^*(892)$, bien establecidas, y las controvertidas escalares $f_0(600)$ y $K_0^*(800)$, también llamadas σ y κ, respectivamente.

Para ello nos hemos servido de la teoría efectiva de baja energía conocida como Teoría de Perturbaciones Quiral (ChPT) [1, 2, 3, 4, 5]. Para el estudio de las resonancias, hemos unitarizado las amplitudes de ChPT usando el Método de la Amplitud Inversa (IAM) [26, 27, 28, 29, 30], que se deriva de una relación de dispersión para el inverso de la amplitud, cuya parte imaginaria en la región elástica se conoce exactamente gracias a la condición de unitariedad. Este método no contiene parámetros espurios y todas las dependencias con los parámetros de QCD aparecen a través de la expansión de ChPT, que se usa para calcular los puntos de substracción a baja energía y el corte izquierdo. Además, el IAM genera polos en

la segunda hoja de Riemann asociados a las resonancias ligeras, sin necesidad de hacer ninguna suposición sobre su existencia y naturaleza. Esto nos ha permitido hacer un estudio sistemático de la dependencia de las amplitudes y resonancias con dos parámetros de QCD: las masas de los quarks y el número de colores, N_c.

Hemos estudiado la extrapolación quiral de los desfases de las amplitudes de dispersión de dos piones, usando $SU(2)$ ChPT estándar y unitarizada, a uno y dos loops. Con ChPT estándar, que está limitada a momentos bajos, hemos estudiado las ondas S, P y D. A continuación, usando ChPT unitarizada, hemos extendido el análisis a energías de alrededor de 1 GeV para las ondas S y P, siendo compatible con ChPT estándar a bajas energías. Hemos hecho una comparación con los resultados de cálculos en el retículo [62, 63, 64] y hemos encontrado que estos están de acuerdo con ChPT estándar por debajo de $p \sim 200$ MeV para los canales I=2, J=0 y I=J=1 y hasta $p \sim 500$ MeV para el canal I=J=2. Hemos mostrado que los desfases calculados con ChPT unitarizada se asemejan más a los de los cálculos en el retículo en los canales escalar y vectorial a energías más altas. Además, hemos llevado a cabo un análisis de Montecarlo para proporcionar una estimación de las incertidumbres.

También hemos estudiado la dependencia con la masa de los quarks ligeros y extraño de los parámetros de las resonancias $f_0(600)$, $K_0^*(800)$, $\rho(770)$ y $K^*(892)$ usando $SU(3)$ ChPT unitarizada con el IAM. Hemos realizado ajustes simultáneos a datos experimentales hasta 0.8-1 GeV junto con resultados de cálculos en el retículo [102, 103, 104, 105] hasta masas del pión de unos 440 MeV. A continuación, hemos variado la masa de los quarks desde el límite quiral hasta valores de interés para los estudios en el retículo. Hemos encontrado que la masa y la anchura de las resonancias $\rho(770)$ y $K^*(892)$ presentan una dependencia con la masa de los quarks suave y similar entre ambas, mientras que las resonacias escalares muestran un comportamiento no analítico para una masa del quark ligero elevada. Además hemos confirmado la suposición que se suele hacer en los estudios en el retículo de que el acoplo de las resonancias vectoriales a dos mesones no depende de la masa de los quarks, y hemos visto que para los escalares la dependencia es muy fuerte.

Se han calculado también las derivadas de las masas de estas resonancias respecto a la masa de los quarks usando el IAM. Hemos calculado los parámetros adimensionales $K_R^f = \frac{m_f}{M_R}\frac{\partial M_R}{\partial m_f}$, donde m_f es la masa de los quarks ligeros o del extraño. Hemos estimado los errores sistemáticos usando dos métodos distintos que sólo se distinguen en órdenes más altos en la expansión de ChPT, y además hemos repetido los cálculos usando el Método Chiral Unitario [21, 18], que es más simple que el IAM pero no incluye toda la dependencia con la masa. Calculando estos parámetros para el pión y el kaón, para los cuales no se necesita la unitarización, hemos comprobado que las LECs que usamos para los cálculos con el IAM ofrecen resultados que son compatibles con los obtenidos usando las LECs estándar de ChPT. De entre los valores estimados que encontramos, destacamos el de σ con la masa del quark extraño, que es muy distinto del valor usado en algunos estudios sobre la variación cosmológica de las constantes fundamentales [53].

En lo que concierne al número de colores, tras repasar resultados previos sobre el comportamiento con la expansión $1/N_c$ de las resonancias generadas con el IAM [128, 83], hemos discutido sobre la aplicabilidad del IAM en el límite $N_c \to \infty$.

A continuación, con el objetivo de extraer información sobre la posible naturaleza $\bar{q}q$ o glueball de las resonancias σ y κ sin tener que extrapolar a valores de N_c no físicos, hemos presentado dos observables adimensionales, cuyo valor es conocido salvo por correcciones en la expansión $1/N_c$ muy suprimidas para estados $\bar{q}q$ y glueball. Así, hemos calculado estos observables en $N_c = 3$, usando análisis del desfase en la dispersión de $\pi\pi$ y πK, recientes y muy precisos [95, 133], sin necesidad de utilizar métodos de unitarización. De este modo hemos demostrado que, si asumimos una naturaleza $\bar{q}q$ para estas resonancias, las correcciones en la expansión $1/N_c$ de los observables son dos órdenes de magnitud demasiado grandes, lo que desfavorece mucho una interpretación $\bar{q}q$ para ambas resonancias escalares, así como una naturaleza glueball para la σ.

Bibliography

[1] S. Weinberg, *Phenomenological Lagrangians*, *Physica* **A96** (1979) 327.

[2] J. Gasser and H. Leutwyler, *Chiral Perturbation Theory to One Loop*, *Annals Phys.* **158** (1984) 142.

[3] J. Gasser and H. Leutwyler, *Low-Energy Expansion of Meson Form-Factors*, *Nucl. Phys.* **B250** (1985) 517–538.

[4] J. Gasser and H. Leutwyler, *eta → 3 pi to One Loop*, *Nucl. Phys.* **B250** (1985) 539.

[5] J. Gasser and H. Leutwyler, *Chiral Perturbation Theory: Expansions in the Mass of the Strange Quark*, *Nucl. Phys.* **B250** (1985) 465.

[6] G. Ecker, J. Gasser, A. Pich, and E. de Rafael, *The Role of Resonances in Chiral Perturbation Theory*, *Nucl. Phys.* **B321** (1989) 311.

[7] J. F. Donoghue, C. Ramirez, and G. Valencia, *The Spectrum of QCD and Chiral Lagrangians of the Strong and Weak Interactions*, *Phys. Rev.* **D39** (1989) 1947.

[8] H. Leutwyler, *Chiral dynamics*, `hep-ph/0008124`. Contribution to the Festschrift in honor of B.L. Ioffe.

[9] A. Dobado, A. Gomez-Nicola, A. L. Maroto, and J. Pelaez, *Effective Lagrangians for the Standard Model*. Texts and Monographs in Physics. Springer-Verlag Berlin/Heidelberg.

[10] A. Pich, *Chiral perturbation theory*, *Rept. Prog. Phys.* **58** (1995) 563–610, [`hep-ph/9502366`].

[11] U. G. Meißner, *Recent developments in chiral perturbation theory*, *Rept. Prog. Phys.* **56** (1993) 903–996, [`hep-ph/9302247`].

[12] G. Ecker, J. Gasser, H. Leutwyler, A. Pich, and E. de Rafael, *Chiral Lagrangians for Massive Spin 1 Fields*, *Phys. Lett.* **B223** (1989) 425.

[13] V. Bernard, N. Kaiser, and U. G. Meißner, *Chiral perturbation theory in the presence of*

resonances: Application to pi pi and pi K scattering, *Nucl. Phys.* **B364** (1991) 283–320.

[14] M. Harada, F. Sannino, and J. Schechter, *Simple description of pi pi scattering to 1-GeV*, *Phys. Rev.* **D54** (1996) 1991–2004, [hep-ph/9511335].

[15] J. Oller and E. Oset, *N/D description of two meson amplitudes and chiral symmetry*, *Phys. Rev.* **D60** (1999) 074023, [hep-ph/9809337].

[16] M. Jamin, J. A. Oller, and A. Pich, *S wave K pi scattering in chiral perturbation theory with resonances*, *Nucl. Phys.* **B587** (2000) 331–362, [hep-ph/0006045].

[17] N. Kaiser, P. Siegel, and W. Weise, *Chiral dynamics and the low-energy kaon - nucleon interaction*, *Nucl. Phys.* **A594** (1995) 325–345, [nucl-th/9505043].

[18] J. Oller, E. Oset, and J. Pelaez, *Nonperturbative approach to effective chiral Lagrangians and meson interactions*, *Phys. Rev. Lett.* **80** (1998) 3452–3455, [hep-ph/9803242].

[19] J. Oller and E. Oset, *Chiral symmetry amplitudes in the S wave isoscalar and isovector channels and the sigma, f0(980), a0(980) scalar mesons*, *Nucl. Phys.* **A620** (1997) 438–456, [hep-ph/9702314].

[20] E. Oset and A. Ramos, *Nonperturbative chiral approach to s wave anti-K N interactions*, *Nucl. Phys.* **A635** (1998) 99–120, [nucl-th/9711022].

[21] J. Oller, E. Oset, and J. Pelaez, *Meson meson interaction in a nonperturbative chiral approach*, *Phys. Rev.* **D59** (1999) 074001, [hep-ph/9804209].

[22] J. Nieves and E. Ruiz Arriola, *Bethe-Salpeter approach for meson meson scattering in chiral perturbation theory*, *Phys. Lett.* **B455** (1999) 30–38, [nucl-th/9807035].

[23] J. Nieves and E. Ruiz Arriola, *Bethe-Salpeter approach for unitarized chiral perturbation theory*, *Nucl. Phys.* **A679** (2000) 57–117, [hep-ph/9907469].

[24] J. Nieves and E. Ruiz Arriola, *Bethe-Salpeter approach for the P(33) elastic pion-nucleon scattering in heavy baryon chiral perturbation theory*, *Phys. Rev.* **D63** (2001) 076001, [hep-ph/0008034].

[25] S. Gupta, *Quantum Electrodynamics*, .

[26] T. N. Truong, *Chiral Perturbation Theory and Final State Theorem*, *Phys. Rev. Lett.* **61** (1988) 2526. Revised version.

[27] T. N. Truong, *Remarks on the unitarization methods*, *Phys. Rev. Lett.* **67** (1991) 2260–2263.

[28] A. Dobado, M. J. Herrero, and T. N. Truong, *Unitarized Chiral Perturbation Theory for Elastic Pion-Pion Scattering*, *Phys. Lett.* **B235** (1990) 134.

[29] A. Dobado and J. Pelaez, *A Global fit of pi pi and pi K elastic scattering in ChPT with dispersion relations*, *Phys. Rev.* **D47** (1993) 4883–4888, [hep-ph/9301276].

[30] A. Dobado and J. Pelaez, *The Inverse Amplitude Method in Chiral Perturbation Theory*, *Phys. Rev.* **D56** (1997) 3057–3073, [hep-ph/9604416].

[31] **Particle Data Group** Collaboration, K. Nakamura *et. al.*, *Review of Particle Physics*, *J. Phys. G* **G37** (2010) 075021.

[32] D. Morgan, *Is the 0+ Nonet Respectable?*, *Phys. Lett.* **B51** (1974) 71.

[33] N. A. Tornqvist, *Understanding the scalar meson q anti-q nonet*, *Z. Phys.* **C68** (1995) 647–660, [hep-ph/9504372].

[34] N. Tornqvist, *Scalar Mesons in the Unitarized Quark Model*, *Phys. Rev. Lett.* **49** (1982) 624–627.

[35] N. A. Tornqvist and M. Roos, *Resurrection of the sigma meson*, *Phys. Rev. Lett.* **76** (1996) 1575–1578, [hep-ph/9511210].

[36] R. L. Jaffe, *Multi-Quark Hadrons. 1. The Phenomenology of (2 Quark 2 anti-Quark) Mesons*, *Phys. Rev.* **D15** (1977) 267.

[37] R. L. Jaffe, *Multi-Quark Hadrons. 2. Methods*, *Phys. Rev.* **D15** (1977) 281.

[38] N. Achasov, S. Devyanin, and G. Shestakov, *On scalar resonances in pi pi $\to$ pi pi, K anti-K, eta eta reactions*, *Z. Phys.* **C22** (1984) 53.

[39] N. Achasov, S. Devyanin, and G. Shestakov, *Is there a 'signature' of the Delta(980) meson four quark nature?*, *Phys. Lett.* **B96** (1980) 168.

[40] N. Achasov, S. Devyanin, and G. Shestakov, *Can Delta (980, 0+) be a broad $qq\bar{q}\bar{q}$ state?*, *Phys. Scripta* **27** (1983) 330.

[41] J. D. Weinstein and N. Isgur, *K anti-K Molecules*, *Phys. Rev.* **D41** (1990) 2236.

[42] J. D. Weinstein and N. Isgur, *Do Multi-Quark Hadrons Exist?*, *Phys. Rev. Lett.* **48** (1982) 659.

[43] J. D. Weinstein and N. Isgur, *The q q anti-q anti-q System in a Potential Model*, *Phys. Rev.* **D27** (1983) 588.

[44] G. Janssen, B. Pearce, K. Holinde, and J. Speth, *On the structure of the scalar mesons f0(975) and a0 (980)*, *Phys. Rev.* **D52** (1995) 2690–2700, [nucl-th/9411021].

[45] F. Close, *Gluonic Hadrons*, *Rept. Prog. Phys.* **51** (1988) 833.

[46] P. Minkowski and W. Ochs, *Identification of the glueballs and the scalar meson nonet of lowest mass*, *Eur. Phys. J.* **C9** (1999) 283–312, [hep-ph/9811518].

[47] J. A. Oller, *The Mixing angle of the lightest scalar nonet*, *Nucl. Phys.* **A727** (2003) 353–369, [hep-ph/0306031].

[48] M. Johnson and E. Teller, *Classical Field Theory of Nuclear Forces*, *Phys. Rev.* **98** (1955) 783–787.

[49] C. J. Hogan, *Why the universe is just so*, *Rev. Mod. Phys.* **72** (2000) 1149–1161, [astro-ph/9909295].

[50] T. Damour and J. F. Donoghue, *Constraints on the variability of quark masses from nuclear binding*, *Phys.Rev.* **D78** (2008) 014014, [arXiv:0712.2968].

[51] T. E. Jeltema and M. Sher, *The Triple alpha process and the anthropically allowed values of the weak scale*, *Phys. Rev.* **D61** (2000) 017301, [hep-ph/9905494].

[52] J. K. Webb, V. V. Flambaum, C. W. Churchill, M. J. Drinkwater, and J. D. Barrow, *Evidence for time variation of the fine structure constant*, *Phys. Rev. Lett.* **82** (1999) 884–887, [astro-ph/9803165].

[53] V. Flambaum and E. Shuryak, *Dependence of hadronic properties on quark masses and constraints on their cosmological variation*, *Phys. Rev.* **D67** (2003) 083507, [hep-ph/0212403].

[54] V. Flambaum and E. Shuryak, *Limits on cosmological variation of strong interaction and quark masses from big bang nucleosynthesis, cosmic, laboratory and Oklo data*, *Phys. Rev.* **D65** (2002) 103503, [hep-ph/0201303].

[55] Y. Nambu and G. Jona-Lasinio, *Dynamical Model of Elementary Particles Based on an Analogy with Superconductivity. I*, *Phys. Rev.* **122** (1961) 345–358.

[56] Y. Nambu and G. Jona-Lasinio, *Dynamical Model of Elementary Particles Based on an Analogy with Superconductivity. II*, *Phys. Rev.* **124** (1961) 246–254.

[57] A. Dobado, M. Herrero, J. Pelaez, E. Ruiz Morales, and M. Urdiales, *Learning about the strongly interacting symmetry breaking sector at LHC*, *Phys. Lett.* **B352** (1995) 400–410, [hep-ph/9502309].

[58] A. Dobado and J. Pelaez, *On the equivalence theorem in the Chiral Perturbation Theory description of the Symmetry Breaking Sector of the Standard Model*, *Nucl. Phys.* **B425** (1994) 110–136, [hep-ph/9401202].

[59] A. Dobado and J. R. Pelaez, *The equivalence theorem for chiral Lagrangians*, *Phys. Lett.* **B329** (1994) 469–478, [hep-ph/9404239].

[60] D. Robson, *A Basic Guide for the Glueball Spotter*, *Nucl. Phys.* **B130** (1977) 328.

[61] J. F. Donoghue, K. Johnson, and B. A. Li, *Low Mass Glueballs in the Meson Spectrum*, *Phys. Lett.* **B99** (1981) 416.

[62] K. Sasaki and N. Ishizuka, *I=2 Two-Pion Wave Function and Scattering Phase Shift*, *Phys. Rev.* **D78** (2008) 014511, [arXiv:0804.2941].

[63] J. J. Dudek, R. G. Edwards, M. J. Peardon, D. G. Richards, and C. E. Thomas, *The phase-shift of isospin-2 pi-pi scattering from lattice QCD*, *Phys. Rev.* **D83** (2011) 071504, [arXiv:1011.6352].

[64] C. Lang, D. Mohler, S. Prelovsek, and M. Vidmar, *Coupled channel analysis of the rho meson decay in lattice QCD*, *Phys. Rev.* **D84** (2011) 054503, [arXiv:1105.5636].

[65] G. 't Hooft, *A Planar Diagram Theory for Strong Interactions*, *Nucl. Phys.* **B72** (1974) 461.

[66] E. Witten, *Baryons in the 1/N Expansion*, *Nucl. Phys.* **B160** (1979) 57.

[67] Y. Nambu, *Axial vector current conservation in weak interactions*, *Phys.Rev.Lett.* **4** (1960) 380–382.

[68] J. Goldstone, *Field Theories with Superconductor Solutions*, *Nuovo Cim.* **19** (1961) 154–164.

[69] J. Goldstone, A. Salam, and S. Weinberg, *Broken Symmetries*, *Phys.Rev.* **127** (1962) 965–970.

[70] M. Gell-Mann, *The Eightfold Way: A Theory of strong interaction symmetry*, .

[71] S. Okubo, *Note on unitary symmetry in strong interactions*, *Prog.Theor.Phys.* **27** (1962) 949–966.

[72] M. Knecht and J. Stern, *Generalized chiral perturbation theory*, hep-ph/9411253. Contribution to the second edition of the DAPHNE physics handbook, L. Maiani, G. Pancheri and N. Paver Eds.

[73] V. Bernard, N. Kaiser, and U. G. Meißner, *Threshold parameters of pi K scattering in QCD*, *Phys.Rev.* **D43** (1991) 2757–2760.

[74] V. Bernard, N. Kaiser, and U. G. Meißner, *pi K scattering in chiral perturbation theory to one loop*, *Nucl.Phys.* **B357** (1991) 129–152.

[75] V. Bernard, N. Kaiser, and U. G. Meißner, *pi eta scattering in QCD*, *Phys.Rev.* **D44** (1991) 3698–3701.

[76] J. Bijnens, *Chiral perturbation theory beyond one loop*, *Prog. Part. Nucl. Phys.* **58** (2007) 521–586, [hep-ph/0604043].

[77] S. Weinberg, *Pion scattering lengths*, *Phys.Rev.Lett.* **17** (1966) 616–621.

[78] M. Knecht, B. Moussallam, J. Stern, and N. Fuchs, *The Low-energy pi pi amplitude to one and two loops*, *Nucl.Phys.* **B457** (1995) 513–576, [hep-ph/9507319].

[79] J. Bijnens, G. Colangelo, G. Ecker, J. Gasser, and M. Sainio, *Elastic pi pi scattering to two loops*, *Phys. Lett.* **B374** (1996) 210–216, [hep-ph/9511397].

[80] A. D. Martin and T. D. Spearman, *Elementary particle theory.* North- Holland Pub. Co.

[81] A. Gomez Nicola, J. Pelaez, and G. Rios, *The Inverse Amplitude Method and Adler Zeros*, *Phys. Rev.* **D77** (2008) 056006, [arXiv:0712.2763].

[82] J. Nieves, M. Pavon Valderrama, and E. Ruiz Arriola, *The Inverse amplitude method in pi pi scattering in chiral perturbation theory to two loops*, *Phys. Rev.* **D65** (2002) 036002, [hep-ph/0109077].

[83] J. Pelaez and G. Rios, *Nature of the f0(600) from its N(c) dependence at two loops in unitarized Chiral Perturbation Theory*, *Phys. Rev. Lett.* **97** (2006) 242002, [hep-ph/0610397].

[84] J. Oller, E. Oset, and J. Pelaez, *The phi $\to$ pi+ pi- decay within a chiral unitary approach*, *Phys. Rev.* **D62** (2000) 114017, [hep-ph/9911297].

[85] A. Gomez Nicola and J. Pelaez, *Meson meson scattering within one loop chiral perturbation theory and its unitarization*, *Phys. Rev.* **D65** (2002) 054009, [hep-ph/0109056].

[86] J. Pelaez, *Light scalars as tetraquarks or two-meson states from large N(c) and unitarized Chiral Perturbation Theory*, *Mod. Phys. Lett.* **A19** (2004) 2879–2894, [hep-ph/0411107].

[87] P. Buettiker, S. Descotes-Genon, and B. Moussallam, *A new analysis of pi K scattering*

from Roy and Steiner type equations, *Eur. Phys. J.* **C33** (2004) 409–432, [hep-ph/0310283].

[88] G. Amoros, J. Bijnens, and P. Talavera, *QCD isospin breaking in meson masses, decay constants and quark mass ratios*, *Nucl. Phys.* **B602** (2001) 87–108, [hep-ph/0101127].

[89] G. Colangelo, J. Gasser, and H. Leutwyler, *pi pi scattering*, *Nucl. Phys.* **B603** (2001) 125–179, [hep-ph/0103088].

[90] L. Girlanda, M. Knecht, B. Moussallam, and J. Stern, *Comment on the prediction of two loop standard chiral perturbation theory for low-energy pi pi scattering*, *Phys. Lett.* **B409** (1997) 461–468, [hep-ph/9703448].

[91] G. Colangelo, S. Durr, A. Juttner, L. Lellouch, H. Leutwyler, *et. al.*, *Review of lattice results concerning low energy particle physics*, *Eur. Phys. J.* **C71** (2011) 1695, [arXiv:1011.4408].

[92] A. Bazavov, C. Bernard, C. DeTar, X. Du, W. Freeman, *et. al.*, *Staggered chiral perturbation theory in the two-flavor case and SU(2) analysis of the MILC data*, *PoS* **LATTICE2010** (2010) 083, [arXiv:1011.1792]. Long author list - awaiting processing.

[93] R. Baron, P. Boucaud, J. Carbonell, A. Deuzeman, V. Drach, *et. al.*, *Light hadrons from lattice QCD with light (u,d), strange and charm dynamical quarks*, *JHEP* **1006** (2010) 111, [arXiv:1004.5284].

[94] J. Nebreda, J. Pelaez, and G. Rios, *Chiral extrapolation of pion-pion scattering phase shifts within standard and unitarized Chiral Perturbation Theory*, *Phys. Rev.* **D83** (2011) 094011, [arXiv:1101.2171].

[95] R. Garcia-Martin, R. Kaminski, J. Pelaez, J. Ruiz de Elvira, and F. Yndurain, *The Pion-pion scattering amplitude. IV: Improved analysis with once subtracted Roy-like equations up to 1100 MeV*, *Phys. Rev.* **D83** (2011) 074004, [arXiv:1102.2183].

[96] J. Nebreda, J. Pelaez, and G. Rios, *Mass dependence of pion-pion phase shifts within standard and unitarized ChPT versus Lattice results*, arXiv:1108.5980. * Temporary entry *.

[97] C. Hanhart, J. Pelaez, and G. Rios, *Quark mass dependence of the rho and sigma from dispersion relations and Chiral Perturbation Theory*, *Phys. Rev. Lett.* **100** (2008) 152001, [arXiv:0801.2871].

[98] J. Pelaez and G. Rios, *Chiral extrapolation of light resonances from one and two-loop unitarized Chiral Perturbation Theory versus lattice results*, *Phys. Rev.* **D82** (2010)

114002, [arXiv:1010.6008].

[99] J. Bijnens, G. Colangelo, G. Ecker, J. Gasser, and M. E. Sainio, *Pion pion scattering at low energy*, *Nucl. Phys.* **B508** (1997) 263–310, [hep-ph/9707291].

[100] **MILC Collaboration** Collaboration, A. Bazavov *et. al.*, *MILC results for light pseudoscalars*, *PoS* **CD09** (2009) 007, [arXiv:0910.2966].

[101] J. Nebreda and J. Pelaez., *Strange and non-strange quark mass dependence of elastic light resonances from SU(3) Unitarized Chiral Perturbation Theory to one loop*, *Phys. Rev.* **D81** (2010) 054035, [arXiv:1001.5237].

[102] **NPLQCD Collaboration** Collaboration, S. R. Beane *et. al.*, *The K+ K+ scattering length from lattice QCD*, *Phys. Rev.* **D77** (2008) 094507, [arXiv:0709.1169].

[103] S. R. Beane, T. C. Luu, K. Orginos, A. Parreno, M. J. Savage, *et. al.*, *Precise Determination of the I=2 pi pi Scattering Length from Mixed-Action Lattice QCD*, *Phys. Rev.* **D77** (2008) 014505, [arXiv:0706.3026].

[104] S. R. Beane, P. F. Bedaque, T. C. Luu, K. Orginos, E. Pallante, *et. al.*, *pi K scattering in full QCD with domain-wall valence quarks*, *Phys. Rev.* **D74** (2006) 114503, [hep-lat/0607036].

[105] **ETM collaboration** Collaboration, P. Boucaud *et. al.*, *Dynamical Twisted Mass Fermions with Light Quarks: Simulation and Analysis Details*, *Comput. Phys. Commun.* **179** (2008) 695–715, [arXiv:0803.0224].

[106] L. Montanet, *The positive parity mesons*, *Rept.Prog.Phys.* **46** (1983) 337.

[107] D. Morgan and M. Pennington, *The Scalar meson enigma*, *Nucl.Phys.Proc.Suppl.* **21** (1991) 37–42.

[108] A. V. Manohar, *Large N QCD*, hep-ph/9802419. From 'Probing the Standard Model of Particle Interactions', F. David & R. Gupta eds.

[109] S. Peris and E. de Rafael, *On the large N(c) behavior of the L(7) coupling in ChPT*, *Phys. Lett.* **B348** (1995) 539–542, [hep-ph/9412343].

[110] J. Pelaez, J. Nebreda, and G. Rios, *Properties of light resonances from unitarized Chiral perturbation theory: Nc behavior and quark mass dependence*, *Prog. Theor. Phys. Suppl.* **186** (2010) 113–123, [arXiv:1007.3461].

[111] J. Nebreda, J. Pelaez, and G. Rios, *Enhanced non-quark-antiquark and non-glueball Nc behavior of light scalar mesons*, *Phys. Rev.* **D84** (2011) 074003, [arXiv:1107.4200].

[112] C. W. Bernard, T. Burch, K. Orginos, D. Toussaint, T. A. DeGrand, *et. al.*, *The QCD spectrum with three quark flavors*, *Phys.Rev.* **D64** (2001) 054506, [hep-lat/0104002].

[113] **ETM Collaboration** Collaboration, P. Boucaud *et. al.*, *Dynamical twisted mass fermions with light quarks*, *Phys. Lett.* **B650** (2007) 304–311, [hep-lat/0701012].

[114] **RBC and UKQCD Collaborations** Collaboration, C. Allton *et. al.*, *2+1 flavor domain wall QCD on a (2 fm)*83 lattice: Light meson spectroscopy with L(s) = 16*, *Phys. Rev.* **D76** (2007) 014504, [hep-lat/0701013].

[115] C. Allton, W. Armour, D. B. Leinweber, A. W. Thomas, and R. D. Young, *Chiral and continuum extrapolation of partially-quenched lattice results*, *Phys. Lett.* **B628** (2005) 125–130, [hep-lat/0504022].

[116] **QCDSF Collaboration** Collaboration, M. Gockeler *et. al.*, *Extracting the rho resonance from lattice QCD simulations at small quark masses*, *PoS* **LATTICE2008** (2008) 136, [arXiv:0810.5337].

[117] X. Feng, K. Jansen, and D. B. Renner, *The pi+ pi+ scattering length from maximally twisted mass lattice QCD*, *Phys. Lett.* **B684** (2010) 268–274, [arXiv:0909.3255].

[118] J. Nagata, S. Muroya, and A. Nakamura, *Lattice study of K pi scattering in I = 3/2 and 1/2*, *Phys. Rev.* **C80** (2009) 045203, [arXiv:0812.1753].

[119] S. Prelovsek, T. Draper, C. B. Lang, M. Limmer, K.-F. Liu, *et. al.*, *Lattice study of light scalar tetraquarks with I=0,2,*1/2,3/2*: Are σ and κ tetraquarks?*, *Phys. Rev.* **D82** (2010) 094507, [arXiv:1005.0948].

[120] P. C. Bruns and U.-G. Meißner, *Infrared regularization for spin-1 fields*, *Eur. Phys. J.* **C40** (2005) 97–119, [hep-ph/0411223].

[121] **CP-PACS Collaboration** Collaboration, S. Aoki *et. al.*, *Lattice QCD Calculation of the rho Meson Decay Width*, *Phys. Rev.* **D76** (2007) 094506, [arXiv:0708.3705].

[122] K. Kawarabayashi and M. Suzuki, *Partially conserved axial vector current and the decays of vector mesons*, *Phys. Rev. Lett.* **16** (1966) 255.

[123] Riazuddin and Fayyazuddin, *Algebra of current components and decay widths of rho and K* mesons*, *Phys. Rev.* **147** (1966) 1071–1073.

[124] E. Epelbaum, V. Flambaum, C. Hanhart, U. G. Meißner, J. Nebreda, and J. R. Pelaez, *Varying quark masses and its impact in bbn*, *In preparation.*

[125] V. F. Dmitriev, V. V. Flambaum, and J. K. Webb, *Cosmological variation of deuteron*

binding energy, strong interaction and quark masses from Big Bang nucleosynthesis, *Phys. Rev.* **D69** (2004) 063506, [astro-ph/0310892].

[126] M. T. Murphy *et. al.*, *Possible evidence for a variable fine structure constant from QSO absorption lines: motivations, analysis and results*, *Mon. Not. Roy. Astron. Soc.* **327** (2001) 1208, [astro-ph/0012419].

[127] U. Burgi, *Charged pion pair production and pion polarizabilities to two loops*, *Nucl. Phys.* **B479** (1996) 392–426, [hep-ph/9602429].

[128] J. R. Pelaez, *On the nature of light scalar mesons from their large N_c behavior*, *Phys. Rev. Lett.* **92** (2004) 102001, [hep-ph/0309292].

[129] J. Ruiz de Elvira, J. Pelaez, M. Pennington, and D. Wilson, *Chiral Perturbation Theory, the $1/N_c$ expansion and Regge behaviour determine the structure of the lightest scalar meson*, *Phys.Rev.* **D84** (2011) 096006, [arXiv:1009.6204].

[130] J. Nieves, A. Pich, and E. Ruiz Arriola, *Large-Nc Properties of the rho and f0(600) Mesons from Unitary Resonance Chiral Dynamics*, *Phys.Rev.* **D84** (2011) 096002, [arXiv:1107.3247].

[131] Z.-H. Guo and J. Oller, *Resonances from meson-meson scattering in U(3) CHPT*, *Phys. Rev.* **D84** (2011) 034005, [arXiv:1104.2849].

[132] J. Nieves and E. Ruiz Arriola, *Meson Resonances at large N(C): Complex Poles versus Breit-Wigner Masses*, *Phys. Lett.* **B679** (2009) 449–453, [arXiv:0904.4590].

[133] S. Descotes-Genon and B. Moussallam, *The K*0 (800) scalar resonance from Roy-Steiner representations of pi K scattering*, *Eur. Phys. J.* **C48** (2006) 553, [hep-ph/0607133].